RAB27A AND MUNC18 AS MOLECULAR DETERMINANTS OF SNARE-MEDIATED VESICLE DOCKING, PRIMING, AND FUSION IN GLUCOSE REGULATORY TISSUES

by

Matthew J. Merrins

A dissertation submitted in partial fulfillment
of the requirements for the degree of
Doctor of Philosophy
(Molecular and Integrative Physiology)
in The University of Michigan
2008

Doctoral Committee:

Professor Edward L. Stuenkel, Co-chair
Associate Professor Richard M. Mortensen, Co-chair
Professor John A. Williams
Professor Robert T. Kennedy
Assistant Professor Anatoli N. Lopatin

TABLE OF CONTENTS

LIST OF FIGURES

CHAPTER I:

CHAPTER II:

CHAPTER III:

ABSTRACT

Vesicle exocytosis involves number of essential protein families that cooperatively mediate physical attachment between the vesicle and the plasma membrane, including Rab GTPases, Sec1/Munc18 proteins, and SNARE proteins. We have examined two specific molecules in the regulated exocytotic pathway, Munc18c and Rab27a, at sites of SNARE-mediated vesicle fusion in tissues integral to the controlled maintenance of blood glucose, adipocytes and pancreatic β-cells. We have hypothesized that Munc18c regulates the progression of GLUT4 storage vesicle (GSV) trafficking and fusion via the insulin-induced alteration of its binding to the t-SNARE syntaxin4. Our results indicate that Munc18c interaction with a conformationally folded syntaxin4 acts as a negative regulator GSV docking. By comparison, syntaxin4 mutants that promote a SNARE complex-forming conformation demonstrate a shift in the state of Munc18c interaction that is sufficient for GSV docking, and is likely to mimic insulin activation of GSV trafficking, resulting in increased GLUT4 at the plasma membrane. Upstream of SM proteins, Rab GTPases and their effector proteins assist with the transport to and docking of vesicles at the plasma membrane, where they are believed to interact directly with the Munc18/syntaxin complex. We focused on identifying sites of Rab27a action in the insulin secretory pathways using membrane capacitance measurements of pancreatic β-cells isolated from Rab27a-null (*ashen*) mice. We demonstrate that Rab27a exerts dual roles in insulin granule exocytosis, facilitating the glucose-induced refilling of releasable granule pools while also limiting release from these pools. In summary, the investigations of this dissertation support a role for Munc18c and Rab27a in controlling both the timing and magnitude of vesicle docking and priming (*i.e.*, SNARE complex formation) at the plasma membrane, thereby acting as crucial regulators in the regulated exocytotic pathways in glucose regulatory tissues.

CHAPTER I

BACKGROUND

Introduction

'*If you love me, don't feed me junk food.*' ~ children's t-shirt slogan

The global burden of diabetes

Underlying diabetes mellitus is an insufficiency of the hormone insulin. Insulin is essential for growth and tissue development, and relevant to diabetes, the maintenance of whole body glucose homeostasis. After a meal, glucose and amino acids stimulate insulin secretion from β-cells in the pancreatic islets of Langerhans. At several tissues, insulin then promotes the synthesis and storage of carbohydrates, lipids and proteins while concurrently inhibiting their degradation and return into circulation. For example, hepatic glucose output is reduced via reduced gluconeogenesis and glycogenolysis, and glucose uptake is increased, primarily at striated muscle and adipose tissue. In type 1 diabetes mellitus, reduced insulin secretion results from the destruction of β-cells owing to immune system dysregulation. Comparatively, in type 2 diabetes mellitus the relative insulin deficiency is due to (1) an insensitivity of peripheral tissues to the hormone combined with (2) dramatically reduced insulin secretion from pancreatic β-cells. 95% of diabetics have type 2 diabetes. Currently, the treatment strategies encompass lifestyle alterations (principally diet and exercise) and frequently administration of pharmacologic agents

(*e.g.*, hypoglycemic sulphonylureas, metformin, *etc.*) or exogenous insulin, although alternative interventions including cell therapies are being pursued.

Currently, the American Diabetes Association estimates that 20.8 million Americans have diabetes (defined as >125 mg/dl fasting blood glucose) and an additional 54 million have pre-diabetic sugar levels (100-125 mg/dl). Globally, data collected by the World Health Organization (WHO) and the United Nations indicates that diabetes is most prevalent in India, China, and the United States. Particularly disturbing is the prevalence of diabetes in the U.S. (6.9%) considering the population (300 million) is roughly 23% that of China (1.31 billion), which harbored 16 million diabetics when the survey was completed in 1998. A 42% increase in type 2 diabetes is predicted in the United States and other industrialized countries by 2025, and projections are even worse in countries WHO statisticians termed 'developing' (non-industrialized), which are expected to see an average 170% increase per capita (King *et al.* 1998). The specific cultural or environmental factors that have triggered this recent precipitous increase in the prevalence of type 2 diabetes remains unclear.

For the individual, the impact of a diabetes diagnosis has substantial social and lifestyle implications including the planning and timing of meals, frequent self-measurement of blood glucose, the administration of insulin or oral medications, adjustments and precautions for physical activity, and avoidance of short term complications such as hypoglycemic episodes. A major goal of this thesis and an important step in addressing and eventually treating type 2 diabetes is to develop a better understanding of the cellular and molecular underpinnings of processes that underlie the control of blood glucose. As more information becomes available about these pathways, medicine will be better equipped to deal with the impending diabetes epidemic. More broadly, information gleaned from this thesis may also assist in the development of treatments for the multitude of other diseases, particularly those affecting neuroendocrine cells that are manifested by dysfunction of membrane trafficking pathways.

The role of membrane trafficking in glucose homeostasis

Membrane trafficking, in general, is an essential feature of all eukaryotic cells. Cargo molecules, either membrane bound or soluble, are carried by specific classes of membrane delimited granules or vesicles. The vesicles that undergo transport and fusion with the plasma membrane, exocytosis, must go through at least four basic processes: *translocation* of vesicles to the plasma membrane along the cytoskeletal network; tight *docking*, the physical attachment to the plasma membrane; *priming* of the granules to allow assembly of exocytotic machinery; and, finally, *fusion* of the granule membrane with the plasma membrane.

Exocytotic pathways can be categorized as either constitutive or regulated, the latter of which allows cells to temporally control vesicle release. The most common mechanism of regulated secretion for release of neurotransmitters or hormones is Ca^{2+}-triggered exocytosis. This form of membrane fusion is engineered specifically for high-speed execution, with fusion following Ca^{2+} entry by only milliseconds (Schneggenburger and Neher 2000). In this dissertation, Ca^{2+}-triggered exocytosis is examined in pancreatic β-cells, which releases the hypoglycemic hormone insulin in response to glucose and other physiologic stimuli. This process is dysfunctional in the diabetic state when β-cells decompensate and lose their capacity to secrete insulin. In addition to cell-to-cell communication, the secretory pathway allows for transport of membrane and membrane proteins to the cell surface, which in some cases relies on second messengers other than Ca^{2+} to trigger vesicle movement and membrane fusion. This case is examined here in adipocytes, which control blood sugar in response to insulin through the cell-surface presentation of the glucose transporter GLUT4 (Slc2a4) when triggered by the insulin signaling cascade, independently of intracellular Ca^{2+} levels. Thus, this thesis links these two key systems of blood glucose regulation, pancreatic β-cells and adipocytes, through the study of protein families critical to the physical attachment and fusion of vesicles to the plasma membrane in the regulated exocytotic pathways.

Vesicle trafficking involves a number of essential protein families that cooperate to provide attachment (tethering and docking) between the vesicle and the plasma membrane. Among these, Rab GTPases, Sec1/Munc18 (SM) proteins, and soluble N-ethylmaleimide-sensitive receptor (SNARE) proteins represent gene families that cooperatively mediate the final stages of the exocytotic pathway. Rab GTPases become localized to specific organelles when activated by GTP-binding, regulate vesicle transport along the cytoskeleton, as well as mediate vesicle tethering and docking through interaction with specific effector complexes (Fukuda 2005; Pfeffer 2007). Sec1/Munc18 proteins are believed to be Rab effector molecules that have dual roles in both docking and fusion, due to direct binding of SNARE proteins (Toonen and Verhage 2003). Ultimately, SNARE proteins anchored to both vesicles and their target membranes form the molecular machine responsible for generating the forces necessary for fusion (Chen and Scheller 2001; Jahn and Scheller 2006).

The over-arching hypothesis of this dissertation is that molecular docking and priming of vesicles is strongly regulated by two specific molecules in the exocytotic pathway, Rab27 and Munc18, at sites of SNARE-mediated fusion. The experiments of this dissertation demonstrate that both molecules work in concert to exert spatial and temporal control over membrane fusion reactions. Below I introduce the fusion processes carried out by the SNARE proteins in adipocytes and identify their potential sites of regulation. The evidence for the necessity of Munc18 as a syntaxin chaperone to define specific sites of exocytosis is discussed. Subsequently, the potential for Munc18 family members to exert inhibitory and potentiating actions on vesicle docking and priming is outlined across cell types, and the actions of Munc18c are then addressed specifically within the context of the adipocyte. The second half of this chapter reviews the literature supporting an important role of Rab27a GTPase for glucose-stimulated insulin secretion from pancreatic β-cells. Finally, evidence is presented for the specific hypothesis that Rab27a acts to finely adjust the number of vesicles that are docked and appear in a primed and release-competent state at the plasma membrane.

Regulation of glucose uptake by adipocytes

The molecular basis of insulin resistance

A decline in glucose uptake by peripheral tissues (*i.e.*, muscle and fat) is a known pre-diabetic condition, which only worsens with onset of type 2 diabetes. At the simplest level, it results from the failure of insulin to properly stimulate the surface presentation of the facilitative glucose transporter GLUT4 (Zierath *et al.* 1996; King *et al.* 1998). The first theory behind this 'insulin resistance' postulated that insulin receptors (IR) themselves were down-regulated, resulting in immediate termination of the hormonal signal. However, based on individuals with IR mutations it was soon realized that the loss of insulin-dependent stimulus-secretion coupling arises primarily from defects in intracellular signaling events downstream of insulin receptors (Pessin and Saltiel 2000). Consistently, tissue-specific deletion of the IRs in either muscle or fat (MIRKO and FIRKO mice, respectively) results in mild insulin resistance, whereas severe diabetes ensues upon deletion of GLUT4 in the same tissues (reviewed in (Huang and Czech 2007). These findings prompted a detailed analysis of signal transduction pathways in these tissues. This is a difficult task, as IR signaling through its tyrosine kinase activity quickly diverges to accomplish numerous tasks. These include cell growth and differentiation, activation/repression of transcription, and importantly to this work, stimulation of kinases/phosphatases that regulate the trafficking of vesicles containing GLUT4 to the membrane upon insulin stimulation (Saltiel and Pessin 2002).

Insulin regulation of GLUT4 compartmentalization and cycling

Changes in the location of GLUT4 determine the rate of glucose uptake in adipocytes and muscle. Pathways of continuous cycling within an intramembrane system keep GLUT4 sequestered in the absence of insulin. Upon synthesis, GLUT4 is membrane anchored via 12 transmembrane domains. Following this process, GLUT4 exits from the trans-Golgi network into a pool of insulin-responsive GLUT4 storage vesicles (GSVs). This newly synthesized GLUT4 is joined by 'old' GLUT4 contained in membrane contributed from the endosomal-recycling

compartment. Flux from both pathways is increased in response to insulin. Insulin stimulation increases GLUT4 at the PM ~20-fold in rat adipocytes, ~2-3 fold in human adipocytes, and ~10-fold in 3T3L1 adipocytes, a widely used cell line derived from mouse embryonic fibroblasts (Ishiki and Klip 2005). Insulin is also capable of simultaneously slowing the endocytosis of GLUT4 on the plasma membrane (PM). Upon exit from the PM, GLUT4 enters sorting endosome/early endosome membranes. There the pathway diverges. Most GLUT4 is recycled into the endosomal membrane-recycling compartment where it can be returned to the PM. In a second pathway, GLUT4 enters the late endosome, and is either recycled back through the trans-Golgi network or is degraded by lysosomes.

The use of total internal reflection (TIRF) microscopy to follow GLUT4-GFP localization has recently been used to study events within 100-250 nm of the adipocytes plasma membrane, revealing a previously undiscovered insulin-regulated step proximally to GSV fusion. Overall, insulin is found to stimulate a 2- to 3-fold increase in GLUT4 in the TIRF zone within a 10-20 min period (Tengholm and Meyer 2002; Gonzalez and McGraw 2006). This population includes vesicles moving along cytoskeletal tracks within the TIRF field, tethered/docked vesicles, and those that have accumulated in static clathrin coats during endocytosis (Bellve *et al.* 2006; Huang and Czech 2007). In studies of single GSV exocytosis, insulin stimulation was shown to result in a 4-fold increase in the frequency of vesicle fusion and significant shortening of the duration of vesicle tethering/docking prior to fusion (Bai *et al.* 2007; Huang *et al.* 2007). Of significant importance will be the correlation of these insulin-stimulated events (*i.e.*, GSV translocation, docking, and fusion) with the actions of specific proteins.

Stimulus-secretion coupling in the adipocyte

As shown in Figure 1.1, insulin binds a receptor tyrosine kinase on the extracellular alpha subunits of an $\alpha 2\beta 2$ heterotetrameric complex. The β-subunits contain tyrosine kinase activity, and the two subunits phosphorylate each other, allowing proximal effectors including four insulin receptor substrate (IRS 1/2/3/4) proteins to bind. Phosphorylation of IRS proteins then creates a

binding site for Src homology 2 (SH2) domain proteins. Most importantly for glucose uptake is the binding of type 1A phosphatidylinositol-3-kinase (PI3K). Interestingly, homozygous deletion of IRS1 protein, which couples to PI3K, induces mild insulin resistance but not diabetes, probably because of β-cell compensation (Araki *et al.* 1994; Tamemoto *et al.* 1994). However, inhibition of PI3K activity by a variety of pharmacologic inhibitors, interfering antibodies, and dominant-interfering mutants (reviewed in (Cheatham *et al.* 1994; Okada *et al.* 1994; Czech and Corvera 1999)) have clearly demonstrated that PI3K is the only enzyme that is absolutely essential to insulin-stimulated glucose uptake and GLUT4 surface presentation.

PI3K catalyzes the conversion of phosphatidylinositol-4,5-bisphostphate (PIP_2) into phosphatidylinositol-3,4,5-bisphostphate (PIP_3). However, PIP_3 is unable to mimic insulin stimulation in stimulating glucose uptake, which has been taken to mean that PI3K by itself is not a sufficient signal (Jiang *et al.* 1998). Subsequently, knockdown studies have suggested an alternative pathway involving activation of the small GTPase TC10 by CAP is required (Chiang *et al.* 2001; Chang *et al.* 2006), although this hypothesis has been challenged by studies showing a lack of effect of RNAi experiments directed against these signaling intermediates (Mitra *et al.* 2004; Zhou *et al.* 2004). Chang *et al.* (Chang *et al.* 2006) also showed that TC10 catalyzes GSV movement to the plasma membrane. The physiologic relevance of this step has been questioned by numerous studies using TIRFM showing that GSVs pass into the evanescent field (*i.e.*, within 100 nm of the PM) regularly in the absence of insulin in 3T3L1 adipocytes (Gonzalez and McGraw 2006; Bai *et al.* 2007; Sano *et al.* 2007) and rat adipocytes (Lizunov *et al.* 2005). Collectively, however, there is near unanimous agreement that PI3K is a primary signal transduction pathway downstream of insulin in GSV targeting.

Downstream of PI3K, PIP3 activates phosphoinositide-dependent kinase 1 (PDK1). At the level of PDK1 the wortmannin-sensitive (PI3K-dependent) signaling cascade diverges (Figure 1.1). In one pathway, PI3K stimulates the activity of atypical protein kinase C (aPKC) isoforms (Bandyopadhyay *et al.* 2002; Sajan *et al.* 2006), although their downstream targets have not yet

been identified. In a second pathway, PI3K stimulates the activation and translocation of Akt2 to the PM. In 3T3L1 adipocytes, the expression of a constitutively active membrane-delimited Akt2 results in dramatically increased glucose uptake and persistent PM GLUT4 localization (Kohn *et al.* 1996; Kohn *et al.* 1998). Consistently, a dominant negative Akt2 inhibits glucose uptake (Wang *et al.* 1999). At the level of Akt2, the insulin-signaling cascade diverges again. One important Akt2 substrate, AS160, has a Rab GTPase activating protein (GAP) domain that is required for its ability to regulate glucose uptake (Sano *et al.* 2003; Eguez *et al.* 2005; Larance *et al.* 2005; Miinea *et al.* 2005). Akt2, through inhibition of AS160, is thereby able to activate one of the master regulators of membrane trafficking, vesicle-associated Rab10 (Sano *et al.* 2007). Importantly, knockdown of AS160 is sufficient to increase glucose uptake in the basal state (Eguez *et al.* 2005; Larance *et al.* 2005). Subsequently, Gonzales et al. (Gonzalez and McGraw 2006) demonstrated the necessity of Akt2 for a pre-fusion step that includes GSV recruitment and/or docking, but somewhat inconsistently with the AS160 knockdown studies (Eguez *et al.* 2005; Larance *et al.* 2005), fusion was shown to be dependent on the activity of PI3K but independent of Akt2 (Gonzalez and McGraw 2006). Further kinetic analysis again using TIRFM has shown that GSV docking, in particular, is regulated by PI3K/AS160 (Bai *et al.* 2007). This step brings GSVs close enough the plasma membrane to be acted up by the SNARE fusion machinery and its regulatory molecules. Another outcome of the kinetic analysis performed by Bai and colleagues (Bai *et al.* 2007) indicates that insulin dramatically accelerates a priming step after docking, thereby contributing to the ~6-fold increase in the frequency of fusion seen in the presence of insulin. This result specifically implicates SNARE complex formation as a key molecular event for surface presentation of GLUT4, which is a central aspect of this dissertation.

Vesicle Fusion Machinery: SNARE proteins

The SNARE hypothesis

Soluble N-ethylmaleimide-sensitive factor (NSF) attachment protein receptors (SNAREs) are recognized as central to vesicle fusion events in all eukaryotes. The superfamily has 25 members in *S. cerivisiae* and 36 members in humans. The adaptive advantage of this diversity is that SNARE proteins are directed to catalyze fusion in specific intracellular membrane compartments (reviewed in (Hay 2001)). The first SNARE complex to be discovered comprised syntaxin1A (Bennett *et al.* 1992), SNAP25 (25 kDa synaptosome-associated protein) (Oyler *et al.* 1989), and VAMP/synaptobrevin (Trimble *et al.* 1988; Baumert *et al.* 1989). Each SNARE protein possesses a hallmark SNARE motif, a 60-70 amino acid sequence composed of evolutionarily conserved heptad repeat sequences that formed coiled-coil interactions (Figure 1.2). The 'SNARE hypothesis', in its original form, postulated that pre-assembled SNARE complexes at the sites of vesicle docking were acted on by the ATPase *N*-ethylmaleimide-sensitive factor (NSF) and its cofactor α-SNAP (soluble NSF attachment protein) to drive membrane fusion (Sollner *et al.* 1993; Sollner *et al.* 1993). Soon after, it was discovered that NSF and α-SNAP were not involved in fusion itself, but in SNARE complex disassembly (Mayer *et al.* 1996), and the hypothesis was altered to its present form, that assembly of SNARE core complexes is coincident with fusion events in the constitutive pathway of vesicle fusion. Indeed, reconstitution of SNAREs into separate lipid bilayer vesicles (liposomes) is sufficient for membrane fusion (Weber *et al.* 1998), and requires the presence of SNARE transmembrane domains (Nichols *et al.* 1997; McNew *et al.* 1999). A further advancement of the SNARE hypothesis came with ultrastructural analysis, using EM, which directly visualized the parallel alignment of neuronal SNAREs in the membrane from N- to C-termini (Hanson *et al.* 1997; Lin and Scheller 1997). This finding subsequently led to the hypothesis that N- to C-terminal 'zippering' of the SNARE motifs of these proteins provides the forces necessary to initiate vesicle-target membrane lipid mixing (Pobbati *et al.* 2006).

SNARE structure and core complex formation

In isolated SNARE proteins, the α-helical SNARE domains remain unstructured. However, SNARE core complexes are characterized by four parallel intertwined α-helices, one from each SNARE motif (Figure 1.2). The crystal structure has been solved for two SNARE core complexes, syntaxin1A/SNAP25/VAMP (Sutton *et al.* 1998) and an endosomal SNARE complex containing syntaxin 7, syntaxin 8, vti1b, and VAMP8/endobrevin (Antonin *et al.* 2002). In the former, SNAP25 contributes two SNARE domains to the four-helix bundle, while each SNARE motif is present on a separate protein in the endosomal complex. In this dissertation, the syntaxin4/SNAP23/VAMP2 complex is extensively studied in the plasma membrane docking and fusion of GLUT4 storage vesicles in adipocytes. Comparatively, the syntaxin1A/SNAP25/VAMP2 is believed to catalyze the fusion of insulin granules in β-cells. The high stability of these ternary complexes is evidenced by a melting temperature of 90°C (Sollner *et al.* 1993; Hayashi *et al.* 1995; Fasshauer *et al.* 1997). The stability arises from interacting side chains that form 16 hydrophobic 'layers', excepting the 0-layer which contains a highly-conserved arginine or glutamine residue that classifies SNARES as Q- or R-SNAREs (Fasshauer *et al.* 1998). Mutating amino acids in the center of this bundle impairs fusion (Fasshauer *et al.* 1998; Chen *et al.* 1999).

Regions outside the helical SNARE bundle are also of utmost importance for SNARE proteins to function. Most SNARE proteins contain transmembrane domains at their C-terminal ends, which are separated from the SNARE motif by a short linker (Jahn and Scheller 2006). Upstream of the conserved SNARE motifs there are independently folded domains. In SNAP23 and SNAP25, for example, a loop region covalently connects the two SNARE coils. While this loop region is not required for fusogenic activity (Parlati *et al.* 1999; Fukuda *et al.* 2000; Scales *et al.* 2000), it is likely that the cysteine-palmitolyation anchors permit high local concentrations of the two SNARE coils at the plasma membrane. Some Q-SNAREs like syntaxin (Fernandez *et al.* 1998; Misura *et al.* 2000; Misura *et al.* 2002; Dietrich *et al.* 2003) have an N-terminally folded 3-

helix bundle, whereas others such as Ykt6 contain a profilin-like fold (a.k.a. longin domain) (Gonzalez *et al.* 2001). These two motifs each possess an auto-inhibitory function, despite being structurally disparate (Tochio *et al.* 2001).

The function of the syntaxin N-terminal helices varies significantly between syntaxins. In the exocytotic pathway syntaxin1A is thought to assume multiple conformations that determine its ability to form into SNARE complexes. The autonomously folded N-terminal three helix bundle, termed the Habc domain, reversibly folds the SNARE motif (H3 domain) (Dulubova *et al.* 1999; Misura *et al.* 2000; Margittai *et al.* 2003). These two motifs are separated by a short structured linker. By itself, syntaxin1A *in vitro* rapidly fluctuates between a folded (closed) conformation and an unfolded (open) conformation every 0.8 ms (Margittai *et al.* 2003). The open conformation facilitates SNARE-SNARE pairing, resulting from accessibility of the SNARE motif. In the closed (SNARE-pairing inactive) conformation of syntaxin1A, the N-terminal bundle competes with SNAP25 and VAMP2 for binding to the H3 SNARE motif. Hence, removing the N-terminal helices of syntaxin1A increases the rate of ternary complex formation between synthetic liposomes reconstituted with SNAP25 and VAMP2 (Parlati *et al.* 1999), and between the yeast homologues Sso1p/syntaxin, Sec9p, and the vesicle SNARE Snc2p in solution (Nicholson *et al.* 1998). Comparatively, syntaxins 5 and 18, which regulate intracellular transport events, do not fold (Dulubova *et al.* 2002; Yamaguchi *et al.* 2002; Bryant and James 2003). In other cases, such as syntaxin4, no direct structural information currently exists.

SNARE complex assembly and cycling

The assembly of the ternary SNARE complex is believed to begin when the N-terminal ends of the Q-SNARE motifs on the acceptor complexes (*e.g.*, syntaxin1A and SNAP25) nucleate the formation of a three-helix complex (Fasshauer *et al.* 1997), which is joined by vesicle bound VAMP2 to nucleate a four-helix *trans*-complex (Sutton *et al.* 1998). Fluorescence anisotropy studies suggest that a loose state, in which only the N-terminal ends of the SNARE complex are

'zipped' up, then proceeds to a tight state (zippering is mostly completed) (Pobbati *et al.* 2006). This may be the point at which SNARE complex assembly can be arrested by interaction with other regulatory proteins (*e.g.*, complexin) without fusion occurring. Alternative models suggest that no directionality is required for the electrostatic interactions of the SNARE bundles to associate, akin to a 'Velcro' strip (Durrieu *et al.* 2008). Significant evidence indicates that SNARE complexes are intact as late as the final few milliseconds prior to Ca^{2+}-stimulated fusion, based on their continued sensitivity to SNARE-cleaving Botulinum neurotoxins (Bruns and Jahn 1995; Parsons *et al.* 1995). In regulated exocytosis, these assembly transition states are kinetically controlled by late regulatory proteins such as complexins (small proteins that bind to the surface of SNARE complexes and hinder fusion) and synaptotagmin, which is activated by Ca^{2+} to trigger fusion (Tucker *et al.* 2004; Giraudo *et al.* 2006; Dai *et al.* 2007). After *trans*-complexes are transformed into *cis*-complexes during fusion, the AAA+ ATPase N-ethylmaleimide sensitive factor (NSF) together with α-SNAP (soluble NSF attachment protein) cofactors disassemble the complex (Whiteheart *et al.* 1994; DeBello *et al.* 1995). A high constitutive activity of NSF constantly regenerates free (uncomplexed) SNAREs.

The actual configuration of the SNARE machinery required for rapid, sub-millisecond fusion (Sabatini and Regehr 1996), remains controversial. Primarily, the number of copies of SNARE complexes required for fusion is not precisely known. Hua and Scheller (Hua and Scheller 2001) calculated that three SNARE complexes are required to fuse large dense-core vesicles in cracked PC12 cells, while Han and Jackson (Han *et al.* 2004) calculated that between 5 and 8 transmembrane segments of syntaxin lining the fusion pore are required, and Keller and Neale (Keller and Neale 2001; Keller *et al.* 2004) estimated ~10-15 complexes in studies using Botulinum neurotoxins to cleave the SNAREs. On a larger scale, it is also known that SNARE complexes cluster in cholesterol-dependent nanodomains, which are not evenly distributed in the membrane (Chamberlain *et al.* 2001; Lang *et al.* 2001; Predescu *et al.* 2005). However, it is not clear that this clustering is a trademark of SNAREs in general; clustering may be a particular

feature of steroid-rich membranes. Since secretory vesicles dock at SNARE clusters, the high local SNARE concentration may lead to more efficient fusion (Lang *et al.* 2001).

SNARE complex nucleation is a rate-limiting step in the SNARE cycle that is thought to be ordered. Most data suggests that formation of a Q-SNARE complex (*e.g.*, syntaxin4/SNAP23 or syntaxin1A/SNAP25) likely precedes entry of the final R-SNARE domain (Fasshauer *et al.* 1997; Nicholson *et al.* 1998; Fiebig *et al.* 1999; Fasshauer and Margittai 2004). *In vivo*, both SNARE binding studies (Lang *et al.* 2002) and live cell imaging (An and Almers 2004) indirectly support the presence of Q-SNARE complexes. In contrast, kinetic analyses of exocytosis in the presence of various SNARE motif combinations suggest that prior to fusion, VAMP2 and SNAP25 become associated before syntaxin1A binds (Chen *et al.* 2001). A critical advancement to understanding SNARE complex formation will be direct evidence of ordered assembly.

SNARE complex nucleation is furthermore potentially the most highly regulated step in the SNARE complex assembly cycle, owing to SNARE-binding regulatory proteins that either inhibit or activate this process. One group of enzymatic regulators is the protein kinases. For example, potentiation of complex formation and exocytosis occurs in neuroendocrine cells via phosphorylation of SNAP25 by PKC (Nagy *et al.* 2002; Shu *et al.* 2008), PKA (Hepp *et al.* 2002), and calcium/calmodulin-dependent protein kinase II (CaMKII) (Risinger and Bennett 1999). Syntaxin, meanwhile, is phosphorylated by casein kinase 2 (Hepp *et al.* 2002). Apart from tonic regulators are molecules required for the SNARE assembly process. Isoforms of the Munc13 family, for example, are essential priming factors that function by stabilizing the open conformation of syntaxin, and thus permitting SNARE complex nucleation (Augustin *et al.* 1999; Richmond *et al.* 1999; Brose *et al.* 2000; Richmond *et al.* 2001). Consequently, both the size and release probability of readily-releasable vesicles are increased in neurons and β-cells overexpressing Munc13 (Rhee *et al.* 2002; Kwan *et al.* 2006). Apart from Munc13, the Sec1/Munc18 (SM) proteins are the only other family of SNARE binding partners found to be

essential for secretion. The molecular basis of when and how SM proteins are believed to regulate SNARE assembly is discussed in detail in the next section.

Vesicle Docking and Priming Machinery: Role of Munc18

The Sec1/Munc18 (SM) protein family

The first family member of the Sec1/Munc18 (SM) proteins, unc18, was isolated in a genetic screen of uncoordinated (*unc*) mutants in *C. elegans* (Brenner 1974). Independently, the *S. Ceriviseae* homolog Sec1 was isolated through studies of a secretion-defective mutant strain (Novick and Schekman 1979). The discovery of mammalian unc18 (Munc18) homologues followed, and seven vertebrate SM gene family members (Munc18a/b/c, Sly1, Vps45, Vps33a/b) have now been described. The family is conserved throughout their ~600 aa, which fold three-dimensionally into an arch-shaped molecule (Misura *et al.* 2000; Bracher and Weissenhorn 2001) (Figure 1.3).

As discussed in the previous section, the formation of SNARE core complexes is sufficient for membrane fusion (Weber *et al.* 1998; Parlati *et al.* 1999). However, SM proteins are the only family apart from the Munc13 family identified as essential to exocytosis. In fact, deletion of Munc18a in the nervous system results in the complete loss of spontaneous and evoked secretion (Verhage *et al.* 2000). This effect on exocytosis is greater than deletion of either SNARE protein SNAP25 or syntaxin1A (Schoch *et al.* 2001; Washbourne *et al.* 2002), perhaps as a result of partial redundant actions among compartmentalized SNAREs. Mechanistically, SM proteins affect membrane trafficking in distinct subcellular pathways, predominantly through their association with specific syntaxin Q-SNAREs (Toonen and Verhage 2003).

SM proteins and exocytosis

Historically, the first clues to understanding SM function in exocytosis stemmed from discovery of Munc18a as a syntaxin1A binding partner involved in regulated neuroexocytosis (Hata *et al.* 1993; Garcia *et al.* 1994; Pevsner *et al.* 1994). As stated above, syntaxin1A fluctuates between closed and open conformations, and the closed conformation of syntaxin1A is stabilized by interaction with Munc18a (Dulubova *et al.* 1999; Misura *et al.* 2002). Subsequently it was hypothesized that Munc18a directs syntaxin conformation, and more broadly, temporal control over secretion.

Considering that SNARE complex formation is critical for membrane fusion, and exocytotic vertebrate SM proteins impair closed syntaxin interaction with other cognate SNAREs (Calakos *et al.* 1994; Liu *et al.* 2004; Medine *et al.* 2007), one might anticipate an overall negative role of SM proteins. Although this hypothesis has been at the forefront for over a decade, it is difficult to reconcile with most structural, genetic data, and overexpression studies. Primarily, there is a lack of general correlation between SM function and a particular conformation of syntaxin. The situation is further complicated because not all syntaxins assume folded conformations. For instance, the SM proteins Sly1 and Vps45, which regulate trafficking of intracellular transport vesicles, bind to a conserved N-terminal domain found upstream of the Habc domain in their cognate syntaxins (Sly1 to syntaxins 5 and 18, and Vps45 to syntaxin16) (Dulubova *et al.* 2002; Yamaguchi *et al.* 2002; Bryant and James 2003). This subset of SM proteins does not hinder the kinetics of SNARE pairings (Peng and Gallwitz 2002). In fact, yeast Q-SNARE Tlg2p/syntaxin cannot form SNARE complexes in the cells lacking Vps45p (Bryant and James 2001). Likewise, Vps33p is thought to prepare SNAREs for vacuole fusion (Collins *et al.* 2005). Comparatively, the yeast Munc18 homologue Sec1p stimulates fusion through its interaction with the ternary SNARE complex, only binding weakly to monomeric Sso1p/syntaxin (Carr *et al.* 1999; Scott *et al.* 2004). In mice and *C. elegans*, deletion of Munc18a leads to a complete block of neurotransmitter release, largely due to an absence of docked vesicles (Verhage *et al.* 2000; Weimer *et al.* 2003). Furthermore, in most systems including chromaffin

cells (Voets *et al.* 2001; Graham *et al.* 2004) and PC-12 cells (Graham *et al.* 1997; Fisher *et al.* 2001), overexpression of Munc18a has no deleterious effect on exocytosis, excepting a single report on the SM homolog Rop in Drosophila (Schulze *et al.* 1994). Thus, the majority of studies indicate an activating or essential role for SM proteins. One notable and surprising counterexample is Munc18c, whose functions have been touted as largely inhibitory.

Munc18c and GLUT4 vesicle cycling

As discussed above, upon activation of the insulin signaling cascade (Figure 1.1), GLUT4 storage vesicles (GSV) move to and fuse with the plasma membrane. In the final stages of this process, Munc18c-syntaxin4 interactions are believed to exert a critically important role in the temporal control of insulin-stimulated GSV exocytosis in muscle and adipose tissue (Tellam *et al.* 1997; Tamori *et al.* 1998; Thurmond *et al.* 1998; Dugani and Klip 2005). Of significant importance is that insulin signaling to Munc18c is disrupted in the diabetic state (James 2005; Kanda *et al.* 2005; Karlsson *et al.* 2006).

Based on overexpression studies, Munc18c was initially proposed to function as a negative regulator of GLUT4 vesicle translocation in 3T3L1 adipocytes (Tellam *et al.* 1997; Thurmond *et al.* 1998). Notably, the failure of the phosphatidylinositol-3-phosphate kinase (PI3K) inhibitor wortmannin to suppress GLUT4 externalization in adipocytes derived from Munc18c-null mice suggests that Munc18c specifically inhibits a priming and/or fusion step under the control of the PI3K pathway (Kanda *et al.* 2005). Although the exact mechanism for this inhibition is not fully understood, Munc18c has been proposed to preclude the binding of syntaxin4 to its cognate SNAREs, vesicle-associated membrane protein 2 (VAMP2) and synaptosomal-associated protein of 23-kDa (SNAP23), preventing GLUT4 externalization in the absence of insulin (Araki *et al.* 1997; Tellam *et al.* 1997; Thurmond *et al.* 1998). This interpretation would be consistent with the ability of its homologue Munc18a to inhibit the *in vitro* binding of syntaxin1A to VAMP2 and SNAP25, consistent with the closed conformation of syntaxin1A seen in the crystal structure with Munc18a (Figure 1.3) (Misura *et al.* 2000).

Therefore, by analogy, the most prevalent model for Munc18c regulation of SNARE complex formation equates the association of Munc18c and closed syntaxin4 to the inhibition of GLUT4 transport vesicle externalization. However, given the absence of fine structural information, a model of Munc18c control over syntaxin4/SNARE complex formation is not easily predicted by other SM-syntaxin interactions due to the diversity in their modes of action.

Recent evidence suggests that SM-syntaxin interactions regulating exocytosis at the plasma membrane may possess multiple binding and functional states. Widberg and colleagues (Widberg *et al.* 2003) showed that Munc18c associates with the ternary SNARE complex *in vitro*. This finding seemed incongruous with other SM-syntaxin protein interactions until it was shown that Munc18c possesses an interaction site for the N-terminal amino acids of syntaxin4 resembling the syntaxin binding sites on Sly1 and Vps45 (Figure 1.3) (Latham *et al.* 2006; Hu *et al.* 2007), which bind to open conformations of their cognate syntaxins (5 and 18) (Dulubova *et al.* 2002; Yamaguchi *et al.* 2002; Bryant and James 2003). Subsequently, although Munc18a binding to the closed form of syntaxin1a has been extensively established, Munc18a has been very recently shown to also bind to SNARE complexes and facilitate SNARE-mediated fusion *in vitro* (Dulubova *et al.* 2007; Khvotchev *et al.* 2007; Shen *et al.* 2007). The basis of Munc18a/SNARE complex binding involves Munc18a utilizing both the N-terminus of syntaxin1A as well as interactions with the SNARE bundle (Dulubova *et al.* 2007; Khvotchev *et al.* 2007).

In spite of similar binding modes of Munc18a and Munc18c to syntaxins 1 and 4, genetic studies suggest that the mechanism of Munc18c action may be different than Munc18a. For example, the insulin-induced fusion of GLUT4 vesicles was enhanced in adipocytes prepared from Munc18c-null mice (Kanda *et al.* 2005), while Munc18a deficiency was demonstrated to eliminate both evoked and spontaneous synaptic exocytosis (Verhage *et al.* 2000). Additionally, insulin (Thurmond *et al.* 1998) as well as N-ethylmaleimide (NEM) (Widberg *et al.* 2003), which inhibits NSF-mediated SNARE core complex disassembly, have been reported to dissociate

Munc18c from syntaxin4. Thus, the Munc18c-syntaxin4 interaction may be unique in negatively regulation of vesicle docking, priming, or fusion.

Munc18c and vesicle docking

Of the several potential roles for Munc18c in GLUT4 vesicle cycling, the most convincing studies suggest that it may function as a link between the vesicle docking and fusion machinery through Rab proteins. Indeed, genetic interactions between SM proteins and Rab proteins have been described in yeast (Toonen and Verhage 2003), suggesting that Rabs and SM proteins work in tandem. For example, the yeast SM protein Sly1 is named as suppressor of loss of ypt1, the Rab homologue that functions in ER-to-Golgi vesicle trafficking (Peng and Gallwitz 2002). In fact, the blockage of vesicle fusion upon deletion of SM proteins is principally due to docking defects (Voets *et al.* 2001; Weimer *et al.* 2003; Korteweg *et al.* 2005). Furthermore, in the exocytosis of synaptic vesicles in neurons, the enhanced docking seen by Rab3a overexpression does not occur in the absence of Munc18a (van Weering *et al.* 2007). Thus, a relationship between SM proteins, Rab proteins, and vesicle docking is well supported in several cell types. A critical question remaining is whether Munc18c likewise functions downstream of Rab proteins in GLUT4 vesicle docking processes.

The identity of critical Rab protein(s) involved in GLUT4 trafficking is/are still being elucidated. Rab10 appears critical to the process, as overexpression of a Rab10 mutant defective in GTP hydrolysis increases basal surface GLUT4 while Rab10 knockdown inhibits the rate of exocytosis (Sano *et al.* 2007). In the absence of insulin stimulation, Rab10 activation is inhibited by constitutive activity of the Rab GTPase activating protein (GAP) AS160. Upon activation of the insulin signaling cascade, AS160 is inactivated via direct phosphorylation by PI3K/Ak2. Indeed, expression of dominant negative AS160 mutant that lacks Akt2 phosphorylation sites inhibits GLUT4 translocation (Sano *et al.* 2003; Karylowski *et al.* 2004), while RNAi of AS160 increases basal levels of GLUT4 on the adipocyte surface (Eguez *et al.* 2005; Larance *et al.* 2005). Of interest, the phosphorylation of AS160 is impaired in the skeletal muscle of patients

with type 2 diabetes (Karlsson *et al.* 2006). Since the functional activity of both Munc18c and AS160 are sensitive to the PI3K inhibitor wortmannin (Kanda *et al.* 2005), it is furthermore likely that they function in the same pathway. The model that emerges is that Munc18c might link to Rab10 upon activation of the PI3K/Akt2 pathway, ultimately resulting in a conformational change in the Munc18c-syntaxin4 interaction which results in GLUT4 vesicle docking, priming, and fusion.

Summary

The experiments in Chapter II of this dissertation test the hypothesis that Munc18c exerts spatial and temporal control over GLUT4 vesicle docking and fusion. Experiments are presented that examine the relevant molecular mechanisms. This hypothesis arises, in part, from evidence that the N-terminal domain of syntaxin retards binding of syntaxin to other SNAREs, which is the rate-limiting step in SNARE complex formation. Munc18, as a governor of syntaxin conformation, is therefore likely to have effects on the ability of vesicles to undergo priming and tightly dock with SNARE complexes. Underlying this feature of SM proteins is their ability to confer specificity on membrane trafficking pathways by serving as high affinity syntaxin chaperones at the sites of fusion.

As discussed above, increasing evidence is available that SM proteins are directly regulated by Rab GTPases. The next section addresses how the kinetics of fast Ca^{2+}-dependent secretion in pancreatic β-cells may be facilitated by the actions of Rab27a GTPase under conditions of stimulation and vesicle replenishment.

Vesicle Docking and Priming Machinery: Role of Rab27a

The small GTPase Rab27

The process of vesicle targeting includes all the steps necessary to deliver a newly formed transport vesicle to its target membrane. Central to this process from start to finish are the Rab

family of small GTPases, which facilitate vesicle budding, transport, tethering, and docking through a plethora of effector molecules. Evolutionarily, Rab proteins belong to the Ras-related superfamily of small monomeric GTPases. More than 60 mammalian and 11 yeast Rab proteins have been identified, and are involved in intracellular fusion reactions of vesicles or organelles with their target membranes (Takai *et al.* 2001; Zerial and McBride 2001; Gurkan *et al.* 2005).

Two Rab27 isoforms, Rab27a and Rab27b, have been described, which share ~70% homology (Fukuda 2005). While both of these molecules are located on secretory granules (Tolmachova *et al.* 2007), our interest was in the cellular function of insulin-secreting pancreatic β-cells, which contain Rab27a but lack Rab27b (Yi *et al.* 2002; Tolmachova *et al.* 2004; Tsuboi and Fukuda 2006). Additionally, Rab27a is singularly involved in exocytosis cytotoxic T cells (Stinchcombe *et al.* 2001), histamine granule secretion in mast cells, as well as dense core ADP- and serotonin-granule secretion in platelets (Kondo *et al.* 2006). Rab27a expression is also evident in the pigment epithelium and choriocapillaris of the retina (Futter *et al.* 2004). Recently it has been shown that Rab27 is also involved in synaptic transmission in *C. elegans* (Mahoney *et al.* 2006). Vesicular trafficking in each of these cell types is affected by Rab27a deficiency.

Clinical manifestations of Rab27a deficiency

Our understanding of the function of Rab27a in the exocytosis pathway has been greatly accelerated by studies of human disease. Mutations in the human Rab27A gene result in Griscelli syndrome (hemophagocytic syndrome), an often fatal disease which is characterized by pigment dilution of the hair (albinism) and uncontrolled T-lymphocyte and macrophage activation, resulting in immunodeficiency. These symptoms are likely due to the dysregulation of membrane transport of melanosomes in melanocytes and lytic granules in cytotoxic T lymphocytes, respectively (Mancini *et al.* 1998; Stinchcombe *et al.* 2001; Aslan *et al.* 2006). Less common are the phenotypically-related Rab27 disorders choroideremia and Hermansky-Pudlack syndrome, which result from Rab27-prenylation defects due to Rab escort protein and Rab geranylgeranyltransferase defects, respectively (Seabra *et al.* 2002).

Insights into the human conditions were largely facilitated by positional cloning studies identifying Rab27a-deficiency as the cause of vesicle secretion defects in the *ashen* mouse, a model of both Griscelli and Hermansky-Pudlack syndromes (Wilson *et al.* 2000). The murine Rab27a gene, first isolated from a melanocyte library, has five exons, similar to human RAB27A. In *ashen* mice (Wilson *et al.* 2000; Kasai *et al.* 2005), a single A-to-T transversion in the splice donor site downstream of exon 4 results in a larger than normal transcript due to the insertion of 235 or 252 base pairs of intron into the Rab27a message. An in-frame stop codon in the intron sequence leads to the production of a non-functional protein lacking two critical domains of the GTP-binding pocket. Genetic experiments using overexpressed GFP-Rab27a to rescue Rab27a deficiency subsequently revealed that Rab27a is expressed in a broad range of secretory cells, including ovarian cells, hematapoietic cells, and pancreatic β-cells, most of which undergo regulated exocytosis (Tolmachova *et al.* 2004). Interestingly, Rab27a is functionally redundant with Rab27b (Barral *et al.* 2002), which can compensate for Rab27a-deficiency in cells where both are present (*e.g.*, platelets) but not in tissues where only one isoform is present, resulting in the *ashen* phenotype (Barral *et al.* 2002; Tolmachova *et al.* 2007).

Rab27a deficiency results in defective granule exocytosis

Studies of *ashen* mice suggest that Rab27 has multiple functions in vesicle exocytosis. Particularly well characterized are the functions of Rab27a to transport and dock granules and vesicles to the PM. For example, melanosomes were found clumped in peri-nuclear regions in *ashen* melanocytes, while re-expression of Rab27a restores melanosome trafficking to the dendrite tips (Wilson *et al.* 2000; Bahadoran *et al.* 2001; Hume *et al.* 2001). The role of Rab27a was further clarified when melanosome movement by Myosin Va was shown to require Rab27a (Hume *et al.* 2001; Wu *et al.* 2002), through the Rab effector melanophilin (Nagashima *et al.* 2002; Provance *et al.* 2002). Likewise, *ashen* lytic granules do not reach the PM, dramatically reducing the cytotoxicity of T-lymphocytes (Stinchcombe *et al.* 2001).

Of significant interest to this work, a marked deficit in the replenishment of docked insulin granules at the plasma membrane during glucose stimulation was reported in pancreatic β-cells of *ashen* mice (Kasai *et al.* 2005). Consistently, *ashen* mice are glucose intolerant owing to defective glucose-stimulated insulin secretion (GSIS) (Kasai *et al.* 2005). However, this docking defect alone cannot account for the reduced secretion, as EM shows that the number of granules docked/adjacent to the plasma membrane is similar in wildtype and *ashen* β-cells prior to stimulation (Kasai *et al.* 2005). Kasai and colleagues (Kasai *et al.* 2005) furthermore demonstrated by TIRFM a reduced release of vesicles pre-docked on the plasma membrane. These results collectively suggest that in addition to defects in vesicle transport/docking, defective insulin granule *priming* may underlie the secretory defect in *ashen* β-cells. This hypothesis can be rationalized after consideration of the numerous studies linking (1) Rab activation and (2) Rab27a-binding proteins to the vesicle priming reactions that govern SNARE complex formation in pancreatic β-cells.

The Rab27 activation cycle in β-cells

In response to continued activation, Rab proteins are thought to cycle repeatedly through active and inactive states. Like other GTPases, the activity of Rab27a is regulated by its GDP/GTP binding state, with Rab27a in its GTP state strongly facilitating and Rab27a-GDP potently inhibiting insulin secretion (Yi *et al.* 2002; Fukuda 2003). In general, Rab proteins are inactive in the GDP bound state and active in the GTP bound state. To maintain their inactive conformation, interaction of GDP-Rab with a Rab-specific GDP dissociation factor (Rab-GDI) maintains the complex in the cytosol by forming a 1:1 complex (Ullrich *et al.* 1993; Wu *et al.* 1996; Takai *et al.* 2001; Alory and Balch 2003). The Rab-GDI interaction masks the prenylation sites required for membrane anchoring and prevents unwanted association with lipids in non-target membranes (Peter *et al.* 1992; Maltese *et al.* 1996). In some signaling pathways, the activation of Rabs is facilitated by GDI displacement factors (GDFs), which catalyze the

dissociation of Rab proteins from GDI (Novick and Zerial 1997; Pfeffer 2001; Zerial and McBride 2001; Seabra *et al.* 2002). This allows Rab escort protein (REP) to recruit GDP-Rab to Rab geranylgeranyltransferase (RabGGTase) resulting in the anchoring of one or two geranyl groups to C-terminal cysteines (Andres *et al.* 1993). REP is additionally necessary to maintain the solubility of prenlyated Rab in aqueous solution (Wu *et al.* 2007). Guanine exchange factors (GEFs) subsequently assist the replacement of GDP by GTP, while GTPase activating proteins (GAPs) complete the activity cycle, deactivating Rab27.

In pancreatic β-cells, several properties governing its activity/cycling set Rab27a, and the four isoforms of Rab3 (a/b/c/d), apart from other Rab GTPases. First, Rab3/27 isoforms function specifically in the secretory process and are localized to insulin granules (Tsuboi and Fukuda 2006). Second, is that GTP-Rab27a tends to remain active (~80%) due to a low intrinsic GTPase activity, until further catalyzed by GAPs (Becker *et al.* 1991; Kondo *et al.* 2006). Rab3d, for example, is also ~80% in the GTP-bound form (Chen *et al.* 2003), while other Rab family members (*e.g.*, Rab5) are mostly maintained in an inactive GDP-bound state (Barbieri *et al.* 2000). In fact, the larger Ras and Rho/Rac/CDC42 GTPase families are largely maintained in the inactive GDP-bound state (Takai *et al.* 2001). Third, Rab3 and Rab27 were recently shown to be connected by a common GEF (termed Rab3GEP) (Figueiredo *et al.* 1997), which is active on at least the a/c/d isoforms of Rab3 (Fukui *et al.* 1997). Likewise, the *C. elegans* homologue of Rab3GEP is AEX-3 is also active on both Rab3 and Rab27 (Iwasaki *et al.* 1997; Mahoney *et al.* 2006). Other Rab GEFs are more specific. For example, Rabex-5 is specific for the Rab5 subfamily (Horiuchi *et al.* 1997), and yeast Sec2p (the GEF) is specific for Sec4p GTPase (Walch-Solimena *et al.* 1997). Predictions based on the human genome project indicate ~50 putative Rab-GAPs (a.k.a. TBC proteins) are present, though only 6 have been characterized as accelerating the cycling of specific Rabs (Bernards 2003). Among those characterized are a Rab3-specific GAP, termed Rab3 GAP (Fukui *et al.* 1997), and two putative Rab27a-specific GAPs (EPI64 and FLJ13130/Rab27a-GAPβ), which were isolated from melanosomes by

screening for molecules pulled down by the Rab27a effector Slac2a (Itoh and Fukuda 2006; Itoh *et al.* 2006). Comparatively less is known about GDIs for Rab3/27. In summary, these parameters favor the predominant association of Rab27a and Rab3 with granules and with their effector molecules. And for Rab27a, cycling is believed to be initiated upon stimulation (Kondo *et al.* 2006), though the rate of cycling *in vivo* remains to be discovered.

The structural basis underlying nucleotide cycling has not yet become available for either Rab27 isoform, although x-ray diffraction information is available for other related Rab GTPases: Rab3a (Dumas *et al.* 1999; Ostermeier and Brunger 1999), *P. falciparum* Rab6 (Chattopadhyay *et al.* 2000; Chattopadhyay *et al.* 2000), yeast Ypt51p (Esters *et al.* 2000), and Sec4p (Sato *et al.* 2007). Shared with the Ras family is a structural fold consisting of a six strand β-sheet, comprising five parallel strands and one antiparallel strand, surrounded by five α-helices. The structural elements responsible for Mg^{2+} and guanine nucleotide binding, and well as GTP hydrolysis, are located in five loops that connect the alpha helices and β-sheets. The major nucleotide induced differences occur in two regions, denoted switch I and II, which are responsible for interaction with regulatory proteins such as GAPs and GEFs (Stenmark and Olkkonen 2001), and create a platform for effector proteins to bind specifically to GTP-Rab (Pfeffer 2005). In turn, Rab effectors function to assist in vesicle transport, docking, and priming.

Rab27 effectors in vesicle priming

In general, Rab27 effectors contain a common ~100 aa GTP-Rab27 binding domain, the synaptotagmin-like protein (Slp) homology domain (SHD). The SHD domain is comprised of two helical domains termed SHD1 and SHD2, which are separated by two zinc-finger motifs (except in Slp1 and Slp2a, in which the SHD domains are directly linked) (Fukuda 2005). These effectors are classified into three main groups: Slp 1-5 and rabphilin contain two tandem calcium-binding C2 domains, which are absent in Slp-lacking C2 domains (Slac2)-a-c as well as

Noc2 (No C2), and the priming factor Munc13. Through a subset of its effectors, most prominently Slp4a, Rab27a is linked to the SNARE fusion machinery.

A critical role for Slp4a (a.k.a. granuphilin) in the docking of large dense core vesicles has been identified in multiple neuroendocrine cell types. For example, β-cells isolated from $Slp4a^{-/Y}$ mice (Gomi *et al.* 2005), as well as PC12 cells expressing $Slp4a^{RNAi}$ (Tsuboi and Fukuda 2006), display a morphological docking defect (as shown by TIRFM and EM), and paradoxically, increased secretion. Comparatively, Slp4a overexpression significantly increases the number of vesicles docked prior to stimulation, yet dramatically decreases the number of exocytotic events in PC12 cells as measured by TIRF microscopy (Tsuboi and Fukuda 2006). Likewise, in Min6 β-cells overexpressing Slp4a, insulin secretion stimulated by high K^+ is reduced by about 50% (Torii *et al.* 2002). Importantly, the inhibitory effects of Slp4a overexpression on secretion in either PC12 cells or Min6 β-cells appear to require Slp4a interaction with both Rab27a and the SM-syntaxin complex. For example, these effects are eliminated by the point mutants $Slp4a^{W118S}$ (which eliminates binding to Rab27a) as well as $Slp4a^{L43A}$ (which maintains binding to Rab27a but eliminates binding of syntaxin1A) (Torii *et al.* 2002; Gomi *et al.* 2005). Thus, interactions between Rab27a/Slp4a on the granule and Munc18/syntaxin on the plasma membrane act in concert to facilitate β-granule docking and secretion.

Rab27a in β-cell stimulus-secretion coupling

As first described in 1968 by Grodsky and colleagues (Curry *et al.* 1968), insulin secretion in response to physiologic stimuli such as glucose is typically biphasic and pulsatile, consisting of a transient (10 min) first stage followed by a sustained second phase. The cellular underpinnings of this process have not been fully elucidated. Depicted in Figure 1.4, the best characterized metabolic coupling event is the increase in ATP/ADP ratio induced by glucose metabolism, which promotes closure of the K_{ATP}-sensitive K+ channel (K_{ATP}). This leads to membrane depolarization and opening of voltage-dependent Ca^{2+} channels (VDCC), with the

subsequent rise in $[Ca^{2+}]_i$ being the critical second messenger that stimulates insulin secretion (Wollheim and Sharp 1981; Ashcroft *et al.* 1984; Hoenig and Sharp 1986). Importantly, the initial phase (K_{ATP}-dependent pathway) does not appear to require access to metabolic energy sources and can be elicited in the absence of any nutrient by depolarization with high extracellular K^+. Second phase release, however, is only apparent in the presence of energy-providing secretagogues. It is induced by glucose via a mechanism distinct from closure of K_{ATP} channels and alterations in $[Ca^{2+}]_i$ via VDCCs (Henquin *et al.* 1994). This so-called K_{ATP}-independent pathway was identified by treating β-cells with diazoxide to hold K_{ATP} channels open and high extracellular K^+ to depolarize the membrane sufficiently to restore Ca^{2+} influx (Gembal *et al.* 1992; Sato *et al.* 1992). Using this protocol, glucose does not increase $[Ca^{2+}]_i$ to high levels yet insulin release is promoted (Gembal *et al.* 1993j; Straub *et al.* 1998). The signaling molecules proposed to mediate second phase secretion include malonyl CoA (and other long chain acyl CoA) (Prentki 1996; Prentki and Corkey 1996), protein kinases (PKA, PKC, AMPK) (Nesher *et al.* 2002), and ATP/ADP (Henquin 2000). Ultimately, the K_{ATP}-dependent and K_{ATP}-independent pathways converge to regulate the size of the readily-releasable pool (RRP) of docked and primed vesicles, thereby controlling the magnitude of insulin secretion. Importantly, Rab27a has been shown to strongly enhance both the K_{ATP}-dependent and K_{ATP}-independent pathways of secretion (Fukuda 2005; Kasai *et al.* 2005).

Since the Rab family of GTPases has a role in essentially all intracellular membrane trafficking, a general hypothesis of this dissertation is that Rab27a is a central effector upon which β-cell signaling pathways converge to regulate granule recruitment, priming, and exocytosis. Consistent with this idea are the basic deficiencies of glucose intolerance and reduced biphasic secretion seen in Rab27a-null *ashen* mice (Wilson *et al.* 2000; Kasai *et al.* 2005). Notably, the actions of Rab27a that underlie these deficiencies remain unclear. Two potential sites of Rab27a action have been proposed. First are the well-studied effects of Rab27a to

promote β-granule transport and tethering/docking to the PM. Following vesicle tethering/docking are absolutely essential *priming* events that result in formation of SNARE complexes, although the effects of Rab27a on these latter processes have not been elucidated. Thus, a major goal of this dissertation was to elucidate the kinetic parameters of priming and exocytosis that are specifically altered by Rab27a deficiency. Inherent in this objective is uncovering the nature of the undefined relationship between Rab27a activity and its ability to augment the size of specific vesicle pools of primed and release-competent granules: the immediately-releasable and readily-releasable pools. The following sections of this chapter detail the mechanisms in the β-cell that control vesicle pool size, as well as the cellular mechanisms that provide for vesicle replenishment under constant stimulation, as both are thought to be under Rab27a control.

β-granule pool dynamics

The pancreatic β-cell contains 10,000-13,000 insulin secretory granules (Dean 1973; Olofsson *et al.* 2002), each of which contains between 150,000-280,000 molecules (1.4-2.5 fg) of insulin (Howell 1974). The maturation of these vesicles occurs beginning with biogenesis and vesicle filling, followed by transport and physical attachment to the plasma membrane (tethering and docking). A rapid secretory response to physiologic stimuli requires that a subset of vesicles is readily available for release (Figure 1.5). Under continued glucose stimulation and depletion of this 'readily-releasable' pool (RRP), continuing exocytosis is supported by the recruitment of granules to the PM, and by priming of those vesicles already at the PM. It has been hypothesized that priming is responsible for second phase secretion, as both are known to have dependence on time, temperature, energy (glucose and ATP), and Ca^{2+} (Straub and Sharp 2002).

The 'readily-releasable' pool (RRP)

Release from the RRP occurs rapidly upon elevation of $[Ca^{2+}]_i$, and is readily apparent as an exocytotic burst stage in experiments that monitor release during prolonged stimulation

(Elmqvist and Quastel 1965). When the number of vesicles present in the RRP, measured electrophysiologically, is compared with the number of docked vesicle using electron microscopy (EM), it is apparent that not all docked vesicles are release competent (Parsons *et al.* 1995; Steyer *et al.* 1997). By EM, the density of granules in β-cells is highest near the plasma membrane, with an estimated 650 (7%) of granules morphologically docked and another 2000 within a granule diameter (300 nm) away from the plasma membrane. The ~650 vesicles in direct contact with the plasma membrane could account for several hours of glucose-induced insulin secretion (Olofsson *et al.* 2002). Yet, by capacitance measurements the RRP has been estimated as 40-50 granules (Eliasson *et al.* 1997). Therefore, the number of granules in the RRP is only 6-8% of the total number of docked granules. This finding has led to the hypothesis that vesicle translocation is not required for conversion of the reserve pool into a readily releasable state (Parsons *et al.* 1995). Instead, the additional maturation steps can be explained by the time- and energy-dependent chemical reactions of priming, during which SNARE complexes are formed and vesicles are prepared for fusion within milliseconds of a sufficient Ca^{2+} signal. Thus, vesicles can exists in (1) undocked, (2) docked but unprimed, or (3) readily-releasable (docked and primed) states.

The 'immediately-releasable' pool (IRP)

When membrane depolarization in applied, the fastest kinetic component of vesicle release comes from the immediately-releasable pool (IRP). Several observations across multiple neuroendocrine cell types have led to the hypothesis that the IRP is a subset of the RRP that is located near Ca^{2+} channels. Principally, in pancreatic β-cells, ~10% of readily releasable granules are found colocalized with ~500 $\alpha 1_C$ L-type Ca^{2+} channels (Gromada *et al.* 1997; Barg *et al.* 2001; Barg *et al.* 2002). Owing to this proximity to the Ca^{2+} stimulus the IRP is less sensitive to introduction of exogenous Ca^{2+} buffers than the slower phase representing RRP release, as demonstrated in adrenal chromaffin cells (Horrigan and Bookman 1994; Moser and Neher 1997) and neurons (Mennerick and Matthews 1996), in addition to pancreatic β-cells (Barg *et al.* 2001).

Furthermore, as no distinct kinetic component corresponding to the IRP has been identified in UV flash photolysis experiments where calcium is uncaged to >20 μM, it is likely that the fast IRP release kinetics in response to voltage depolarization is not due to intrinsically higher calcium sensitivity (Voets *et al.* 1999; Yang and Gillis 2004).

The highly Ca^{2+}-sensitive pool (HCSP)

Flash uncaging experiments using NP-EGTA/Ca^{2+} have revealed a population of vesicles with faster release kinetics than the RRP, termed the highly calcium-sensitive pool (HCSP). Because uncaging experiments elevate $[Ca^{2+}]_i$ almost uniformly throughout the cytosol, vesicle proximity to Ca^{2+} channels is irrelevant, and the direct relationship between $[Ca^{2+}]_i$ and exocytosis can be measured. After its discovery in adrenal chromaffin cells (Yang and Gillis 2004), the HCSP has been described in rat pancreatic β-cells (Wan *et al.* 2004) as well as the INS-1 insulin-secreting cell line (Yang and Gillis 2004). In each cell type, the HCSP is released by low $[Ca^{2+}]_i$ (<4 μM) in response to flash uncaging, as compared to the ~17 μM $[Ca^{2+}]_i$ required to elicit half-maximal response from the RRP (Barg *et al.* 2001).

By all indications, the HCSP is a separate pool from the IRP, although both function in first phase insulin release. The most definitive measure of their independence is that UV flash uncaging to low $[Ca^{2+}]_i$ preceding membrane depolarization does not significantly decrease the size of the IRP (Yang *et al.* 2002), nor does brief membrane depolarization reduce the size of the HCSP (Wan *et al.* 2004). This furthermore indicates that IRP vesicles located close to Ca^{2+} channels are not as highly Ca^{2+}-sensitive as the HCSP. Second, the HCSP is distinguished by responsiveness to activators of PKA and PKC, which likely affects its role in pool refilling. For example, in rat pancreatic β-cells the HCSP was measured as ~20 fF (6-12 vesicles), yet was increased by 4-fold in response to PKC activation by phorbol-12-myristate-13-acetate (PMA), whereas the RRP was only moderately increased (Wan *et al.* 2004). Forskolin, which increases cAMP production, increases the HCSP by an equivalent magnitude. The effects of PKC and

cAMP on HCSP size are not additive, suggesting that their actions converge on the same molecular targets. Glucose, however, has been shown to enhance the effects of PKA and PKC, affecting both the HCSP and the RRP (Yang and Gillis 2004).

As a major focus of this dissertation, the insulin secretion defect in *ashen* mice was exploited to identify how the Rab27a GTPase found on insulin granules facilitate vesicle priming and replenishment under stimulation. Despite considerable studies of Rab effectors discussed above, many of which could affect vesicle priming, no studies to date have reported on potential effects of Rab27a on priming. Our hypothesis is that in addition to its well-characterized role in vesicle trafficking, Rab27a serves as a critically important Rab protein in regulating the terminal events of priming and vesicle exocytosis.

Role of cAMP in insulin secretion

While intracellular calcium is the principal second messenger of glucose-stimulated insulin secretion, hormonal modulation of other second messengers modulate the magnitude of secretion. cAMP is the most powerful potentiator of insulin secretion (Holst and Gromada 2004), via its contribution to both the initial size and the refilling of multiple vesicle pools (Gromada *et al.* 1998; Yang *et al.* 2002; Wan *et al.* 2004; Yang and Gillis 2004; Kwan and Gaisano 2005). A rise in intracellular cAMP in pancreatic β-cells is mediated by incretins such as glucagon-like peptide-1 (GLP-1) and glucose-dependent insulinotropic peptide (GIP), which are secreted after meals from L and K cells, respectively (Meier *et al.* 2002; Drucker 2006) (Figure 1.6). Both protein kinase A (PKA)-dependent and PKA-independent pathways have been discovered. Epac2 (exchange protein directly activated by cAMP) (Ozaki *et al.* 2000) serves as a primary effector of the PKA-independent pathway. It exerts effects on exocytosis via regulation of ion channel activity (K_{ATP}) (Kang *et al.* 2001; Shibasaki *et al.* 2004) and Ca^{2+} release from intracellular stores (Kang *et al.* 2001). However, up to 80% of the effects of cAMP on exocytosis are through direct interaction with the secretory machinery (Ammala *et al.* 1993). This effect is believed to arise in part via the actions of cAMP-Epac2, which serves as a GEF for the small GTPase Rab3a (Holz *et*

al. 2006). The conversion of Rab3a to its GTP-bound state then initiates its binding to the priming factors Rim2 and Munc13-1 (Fujimoto *et al.* 2002; Kwan *et al.* 2007). This mechanism is influenced by PKA-dependent processes, owing to direct phosphorylation of Rim2 by PKA (Lonart *et al.* 2003). However, since cAMP-Epac2 may be promiscuous in binding to other small GTPases localized on insulin granules (Shibasaki *et al.* 2007), it remains unclear whether additional Rab-dependent priming pathways are also involved, including those of Rab27a.

The effects of cAMP to augment secretion are synergistic with those seen under conditions of elevated glucose (Wan *et al.* 2004; Yang and Gillis 2004), suggesting that glucose and cAMP act via separate pathways. This synergism is capable of more than doubling both the HCSP and RRP in rat β-cells and INS-1 cells (Wan *et al.* 2004; Yang and Gillis 2004). As discovered in *ashen* mice, Rab27a is required for both first- and second- phase GSIS (Kasai *et al.* 2005). An outstanding question is whether Rab27a also mediates increased β-granule pool size in response to elevated cAMP levels.

Summary

Secretory granules in pancreatic β-cells exhibit distinct states of competence to undergo secretion. The size of each pool (*i.e.*, RRP, IRP, HCSP) defines the magnitude and kinetics of the cell secretory response to glucose. A limiting feature of these pools is that they require refilling to sustain secretion in the continued presence of secretagogues. Replenishment of the pools is achieved principally through mobilization and priming of granules at the PM. Collectively, the actions of Rab27a and its effector molecules act to expand and/or increase the rate of β-granule replenishment of the docked and primed pool of vesicles. However, a critical unknown is which vesicle pools and molecular targets mediate the Rab27a-induced alterations in vesicle release kinetics. The experiments in Chapter III of this dissertation address these questions and collectively argue that Rab27a GTPase comprises a major regulatory step in membrane transport owing to precise control over its activation, the spatial control and identity they confer on a

particular vesicle or organelle, and their links to the SNARE vesicle fusion machinery through effector molecules.

Statement of Hypothesis and Specific Aims

In type 2 diabetes the exocytotic process is defective in adipocytes and pancreatic β-cells, two tissues critical to the maintenance of blood glucose. This dissertation examines the role of specific members of the Sec1/Munc18 and Rab27 protein families which carry out vesicle docking, priming, and fusion in each of these tissues. The current model of Munc18c function in adipocytes, which is controversial, proposes that Munc18c is inhibitory to SNARE complex formation and hence GLUT4 storage vesicle fusion until its dissociation from syntaxin4. Based on *in vitro* evidence we have alternatively hypothesized that Munc18c participates throughout the formation of SNARE complexes, and has additional facilitative actions on GLUT4 storage vesicle fusion. Thus, there exists a clear need for structural studies to determine the Munc18c-SNARE binding interactions *in vivo*, as well as precisely which steps in the vesicle docking, priming, and fusion processes Munc18c participates in. Upstream of Sec1/Munc18 proteins are the vesicle-associated Rab GTPases. One family member, Rab27a, has been identified as important for insulin secretion from pancreatic islets based on studies of Rab27a-null *ashen* mice. Still lacking are studies of single pancreatic β-cells that identify the specific molecular mechanisms under Rab27a control, and how via these mechanisms Rab27a affects the amplification of secretion by priming factors such as glucose and cAMP. In summary, the specific aims of this dissertation are directed at defining the mechanisms by which Munc18c and Rab27a exert spatial and temporal control over vesicle exocytosis, through their regulation of vesicle docking and priming at the sites of SNARE complex-dependent membrane fusion.

Specific Aim 1: ***Identify the molecular determinants through which Munc18c specifically binds to and serves as a chaperone for the t-SNARE syntaxin4 in adipocytes.***

Specific Aim 2: ***Determine whether Munc18c association and control over syntaxin4 conformation affects competency of GLUT4 storage vesicle docking and priming.***

Specific Aim 3: ***Determine the primary sites at which Rab27a acts to facilitate insulin secretion using patch-clamp measurements of membrane capacitance to resolve specific kinetic parameters of vesicle docking and priming. Sites within the secretory pathway that are affected will be identified by comparison of results obtained from β-cells isolated from ashen (Rab27a deficient) and background control mice.***

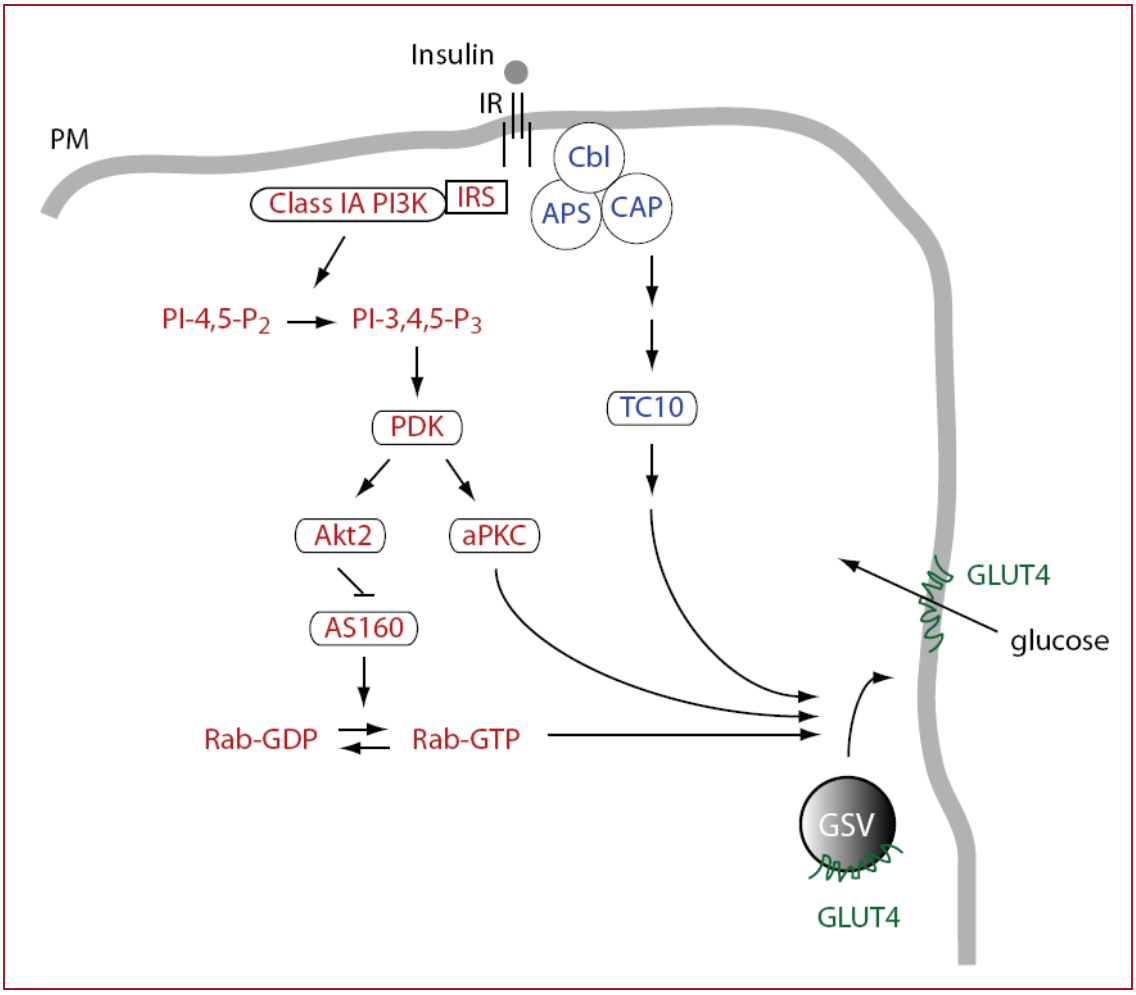

Figure 1.1. **Insulin signaling pathways regulating GLUT4 vesicle translocation.** The canonical insulin signaling cascade is triggered by activation of the insulin receptor (IR) tyrosine kinase activity leading to tyrosine phosphorylation of insulin receptor substrate (IRS) proteins and their recruitment of phosphatidylinositol 3-kinase (PI3K). At this critical node, the insulin signaling pathway diverges such that the delivery of GLUT4 to the cell surface occurs independently of PI3K (*blue*), utilizing a pathway proposed to involve APS (Hu *et al.* 2003), c-Cbl (Ribon *et al.* 1998), CAP, and the small GTPase TC10 (Chiang *et al.* 2001; Saltiel and Kahn 2001; Saltiel and Pessin 2003), although this hypothesis has been challenged by the lack of effect of RNAi experiments directed against these signaling intermediates (Mitra *et al.* 2004; Zhou *et al.* 2004). In a parallel pathway, PI3K directs vesicle docking and fusion (*red*). Conversion of PI-4,5-P2 to PI-3,4,5-P3 activates the intermediate kinases PDK1 (Hajduch *et al.* 2001) and Ak2/PKB (Cho *et al.* 2001; Whiteman *et al.* 2002), which in turn leads to the activation of Rab10 GTPase (Sano *et al.* 2007) and the SNARE-associated vesicle docking and fusion machinery.

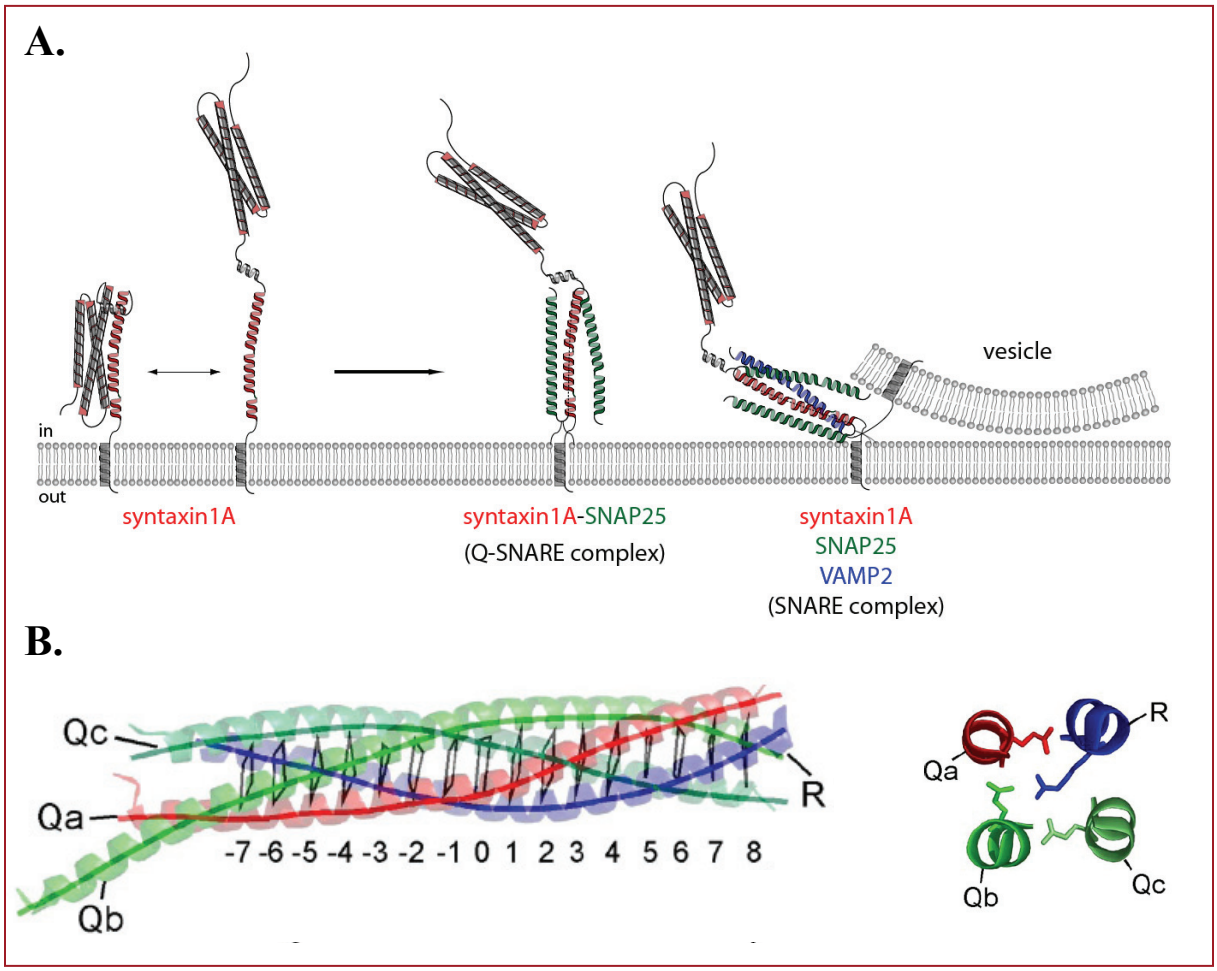

Figure 1.2. **Model of the neuronal SNARE core complex.** *A*, The syntaxin1A (*red*) N-terminal Habc domain folds into a three helix bundle that self-associates with the SNARE domain (closed conformation), preventing interactions with other SNAREs. The open (unfolded) conformation of syntaxin1A is available to form binary Q-SNARE complexes with SNAP25 (*green*), prior to the entry of the final SNARE domain contributed by VAMP2 (*blue*) on the vesicle. *B*, The four helix bundle of the neuronal SNARE complex (syntaxin1A, *blue*; VAMP2, *red*; SNAP25, *green*). The structure of the 0-layer is shown. Figure adapted from (Kloepper *et al.* 2007).

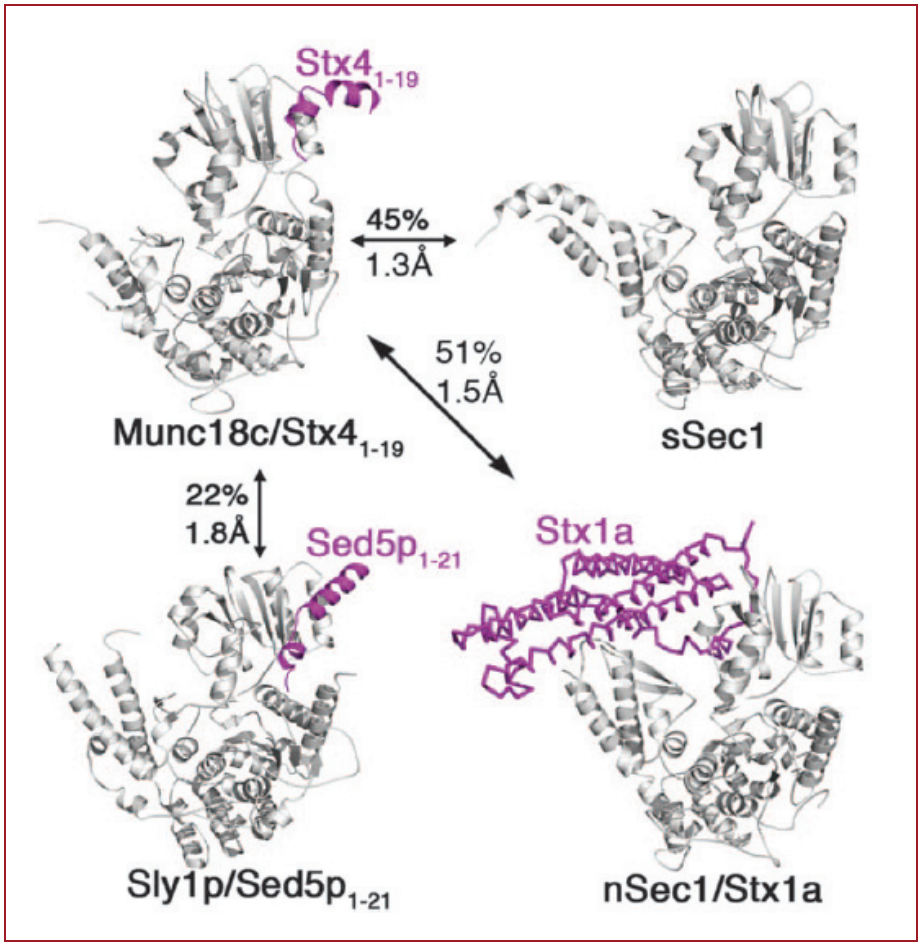

Figure 1.3. **Comparison of Sec1/Munc18 (SM) protein crystal structures** (Hu *et al.* 2007)**.** Mouse Munc18c/syntaxin4$_{1\text{-}19}$ (Hu *et al.* 2007), Squid neuronal Munc18 (sSec1), yeast Sly1p/Sed5p$_{1\text{-}21}$ (Bracher and Weissenhorn 2002), and rat neuronal Munc18a/syntaxin1A (Misura *et al.* 2000).

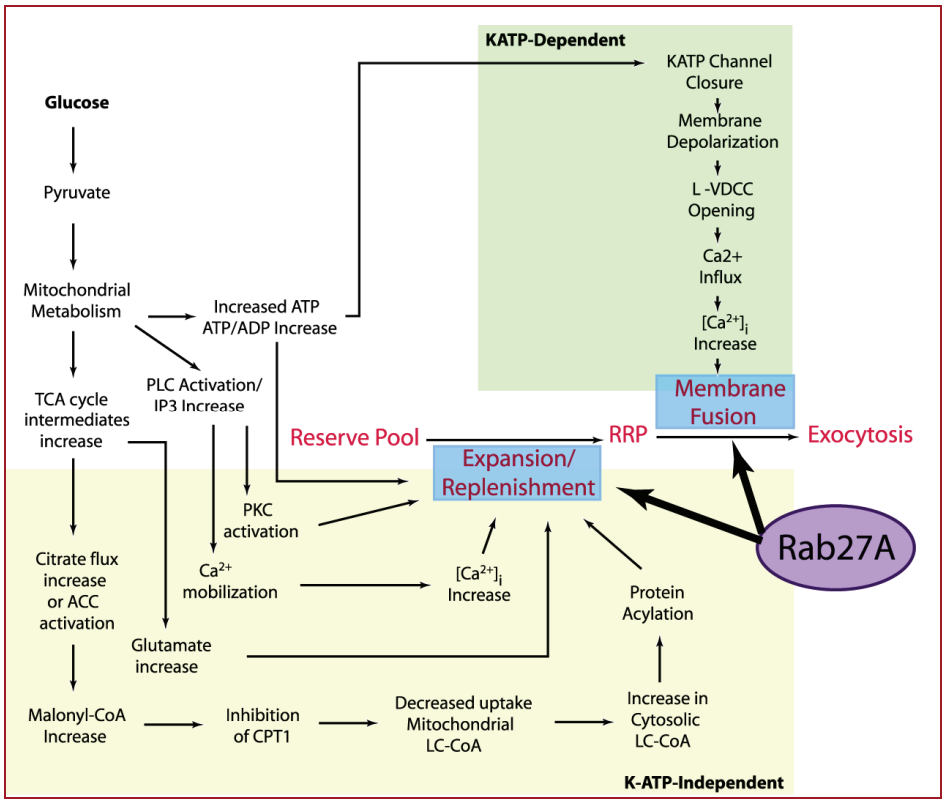

Figure 1.4. **Sites of Rab27a action within the pathways of glucose-stimulated insulin secretion in pancreatic β-cells**. The actions of Rab27a to augment insulin secretion are proposed to occur via enhanced insulin granule recruitment, as well as a step following vesicle-PM docking. Adapted from (Aizawa and Komatsu 2005).

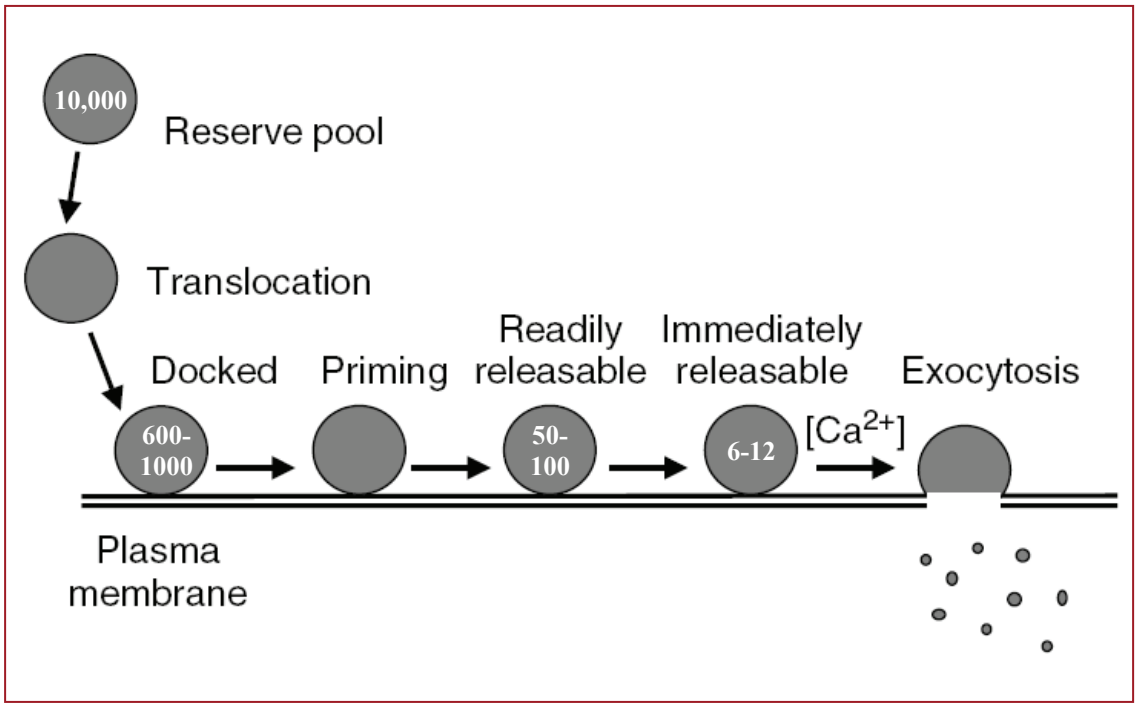

Figure 1.5. **Granule pools in the pancreatic β-cell** (Straub and Sharp 2002). Approximately 95% of the secretory granules in a β-cell reside in a non-releasable pool (reserve pool, ~10,000 granules). The remaining 1-5% of the granules are in a 'readily-releasable' pool (RRP) of 50-100 granules that can be functionally subdivided based on kinetic differences and/or Ca^{2+}-sensitivity. One RRP subset is termed the 'immediately-releasable' pool (IRP; 6-12 granules), comprised of secretory granules situated adjacent to L-type voltage-dependent Ca^{2+} channels, and therefore exhibit a minimal latency from channel opening to membrane fusion (Horrigan and Bookman 1994; Barg *et al.* 2001; Barg *et al.* 2002). A second subset (*not pictured*) is termed the highly calcium-sensitive pool (HCSP; 15 granules) which exhibits rapid kinetics of release at $[Ca^{2+}]_i$ of 1-3 μM, which is a Ca^{2+} level below that required (~15 μM) for rapid release of the bulk of the secretory granules in the IRP and RRP (Yang *et al.* 2002; Wan *et al.* 2004; Yang and Gillis 2004).

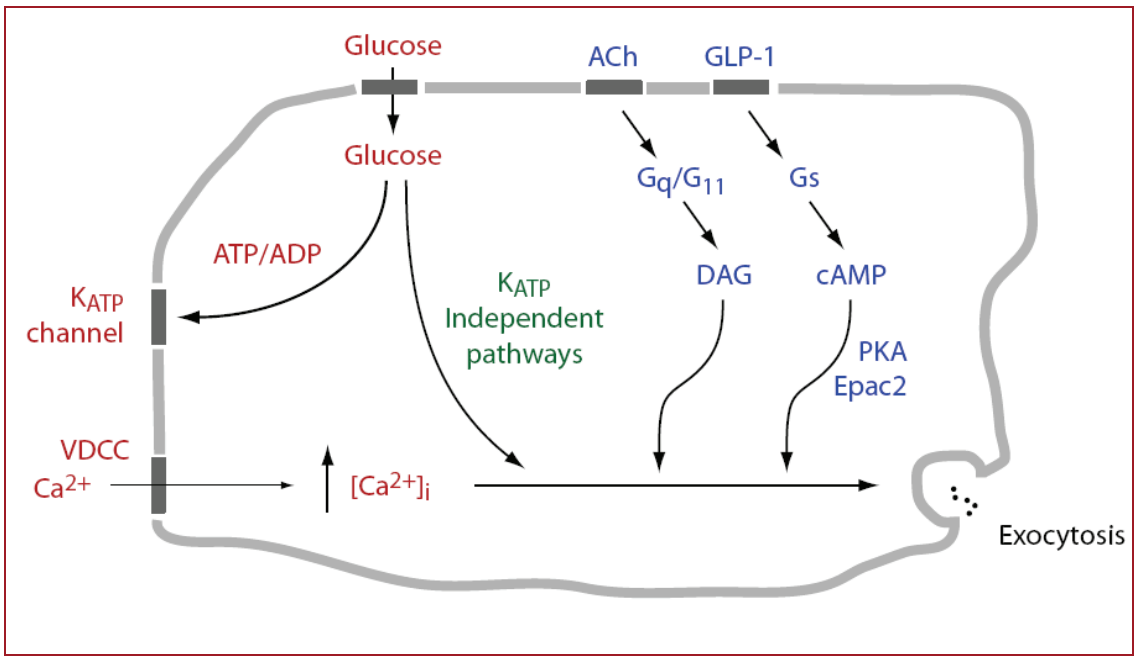

Figure 1.6. **Mechanism of glucose-stimulated insulin secretion in pancreatic β-cells**. After glucose entry through passive glucose transporters, metabolism of glucose increases ATP production, closing K_{ATP} channels, resulting in membrane depolarization and the opening of voltage-dependent Ca^{2+} channels (VDCC), which triggers insulin granule exocytosis (*red*). A secretion-amplifying pathway independent of the K_{ATP} channel has also been discovered (*green*), although its downstream effectors remain unclear. Secretion is also regulated by hormones and neurotransmitters through G-protein coupled receptor pathways (*blue*), which generate intracellular signals such as diacylglycerol (DAG) and cAMP, which directly activates protein kinase A (PKA) and Epac2 (exchange protein directly activated by cAMP) to enhance the secretory response.

References

Aizawa, T. and M. Komatsu (2005). "Rab27a: a new face in beta cell metabolism-secretion coupling." J Clin Invest **115**(2): 227-30.

Alory, C. and W. E. Balch (2003). "Molecular evolution of the Rab-escort-protein/guanine-nucleotide-dissociation-inhibitor superfamily." Mol Biol Cell **14**(9): 3857-67.

Ammala, C.*, et al.* (1993). "Calcium-independent potentiation of insulin release by cyclic AMP in single beta-cells." Nature **363**(6427): 356-8.

An, S. J. and W. Almers (2004). "Tracking SNARE complex formation in live endocrine cells." Science **306**(5698): 1042-6.

Andres, D. A.*, et al.* (1993). "cDNA cloning of component A of Rab geranylgeranyl transferase and demonstration of its role as a Rab escort protein." Cell **73**(6): 1091-9.

Antonin, W.*, et al.* (2002). "Crystal structure of the endosomal SNARE complex reveals common structural principles of all SNAREs." Nat Struct Biol **9**(2): 107-11.

Araki, E.*, et al.* (1994). "Alternative pathway of insulin signalling in mice with targeted disruption of the IRS-1 gene." Nature **372**(6502): 186-90.

Araki, S.*, et al.* (1997). "Inhibition of the binding of SNAP-23 to syntaxin 4 by Munc18c." Biochem Biophys Res Commun **234**(1): 257-62.

Ashcroft, F. M.*, et al.* (1984). "Glucose induces closure of single potassium channels in isolated rat pancreatic beta-cells." Nature **312**(5993): 446-8.

Aslan, D.*, et al.* (2006). "Griscelli syndrome: description of a case with Rab27A mutation." Pediatr Hematol Oncol **23**(3): 255-61.

Augustin, I.*, et al.* (1999). "Munc13-1 is essential for fusion competence of glutamatergic synaptic vesicles." Nature **400**(6743): 457-61.

Bahadoran, P.*, et al.* (2001). "Rab27a: A key to melanosome transport in human melanocytes." J Cell Biol **152**(4): 843-50.

Bai, L.*, et al.* (2007). "Dissecting multiple steps of GLUT4 trafficking and identifying the sites of insulin action." Cell Metab **5**(1): 47-57.

Bandyopadhyay, G.*, et al.* (2002). "PKC-zeta mediates insulin effects on glucose transport in cultured preadipocyte-derived human adipocytes." J Clin Endocrinol Metab **87**(2): 716-23.

Barbieri, M. A.*, et al.* (2000). "Epidermal growth factor and membrane trafficking. EGF receptor activation of endocytosis requires Rab5a." J Cell Biol **151**(3): 539-50.

Barg, S.*, et al.* (2002). "A subset of 50 secretory granules in close contact with L-type Ca2+ channels accounts for first-phase insulin secretion in mouse beta-cells." Diabetes **51 Suppl 1**: S74-82.

Barg, S.*, et al.* (2001). "Fast exocytosis with few Ca(2+) channels in insulin-secreting mouse pancreatic B cells." Biophys J **81**(6): 3308-23.

Barral, D. C.*, et al.* (2002). "Functional redundancy of Rab27 proteins and the pathogenesis of Griscelli syndrome." J Clin Invest **110**(2): 247-57.

Baumert, M.*, et al.* (1989). "Synaptobrevin: an integral membrane protein of 18,000 daltons present in small synaptic vesicles of rat brain." Embo J **8**(2): 379-84.

Becker, J.*, et al.* (1991). "Mutational analysis of the putative effector domain of the GTP-binding Ypt1 protein in yeast suggests specific regulation by a novel GAP activity." Embo J **10**(4): 785-92.

Bellve, K. D.*, et al.* (2006). "Plasma membrane domains specialized for clathrin-mediated endocytosis in primary cells." J Biol Chem **281**(23): 16139-46.

Bennett, M. K.*, et al.* (1992). "Syntaxin: a synaptic protein implicated in docking of synaptic vesicles at presynaptic active zones." Science **257**(5067): 255-9.

Bernards, A. (2003). "GAPs galore! A survey of putative Ras superfamily GTPase activating proteins in man and Drosophila." Biochim Biophys Acta **1603**(2): 47-82.
Bracher, A. and W. Weissenhorn (2001). "Crystal structures of neuronal squid Sec1 implicate inter-domain hinge movement in the release of t-SNAREs." J Mol Biol **306**(1): 7-13.
Bracher, A. and W. Weissenhorn (2002). "Structural basis for the Golgi membrane recruitment of Sly1p by Sed5p." Embo J **21**(22): 6114-24.
Brenner, S. (1974). "The genetics of Caenorhabditis elegans." Genetics **77**(1): 71-94.
Brose, N.*, et al.* (2000). "Regulation of transmitter release by Unc-13 and its homologues." Curr Opin Neurobiol **10**(3): 303-11.
Bruns, D. and R. Jahn (1995). "Real-time measurement of transmitter release from single synaptic vesicles." Nature **377**(6544): 62-5.
Bryant, N. J. and D. E. James (2001). "Vps45p stabilizes the syntaxin homologue Tlg2p and positively regulates SNARE complex formation." Embo J **20**(13): 3380-8.
Bryant, N. J. and D. E. James (2003). "The Sec1p/Munc18 (SM) protein, Vps45p, cycles on and off membranes during vesicle transport." J Cell Biol **161**(4): 691-6.
Calakos, N.*, et al.* (1994). "Protein-protein interactions contributing to the specificity of intracellular vesicular trafficking." Science **263**(5150): 1146-9.
Carr, C. M.*, et al.* (1999). "Sec1p binds to SNARE complexes and concentrates at sites of secretion." J Cell Biol **146**(2): 333-44.
Chamberlain, L. H.*, et al.* (2001). "SNARE proteins are highly enriched in lipid rafts in PC12 cells: implications for the spatial control of exocytosis." Proc Natl Acad Sci U S A **98**(10): 5619-24.
Chang, L.*, et al.* (2006). "TC10{alpha} is Required for Insulin-Stimulated Glucose Uptake in Adipocytes." Endocrinology.
Chattopadhyay, D.*, et al.* (2000). "Structure of the nucleotide-binding domain of Plasmodium falciparum rab6 in the GDP-bound form." Acta Crystallogr D Biol Crystallogr **56**(Pt 8): 937-44.
Chattopadhyay, D.*, et al.* (2000). "Plasmodium falciparum rab6 GTPase: expression, purification, crystallization and preliminary crystallographic studies." Acta Crystallogr D Biol Crystallogr **56**(Pt 8): 1017-9.
Cheatham, B.*, et al.* (1994). "Phosphatidylinositol 3-kinase activation is required for insulin stimulation of pp70 S6 kinase, DNA synthesis, and glucose transporter translocation." Mol Cell Biol **14**(7): 4902-11.
Chen, X.*, et al.* (2003). "Dominant negative Rab3D mutants reduce GTP-bound endogenous Rab3D in pancreatic acini." J Biol Chem **278**(50): 50053-60.
Chen, Y. A.*, et al.* (1999). "SNARE complex formation is triggered by Ca2+ and drives membrane fusion." Cell **97**(2): 165-74.
Chen, Y. A.*, et al.* (2001). "Sequential SNARE assembly underlies priming and triggering of exocytosis." Neuron **30**(1): 161-70.
Chen, Y. A. and R. H. Scheller (2001). "SNARE-mediated membrane fusion." Nat Rev Mol Cell Biol **2**(2): 98-106.
Chiang, S. H.*, et al.* (2001). "Insulin-stimulated GLUT4 translocation requires the CAP-dependent activation of TC10." Nature **410**(6831): 944-8.
Cho, H.*, et al.* (2001). "Insulin resistance and a diabetes mellitus-like syndrome in mice lacking the protein kinase Akt2 (PKB beta)." Science **292**(5522): 1728-31.
Collins, K. M.*, et al.* (2005). "Sec17p and HOPS, in distinct SNARE complexes, mediate SNARE complex disruption or assembly for fusion." Embo J **24**(10): 1775-86.
Curry, D. L.*, et al.* (1968). "Dynamics of insulin secretion by the perfused rat pancreas." Endocrinology **83**(3): 572-84.
Czech, M. P. and S. Corvera (1999). "Signaling mechanisms that regulate glucose transport." J Biol Chem **274**(4): 1865-8.

Dai, H., *et al.* (2007). "A quaternary SNARE-synaptotagmin-Ca2+-phospholipid complex in neurotransmitter release." J Mol Biol **367**(3): 848-63.
Dean, P. M. (1973). "Ultrastructural morphometry of the pancreatic -cell." Diabetologia **9**(2): 115-9.
DeBello, W. M., *et al.* (1995). "SNAP-mediated protein-protein interactions essential for neurotransmitter release." Nature **373**(6515): 626-30.
Dietrich, L. E., *et al.* (2003). "Control of eukaryotic membrane fusion by N-terminal domains of SNARE proteins." Biochim Biophys Acta **1641**(2-3): 111-9.
Drucker, D. J. (2006). "The biology of incretin hormones." Cell Metab **3**(3): 153-65.
Dugani, C. B. and A. Klip (2005). "Glucose transporter 4: cycling, compartments and controversies." EMBO Rep **6**(12): 1137-42.
Dulubova, I., *et al.* (2007). "Munc18-1 binds directly to the neuronal SNARE complex." Proc Natl Acad Sci U S A.
Dulubova, I., *et al.* (1999). "A conformational switch in syntaxin during exocytosis: role of munc18." Embo J **18**(16): 4372-82.
Dulubova, I., *et al.* (2002). "How Tlg2p/syntaxin 16 'snares' Vps45." Embo J **21**(14): 3620-31.
Dumas, J. J., *et al.* (1999). "Structural basis of activation and GTP hydrolysis in Rab proteins." Structure **7**(4): 413-23.
Durrieu, M. P., *et al.* (2008). "Interactions between neuronal fusion proteins explored by molecular dynamics." Biophys J **94**(9): 3436-46.
Eguez, L., *et al.* (2005). "Full intracellular retention of GLUT4 requires AS160 Rab GTPase activating protein." Cell Metab **2**(4): 263-72.
Eliasson, L., *et al.* (1997). "Rapid ATP-dependent priming of secretory granules precedes Ca(2+)-induced exocytosis in mouse pancreatic B-cells." J Physiol **503 (Pt 2)**: 399-412.
Elmqvist, D. and D. M. Quastel (1965). "A quantitative study of end-plate potentials in isolated human muscle." J Physiol **178**(3): 505-29.
Esters, H., *et al.* (2000). "High-resolution crystal structure of S. cerevisiae Ypt51(DeltaC15)-GppNHp, a small GTP-binding protein involved in regulation of endocytosis." J Mol Biol **298**(1): 111-21.
Fasshauer, D., *et al.* (1997). "A structural change occurs upon binding of syntaxin to SNAP-25." J Biol Chem **272**(7): 4582-90.
Fasshauer, D. and M. Margittai (2004). "A transient N-terminal interaction of SNAP-25 and syntaxin nucleates SNARE assembly." J Biol Chem **279**(9): 7613-21.
Fasshauer, D., *et al.* (1998). "Conserved structural features of the synaptic fusion complex: SNARE proteins reclassified as Q- and R-SNAREs." Proc Natl Acad Sci U S A **95**(26): 15781-6.
Fernandez, I., *et al.* (1998). "Three-dimensional structure of an evolutionarily conserved N-terminal domain of syntaxin 1A." Cell **94**(6): 841-9.
Fiebig, K. M., *et al.* (1999). "Folding intermediates of SNARE complex assembly." Nat Struct Biol **6**(2): 117-23.
Fisher, R. J., *et al.* (2001). "Control of fusion pore dynamics during exocytosis by Munc18." Science **291**(5505): 875-8.
Fujimoto, K., *et al.* (2002). "Piccolo, a Ca2+ sensor in pancreatic beta-cells. Involvement of cAMP-GEFII.Rim2.Piccolo complex in cAMP-dependent exocytosis." J Biol Chem **277**(52): 50497-502.
Fukuda, M. (2003). "Slp4-a/granuphilin-a inhibits dense-core vesicle exocytosis through interaction with the GDP-bound form of Rab27A in PC12 cells." J Biol Chem **278**(17): 15390-6.
Fukuda, M. (2005). "Versatile role of Rab27 in membrane trafficking: focus on the Rab27 effector families." J Biochem (Tokyo) **137**(1): 9-16.

Fukuda, R., *et al.* (2000). "Functional architecture of an intracellular membrane t-SNARE." Nature **407**(6801): 198-202.
Fukui, K., *et al.* (1997). "Isolation and characterization of a GTPase activating protein specific for the Rab3 subfamily of small G proteins." J Biol Chem **272**(8): 4655-8.
Futter, C. E., *et al.* (2004). "The role of Rab27a in the regulation of melanosome distribution within retinal pigment epithelial cells." Mol Biol Cell **15**(5): 2264-75.
Garcia, E. P., *et al.* (1994). "A rat brain Sec1 homologue related to Rop and UNC18 interacts with syntaxin." Proc Natl Acad Sci U S A **91**(6): 2003-7.
Gembal, M., *et al.* (1993). "Mechanisms by which glucose can control insulin release independently from its action on adenosine triphosphate-sensitive K+ channels in mouse B cells." J Clin Invest **91**(3): 871-80.
Gembal, M., *et al.* (1992). "Evidence that glucose can control insulin release independently from its action on ATP-sensitive K+ channels in mouse B cells." J Clin Invest **89**(4): 1288-95.
Giraudo, C. G., *et al.* (2006). "A clamping mechanism involved in SNARE-dependent exocytosis." Science **313**(5787): 676-80.
Gomi, H., *et al.* (2005). "Granuphilin molecularly docks insulin granules to the fusion machinery." J Cell Biol **171**(1): 99-109.
Gonzalez, E. and T. E. McGraw (2006). "Insulin signaling diverges into Akt-dependent and -independent signals to regulate the recruitment/docking and the fusion of GLUT4 vesicles to the plasma membrane." Mol Biol Cell **17**(10): 4484-93.
Gonzalez, L. C., Jr., *et al.* (2001). "A novel snare N-terminal domain revealed by the crystal structure of Sec22b." J Biol Chem **276**(26): 24203-11.
Graham, M. E., *et al.* (2004). "Syntaxin/Munc18 interactions in the late events during vesicle fusion and release in exocytosis." J Biol Chem **279**(31): 32751-60.
Graham, M. E., *et al.* (1997). "Evidence against an acute inhibitory role of nSec-1 (munc-18) in late steps of regulated exocytosis in chromaffin and PC12 cells." J Neurochem **69**(6): 2369-77.
Gromada, J., *et al.* (1997). "Adrenaline stimulates glucagon secretion in pancreatic A-cells by increasing the Ca2+ current and the number of granules close to the L-type Ca2+ channels." J Gen Physiol **110**(3): 217-28.
Gromada, J., *et al.* (1998). "Glucagon-like peptide 1 (7-36) amide stimulates exocytosis in human pancreatic beta-cells by both proximal and distal regulatory steps in stimulus-secretion coupling." Diabetes **47**(1): 57-65.
Gurkan, C., *et al.* (2005). "Large-scale profiling of Rab GTPase trafficking networks: the membrome." Mol Biol Cell **16**(8): 3847-64.
Hajduch, E., *et al.* (2001). "Protein kinase B (PKB/Akt)--a key regulator of glucose transport?" FEBS Lett **492**(3): 199-203.
Han, X., *et al.* (2004). "Transmembrane segments of syntaxin line the fusion pore of Ca2+-triggered exocytosis." Science **304**(5668): 289-92.
Hanson, P. I., *et al.* (1997). "Structure and conformational changes in NSF and its membrane receptor complexes visualized by quick-freeze/deep-etch electron microscopy." Cell **90**(3): 523-35.
Hata, Y., *et al.* (1993). "Synaptic vesicle fusion complex contains unc-18 homologue bound to syntaxin." Nature **366**(6453): 347-51.
Hay, J. C. (2001). "SNARE complex structure and function." Exp Cell Res **271**(1): 10-21.
Hayashi, T., *et al.* (1995). "Disassembly of the reconstituted synaptic vesicle membrane fusion complex in vitro." Embo J **14**(10): 2317-25.
Henquin, J. C. (2000). "Triggering and amplifying pathways of regulation of insulin secretion by glucose." Diabetes **49**(11): 1751-60.
Henquin, J. C., *et al.* (1994). "Multisite control of insulin release by glucose." Diabete Metab **20**(2): 132-7.

Hepp, R., *et al.* (2002). "Differential phosphorylation of SNAP-25 in vivo by protein kinase C and protein kinase A." FEBS Lett **532**(1-2): 52-6.
Hoenig, M. and G. W. Sharp (1986). "Glucose induces insulin release and a rise in cytosolic calcium concentration in a transplantable rat insulinoma." Endocrinology **119**(6): 2502-7.
Holst, J. J. and J. Gromada (2004). "Role of incretin hormones in the regulation of insulin secretion in diabetic and nondiabetic humans." Am J Physiol Endocrinol Metab **287**(2): E199-206.
Holz, G. G., *et al.* (2006). "Cell physiology of cAMP sensor Epac." J Physiol **577**(Pt 1): 5-15.
Horiuchi, H., *et al.* (1997). "A novel Rab5 GDP/GTP exchange factor complexed to Rabaptin-5 links nucleotide exchange to effector recruitment and function." Cell **90**(6): 1149-59.
Horrigan, F. T. and R. J. Bookman (1994). "Releasable pools and the kinetics of exocytosis in adrenal chromaffin cells." Neuron **13**(5): 1119-29.
Howell, S. L. (1974). "The molecular organization of the beta granule of the islets of Langerhans." Adv Cytopharmacol **2**: 319-27.
Hu, J., *et al.* (2003). "Structural basis for recruitment of the adaptor protein APS to the activated insulin receptor." Mol Cell **12**(6): 1379-89.
Hu, S. H., *et al.* (2007). "Structure of the Munc18c/Syntaxin4 N-peptide complex defines universal features of the N-peptide binding mode of Sec1/Munc18 proteins." Proc Natl Acad Sci U S A **104**(21): 8773-8.
Hua, Y. and R. H. Scheller (2001). "Three SNARE complexes cooperate to mediate membrane fusion." Proc Natl Acad Sci U S A **98**(14): 8065-70.
Huang, S. and M. P. Czech (2007). "The GLUT4 glucose transporter." Cell Metab **5**(4): 237-52.
Huang, S., *et al.* (2007). "Insulin stimulates membrane fusion and GLUT4 accumulation in clathrin coats on adipocyte plasma membranes." Mol Cell Biol **27**(9): 3456-69.
Hume, A. N., *et al.* (2001). "Rab27a regulates the peripheral distribution of melanosomes in melanocytes." J Cell Biol **152**(4): 795-808.
Ishiki, M. and A. Klip (2005). "Minireview: recent developments in the regulation of glucose transporter-4 traffic: new signals, locations, and partners." Endocrinology **146**(12): 5071-8.
Itoh, T. and M. Fukuda (2006). "Identification of EPI64 as a GTPase-activating protein specific for Rab27A." J Biol Chem **281**(42): 31823-31.
Itoh, T., *et al.* (2006). "Screening for target Rabs of TBC (Tre-2/Bub2/Cdc16) domain-containing proteins based on their Rab-binding activity." Genes Cells **11**(9): 1023-37.
Iwasaki, K., *et al.* (1997). "aex-3 encodes a novel regulator of presynaptic activity in C. elegans." Neuron **18**(4): 613-22.
Jahn, R. and R. H. Scheller (2006). "SNAREs--engines for membrane fusion." Nat Rev Mol Cell Biol **7**(9): 631-43.
James, D. E. (2005). "MUNC-ing around with insulin action." J Clin Invest **115**(2): 219-21.
Jiang, T., *et al.* (1998). "Membrane-permeant esters of phosphatidylinositol 3,4,5-trisphosphate." J Biol Chem **273**(18): 11017-24.
Kanda, H., *et al.* (2005). "Adipocytes from Munc18c-null mice show increased sensitivity to insulin-stimulated GLUT4 externalization." J Clin Invest **115**(2): 291-301.
Kang, G., *et al.* (2001). "cAMP-regulated guanine nucleotide exchange factor II (Epac2) mediates Ca2+-induced Ca2+ release in INS-1 pancreatic beta-cells." J Physiol **536**(Pt 2): 375-85.
Karlsson, H. K., *et al.* (2006). "Insulin signaling and glucose transport in skeletal muscle from first-degree relatives of type 2 diabetic patients." Diabetes **55**(5): 1283-8.
Karylowski, O., *et al.* (2004). "GLUT4 is retained by an intracellular cycle of vesicle formation and fusion with endosomes." Mol Biol Cell **15**(2): 870-82.
Kasai, K., *et al.* (2005). "Rab27a mediates the tight docking of insulin granules onto the plasma membrane during glucose stimulation." J Clin Invest **115**(2): 388-96.

Keller, J. E., *et al.* (2004). "Uptake of botulinum neurotoxin into cultured neurons." Biochemistry **43**(2): 526-32.
Keller, J. E. and E. A. Neale (2001). "The role of the synaptic protein snap-25 in the potency of botulinum neurotoxin type A." J Biol Chem **276**(16): 13476-82.
Khvotchev, M., *et al.* (2007). "Dual modes of Munc18-1/SNARE interactions are coupled by functionally critical binding to syntaxin-1 N terminus." J Neurosci **27**(45): 12147-55.
King, H., *et al.* (1998). "Global burden of diabetes, 1995-2025: prevalence, numerical estimates, and projections." Diabetes Care **21**(9): 1414-31.
Kloepper, T. H., *et al.* (2007). "An elaborate classification of SNARE proteins sheds light on the conservation of the eukaryotic endomembrane system." Mol Biol Cell **18**(9): 3463-71.
Kohn, A. D., *et al.* (1998). "Construction and characterization of a conditionally active version of the serine/threonine kinase Akt." J Biol Chem **273**(19): 11937-43.
Kohn, A. D., *et al.* (1996). "Expression of a constitutively active Akt Ser/Thr kinase in 3T3-L1 adipocytes stimulates glucose uptake and glucose transporter 4 translocation." J Biol Chem **271**(49): 31372-8.
Kondo, H., *et al.* (2006). "Constitutive GDP/GTP exchange and secretion-dependent GTP hydrolysis activity for Rab27 in platelets." J Biol Chem **281**(39): 28657-65.
Korteweg, N., *et al.* (2005). "The role of Munc18-1 in docking and exocytosis of peptide hormone vesicles in the anterior pituitary." Biol Cell **97**(6): 445-55.
Kwan, E. P. and H. Y. Gaisano (2005). "Glucagon-like peptide 1 regulates sequential and compound exocytosis in pancreatic islet beta-cells." Diabetes **54**(9): 2734-43.
Kwan, E. P., *et al.* (2006). "Munc13-1 deficiency reduces insulin secretion and causes abnormal glucose tolerance." Diabetes **55**(5): 1421-9.
Kwan, E. P., *et al.* (2007). "Interaction between Munc13-1 and RIM is critical for glucagon-like peptide-1 mediated rescue of exocytotic defects in Munc13-1 deficient pancreatic beta-cells." Diabetes **56**(10): 2579-88.
Lang, T., *et al.* (2001). "SNAREs are concentrated in cholesterol-dependent clusters that define docking and fusion sites for exocytosis." EMBO J **20**(9): 2202-13.
Lang, T., *et al.* (2002). "SNAREs in native plasma membranes are active and readily form core complexes with endogenous and exogenous SNAREs." J Cell Biol **158**(4): 751-60.
Larance, M., *et al.* (2005). "Characterization of the role of the Rab GTPase-activating protein AS160 in insulin-regulated GLUT4 trafficking." J Biol Chem **280**(45): 37803-13.
Latham, C. F., *et al.* (2006). "Molecular dissection of the munc18c/syntaxin4 interaction: implications for regulation of membrane trafficking." Traffic **7**(10): 1408-19.
Lin, R. C. and R. H. Scheller (1997). "Structural organization of the synaptic exocytosis core complex." Neuron **19**(5): 1087-94.
Liu, J., *et al.* (2004). "Fluorescence resonance energy transfer reports properties of syntaxin1a interaction with Munc18-1 in vivo." J Biol Chem **279**(53): 55924-36.
Lizunov, V. A., *et al.* (2005). "Insulin stimulates the halting, tethering, and fusion of mobile GLUT4 vesicles in rat adipose cells." J Cell Biol **169**(3): 481-9.
Lonart, G., *et al.* (2003). "Phosphorylation of RIM1alpha by PKA triggers presynaptic long-term potentiation at cerebellar parallel fiber synapses." Cell **115**(1): 49-60.
Mahoney, T. R., *et al.* (2006). "Regulation of synaptic transmission by RAB-3 and RAB-27 in Caenorhabditis elegans." Mol Biol Cell **17**(6): 2617-25.
Maltese, W. A., *et al.* (1996). "Prenylation-dependent interaction of Rab proteins with GDP dissociation inhibitors." Biochem Soc Trans **24**(3): 703-8.
Mancini, A. J., *et al.* (1998). "Partial albinism with immunodeficiency: Griscelli syndrome: report of a case and review of the literature." J Am Acad Dermatol **38**(2 Pt 2): 295-300.
Margittai, M., *et al.* (2003). "Single-molecule fluorescence resonance energy transfer reveals a dynamic equilibrium between closed and open conformations of syntaxin 1." Proc Natl Acad Sci U S A **100**(26): 15516-21.

Mayer, A., *et al.* (1996). "Sec18p (NSF)-driven release of Sec17p (alpha-SNAP) can precede docking and fusion of yeast vacuoles." Cell **85**(1): 83-94.
McNew, J. A., *et al.* (1999). "The length of the flexible SNAREpin juxtamembrane region is a critical determinant of SNARE-dependent fusion." Mol Cell **4**(3): 415-21.
Medine, C. N., *et al.* (2007). "Munc18-1 prevents the formation of ectopic SNARE complexes in living cells." J Cell Sci **120**(Pt 24): 4407-15.
Meier, J. J., *et al.* (2002). "Gastric inhibitory polypeptide: the neglected incretin revisited." Regul Pept **107**(1-3): 1-13.
Mennerick, S. and G. Matthews (1996). "Ultrafast exocytosis elicited by calcium current in synaptic terminals of retinal bipolar neurons." Neuron **17**(6): 1241-9.
Miinea, C. P., *et al.* (2005). "AS160, the Akt substrate regulating GLUT4 translocation, has a functional Rab GTPase-activating protein domain." Biochem J **391**(Pt 1): 87-93.
Misura, K. M., *et al.* (2002). "Three-dimensional structure of the amino-terminal domain of syntaxin 6, a SNAP-25 C homolog." Proc Natl Acad Sci U S A **99**(14): 9184-9.
Misura, K. M., *et al.* (2000). "Three-dimensional structure of the neuronal-Sec1-syntaxin 1a complex." Nature **404**(6776): 355-62.
Mitra, P., *et al.* (2004). "RNAi-based analysis of CAP, Cbl, and CrkII function in the regulation of GLUT4 by insulin." J Biol Chem **279**(36): 37431-5.
Moser, T. and E. Neher (1997). "Rapid exocytosis in single chromaffin cells recorded from mouse adrenal slices." J Neurosci **17**(7): 2314-23.
Nagashima, K., *et al.* (2002). "Melanophilin directly links Rab27a and myosin Va through its distinct coiled-coil regions." FEBS Lett **517**(1-3): 233-8.
Nagy, G., *et al.* (2002). "Protein kinase C-dependent phosphorylation of synaptosome-associated protein of 25 kDa at Ser187 potentiates vesicle recruitment." J Neurosci **22**(21): 9278-86.
Nesher, R., *et al.* (2002). "Beta-cell protein kinases and the dynamics of the insulin response to glucose." Diabetes **51 Suppl 1**: S68-73.
Nichols, B. J., *et al.* (1997). "Homotypic vacuolar fusion mediated by t- and v-SNAREs." Nature **387**(6629): 199-202.
Nicholson, K. L., *et al.* (1998). "Regulation of SNARE complex assembly by an N-terminal domain of the t-SNARE Sso1p." Nat Struct Biol **5**(9): 793-802.
Novick, P. and R. Schekman (1979). "Secretion and cell-surface growth are blocked in a temperature-sensitive mutant of Saccharomyces cerevisiae." Proc Natl Acad Sci U S A **76**(4): 1858-62.
Novick, P. and M. Zerial (1997). "The diversity of Rab proteins in vesicle transport." Curr Opin Cell Biol **9**(4): 496-504.
Okada, T., *et al.* (1994). "Essential role of phosphatidylinositol 3-kinase in insulin-induced glucose transport and antilipolysis in rat adipocytes. Studies with a selective inhibitor wortmannin." J Biol Chem **269**(5): 3568-73.
Olofsson, C. S., *et al.* (2002). "Fast insulin secretion reflects exocytosis of docked granules in mouse pancreatic B-cells." Pflugers Arch **444**(1-2): 43-51.
Ostermeier, C. and A. T. Brunger (1999). "Structural basis of Rab effector specificity: crystal structure of the small G protein Rab3A complexed with the effector domain of rabphilin-3A." Cell **96**(3): 363-74.
Oyler, G. A., *et al.* (1989). "The identification of a novel synaptosomal-associated protein, SNAP-25, differentially expressed by neuronal subpopulations." J Cell Biol **109**(6 Pt 1): 3039-52.
Ozaki, N., *et al.* (2000). "cAMP-GEFII is a direct target of cAMP in regulated exocytosis." Nat Cell Biol **2**(11): 805-11.
Parlati, F., *et al.* (1999). "Rapid and efficient fusion of phospholipid vesicles by the alpha-helical core of a SNARE complex in the absence of an N-terminal regulatory domain." Proc Natl Acad Sci U S A **96**(22): 12565-70.

Parsons, T. D., *et al.* (1995). "Docked granules, the exocytic burst, and the need for ATP hydrolysis in endocrine cells." Neuron **15**(5): 1085-96.
Peng, R. and D. Gallwitz (2002). "Sly1 protein bound to Golgi syntaxin Sed5p allows assembly and contributes to specificity of SNARE fusion complexes." J Cell Biol **157**(4): 645-55.
Pessin, J. E. and A. R. Saltiel (2000). "Signaling pathways in insulin action: molecular targets of insulin resistance." J Clin Invest **106**(2): 165-9.
Peter, M., *et al.* (1992). "Isoprenylation of rab proteins on structurally distinct cysteine motifs." J Cell Sci **102 (Pt 4)**: 857-65.
Pevsner, J., *et al.* (1994). "n-Sec1: a neural-specific syntaxin-binding protein." Proc Natl Acad Sci U S A **91**(4): 1445-9.
Pfeffer, S. R. (2001). "Rab GTPases: specifying and deciphering organelle identity and function." Trends Cell Biol **11**(12): 487-91.
Pfeffer, S. R. (2005). "Structural clues to Rab GTPase functional diversity." J Biol Chem **280**(16): 15485-8.
Pfeffer, S. R. (2007). "Unsolved mysteries in membrane traffic." Annu Rev Biochem **76**: 629-45.
Pobbati, A. V., *et al.* (2006). "N- to C-terminal SNARE complex assembly promotes rapid membrane fusion." Science **313**(5787): 673-6.
Predescu, S. A., *et al.* (2005). "Cholesterol-dependent syntaxin-4 and SNAP-23 clustering regulates caveolar fusion with the endothelial plasma membrane." J Biol Chem **280**(44): 37130-8.
Prentki, M. (1996). "New insights into pancreatic beta-cell metabolic signaling in insulin secretion." Eur J Endocrinol **134**(3): 272-86.
Prentki, M. and B. E. Corkey (1996). "Are the beta-cell signaling molecules malonyl-CoA and cystolic long-chain acyl-CoA implicated in multiple tissue defects of obesity and NIDDM?" Diabetes **45**(3): 273-83.
Provance, D. W., *et al.* (2002). "Melanophilin, the product of the leaden locus, is required for targeting of myosin-Va to melanosomes." Traffic **3**(2): 124-32.
Rhee, J. S., *et al.* (2002). "Beta phorbol ester- and diacylglycerol-induced augmentation of transmitter release is mediated by Munc13s and not by PKCs." Cell **108**(1): 121-33.
Ribon, V., *et al.* (1998). "A novel, multifuntional c-Cbl binding protein in insulin receptor signaling in 3T3-L1 adipocytes." Mol Cell Biol **18**(2): 872-9.
Richmond, J. E., *et al.* (1999). "UNC-13 is required for synaptic vesicle fusion in C. elegans." Nat Neurosci **2**(11): 959-64.
Richmond, J. E., *et al.* (2001). "An open form of syntaxin bypasses the requirement for UNC-13 in vesicle priming." Nature **412**(6844): 338-41.
Risinger, C. and M. K. Bennett (1999). "Differential phosphorylation of syntaxin and synaptosome-associated protein of 25 kDa (SNAP-25) isoforms." J Neurochem **72**(2): 614-24.
Sabatini, B. L. and W. G. Regehr (1996). "Timing of neurotransmission at fast synapses in the mammalian brain." Nature **384**(6605): 170-2.
Sajan, M. P., *et al.* (2006). "Repletion of atypical protein kinase C following RNA interference-mediated depletion restores insulin-stimulated glucose transport." J Biol Chem **281**(25): 17466-73.
Saltiel, A. R. and C. R. Kahn (2001). "Insulin signalling and the regulation of glucose and lipid metabolism." Nature **414**(6865): 799-806.
Saltiel, A. R. and J. E. Pessin (2002). "Insulin signaling pathways in time and space." Trends Cell Biol **12**(2): 65-71.
Saltiel, A. R. and J. E. Pessin (2003). "Insulin signaling in microdomains of the plasma membrane." Traffic **4**(11): 711-6.
Sano, H., *et al.* (2007). "Rab10, a target of the AS160 Rab GAP, is required for insulin-stimulated translocation of GLUT4 to the adipocyte plasma membrane." Cell Metab **5**(4): 293-303.

Sano, H., *et al.* (2003). "Insulin-stimulated phosphorylation of a Rab GTPase-activating protein regulates GLUT4 translocation." J Biol Chem **278**(17): 14599-602.
Sato, Y., *et al.* (1992). "Dual functional role of membrane depolarization/Ca2+ influx in rat pancreatic B-cell." Diabetes **41**(4): 438-43.
Sato, Y., *et al.* (2007). "Crystal structure of the Sec4p.Sec2p complex in the nucleotide exchanging intermediate state." Proc Natl Acad Sci U S A **104**(20): 8305-10.
Scales, S. J., *et al.* (2000). "SNAREs contribute to the specificity of membrane fusion." Neuron **26**(2): 457-64.
Schneggenburger, R. and E. Neher (2000). "Intracellular calcium dependence of transmitter release rates at a fast central synapse." Nature **406**(6798): 889-93.
Schoch, S., *et al.* (2001). "SNARE function analyzed in synaptobrevin/VAMP knockout mice." Science **294**(5544): 1117-22.
Schulze, K. L., *et al.* (1994). "rop, a Drosophila homolog of yeast Sec1 and vertebrate n-Sec1/Munc-18 proteins, is a negative regulator of neurotransmitter release in vivo." Neuron **13**(5): 1099-108.
Scott, B. L., *et al.* (2004). "Sec1p directly stimulates SNARE-mediated membrane fusion in vitro." J Cell Biol **167**(1): 75-85.
Seabra, M. C., *et al.* (2002). "Rab GTPases, intracellular traffic and disease." Trends Mol Med **8**(1): 23-30.
Shen, J., *et al.* (2007). "Selective activation of cognate SNAREpins by Sec1/Munc18 proteins." Cell **128**(1): 183-95.
Shibasaki, T., *et al.* (2004). "Interaction of ATP sensor, cAMP sensor, Ca2+ sensor, and voltage-dependent Ca2+ channel in insulin granule exocytosis." J Biol Chem **279**(9): 7956-61.
Shibasaki, T., *et al.* (2007). "Essential role of Epac2/Rap1 signaling in regulation of insulin granule dynamics by cAMP." Proc Natl Acad Sci U S A **104**(49): 19333-8.
Shu, Y., *et al.* (2008). "Phosphorylation of SNAP-25 at Ser187 mediates enhancement of exocytosis by a phorbol ester in INS-1 cells." J Neurosci **28**(1): 21-30.
Sollner, T., *et al.* (1993). "A protein assembly-disassembly pathway in vitro that may correspond to sequential steps of synaptic vesicle docking, activation, and fusion." Cell **75**(3): 409-18.
Sollner, T., *et al.* (1993). "SNAP receptors implicated in vesicle targeting and fusion." Nature **362**(6418): 318-24.
Stenmark, H. and V. M. Olkkonen (2001). "The Rab GTPase family." Genome Biol **2**(5): REVIEWS3007.
Steyer, J. A., *et al.* (1997). "Transport, docking and exocytosis of single secretory granules in live chromaffin cells." Nature **388**(6641): 474-8.
Stinchcombe, J. C., *et al.* (2001). "Rab27a is required for regulated secretion in cytotoxic T lymphocytes." J Cell Biol **152**(4): 825-34.
Straub, S. G., *et al.* (1998). "Glucose activates both K(ATP) channel-dependent and K(ATP) channel-independent signaling pathways in human islets." Diabetes **47**(5): 758-63.
Straub, S. G. and G. W. Sharp (2002). "Glucose-stimulated signaling pathways in biphasic insulin secretion." Diabetes Metab Res Rev **18**(6): 451-63.
Sutton, R. B., *et al.* (1998). "Crystal structure of a SNARE complex involved in synaptic exocytosis at 2.4 A resolution." Nature **395**(6700): 347-53.
Takai, Y., *et al.* (2001). "Small GTP-binding proteins." Physiol Rev **81**(1): 153-208.
Tamemoto, H., *et al.* (1994). "Insulin resistance and growth retardation in mice lacking insulin receptor substrate-1." Nature **372**(6502): 182-6.
Tamori, Y., *et al.* (1998). "Inhibition of insulin-induced GLUT4 translocation by Munc18c through interaction with syntaxin4 in 3T3-L1 adipocytes." J Biol Chem **273**(31): 19740-6.

Tellam, J. T., *et al.* (1997). "Characterization of Munc-18c and syntaxin-4 in 3T3-L1 adipocytes. Putative role in insulin-dependent movement of GLUT-4." J Biol Chem **272**(10): 6179-86.

Tengholm, A. and T. Meyer (2002). "A PI3-kinase signaling code for insulin-triggered insertion of glucose transporters into the plasma membrane." Curr Biol **12**(21): 1871-6.

Thurmond, D. C., *et al.* (1998). "Regulation of insulin-stimulated GLUT4 translocation by Munc18c in 3T3L1 adipocytes." J Biol Chem **273**(50): 33876-83.

Tochio, H., *et al.* (2001). "An autoinhibitory mechanism for nonsyntaxin SNARE proteins revealed by the structure of Ykt6p." Science **293**(5530): 698-702.

Tolmachova, T., *et al.* (2007). "Rab27b regulates number and secretion of platelet dense granules." Proc Natl Acad Sci U S A **104**(14): 5872-7.

Tolmachova, T., *et al.* (2004). "A general role for Rab27a in secretory cells." Mol Biol Cell **15**(1): 332-44.

Toonen, R. F. and M. Verhage (2003). "Vesicle trafficking: pleasure and pain from SM genes." Trends Cell Biol **13**(4): 177-86.

Torii, S., *et al.* (2002). "Granuphilin modulates the exocytosis of secretory granules through interaction with syntaxin 1a." Mol Cell Biol **22**(15): 5518-26.

Trimble, W. S., *et al.* (1988). "VAMP-1: a synaptic vesicle-associated integral membrane protein." Proc Natl Acad Sci U S A **85**(12): 4538-42.

Tsuboi, T. and M. Fukuda (2006). "Rab3A and Rab27A cooperatively regulate the docking step of dense-core vesicle exocytosis in PC12 cells." J Cell Sci **119**(Pt 11): 2196-203.

Tsuboi, T. and M. Fukuda (2006). "The Slp4-a linker domain controls exocytosis through interaction with Munc18-1.syntaxin-1a complex." Mol Biol Cell **17**(5): 2101-12.

Tucker, W. C., *et al.* (2004). "Reconstitution of Ca2+-regulated membrane fusion by synaptotagmin and SNAREs." Science **304**(5669): 435-8.

Ullrich, O., *et al.* (1993). "Rab GDP dissociation inhibitor as a general regulator for the membrane association of rab proteins." J Biol Chem **268**(24): 18143-50.

van Weering, J. R., *et al.* (2007). "The role of Rab3a in secretory vesicle docking requires association/dissociation of guanidine phosphates and Munc18-1." PLoS ONE **2**: e616.

Verhage, M., *et al.* (2000). "Synaptic assembly of the brain in the absence of neurotransmitter secretion." Science **287**(5454): 864-9.

Voets, T., *et al.* (1999). "Mechanisms underlying phasic and sustained secretion in chromaffin cells from mouse adrenal slices." Neuron **23**(3): 607-15.

Voets, T., *et al.* (2001). "Munc18-1 promotes large dense-core vesicle docking." Neuron **31**(4): 581-91.

Walch-Solimena, C., *et al.* (1997). "Sec2p mediates nucleotide exchange on Sec4p and is involved in polarized delivery of post-Golgi vesicles." J Cell Biol **137**(7): 1495-509.

Wan, Q. F., *et al.* (2004). "Protein kinase activation increases insulin secretion by sensitizing the secretory machinery to Ca2+." J Gen Physiol **124**(6): 653-62.

Wang, Q., *et al.* (1999). "Protein kinase B/Akt participates in GLUT4 translocation by insulin in L6 myoblasts." Mol Cell Biol **19**(6): 4008-18.

Washbourne, P., *et al.* (2002). "Genetic ablation of the t-SNARE SNAP-25 distinguishes mechanisms of neuroexocytosis." Nat Neurosci **5**(1): 19-26.

Weber, T., *et al.* (1998). "SNAREpins: minimal machinery for membrane fusion." Cell **92**(6): 759-72.

Weimer, R. M., *et al.* (2003). "Defects in synaptic vesicle docking in unc-18 mutants." Nat Neurosci **6**(10): 1023-30.

Whiteheart, S. W., *et al.* (1994). "N-ethylmaleimide-sensitive fusion protein: a trimeric ATPase whose hydrolysis of ATP is required for membrane fusion." J Cell Biol **126**(4): 945-54.

Whiteman, E. L., *et al.* (2002). "Role of Akt/protein kinase B in metabolism." Trends Endocrinol Metab **13**(10): 444-51.

Widberg, C. H., *et al.* (2003). "Tomosyn interacts with the t-SNAREs syntaxin4 and SNAP23 and plays a role in insulin-stimulated GLUT4 translocation." J Biol Chem **278**(37): 35093-101.

Wilson, S. M., *et al.* (2000). "A mutation in Rab27a causes the vesicle transport defects observed in ashen mice." Proc Natl Acad Sci U S A **97**(14): 7933-8.

Wollheim, C. B. and G. W. Sharp (1981). "Regulation of insulin release by calcium." Physiol Rev **61**(4): 914-73.

Wu, S. K., *et al.* (1996). "Structural insights into the function of the Rab GDI superfamily." Trends Biochem Sci **21**(12): 472-6.

Wu, X., *et al.* (2002). "Rab27a is an essential component of melanosome receptor for myosin Va." Mol Biol Cell **13**(5): 1735-49.

Wu, Y. W., *et al.* (2007). "Interaction analysis of prenylated Rab GTPase with Rab escort protein and GDP dissociation inhibitor explains the need for both regulators." Proc Natl Acad Sci U S A **104**(30): 12294-9.

Yamaguchi, T., *et al.* (2002). "Sly1 binds to Golgi and ER syntaxins via a conserved N-terminal peptide motif." Dev Cell **2**(3): 295-305.

Yang, Y. and K. D. Gillis (2004). "A highly Ca2+-sensitive pool of granules is regulated by glucose and protein kinases in insulin-secreting INS-1 cells." J Gen Physiol **124**(6): 641-51.

Yang, Y., *et al.* (2002). "A highly Ca2+-sensitive pool of vesicles is regulated by protein kinase C in adrenal chromaffin cells." Proc Natl Acad Sci U S A **99**(26): 17060-5.

Yi, Z., *et al.* (2002). "The Rab27a/granuphilin complex regulates the exocytosis of insulin-containing dense-core granules." Mol Cell Biol **22**(6): 1858-67.

Zerial, M. and H. McBride (2001). "Rab proteins as membrane organizers." Nat Rev Mol Cell Biol **2**(2): 107-17.

Zhou, Q. L., *et al.* (2004). "Analysis of insulin signalling by RNAi-based gene silencing." Biochem Soc Trans **32**(Pt 5): 817-21.

Zierath, J. R., *et al.* (1996). "Insulin action on glucose transport and plasma membrane GLUT4 content in skeletal muscle from patients with NIDDM." Diabetologia **39**(10): 1180-9.

CHAPTER II

MUNC18C INTERACTION WITH SYNTAXIN4 MONOMERS AND SNARE COMPLEX INTERMEDIATES IN GLUT4 VESICLE TRAFFICKING

Abstract

In the process of insulin-stimulated GLUT4 vesicle exocytosis, Munc18c has been proposed to control SNARE complex formation by inactivating syntaxin4 in a self-associated conformation. Using *in vivo* fluorescence resonance energy transfer (FRET) in 3T3L1 adipocytes, co-immunoprecipitation, and *in vitro* binding assays, we provide data to indicate that Munc18c also associates with near equal affinity to a mutant of syntaxin4 in a constitutively open (unfolded) state (L173A/E174A; LE). To bind to the open conformation of syntaxin4, we found that Munc18c requires an interaction with the N-terminus of syntaxin4 which resembles Sly1 interaction with the N-terminus of ER/Golgi syntaxins. However, both N- and C-termini of syntaxin4 are required for Munc18c binding since a mutation in the syntaxin4 SNARE domain (I241A) reduces the interaction, irrespective of syntaxin4 conformation. Using an optical reporter for syntaxin4-SNARE pairings *in vivo*, we demonstrated that Munc18c blocks recruitment of SNAP23 to wildtype syntaxin4, yet associates with syntaxin4^{LE}-SNAP23 Q-SNARE complexes. Fluorescent imaging of GLUT4 vesicles in 3T3L1 adipocytes revealed that syntaxin4^{LE} bypassed the requirement of insulin for GLUT4 vesicle plasma membrane docking, even while Munc18c is bound. Furthermore, as the reduction of the Munc18c-syntaxin4 interaction with the I241A mutation does not promote docking, formation of a Munc18c-syntaxin4 complex is not essential for the docking process. Therefore, in contradiction to previous models, our data indicates that

the conformational 'opening' of syntaxin4 rather than the dissociation of Munc18c is the critical event required for GLUT4 vesicle docking.

Introduction

Soluble N-ethylmaleimide-sensitive factor (NSF) attachment protein receptors (SNAREs) are central to vesicle fusion events in all eukaryotes. SNARE proteins anchored to both transport vesicles and their target membranes overcome the forces necessary for fusion by binding with high affinity in a ternary core complex (Jahn and Scheller 2006). Though formation of the SNARE core complexes are sufficient for membrane fusion (Weber, Zemelman et al. 1998; Parlati, Weber et al. 1999) essential regulatory proteins of the Sec1/Munc18 (SM) family are believed to control SNARE complex formation. Seven vertebrate SM gene family members (Munc18a/b/c, Sly1, Vps45, Vps33a/b) have been described which affect membrane trafficking in distinct subcellular pathways, predominantly through their association with specific syntaxin Q-SNAREs (Toonen and Verhage 2003).

Of the varied SM-syntaxin partners, Munc18c-syntaxin4 interactions are believed to exert a critically important role in the temporal control of insulin-stimulated GLUT4 storage vesicle exocytosis in muscle and adipose tissue (Tellam, Macaulay et al. 1997; Tamori, Kawanishi et al. 1998; Thurmond, Ceresa et al. 1998; Dugani and Klip 2005). The delivery of GLUT4 to the cell surface occurs by distinct signaling processes: (1) GLUT4 vesicle recruitment to the plasma membrane, (2) followed by phosphatidylinositol 3-kinase (PI3K)-dependent vesicle docking and fusion mediated by syntaxin4-containing SNARE complexes (Bose, Robida et al. 2004; Hodgkinson, Mander et al. 2005). Based on overexpression studies, Munc18c was initially proposed to function as a negative regulator of GLUT4 vesicle translocation in 3T3L1 adipocytes (Tellam, Macaulay et al. 1997; Thurmond, Ceresa et al. 1998). However, the failure of the PI3K inhibitor wortmannin to suppress GLUT4 externalization in adipocytes derived from Munc18c-null mice suggests that Munc18c inhibits docking and/or fusion under the control of the PI3K

pathway (Kanda, Tamori et al. 2005). Although the exact mechanism for this inhibition is not fully understood, Munc18c has been proposed to preclude the binding of syntaxin4 to its cognate SNAREs, vesicle-associated membrane protein 2 (VAMP2) and synaptosomal-associated protein of 23-kDa (SNAP23), preventing GLUT4 externalization in the absence of insulin (Araki, Tamori et al. 1997; Tellam, Macaulay et al. 1997; Thurmond, Ceresa et al. 1998).

In the absence of fine structural information, a model of Munc18c control over syntaxin4/SNARE complex formation is not easily predicted by other SM-syntaxin interactions due to the diversity in their modes of action. For example, the Munc18a-syntaxin1A complex participates in regulated neuroexocytosis and has high sequence homology to Munc18c-syntaxin4. Analysis of the syntaxin1A structure showed that an autonomously folded N-terminal three helix bundle, termed the Habc domain, reversibly folds over a helical H3 domain containing the SNARE motif (Dulubova, Sugita et al. 1999; Misura, Scheller et al. 2000; Margittai, Widengren et al. 2003). These two helical domains are separated by a short structured linker proposed to allow syntaxin1A to rapidly fluctuate between a folded (closed) conformation and an unfolded (open) conformation (Margittai, Widengren et al. 2003). The open conformation facilitates SNARE-SNARE pairing resulting from accessibility of the SNARE motif. The closed (SNARE-pairing inactive) conformation of syntaxin1A is stabilized by interaction with Munc18a (Dulubova, Sugita et al. 1999), precluding interactions with other SNAREs (Calakos, Bennett et al. 1994; Liu, Ernst et al. 2004). Thus, the association-disassociation of Munc18a suggests a mechanism for the regulation of the syntaxin SNARE motif through the control of syntaxin conformation. Yet, there is a lack of general correlation between SM function and a particular conformation of syntaxin. The situation is further complicated because not all syntaxins assume folded conformations. For instance, the SM proteins Sly1 and Vps45, which regulate trafficking of intracellular transport vesicles, bind to a conserved N-terminal domain found upstream of the Habc domain in their cognate syntaxins (Sly1 to syntaxins 5 and 18, and Vps45 to syntaxin16) (Dulubova, Yamaguchi et al. 2002; Yamaguchi, Dulubova et al. 2002; Bryant and James 2003).

This subset of SM proteins does not hinder the kinetics of SNARE pairings (Peng and Gallwitz 2002). Comparatively, the yeast Munc18 homologue Sec1p stimulates fusion through its interaction with the ternary SNARE complex, only binding weakly to monomeric Sso1p/syntaxin (Carr, Grote et al. 1999; Scott, Van Komen et al. 2004).

By analogy to the Munc18a-syntaxin1A interaction, the most prevalent model for Munc18c regulation of SNARE complex formation equates the association of Munc18c with syntaxin4 to the inhibition of GLUT4 storage vesicle docking and fusion. Yet, genetic studies suggest that the mechanism of Munc18c action may be different than Munc18a. For instance, the insulin-induced presentation of GLUT4 was enhanced in adipocytes prepared from Munc18c-null mice (Kanda, Tamori et al. 2005), while Munc18a deficiency was demonstrated to eliminate both evoked and spontaneous synaptic exocytosis (Verhage, Maia et al. 2000). Furthermore, it remains unclear whether Munc18c interacts solely with a single closed conformation of syntaxin4 as modeled by Munc18a-syntaxin1A interactions (Calakos, Bennett et al. 1994; Pevsner, Hsu et al. 1994), or additionally to an open conformation in the SNARE complex. Recent evidence indicates that *in vitro* Munc18c associates with the ternary SNARE complex (Widberg, Bryant et al. 2003; Latham, Lopez et al. 2006). In addition, Munc18c possesses an interaction site for the N-terminal amino acids of syntaxin4 resembling the syntaxin binding sites on Sly1 and Vps45 (Latham, Lopez et al. 2006). Yet, insulin (Thurmond, Ceresa et al. 1998) as well as N-ethylmaleimide (NEM) (Widberg, Bryant et al. 2003), which inhibits NSF-mediated SNARE core complex disassembly, have been reported to dissociate Munc18c from syntaxin4. Thus, there is growing evidence to suggest that the Munc18c-syntaxin4 association does not fit any single model for SM-syntaxin interactions.

The purpose of this study was to define the molecular properties of the Munc18c interaction with syntaxin4. Specifically, how the Munc18c-syntaxin4 complex influences SNARE core complex formation in the pathway of GLUT4 cycling. Our investigations utilized quantitative optical techniques including fluorescence resonance energy transfer (FRET) and

biochemical approaches to directly report the state of the Munc18c-syntaxin4 interaction *in vivo*. Using mutational analyses we address the mode of Munc18c binding to syntaxin4, including where and when the interaction occurs, and which structural motifs are important for function. Our findings indicate that syntaxin4 exists in a closed conformation which is stabilized by Munc18c, thus rendering the syntaxin4 SNARE domain unavailable for SNARE complex formation. Using the system of insulin-stimulated GLUT4 exocytosis, we furthermore demonstrate that the binding of Munc18c to an open conformation of syntaxin4 is not inhibitory to GLUT4 vesicle docking, yet is inhibitory to vesicle fusion in the absence of insulin. The maintenance of the Munc18c-SNARE interaction with such proximity to fusion suggests that Munc18c functions as a critical regulatory point in the temporal sequence for the initiation of fusion events.

Experimental Procedures

Chemicals and expression constructs – The following antibodies were used at 1:1000 dilution for Western Blotting: anti-syntaxin4 rabbit polyclonal (Sigma), anti-syntaxin1A mouse monoclonal HPC-1 (Sigma), anti-SNAP23 polyclonal (Synaptic Systems), anti-FLAG polyclonal (Sigma), and anti-c-myc mouse monoclonal 9B11 (Cell Signaling). To generate N-terminal fluoroprotein-labeled constructs, the following cDNAs were sub-cloned into the SalI-XbaI sites of pDNR-dual for use with the cre recombinase-mediated Creator System (Clontech): rat Munc18a (pGex-KG-Munc18a), rat syntaxin1A (pGEX-syntaxin1A[11]), rat Munc18c (pcDNA3-FLAG-Munc18c), human syntaxin4 (pcDNA4/TO/syntaxin4-myc$_2$-his) and human SNAP23 (pcDNA3-SNAP23) (gifts from J. Pevsner, R. Scheller, J. Pessin, T. Weimbs (syntaxin4 and SNAP23), respectively). The recipient vectors pLoxP-ECFP-C1 and pLoxP-EcYFP-C1 (Q39M mutant of pEYFP-C1; citrine) were generated and mutated to their monomeric forms (A206K) from pLoxP-EGFP-C1 (Clontech) as described previously (Liu, Ernst et al. 2004). To prepare pLoxP-mRFP1-C1, the cYFP sequence from pLoxP-EcYFP-C1 was replaced with mRFP1 (monomeric form) from

pRSETB-mRFP1 (a gift from R. Tsien) by PCR cloning. cDNAs in pDNR-dual were subcloned into the indicated recipient vectors using cre recombinase according to the manufacturer's instructions. To prepare recombinant fusion proteins in E. coli, syntaxin4_{1-275} (I276stop) and Munc18c were PCR amplified and cloned downstream of glutathione *S*-transferase (GST) cDNA contained in the pGEX-KG plasmid; pGEX-syntaxin$1A^{11}$ (syntaxin$1A_{1-267}$) was a gift from R. Scheller. pGex-KG-FLAG-loxP-Munc18c was created using a pGex-KG construct modified to include a loxP site suitable for use with the Clontech Creator system and an N-terminal FLAG epitope. The PCR-based Quikchange Site-Directed Mutagenesis kit (Stratagene) was used to construct the following mutants: EGFP-$SNAP23^{C/A}$, a cytosolic mutant lacking cysteine palmitoylation sites at 80, 83, 85 and 87, which were mutated to alanine; Munc18c (R240L); syntaxin1A (L165A/E166A, LE; I209A; and I233A), and the homologous mutations in syntaxin4 (L173A/E174A, LE; I217A; and I241A). Syntaxin4_{1-188} (ΔH3/TM) and syntaxin$1A_{1-181}$ were created by inserting an XbaI site with the TAG stop codon in frame at L189 and I182, respectively. The same XbaI site along with a SalI site upstream of the start codon was used to facilitate construction of the following syntaxin chimeras: syntaxin41 (syntaxin4_{1-188} + syntaxin$1A_{182-288}$) and syntaxin14 (syntaxin$1A_{1-181}$ + syntaxin$4_{189-297}$). Before use, the XbaI restriction sites were back-mutated in the syntaxin14 and syntaxin41 plasmids to eliminate the stop codon and restore the L189 in the syntaxin4 fragments and the I182 in the syntaxin1A fragments. The sequence fidelity of all expression constructs was confirmed by DNA sequencing (University of Michigan DNA Sequencing Core).

Cell culture and transfection – 3T3L1 fibroblasts (American Type Tissue Culture, Rockville, MD) were maintained in DMEM containing 10% bovine serum (Invitrogen). Following two days of confluence, differentiation was induced by addition of DMEM with 10% fetal bovine serum (FBS) containing 167 nM insulin, 0.25 μm dexamethasone, and 0.25 mM isobutylmethylxanthine

(IBMX) for three days, followed by DMEM/FBS containing insulin for 2 days, and subsequent removal of insulin for two days. Adipocytes were transfected by electroporation (0.16 kV, 950 μF) in PBS pH 7.4 (Invitrogen) with 50-200 μg of each plasmid. After electroporation, cells were allowed to adhere to coverglass for 18-24 hours in DMEM/FBS prior to imaging. In selected experiments cells were exposed to 100 nM insulin after 3 hours serum starvation in DMEM low glucose (Invitrogen) containing 0.5% FBS. HEK293-S3 cells, which contain a stably transfected N-type calcium channel (Liu, Ernst et al. 2004), were cultured in RPMI-1640 (Invitrogen) supplemented with 10% FBS (Invitrogen), 0.4 mg/ml hygromycin (Invitrogen), 0.4 mg/ml Geneticin (Invitrogen), and 1% penicillin/streptomycin (Invitrogen). Cells were plated on coverglass affixed to the bottom of 35mm dishes 12-24 hours prior to transfection using Lipofectamine2000 (Invitrogen). Before live cell imaging, cells were transferred to physiologic saline solution (PSS) containing 140 mM NaCl, 5 mM KCl, 5 mM glucose, 1 mM $MgCl_2$, 2.2 mM $CaCl_2$, 5 mM $NaHCO_3$, and 10 mM HEPES (pH 7.4).

Homology modeling of Munc18c-syntaxin4 complex – Rat Munc18c (Stxbp3; GenBank accession No. NP_446089) and syntaxin4 (STX4; GenBank accession No. NP_112387) sequences were threaded into the Munc18a-syntaxin1A structure (PDB No. 1DN1) using O, based on a ClustalW alignment. Helical register, assessed using PredictProtein, was comparable; sequence gaps and insertions were not modeled. Figures were made with MOLSCRIPT, RASTER 3D v2.1.2, and GIMP.

GST fusion proteins – Chemically competent BL21DE3(RIPL) *E. coli* (Invitrogen) containing pGex-KG-syntaxin$4_{1\text{-}275}$, pGex-KG-syntaxin$4_{1\text{-}275}^{LE}$, or pGEX-KG-Munc18c were cultured and induced with 100 nM IPTG for 5-6 hours at 27°C. Bacteria were lysed by French press (15000 PSI pressure differential) and the eluent was solubilized in PBS containing 1% Triton X-

100 for 1 h on ice. Proteins were subsequently purified using Glutathione-Sepharose (Pharmacia). Cleavage of the GST moiety from the fusion protein was accomplished by treatment with 1.4 NIH units human thrombin (Amersham) for 16 hours at 4°C. Purity of all isolated fusion proteins was confirmed by SDS-PAGE fractionation and subsequent visualization with Coomassie Blue or Western Blotting. Protein concentration was measured using the DC Protein Assay (Bio-RAD) against a BSA standard (Sigma).

Trypsin proteolysis assay – Trypsin digest of recombinant GST-syntaxin4$_{1\text{-}275}$ and GST-syntaxin4$_{1\text{-}275}^{LE}$ was modeled after Graham et al. (Graham, Barclay et al. 2004). Proteins were incubated at 5 μM concentration in a total volume of 50 μl containing 60 nM Trypsin (Type IX-S; Sigma) in PBS (pH 7.4) for the times indicated. During trypsin incubation, GST fusion proteins remained bound to Glutathione-Sepharose beads. The reactions were terminated by the addition of SDS sample buffer and immediate boiling. After separation by 12% SDS PAGE, the samples were transferred to nitrocellulose and probed for syntaxin1A or syntaxin4. Proteins were visualized with a HRP-conjugated secondary antibody and ECL substrate (Amersham).

Co-immunoprecipitation – For each treatment, a 6-well plate of confluent HEK293-S3 cells was transiently transfected with pcDNA4/TO/syntaxin4^{LE}-myc$_2$ ± pcDNA3-FLAG-Munc18c. After a two day expression period, cells were rinsed twice in PSS and lysed in a Dounce homogenizer in a buffer containing 2% sucrose, 1 mM EDTA, and 20 mM Tris (pH 7.5). After the homogenate was centrifuged (300 x *g* for 3 minutes) to pellet the nuclei, the supernatant was diluted 1:1 in IP Buffer (150 Tris, pH 7.4; 1 mM $MgCl_2$; 0.1 mM EGTA; 2% Triton X-100). Samples were normalized for lysate volume and concentration (2-3 μg/μl), and incubated with 10 μg anti-myc 9B11 monoclonal antibody (Cell Signaling) for 4 hours at 4°C. The samples were then incubated with ProteinG-Sepharose beads (Pierce) for 1 hour, and washed in IP Buffer. Finally the pellet

was resuspended in SDS sample buffer and subject to fractionation by SDS PAGE and Western blotting.

In vitro binding assay – For all binding reactions *in vitro* the GST moiety was cleaved from purified GST-syntaxin4$_{1\text{-}275}$, GST-syntaxin4$_{1\text{-}275}^{LE}$, and GST-Munc18c. Reactions used 0.03-30 pmols of Munc18c in a dilution series spotted in quadruplicate on nitrocellulose (BA-83, Schleicher and Schuell). After blocking in 2% milk, the blots were incubated with 500 nM syntaxin4$_{1\text{-}275}$ or syntaxin4$_{1\text{-}275}^{LE}$ for ≥12 hours at 4°C. Syntaxin4 proteins were visualized using an anti-syntaxin4 polyclonal antibody and HRP-conjugated secondary antibody as described above. Integrated intensity (area*intensity) was quantified using Metamorph (version 6.3r5, Universal Imaging, Inc., Malvern, PA).

Measurement of FRET stoichiometry by sensitized emission – Live cell imaging of FRET was performed on transfected 3T3L1 adipocytes and HEK293 cells 24 hours after transfection. As false positive FRET signals have been observed when cytoplasmic donors come into contact with membrane compartmentalized acceptors (Vogel, Thaler et al. 2006), syntaxin4 was purposefully tagged with CFP. However, performing the experiments using CFP-Munc18c and cYFP-syntaxin4 resulted in similar FRET efficiency values (data not shown). Measurement of sensitized emission FRET was carried out as previously described (Hoppe, Christensen et al. 2002; Liu, Ernst et al. 2004). The methodology employed an inverted fluorescence microscope (Olympus, IX71) equipped with the following components: a TILL-Photonics Polychrome IV xenon-lamp based monochrometer (TILL-Photonics, Grafelfing, Germany), polychroic mirror that allowed excitation of multiple fluorophores (436-500nm, Chroma Technology Corp., Brattleboro, VT), a Planapo 60x water immersion objective (1.2 NA), a multispec microimager (Optical Insights, Santa Fe, NM) containing dichroic splitter (505dcxr) and emission filters

(D465/30 and HQ535/30) to allow simultaneous two channel monitoring of emission fluorescence, and a cooled digital CCD camera (TILL IMAGO QE). The multispec microimager hardware was calibrated to allow pixel-by-pixel alignment of images, and offline adjustments were made using the TILL-Vision software. All analyses of the acquired images were performed using Metamorph image-processing software as previously described (Hoppe, Christensen et al. 2002; Liu, Ernst et al. 2004). The apparent efficiency of acceptor (monomeric cYFP) in complex (E_A), the apparent efficiency of donor (monomeric ECFP) in complex (E_D) and mole fraction of acceptor to donor (*RATIO*) values were determined using the following equations: $E_A = \gamma[((DA - \beta*DD)/\alpha*AA) - 1](1/E_C)$; $E_D = [1 - (DD/((DA - \alpha*AA - \beta*DD)*(\xi/\gamma) + DD))](1/E_C)$;; and $RATIO = (\xi/\gamma^2)*[\alpha*AA/((DA - \alpha*AA - \beta*DD)*(\xi/\gamma) + DD)]$ (Hoppe, Christensen et al. 2002), where images are abbreviated as follows: *DD*, donor excitation-donor emission; *DA*, donor excitation-donor emission; *AA*, acceptor excitation-acceptor emission; E_C, characteristic efficiency (0.37; (Hoppe, Christensen et al. 2002)). Donor and acceptor excitations were 436 nm and 500 nm, respectively. Empirically determined constants were established in HEK293 cells: α, 0.017; β, 0.9406; γ, 0.0658; ξ, 0.0147. For all measurements E_A values were determined in regions of the cell where the mole fraction between cYFP-Munc18c and CFP-syntaxin4 (*RATIO*) was between 0.9-1.1; E_D is comparable to E_A over this *RATIO* range.

Resolution of SNAP23$^{C/A}$-SNARE interactions by cytosolic photobleach and membrane FRAP – GFP-SNAP23$^{C/A}$ bound to syntaxin4 at the plasma membrane was observed by expression of the proteins when viewed with the FV500 Olympus FluoView laser scanning confocal microscope. In order to resolve the relative amount of plasmalemmal GFP-SNAP23$^{C/A}$, images were taken before and after 1 min cytosolic photobleach (>90% bleach) using the 488 nm laser line of the argon laser. The localization of GFP-SNAP23$^{C/A}$ fluorescence intensity remaining after photobleach was quantified using linescans averaged over a 10 pixel width (~1/8 cell diameter)

normalized to peak intensity for each cell. For FRAP experiments, cytosolic photobleach was followed by a 10s photobleach (>50%) of the cell membrane using simultaneous excitation with the 488 nm line of the Argon laser and 543 nm line of the Helium Neon laser to facilitate simultaneous bleach of GFP and RFP, respectively. FRAP images were taken following a 1.5 minute recovery period.

Quantification of insulin-induced GLUT4 plasma membrane insertion – 3T3L1 adipocytes stably expressing myc_7-GLUT4-GFP were prepared as previously described (Chang, Chiang et al. 2006) using a retroviral vector pMX-GLUT4*myc7*-EGFP (a gift from H. Lodish) (Bogan, McKee et al. 2001). Cells were electroporated as described above with pcDNA-FLAG-Munc18c and pLoxP-ECFP-syntaxin4, or mutants of syntaxin4 as described in the figures. As a control experiment to verify the functionality of N-terminally tagged syntaxin4 (Fig. 2.11), adipocytes were electroporated with pcDNA-syntaxin4^{LE} and pLoxP-mCerulean-Munc18c. 24 hours after electroporation, adipocytes were serum starved for 3 hours in DMEM containing 0.5% FBS. Subsequently, cells were treated with 100 nM insulin for the times indicated, fixed in PBS containing 4% paraformaldehyde, and quenched with 50 mM glycine for 5 minutes. Externalized myc_7-GLUT4-GFP was visualized by exposing the cells to an anti-myc monoclonal antibody 9E10 (Santa Cruz Biotechnology) without permeabilization, followed by Alexa^{594}-conjugated goat anti-mouse secondary antibody (Molecular Probes) as discussed (Chang, Chiang et al. 2006). For cell counting experiments, ≥75 cells from each treatment possessing peripheral CFP-syntaxin4 fluorescence were blindly examined for peripheral GFP fluorescence and/or surface Alexa594 fluorescence using an Olympus IX71 microscope equipped with a dual-pass GFP/mRFP1 filter set (Chroma Technology Corp). For quantification of GLUT4 localization, cells with equivalent CFP (syntaxin) and GFP (GLUT4) were chosen based on equivalent integrated density (cell area x intensity) from a 500 ms image taken at 436 and 480 nm, respectively. To quantify CFP and GFP localization, linescans (10 pixel-width averages) drawn

from the outside of the cell to the interior were normalized to fluorescence intensity at the plasma membrane region and plotted as a function of distance from the plasma membrane.

Results

Modeling of syntaxin4 structure and generation of a constitutively open syntaxin4 mutant – To facilitate design of specific syntaxin4 mutations that would aid in characterization of the conformational states and important domains of syntaxin4 for Munc18c binding, we initially constructed a homology model of syntaxin4 based on the reported crystal structure of syntaxin1A in complex with Munc18a (nSec1/Munc18-1) (Misura, Scheller et al. 2000). The Munc18c and syntaxin4 sequences (identity: 50%, Munc18; 46%, syntaxin) were threaded directly on the crystal structure of the Munc18a-syntaxin1A complex (Protein Data Bank 1DN1). No modeling predictions were made in areas with sequence gaps or insertions. Figure 2.1A shows the generated Munc18c-syntaxin4 homology model. An analysis of the model over highly conserved regions between syntaxin1A and syntaxin4 yielded two important observations. First, the outer surface of the syntaxin4 Habc helices contain most of the non-conserved residues, whereas the regions of intramolecular interactions between the Habc domain and the H3 domain were found to be highly conserved (Fig. 2.1B, circled). This structural similarity suggested that the helical packing which allows syntaxin1A to adopt a closed conformation would also allow syntaxin4 to adopt a closed conformation. Second, the Habc-H3 linker region is stabilized against the Habc and H3 domains by a highly conserved hydrophobic pocket. A mutation in the syntaxin1A linker helix (L165A/E166A; LE) has been reported to destabilize the N-terminal helices from interaction with the SNARE motif and result in a constitutively open syntaxin1A conformation (Dulubova, Sugita et al. 1999). This open conformation impairs Munc18a binding to syntaxin1A, strongly facilitating its interaction with other SNAREs (Parlati, Weber et al. 1999; Richmond, Weimer et al. 2001; Graham, Barclay et al. 2004; Liu, Ernst et al. 2004). From the structural prediction (Fig. 2.1C), the homologous residues in syntaxin4, L173 and E174, lie in a conserved

pocket of the linker helix. The hydrophobic contacts of L173 are maintained with I156, L160, and the semiconserved V168 (I149, L153, and T160 in syntaxin1A). The hydrophobic regions of the non-conserved residues, D170 and R157 (S162 and Q150 in syntaxin1A), may form Van der Waal's interactions contributing to the hydrophobic pocket for L173, whereas their charged portions are solvent exposed. E174 maintains one conserved salt bridge with R149, although a second with V153 (R142 and K146 in syntaxin1A) is lost. Taken together, the model predicts that significant L173 and E174 interactions are likely to be disrupted by dual mutation to alanine (L173A/E174A), hereafter termed syntaxin4^{LE}, and to confer a constitutively open conformation on the syntaxin4 mutant.

To determine whether the syntaxin4^{LE} conformation is different from the wildtype protein in a manner consistent with a constitutively 'open' syntaxin4, we examined the effect of partial trypsin proteolysis on GST-syntaxin4$_{1-275}$ and GST-syntaxin4$_{1-275}^{LE}$. Figure 2.1A shows that proteolytic treatment of wildtype GST-syntaxin4$_{1-275}$ resulted in two dominant cleavage products recognized by the anti-syntaxin4 polyclonal antibody which fractionated at 15- and 30-kDa. After equivalent incubation, these products were dramatically reduced or absent in the GST-syntaxin4$_{1-275}^{LE}$ digest. The increased resistance of wildtype syntaxin4 to trypsin relative to the LE mutant suggests that the wildtype protein is more compact in structure, thereby limiting proteolysis, whereas the LE mutation promotes a more accessible, or open, structure for the proteolytic activity of the enzyme. As a control experiment, we also tested the trypsin sensitivity of GST-syntaxin1A$_{1-267}^{LE}$ (L165A/E166A) relative to wildtype GST-syntaxin1A$_{1-267}$. Figure 2.1B shows that the wildtype syntaxin1A was more resistant to trypsin than that of syntaxin1A carrying the L165A/E166A mutation, confirming the efficacy of the approach initially published by Graham and colleagues (Graham, Barclay et al. 2004). These parallel results suggest that syntaxin4, like syntaxin1A, forms a self-associated structure folded about the linker region. The syntaxin4 LE mutation allowed investigation of the effects of a less restricted syntaxin4 conformation on Munc18c binding.

Munc18c interaction with the closed and open conformations of syntaxin4 in vivo – Syntaxin4 has been reported to facilitate insulin-regulated GLUT4 vesicle externalization in 3T3L1 adipocytes. By comparison, Munc18c overexpression exerts an inhibitory effect on the same pathway through its interaction with syntaxin4 (Tellam, Macaulay et al. 1997; Tamori, Kawanishi et al. 1998; Thurmond, Ceresa et al. 1998), signifying that the level of complexation of Munc18c with syntaxin4 is an important determinant of SNARE complex formation. To measure the structural parameters important for the direct Munc18c-syntaxin4 protein interaction in living 3T3L1 adipocytes, we employed expression of cYFP-Munc18c and CFP-syntaxin4 as a fluorescence resonance energy transfer (FRET) pair. Sensitized emission FRET stoichiometry yields a spatial map of the apparent FRET efficiency of CFP donor (E_D) and cYFP acceptor (E_A) in complex, as well as the mole fraction of acceptor to donor (*RATIO*) (Hoppe, Christensen et al. 2002). Figure 2.3A (*upper panel*) shows an image series of a representative adipocyte coexpressing cYFP-Munc18c and CFP-syntaxin4. Both the CFP and cYFP fluorescence is enriched at the plasma membrane region relative to the cytosol, as expected for the plasma membrane localization of the Munc18c-syntaxin4 complex. Moreover, the corresponding FRET images E_A and E_D for this cell indicated that substantial FRET occurred between the coexpressed cYFP-Munc18c and CFP-syntaxin4 proteins, thereby indicating direct protein-protein interactions. The absolute values of FRET (E_A and E_D) are sensitive to the relative levels of expression of the FRET donor to acceptor (*RATIO*). Therefore, Figure 2.3B compares E_A values averaged from many cells where the range over which the FRET values are averaged was restricted to pixels where the molar ratio of cYFP to CFP expression is within the range of 0.9-1.1. This strategy allowed us to compare E_A values between cells and across treatments. Importantly, as a control to confirm that the FRET signal resulted from a specific and direct interaction between Munc18c and syntaxin4, we tested the effect of CFP-syntaxin4 coexpressed with a single point mutant of Munc18c (cYFP-Munc18c^{R240L}). This temperature-insensitive

mutant was based on the previously characterized temperature-sensitive SM mutants, Munc18c^{R240K} and the *S. ceriviseae* homolog Sly1p^{R266K}, which demonstrated a strongly reduced affinity of interaction with syntaxin4 and Sed5p, respectively (Cao, Ballew et al. 1998; Thurmond and Pessin 2000). In following, the measured FRET efficiency was reduced by ~7-fold with respect to control on coexpression of cYFP-Munc18c^{R240L} with CFP-syntaxin4. These results establish that FRET between cYFP-Munc18c and CFP-syntaxin4 is specific to the bimolecular interaction in 3T3L1 adipocytes and sensitive to changes in Munc18c-syntaxin4 binding affinity. Notably, that CFP-syntaxin4, but not cYFP-Munc18c^{R240L}, localized to the plasma membrane suggests that syntaxin4 does not require a stable interaction with Munc18c for plasma membrane targeting. We next used the FRET assay to determine if the constitutively open mutant of syntaxin4 (CFP-syntaxin4^{LE}) was capable of direct interaction with Munc18c. Remarkably, we observed only a slight reduction (~10%) in cYFP-Munc18c energy transfer with CFP-syntaxin4^{LE} as compared to the wildtype control, indicating the strong association of Munc18c with both closed and open conformations of syntaxin4.

Our above FRET experiments in adipocytes demonstrated a significant interaction of Munc18c to syntaxin4^{LE}, which contrasts with the strongly reduced interaction reported for the LE mutant of syntaxin1A with Munc18a *in vitro* and *in vivo* (Graham, Barclay et al. 2004; Liu, Ernst et al. 2004). This indicates that divergence occurs among vertebrate SM-syntaxin protein interactions. To directly compare the interaction of Munc18c and Munc18a with their cognate syntaxins *in vivo*, we measured FRET between the protein pairs when expressed in a common reporter cell line, HEK293 cells. Figure 2.4A indicates that the apparent efficiency (E_A) of cYFP-Munc18c in complex with CFP-syntaxin4^{LE} was mildly reduced from that measured with CFP-syntaxin4. By contrast, the apparent efficiency of energy transfer between Munc18a and syntaxin1A^{LE} was ~50% lower than that measured for syntaxin1A, a result consistent with the strong reduction in affinity conferred by the syntaxin1A^{LE} mutation reported in other studies (Graham, Barclay et al. 2004; Liu, Ernst et al. 2004). To further gauge the competence of

Munc18c to interact with syntaxin4^{LE} in live cells we examined the ability of RFP-syntaxin4^{LE} to compete with wildtype CFP-syntaxin4 for the binding of cYFP-Munc18c (Fig. 2.4B). The use of an RFP probe facilitated the setting of roughly equivalent levels of the RFP-syntaxins between treatments. We found that RFP-syntaxin4^{LE} expression impaired cYFP-Munc18c energy transfer to CFP-syntaxin4 by ~70%. When the RFP and CFP probes were exchanged to measure FRET between cYFP-Munc18c and CFP-syntaxin4^{LE} in the presence of RFP-syntaxin4, energy transfer was similarly reduced. Taken together, these data demonstrate that Munc18c binds efficiently to syntaxin4 in either a closed or open conformation.

FRET efficiency is a sensitive function of the distance between the donor and acceptor fluorophores, and is also sensitive to the relative orientation of the donor emission dipole and the acceptor absorption dipole. Therefore, we next investigated whether the small difference in the apparent FRET efficiency (E_A) of cYFP-Munc18c with CFP-syntaxin4 and CFP-syntaxin4^{LE} could be attributed to a change in the characteristic efficiency of the interaction (E_C) associated with conformational differences between syntaxin4 and syntaxin4^{LE}, or to changes in the affinity of the interaction. To obtain an estimate of E_C for the interactions in live cells we varied the expression ratio of cYFP-Munc18c to CFP-syntaxin4 such that it encompassed an extended *RATIO* range, thus driving the apparent efficiency to asymptote to E_C. Figure 2.4C shows the combined data for the imaged cells, plotting the calculated E_A values of each image pixel versus the corresponding inverse *RATIO* values. A statistically significant difference in apparent E_C was found between the LE mutant (E_C=26.92±0.05, n=67) and the wildtype syntaxins (E_C=29.59±0.04, n=61). This difference may account for the reduced FRET between cYFP-Munc18c and CFP-syntaxin4^{LE} when compared with wildtype CFP-syntaxin4. However, the fit rate constants also differed slightly between conditions, indicating that small differences may also occur in the affinity of the protein-protein interactions. To test for differences in affinity, we measured the *in vitro* binding of bacterially expressed and purified syntaxin4$_{1\text{-}275}$ or syntaxin4$_{1\text{-}275}^{LE}$ to Munc18c spotted in a dilution series (0.03-30 pmols) on nitrocellulose (Fig. 2.5). To

verify that equal amounts of each syntaxin4 protein were used in the binding reaction, small standardized amounts of syntaxin4$_{1\text{-}275}$ or syntaxin4$_{1\text{-}275}^{LE}$ were spotted alongside Munc18c. No apparent differences were observed between the wildtype or syntaxin4^{LE} binding to Munc18c as measured over a 3 log concentration range, further confirming the promiscuous interaction of Munc18c with both the closed and open conformations of syntaxin4.

The syntaxin4 binding sites for Munc18c – The interaction of Munc18c with multiple conformations of syntaxin4 is in direct contrast to belief that vertebrate exocytotic SM proteins bind solely to the closed form of syntaxin. As a possible explanation, Munc18c-syntaxin4 interactions may resemble a subset of SM proteins that function in the ER, Golgi, TGN, and endosomal networks, Sly1 and Vps45, which are known to require only short N-terminal sequences of their cognate syntaxins (Dulubova, Yamaguchi et al. 2002; Yamaguchi, Dulubova et al. 2002; Bryant and James 2003). Since syntaxin4 shares some sequence homology with the motif that allows rSly1 to bind the N-terminus of syntaxins 5 and 18 (Fig. 2.6A), it remained possible that the N-terminus of syntaxin4 upstream of the Habc domain could be important for binding to Munc18c, as first suggested by *in vitro* studies (Latham, Lopez et al. 2006). Yamaguchi and colleagues (Yamaguchi, Dulubova et al. 2002) previously demonstrated that an arginine substitution at D5 in Sed5p/syntaxin5, a residue common to syntaxins 1-4 as D3, resulted in complete loss of Sly1p binding when mutated to arginine. Shown in Figure 2.6B, CFP-syntaxin4^{D3R} results in a ~40% reduction in FRET with cYFP-Munc18c when compared with the wildtype proteins expressed in HEK293-S3 cells. Moreover, the D3R mutant completely eliminated Munc18c binding to the constitutively open mutant of syntaxin4. However, the N-terminus of syntaxin4 is insufficient to bind Munc18c since a mutant of CFP-syntaxin4 lacking its H3 and transmembrane domains (ΔH3/TM) exhibited negligible energy transfer with cYFP-Munc18c. The N-terminus of syntaxin4 could therefore stabilize the association of Munc18c with both the closed and open syntaxin4 conformations. Furthermore, these results point to a

mode of Munc18c-syntaxin4 binding that shares the characteristics of SM binding to both ER/Golgi syntaxins as well as the exocytotic syntaxins, which require both the N- and C-termini of syntaxin for SM binding.

We next assessed the extent of divergence between the Munc18c-syntaxin4 binding interaction and the Munc18a-syntaxin1A interaction, which facilitates neuroexocytosis. To ascertain whether conserved C-terminal syntaxin4 residues are important for Munc18c binding specificity, we substituted the syntaxin1A H3 domain into syntaxin4 after residue 189 (syntaxin41) (Fig. 2.6B). FRET between Munc18c and syntaxin41 was not different from wildtype syntaxin4, indicating that Munc18c likely utilizes residues conserved between the two syntaxins to bind the SNARE domain. Mutation of syntaxin1A at two conserved residues, I209 and I233, have been reported to reduce binding with SNAP25 and Munc18a, respectively (Kee, Lin et al. 1995; Wu, Fergestad et al. 1999; Graham, Barclay et al. 2004; Liu, Ernst et al. 2004). These two amino acids lie within the group of hydrophobic residues that form the interior of the fully assembled SNARE complex. Therefore, we tested the homologous alanine mutations in syntaxin4, I217A and I241A on Munc18c binding. FRET between cYFP-Munc18c and CFP-syntaxin4^{I217A} was found to be reduced moderately (~16%) when compared with wildtype syntaxin4. Yet, I217A did not affect binding of Munc18c to constitutively open syntaxin4. These results are consistent with the prediction of the model of Figure 2.1A: I217A is not expected to directly contact Munc18c, but may disrupt the helical packing of syntaxin4 in the closed conformation. Comparatively, I241 is predicted to be a critical residue for contacting the central cavity of Munc18c, and it reduced interaction with wildtype syntaxin4 by approximately 60%. To an equivalent extent, the I241A mutation impaired the interaction of Munc18c with the open mutant of syntaxin4, revealing that the membrane-adjacent SNARE domain is critically important for Munc18c binding regardless of syntaxin4 conformation. Given the effects of the D3R mutant and the I241A mutant on Munc18c binding, our data indicate that Munc18c's actions

to regulate SNARE complex formation require association with both the N- and C-termini of syntaxin4.

*Effects of syntaxin4 conformation and Munc18c binding on Q-SNARE complex formatio*n – The nucleation of syntaxin4-mediated SNARE complex formation is believed to be negatively regulated by Munc18c (Araki, Tamori et al. 1997; Tellam, Macaulay et al. 1997; Tamori, Kawanishi et al. 1998; Thurmond, Ceresa et al. 1998; Thurmond and Pessin 2000; Kanda, Tamori et al. 2005). As Munc18c binds to both closed and open conformations of isolated syntaxin4 (Figs. 2.3-6) as well as to the syntaxin4-SNAP23-VAMP2 complex *in vitro* (Widberg, Bryant et al. 2003; Latham, Lopez et al. 2006), we next investigated whether the opening of syntaxin4 is sufficient to relieve Munc18c's inhibition of SNARE complex nucleation *in vivo*. To address this question we developed an optical reporter system to assess how Munc18c affects the interaction of closed or constitutively open syntaxin4 with SNAP23 (Fig. 2.7A). We expressed limiting quantities of syntaxin4 in living HEK293-S3 cells with an excess of GFP-SNAP23$^{C/A}$, a cytosolic mutant of SNAP23 lacking its four-cysteine palmitoylation sequence (Vogel, Cabaniols et al. 2000). After a 1 minute photobleach of a delimited region within the cytosol, GFP-SNAP23$^{C/A}$ was resolved at the plasma membrane, consistent with the formation of a dimeric SNAP23-syntaxin4 complex. The additional expression of mRFP-Munc18c resulted in the complete loss of GFP-SNAP23$^{C/A}$ signal after photobleach, signifying that GFP-SNAP23$^{C/A}$ was freely diffusible and not tethered at the plasma membrane. This result intimates that Munc18c binding to syntaxin4 occludes SNAP23 binding to syntaxin4. Indeed, the presence of membrane-associated mRFP-Munc18c was observed after the photobleach, indicative of its binding to syntaxin4. The membrane association of Munc18c was not due to binding of endogenous proteins in the HEK293 cells, since expressed Munc18c was cytosolic in the absence of expressed syntaxin4 (data not shown). In summary, the data are consistent with Munc18c occluding

syntaxin4 interactions with SNAP23 *in vitro* (Araki, Tamori et al. 1997). Of specific importance, we next investigated if the association of Munc18c with the open form of syntaxin4 inhibits SNAP23 binding. For this analysis we coexpressed syntaxin4^{LE} with GFP-SNAP23$^{C/A}$ in the absence or presence of mRFP-Munc18c. After photobleach, GFP-SNAP23$^{C/A}$ remained bound to syntaxin4^{LE} despite the association of RFP-Munc18c at the membrane, signifying that the conformational transition of syntaxin4 is sufficient to relieve the inhibition of Munc18c on SNAP23 binding. The localization of GFP-SNAP23$^{C/A}$ in both experiments was quantified using linescans drawn from the outside of the cell to its center (Fig. 2.7B). The sharp "ear" in the linescan is consistent with membrane localization of GFP-SNAP23$^{C/A}$, whereas the GFP-intensity plateaus in cells where photobleach of diffusible GFP-SNAP23$^{C/A}$ has occurred upon addition of mRFP1-Munc18c. To confirm that a Munc18c-syntaxin4^{LE}-SNAP23$^{C/A}$ complex is formed on the plasma membrane, we performed fluorescence recovery after photobleaching (FRAP) experiments on the plasma membrane following the cytosolic photobleach. As anticipated, in the syntaxin4^{WT}/RFP-Munc18c/GFP-SNAP23$^{C/A}$ coexpression condition, no further bleaching of GFP was observed on the membrane, although membrane-associated RFP-Munc18c signal recovered after membrane photobleach, consistent with the Munc18c inhibition of Q-SNARE complex formation (Fig. 2.9). However, that both RFP-Munc18c and GFP-SNAP23$^{C/A}$ signals recover after a subsequent plasma membrane photobleach when coexpressed with syntaxin4^{LE} supports the interpretation that a Munc18c-syntaxin4^{LE}-SNAP23$^{C/A}$ complex is formed specifically at the plasma membrane.

As a final measure of whether the interaction of Munc18c affects Q-SNARE complex formation, we tested for co-immunoprecipitation of the proteins when coexpressed in HEK293-S3 cells. Since the HEK293 cell line contains endogenous syntaxin4, an epitope tag was used to limit immunoprecipitation to proteins interacting with the open mutant of syntaxin4 (syntaxin4^{LE}-myc$_2$), thereby facilitating a direct comparison with syntaxin4^{WT}-myc$_2$. As shown in Figure 2.7C, immunoprecipitation with an anti-myc antibody resulted in a co-precipitation of endogenous

SNAP23 only when syntaxin4^{LE}, not syntaxin4^{WT}, was used for pulldown. Moreover, the syntaxin4^{LE}-SNAP23 complex was not dissociated by the additional overexpression of FLAG-Munc18c, which also bound to expressed syntaxin4^{LE}. Comparatively, coexpression of FLAG-Munc18c inhibited the binding of syntaxin4^{WT}-myc$_2$ to SNAP23. Importantly, detectable levels of both SNAP23 and FLAG-Munc18c were present equivalently in the lysate and supernatant in cells lacking expressed syntaxin4, which demonstrates that both proteins were specifically pulled down by the myc-tagged syntaxins. Since coprecipitation of Munc18c and SNAP23 may be explained by immunoprecipitation of a mixture of syntaxin4^{LE} in heterodimeric complex with Munc18c and SNAP23, we tested for a Munc18c-syntaxin4^{LE}-SNAP23 tripartite complex, as suggested by the i*n vitro* binding of Munc18c to preformed syntaxin4$^{\Delta TM}$-SNAP23 binary complexes (Latham, Lopez et al. 2006). While expression of Munc18c inhibited co-precipitation of syntaxin4^{WT} by myc-SNAP23 (Fig. 2.8, *left panel*), immunoprecipitation of myc-tagged SNAP23 resulted in co-precipitation of both expressed syntaxin4^{LE} and FLAG-Munc18c (Fig. 2.8, *middle panel*). Notably, SNAP23 did not bind directly to Munc18c such that pulldown of Munc18c must have occurred through a trimeric complex (Fig. 2.8, *right panel*). Endogenous VAMP2 was not found associated with this complex, suggesting that either VAMP2 is prohibited from entering SNARE complexes when Munc18c is bound (Tellam, Macaulay et al. 1997), or that ternary SNARE complex formation was transient and went undetected by our assay. However, it is possible to conclude from both the photobleach analysis and immunoprecipitation experiments that (1) Munc18c inhibition of Q-SNARE complex formation is relieved by a conformational change in syntaxin4, and (2) Munc18c binding to Q-SNARE complexes suggests an additional regulatory capacity on downstream fusion events.

Functional effects of Munc18c-syntaxin4 binding states on GLUT4 trafficking – The above results demonstrate two distinct binding states of the Munc18c-syntaxin4 interaction: Munc18c binding to a conformation of syntaxin4 that is inhibitory to SNARE complexes, and furthermore

to an open conformation, through binding to Q-SNARE complexes (Figs. 2.7-9). We next sought to determine the functional correlate of each Munc18c-syntaxin4 binding state on GLUT4 vesicle plasma membrane recruitment and fusion under expression conditions favoring Munc18c's interaction with either the closed or open forms of syntaxin4. Our assay of SNARE complex formation was based on quantification of the insulin-stimulated plasma membrane insertion of GLUT4 storage vesicles in 3T3L1 adipocytes stably expressing myc_7-GLUT4-GFP (Bogan, McKee et al. 2001; Chang, Chiang et al. 2006). In these cells, the resting distribution of GLUT4 vesicles is primarily in intracellular compartments, whereas insulin promotes a large net increase in the number of plasma membrane-bound transporters, catalyzed by syntaxin4/SNARE complexes (Dugani and Klip 2005). The movement of GLUT4 was monitored by measuring GFP fluorescence at the cell periphery. Immunostaining of the exofacial myc_7 epitope, contained in the first extracellular loop of GLUT4, was used to distinguish vesicle fusion from vesicle plasma membrane localization.

We examined the effect of Munc18c overexpressed with CFP-syntaxin4^{WT}, CFP-syntaxin4^{LE}, or CFP-syntaxin4^{I241A} on GLUT4 trafficking in 3T3L1 adipocytes. The cells were fixed before or after stimulation with 100 nM insulin, immunostained against the myc epitope, and blindly scored for the presence of translocated (peripheral GFP) or fused (peripheral indirect myc immunofluorescence) GLUT4 vesicles (summarized in Table 2.1). Representative confocal images for each treatment are shown in Figure 2.10A. In the absence of insulin, the extent of GLUT4 movement to the cell periphery in cells expressing CFP-syntaxin4^{WT} and Munc18c was limited to 18±10% of cells (n=75), with very little vesicle fusion (2.5±1.5%). Insulin stimulated a ~4.5-fold increase in vesicle recruitment (83±4%, n=114). These results are comparable to GLUT4 recruitment in untransfected adipocytes in the absence (12±8%, n=75) and presence (95±3%, n=75) of insulin. By comparison, 79±3% (n=100) of the cells expressing CFP-syntaxin4^{LE} displayed unregulated recruitment of GLUT4 vesicles to the plasma membrane in the

absence of insulin, despite the presence of coexpressed Munc18c (Table 2.1). To rigorously quantify the GLUT4 localization changes induced by in the Munc18c/syntaxin4^{LE}-expressing cells in the absence of insulin, we examined cells exhibiting equivalent expression of both CFP-syntaxin4 (or mutants) and myc$_7$-GLUT4-GFP across treatments (Fig. 2.10B). As depicted in Fig. 2.10C, CFP and GFP fluorescence intensity was measured along a 10 pixel wide line, and average fluorescence intensities were plotted as a function of distance from the plasma membrane. CFP-syntaxin4^{WT} and CFP-syntaxin4^{LE}, each exhibited proper membrane localization when expressed with Munc18c. Yet, only cells expressing CFP-syntaxin4^{LE} exhibited high amounts of plasma membrane localized myc$_7$-GLUT4-GFP. Thus, GLUT4 vesicle recruitment was strictly promoted by the conformational change in syntaxin4. However, that only 5±3% of the cells co-expressing syntaxin4^{LE} and Munc18c exhibited GLUT4 fusion (without insulin) (Table 2.1) suggests a further mechanism exists to arrest GLUT4 vesicles at the plasma membrane without permitting vesicle fusion. To eliminate the possibility that the CFP tag used on the syntaxin4 constructs inhibits fusion, we transfected adipocytes with unlabeled syntaxin4^{WT} or syntaxin4^{LE} cotransfected with Cerulean-Munc18c. Coexpression of syntaxin4 was confirmed based on the plasma membrane targeting of Cerulean-Munc18c (Fig. 2.11), which does not occur to a significant extent in the absence of overexpressed syntaxin4. As before, GLUT4 vesicles were found abnormally docked in the absence of insulin in cells expressing syntaxin4^{LE} (but not syntaxin4^{WT}) and Cerulean-Munc18c. These complementary results support the interpretation that a conformational change in syntaxin4 is sufficient to tether GLUT4 vesicles to the plasma membrane without allowing their fusion.

Notably, our syntaxin4 experiments were performed with overexpressed Munc18c, which leaves open the possibility that Munc18c is required for either GLUT4 vesicle docking or the conformational switch in syntaxin4 at either the docking or fusion stages of GLUT4 trafficking. To test these possibilities, we overexpressed Munc18c with CFP-syntaxin4^{I241A}, which exhibits reduced binding with Munc18c regardless of syntaxin4 conformation. In

unstimulated adipocytes GLUT4 movement to the plasma membrane was unaffected (12±4%, *n*=75) (Fig. 2.10D), indicating Munc18c binding to syntaxin4 is not strictly required to inhibit GLUT4 vesicle recruitment, consistent with results in Munc18c-null cells (Kanda, Tamori et al. 2005). In insulin-stimulated cells, CFP-syntaxin4^{I241A} displayed a slight but significant increase in the percentage of cells displaying GLUT4 fusion (65±1%, *n*=75) when compared with coexpression of Munc18c and CFP-syntaxin4^{WT} (46±2%, *n*=114) or CFP-syntaxin4^{LE} (52±2%, *n*=125). Thus, the association of Munc18c with syntaxin4 may correlate with the extent of insulin-regulated GLUT4 fusion.

Discussion

Sec1/Munc18 (SM) proteins exert functional effects at different stages of SNARE complex assembly primarily through specific, non-conserved, interactions with cognate syntaxins. In this study we have focused on identifying and characterizing the molecular underpinnings of the interactions between the ubiquitous SM protein Munc18c and its Q-SNARE cognate, syntaxin4, an interaction of critical importance in the regulation of insulin-stimulated GLUT4 vesicle exocytosis in adipose tissue and muscle (Dugani and Klip 2005). Using a combination of optical techniques and biochemical approaches, we have demonstrated that Munc18c is capable of multiple binding interactions with syntaxin4 *in vivo* which likely occur during the stepwise assembly of SNARE complexes. These interactions include Munc18c binding to a closed conformation of syntaxin4 that is inhibitory to SNARE complex nucleation, as well as to an open conformation, which permits Munc18c binding to heteromeric Q-SNARE complexes. Point mutants were used to identify the syntaxin4 SNARE domain as essential for mediating Munc18c interaction with both syntaxin4 conformations, although the N-terminus of syntaxin4 was strictly required, but insufficient, for Munc18c binding to the open conformation. Lastly, we provide evidence that these multiple Munc18c binding states with Q-SNAREs *in vivo*

are critical determinants of distinct functional effects on Glut4 vesicle translocation in differentiated 3T3L1 adipocytes.

Recent reports have indicated that Munc18c possesses an ability to directly interact with syntaxin4 while it is bound to other SNARE proteins (Widberg, Bryant et al. 2003; Latham, Lopez et al. 2006). Our findings in living 3T3L1 adipocytes extend the analysis of direct Munc18c interactions to an *in vivo* situation, with a specific focus on its interactions with syntaxin4. We report that Munc18c exhibited nearly equal FRET efficiency with either wildtype syntaxin4 or a mutant that maintains a constitutively open conformation (L173A/E174A; LE). Therefore, the affinity of Munc18c for syntaxin4 appears to be largely unaffected by the conformational state of syntaxin4. Our direct *in vitro* binding studies using bacterially expressed GST fusion proteins, as well as co-immunoprecipitation results from cell lysates confirmed the *in vivo* findings. We and others have previously reported that Munc18a also exhibits limited binding to the constitutively open LE mutant of syntaxin1A *in vivo*, (Dulubova, Sugita et al. 1999; Liu, Ernst et al. 2004), which has been recently extended to include Munc18a interaction with syntaxin1A in heteromeric Q-SNARE complexes (Zilly, Sorensen et al. 2006) and fully assembled SNARE complexes (Dulubova, Khvotchev et al. 2007; Shen, Tareste et al. 2007). Comparatively, the yeast exocytotic SM protein Sec1p interacts weakly with a closed conformation of Sso1p, favoring binding to Sso1p-Snc2p Q-SNARE complexes (Carr, Grote et al. 1999; Scott, Van Komen et al. 2004). Therefore, the interaction of exocytotic SM proteins with their cognate syntaxins appears to be converging on a general model where exocytotic Sec/Munc18 proteins demonstrate multiple binding states.

Our data establishing that Munc18c is able to interact with an open conformation of syntaxin4 *in vivo* prompted experiments to map the primary structural sites that mediate the interaction. To date, the interaction sites between these proteins have been based on the crystal structure of Munc18-1 in complex with syntaxin1A (Misura, Scheller et al. 2000). Indeed, our initial threading of the Munc18c and syntaxin4 sequences directly into the Munc18a-syntaxin1A

crystal structure predicted similar interactions between Munc18c and the C-terminus of syntaxin4, when it is in its closed conformation. In confirmation of this prediction, homologous I241A and I233A mutations in syntaxin4 and syntaxin1A, respectively, both dramatically reduced binding to their SM partners (Graham, Barclay et al. 2004; Liu, Ernst et al. 2004). Furthermore, the entire SNARE domain of syntaxin1A substituted for the syntaxin4 SNARE domain exhibited no consequence for Munc18c binding. Notably, the complementary substitution (*i.e.*, replacement of syntaxin1A SNARE motif with syntaxin4 sequence) resulted in a complete loss of Munc18a binding to the syntaxin1A chimera (data not shown). These results correlate well with the binding of Munc18c to both syntaxin4 and, with lesser affinity, to syntaxin1A, whereas Munc18a shows specificity for syntaxin1A (Dulubova, Yamaguchi et al. 2003).

By comparison to the relatively well-defined interactions of Munc18c with a closed state of syntaxin4, the specific structural determinants that allow interaction of Munc18c with an open conformation of syntaxin4 have been largely unstudied. In the current study, we show that the N-terminus of syntaxin4 is required for binding of Munc18c to the open mutant of syntaxin4, but not to wildtype syntaxin4, via examination of an arginine substitution at syntaxin4 D3 in FRET binding assays. Notably, this residue is conserved in both exocytotic and ER/Golgi syntaxins (syntaxins 1-4, 5 and 18), suggesting that SM protein interaction with the N-terminus of syntaxin is a common mechanism for association with the open conformation in intracellular SNARE complexes. This is consistent with the N-terminal motif of Sed5p/syntaxin5 an Ufe1p/syntaxin18 providing a platform for their SM partner, Sly1p, to bind both monomeric syntaxin proteins and SNARE complexes (Peng and Gallwitz 2002; Yamaguchi, Dulubova et al. 2002). Our findings complement a recent report that used an *in vitro* binding assay to elucidate the Munc18c binding pocket predicted to hold the N-terminus of syntaxin4 (Latham, Lopez et al. 2006). However, a notable discrepancy between these collective findings is whether the syntaxin4 N-terminus is sufficient for Munc18c binding. Using an *in vitro* binding assay, Latham *et al*. (Latham, Lopez et al. 2006) reported significant association between Munc18c and a mutant syntaxin4 that lacked

the SNARE motif (H3 domain) and transmembrane domain (syntaxin4$^{\Delta H3/TM}$). However, our *in vivo* analysis using a FRET based assay demonstrated a lack of Munc18c interaction with syntaxin4$^{\Delta H3/TM}$, thereby suggesting that the N-terminal interaction is insufficient to mediate a Munc18c-syntaxin4 interaction, in parallel to the *in vitro* findings of Ter Beest *et al.* (ter Beest, Chapin et al. 2005). The necessity of the syntaxin4 C-terminus was additionally confirmed using the I241A mutation of syntaxin4, a residue predicted to bind to the central cavity of Munc18c. The syntaxin4^{I241A} mutant eliminated Munc18c binding to constitutively open syntaxin4 and severely reduced interaction with wildtype syntaxin4. Therefore, our data favor a model in which Munc18c interaction with either the open or closed conformation of syntaxin4 depends upon SNARE motif interactions, and with an additional requirement for an N-terminal interaction with syntaxin4 in the open conformation. A similar requirement has been demonstrated for Munc18a binding to the open conformation of syntaxin1A in SNARE complexes (Dulubova, Khvotchev et al. 2007).

The SNARE assembly cycle begins with syntaxin nucleation of Qb- and Qc-SNARE complexes followed by the final SNARE motif contributed by vesicular R-SNAREs (Parlati, McNew et al. 2000). It has remained unclear which steps are the relevant sites of action for the exocytotic SM proteins. In the present study we demonstrate that Munc18c can interact with a SNARE pairing-competent conformation of syntaxin4 *in vivo*. These findings extend the recent report using *in vitro* binding studies which showed Munc18c associated with pre-formed syntaxin4-SNAP23 Q-SNARE complexes as well as a ternary SNARE complex composed of syntaxin4, SNAP23, and VAMP2 (Widberg, Bryant et al. 2003; Latham, Lopez et al. 2006). It is difficult to directly demonstrate that Munc18c-containing SNARE complexes form *in vivo* within the regulated secretory pathway. However, as support that these complexes form we show that constitutively open syntaxin4^{LE} recruits both Munc18c and diffusible GFP-SNAP23$^{C/A}$ to the plasma membrane as resolved by photobleach/FRAP of GFP and RFP. Our SNAP23 immunoprecipitation data additionally confirms that a Munc18c-syntaxin4^{LE}-SNAP23 complex

can be co-precipitated from lysates of HEK293-S3 cells overexpressing these proteins. This complex is prohibited from forming by Munc18c binding to syntaxin4^{WT}. Thus, the stabilization of an open syntaxin4 conformation relieves Munc18c's block on SNARE complex nucleation, although the functional significance of the Munc18c-Q-SNARE complexes remains unclear. That endogenous VAMP2 was not found associated with this complex in immunoprecipitation experiments is difficult to interpret. Either the Q-SNARE-Munc18c complex is prohibitive of VAMP2 binding despite the constitutive secretion in these cells, or ternary SNARE complex formation was transient and went undetected.

Of fundamental importance is to correlate the distinct conformational states of syntaxin4 with specific functional effects on the GLUT4 translocation pathway. The accumulation of GLUT4 vesicles at the plasma membrane prior to detectable increases in glucose uptake or to the accessibility of exofacial GLUT4 epitopes (Jhun, Rampal et al. 1992; Satoh, Nishimura et al. 1993) has led to a trafficking model that identifies separate tethering, docking and fusion steps as the critical sites of hormone action on exocytosis. To distinguish these separate kinetic steps we performed functional assays in differentiated 3T3L1 adipocytes in which dual-labeled myc$_7$-GLUT4-GFP was used as a tool to differentiate between GLUT4-vesicle docking and GLUT4-vesicle fusion. Our results suggest that the specific conformation of syntaxin4 together with its state of interaction with Munc18c defines whether GLUT4 vesicles are retained in recycling pathways or undergo fusion. GLUT4 vesicles were observed to accumulate at the plasma membrane regions following overexpression of the constitutively open LE mutant of syntaxin4 with Munc18c, even in the absence of insulin stimulation. By comparison, no such accumulation was observed upon coexpression of wildtype syntaxin4 with Munc18c. Indeed, reports from other groups indicate that GLUT4 vesicles cycle to the plasma membrane in the absence of insulin, although studies using TIRFM indicate that these vesicles do not normally dock (Lizunov, Matsumoto et al. 2005; Gonzalez and McGraw 2006). Our results indicate that the constitutively open conformation of syntaxin4^{LE} bypasses the requirement for insulin-regulated

signaling pathways, uncoupling the normal checkpoint between vesicle recycling and vesicle docking. Interestingly, while SNARE proteins are not traditionally thought of as docking factors, particularly in neurons, it has been recently reported that syntaxin1A is required for vesicle docking in adrenal chromaffin cells (de Wit, Cornelisse et al. 2006).

Although we cannot rule out a role for Munc18c in promoting either vesicle docking or assisting in the conformational transition of syntaxin4, it does not appear that Munc18c is strictly required for either of these processes. For example, overexpression of the Munc18c with the syntaxin4^{I241A} mutant, which demonstrates greatly reduced Munc18c binding, exhibited no abnormal docking in the absence of insulin. Moreover, GLUT4 vesicles dock normally in an insulin-regulated fashion in adipocytes lacking Munc18c (Kanda, Tamori et al. 2005). However, the necessity of insulin to drive GLUT4 vesicle fusion with syntaxin4^{LE}-Munc18c coexpression may be to promote disassembly of Munc18c from syntaxin4. Complementary to this interpretation, several lines of evidence suggest that insulin ultimately reduces Munc18c-syntaxin4 complexation through the activity of phosphatidylinositol 3-kinase (PI3K) and protein kinase Cξ (PKCξ) (Hodgkinson, Mander et al. 2005; Kanda, Tamori et al. 2005). A model whereby Munc18c dissociates from syntaxin4 proximal to fusion may explain why we observed an increased frequency of insulin-stimulated fusion events in adipocytes coexpressing Munc18c with the syntaxin4^{I241A} mutant relative to syntaxin4^{WT} or syntaxin4^{LE}.

In summary, our data indicate that Munc18c likely regulates syntaxin4-mediated SNARE complex formation at two discrete stages: (1) Munc18c prevents monomeric syntaxin4 from entering into Q-SNARE complexes with SNAP23, preventing unwanted vesicle docking through an inhibition which is probably overcome by the priming factors which open syntaxin4; (2) through binding of the SNARE complexes, Munc18c may place an additional inhibitory clamp on vesicle fusion, and may also serve as a scaffold for additional proteins to further regulate SNARE disassembly or recycling. An important focus of future experiments will be to elucidate the

specific signaling pathways that alter the binding of Munc18c to syntaxin4 and of the specific priming factors that control syntaxin4 conformation in insulin-stimulated adipocytes.

Addendum: Molecular Characterization of Munc18 as a Syntaxin Chaperone

Introduction

Syntaxin is a C-terminally anchored integral membrane protein that participates in the catalysis of membrane fusion through its SNARE domain. The ability of Sec1/Munc18 (SM) proteins to specifically bind syntaxin partners with high affinity underscores three potential functions of SM proteins as syntaxin chaperones: to (1) prevent undesired syntaxin-SNARE pairings, (2) enhance fusion specificity, and (3) prime the SNAREs to accelerate fusion.

First, through binding to closed syntaxin, SM proteins may be required to protect the SNARE domain from forming undesired SNARE-SNARE pairings as syntaxin is transported from its site of synthesis at the ER to the plasma membrane sites of exocytosis (Medine, Rickman et al. 2007; Arunachalam, Han et al. 2008). This hypothesis is generally supported by genetic ablation studies indicating that Munc18 and syntaxin tightly regulate each others expression to achieve a 1:1 stoichiometric ratio (Verhage, Maia et al. 2000; Voets, Toonen et al. 2001; Toonen, de Vries et al. 2005). Moreover, syntaxin1A is retained intracellularly when overexpressed in epithelial cells, with its delivery to the cell surface being strongly facilitated by Munc18 co-expression (Rowe, Corradi et al. 1999; Rowe, Calegari et al. 2001; Liu, Ernst et al. 2004). However, an absolute requirement for Munc18 in syntaxin trafficking is unlikely, as syntaxin correctly targets to the plasma membrane in neurons lacking Munc18 (Toonen, de Vries et al. 2005).

A second chaperone function of SM proteins may be to confer specificity to membrane trafficking, thus appropriately pairing incoming vesicles with their target membranes. This hypothesis first arose when it was observed that SNARE interactions are not, alone, intrinsically selective. For example, SNARE complexes form with comparable thermal stability even when

the SNARE motifs of VAMP 4, 7, or 8 replace VAMP2 in the SNARE complex with either syntaxin1A/SNAP25 or syntaxin4/SNAP23 (Yang, Gonzalez et al. 1999; Lang, Margittai et al. 2002). Biochemical analysis of SM proteins, meanwhile, indicates they typically interact with just one or two syntaxins with nanomolar affinity (Pevsner, Hsu et al. 1994; Dulubova, Yamaguchi et al. 2003), placing them in a position to confer specificity. *In vivo* rescue experiments have additionally shown that SM proteins can rescue null mutations from a different species, provided that both isoforms are acting in the same membrane trafficking pathway (*e.g.*, exocytosis). For example, deficiency of the SM protein unc-18 in *C. elegans* is rescued by expression of (mammalian) Munc18-1, but not Munc18-2 (Gengyo-Ando, Kitayama et al. 1996). Likewise, mutants lacking neuronal Drosophila VAMP2/synaptobrevin are rescued by a non-neuronal paralog (Bhattacharya, Stewart et al. 2002). Comparatively, the absence of Munc18c, which perturbs normal GLUT4 trafficking in adipose tissue and skeletal muscle, cannot be rescued by Munc18b despite the existence of both isoforms in the same tissue. Thus, a natural consequence of SM-syntaxin specificity and affinity is that trafficking pathways are marked by unique pairings (Dulubova, Yamaguchi et al. 2003; Toonen and Verhage 2003).

Finally, SM proteins can act as stimulatory subunits of the SNARE complex (*i.e.*, as priming factors). Shen and colleagues (Shen, Tareste et al. 2007) established the ability of Munc18-1 to dose-dependently accelerate *in vitro* liposome fusion reactions catalyzed by the neuronal SNAREs (syntaxin1A/SNAP25/VAMP2). Underlying this feature is the ability of SM proteins to bind SNARE complexes, as evidenced in constitutive exocytosis (Sec1p), regulated exocytosis (Munc18-1), endocytosis (Vps45p), and ER-Golgi transport (Sly1p) (Carr, Grote et al. 1999; Peng and Gallwitz 2004; Scott, Van Komen et al. 2004; Dulubova, Khvotchev et al. 2007). Furthermore, the ability of SM proteins to block SNARE assembly, discussed above, is biochemically separable from their function to speed fusion. For example, SM binding to the N-terminus of syntaxin is required only for the latter (Khvotchev, Dulubova et al. 2007).

Additionally, point mutations in the Drosophila SM homolog ROP that block its inhibitory actions do not affect the ability of Munc18-1 to stimulate fusion (Shen, Tareste et al. 2007).

The purpose of this study was to provide direct information on the molecular interactions underlying syntaxin trafficking by Munc18, as well as to determine how specificity of the trafficking pathways are maintained by specific SM-syntaxin partnerships. Our investigations utilized fluoroprotein-labeled syntaxin and Munc18 to visualize their subcellular localization in living secretory cells, as well as to study their function in vesicle-plasma membrane fusion reactions. Our findings support the conclusion that SM proteins act as syntaxin chaperones in two main ways: (1) SM levels in excess of syntaxin are required for syntaxin to plasma membrane target; (2) the ability of specific SM-syntaxin pairs to catalyze constitutive versus fast Ca^{2+}-dependent exocytosis is adaptable and dependent on the levels of each pair.

Experimental Procedures

Cell culture and transfection – 3T3L1 fibroblasts and HEK293-S3 cells were maintained in culture as described in Chapter II *Experimental Procedures*. PC-12 cells were cultured in 10% CO_2 in DMEM supplemented with 10% horse serum, 5% fetal bovine serum, penicillin (100 U/ml), streptomycin (100 μg/ml), and gentamicin (10 μg/ml) (Invitrogen). Cells were plated on coverglass affixed to the bottom of 35mm culture dishes 12-24 hours prior to transfection using Lipofectamine2000 (Invitrogen).

Quantification of plasma membrane targeting of Munc18 and syntaxin – The targeting of cYFP-Munc18 or CFP-syntaxin to a region adjacent to the plasma membrane was quantified relative to the cytoplasm according to the equation

$$\text{plasma membrane targeting (TF)} = \frac{\left(I_{tot} \cdot A_{tot}\right) - \left(I_{cyt} \cdot A_{cyt}\right)}{\left(A_{tot} - A_{cyt}\right)} \div I_{cyt},$$

where A_{tot} is the total area of the cell, I_{tot} is the averaged intensity of the cell, A_{cyt} is the total area of the cytoplasm (defined as the region inside of and exclusive of the plasma membrane), and I_{cyt} is the averaged intensity of the cytoplasm. Regions were selected and computation of average fluorescence intensity and area were performed using Metamorph (Universal Imaging, v6.3r5).

Human growth hormone (hGH) Secretion Assay– PC-12 cells were plated onto 24-well plates and transfected with expression plasmids containing cDNAs for hGH, ± the light chain of the Botulinum neurotoxin C (BotC). Rescue of secretion from BotC cleavage of syntaxin1A was facilitated by the further addition of Munc18a + BotC resistant CFP-syntaxin1A^{K253I}, or Munc18c + CFP-syntaxin4. The total DNA concentration during transfection was held constant across treatments by addition of a neomycin control plasmid. At 48–72 h following transfection, cells were rinsed for 6 min in a physiological saline solution (PSS, in mM: 145 NaCl, 5.6 KCl, 15 NaHEPES, 0.5 $MgCl_2$, 2.2 $CaCl_2$, 5.6 glucose, 0.5 Na ascorbate, 2 mg/ml bovine serum albumin, pH 7.3), followed by a 6-min stimulation with 50 mM K^+ (same as PSS, with equimolar substitution of K^+ for Na^+). PSS containing the secreted hGH was collected, and cells were lysed (lysis buffer, in mM: 0.2 EDTA, 10 HEPES, 1% Triton X-100, pH 7.4). To determine the percent of total hGH secreted, an hGH ELISA kit (Roche Diagnostics) was used to measure the hGH content of the secreted fraction as a percentage of the hGH contained in the cell lysates. Each experiment was performed with quadruplicate replicates for each treatment.

Human growth hormone (hGH) Secretion Assay– PC-12 cells were plated onto 24-well plates and transfected with expression plasmids containing cDNAs for hGH, ± the light chain of the Botulinum neurotoxin C (BotC). Rescue of secretion from BotC cleavage of syntaxin1A was facilitated by the further addition of Munc18a + BotC resistant CFP-syntaxin1A^{K253I}, or Munc18c + CFP-syntaxin4. The total DNA concentration during transfection was held constant across treatments by addition of a neomycin control plasmid. At 48–72 h following transfection, cells

were rinsed for 6 min in a physiological saline solution (PSS, in mM: 145 NaCl, 5.6 KCl, 15 NaHEPES, 0.5 $MgCl_2$, 2.2 $CaCl_2$, 5.6 glucose, 0.5 Na ascorbate, 2 mg/ml bovine serum albumin, pH 7.3), followed by a 6-min stimulation with 50 mM K^+ (same as PSS, with equimolar substitution of K^+ for Na^+). PSS containing the secreted hGH was collected, and cells were lysed (lysis buffer, in mM: 0.2 EDTA, 10 HEPES, 1% Triton X-100, pH 7.4). To determine the percent of total hGH secreted, an hGH ELISA kit (Roche Diagnostics) was used to measure the hGH content of the secreted fraction as a percentage of the hGH contained in the cell lysates. Each experiment was performed with quadruplicate replicates for each treatment.

Results

Requirements for Munc18 and syntaxin membrane targeting– To determine whether Munc18c and syntaxin4 are reciprocally required for each others membrane targeting, we initially used optical imaging of N-terminally labeled cYFP-Munc18c and CFP-syntaxin4 (Figure 2.12A**A**) to follow their subcellular localization when expressed in living differentiated 3T3L1 adipocytes. These cells utilize Munc18c and syntaxin4 for cycling of GLUT4 transporters on and off the plasma membrane, thereby regulating blood sugar (Dugani and Klip 2005).. Expressed individually, cYFP-Munc18c was found to distribute evenly throughout the cytosol, while CFP-syntaxin4 fluorescence appeared punctate resulting from intracellular clustering (Fig. 2.12B). The restricted ability of syntaxin1A, when overexpressed alone, to target to the plasma membrane region has been reported previously in HEK293, MDCK, and Caco-2 cells as a result of limiting levels of Munc18-1 expression (Rowe, Corradi et al. 1999; Liu, Ernst et al. 2004). Accordingly, coexpression of CFP-syntaxin4 and cYFP-Munc18c localized both proteins to the plasma membrane region, a distribution consistent with that previously reported for the endogenously expressed proteins (Tellam, Macaulay et al. 1997). These results also indicate that the fluoroprotein tags used in the fusion protein constructs do not interfere with the plasma membrane targeting function of these proteins.

It has been reported that the association of these Munc18 and syntaxin is initiated on intracellular membranes and continues through trafficking pathways to the plasma membrane (Rowe, Corradi et al. 1999; Yang, Xu et al. 2006). To test whether a stable Munc18c interaction is required for targeting of syntaxin4 to the plasma membrane region, we tested the effect of CFP-syntaxin 4 coexpressed with a single point mutant of Munc18c (cYFP-Munc18c^{R240L}). This mutant was based on the previously characterized temperature-sensitive SM mutants, Munc18c^{R240K} and the *Saccharomyces cerivisiae* homolog Sly1p^{R266K}, which are known to exhibit a strongly reduced affinity of interaction with syntaxin 4 and Sed5p, respectively (Cao, Ballew et al. 1998; Thurmond and Pessin 2000). When Munc18c^{R240L} was coexpressed with CFP-syntaxin4, only the CFP-syntaxin4 localized to the plasma membrane (Fig. 2.13B), suggesting that syntaxin4 does not require a high affinity interaction with Munc18c for plasma membrane targeting. However, these data indicate that Munc18c does require syntaxin4 interaction for membrane localization (Fig. 2.13B). To quantify the Munc18c-syntaxin4 interaction the subcellular targeting of Munc18c was calculated as an averaged plasma membrane 'targeting factor' (TF). This TF relates the average cYPF-Munc18c fluorescence intensity in the membrane region with its average fluorescence intensity in the cytosol (see *Experimental Procedures* for equation). A targeting factor (TF)>1 indicates predominant membrane localization, whereas TF<1 indicates predominant cytosolic localization. As shown in Figure 2.13C, cYFP-Munc18c was principally found in the membrane region when cotransfected with CFP-syntaxin4. When Munc18c was expressed alone or when it was mutated at R240L, it remained primarily cytosolic. Collectively, these results suggest that although the presence of Munc18c is required for efficient syntaxin4 membrane targeting, neither a high affinity nor high stability interaction with syntaxin4 is necessary.

Molecular requirements for the specificity of Munc18 and syntaxin pairings – As SNARE-SNARE interactions are not intrinsically selective in vitro (Yang, Gonzalez et al. 1999), it has been hypothesized that the high (nM) affinity SM-syntaxin interactions confer specificity

on particular membrane trafficking pathways in cell types where multiple SM-syntaxin pairs are present. For example, in neuroendocrine cells (*e.g.*, neurons, pancreatic β-cells, chromaffin cells), Munc18a/syntaxin1A is believed to primarily mediate Ca^{2+}-triggered exocytosis despite the presence of Munc18c/syntaxin4 at the PM. Comparatively, 3T3L1 adipocytes contain Munc18a/b/c (Tellam, McIntosh et al. 1995) although the Munc18c/syntaxin4 complex is implicated in the insulin-dependent surface presentation of GLUT4 (Tellam, Macaulay et al. 1997; Thurmond, Ceresa et al. 1998). To probe the intrinsic molecular requirements for this apparent cell-type specificity we examined 'heterologous' SM-syntaxin pairings in 3T3L1 adipocytes.

Using the membrane targeting assay, we initially introduced cYFP-Munc18a and/or CFP-syntaxin1A into 3T3L1 adipocytes. Munc18a was found dispersed throughout the cytosol when coexpressed with syntaxin4 (TF_{Munc18}=0.79±0.01, *n*=31), but localized to the plasma membrane (PM) regions in cells co-expressing syntaxin1A (TF_{Munc18}=1.17±0.02, *n*=25) (Fig 2.12C). Importantly, the extent of Munc18a membrane targeting in Munc18a/syntaxin1A-expressing cells was comparable to that found for Munc18c in the Munc18c/syntaxin4 cotransfection condition (TF_{Munc18}=1.22±0.03, *n*=20). By comparison, cYFP-Munc18c demonstrated membrane targeting to a lesser but significant extent to when coexpressed with neuronal CFP-syntaxin1A (TF_{Munc18}=0.92±0.03, *n*=25). In summary, the Munc18a interaction is specific for syntaxin1A, while Munc18c is promiscuous in its targeting of both syntaxins 1 and 4 to the PM.

To address the possibility that the targeting function of SM-syntaxin complexes to the PM is cell-type specific or regulated by the activation state of the 3T3L1 adipocytes, the experiments were repeated in HEK293-S3 cells, which exhibit constitutive rather than regulated secretion. As in adipocytes, these cells contain syntaxin4/Munc18c, but not Munc18a/syntaxin1A (Gladycheva, Ho et al. 2004). Similar results to those found in adipocytes were observed in HEK293-S3 cells (*c.f.*, Fig. 2.12 D and E with Fig. 2.13 B and C). Notably, the targeting of syntaxin to the plasma membrane by Munc18 was found to correlate directly with the

previously reported biochemical measurements of the SM-syntaxin binding affinity performed in vitro: Munc18a-syntaxin4 <<< Munc18c-syntaxin1A < Munc18a-syntaxin1A ≅ Munc18c-syntaxin4 (Dulubova, Yamaguchi et al. 2003). Therefore, we hypothesized that reducing the affinity of SM-syntaxin interaction would also consequently reduce the trafficking of syntaxin. To test this hypothesis we took advantage of the intermediate binding/trafficking phenotype seen in the cYFP-Munc18c/CFP-syntaxin1A co-transfection condition by adjusting the relative levels of Munc18c << syntaxin1A. We found syntaxin1A co-localized to the peri-nuclear region with Munc18c (Fig. 2.12F). In the experiments of Fig 2.12 B-E, where the Munc18c:syntaxin1A ratio was set to 1, significant syntaxin1A and Munc18c was present at the plasma membrane. As a test of non-interacting proteins, we demonstrate that CFP-syntaxin4 when coexpressed with Munc18a was found predominantly on the peri-nuclear and surrounding inner membranes but was not co-localized with Munc18a. Collectively, these results suggest that the relative level of Munc18 to syntaxin is a critical determinant for the proper targeting of Munc18c and syntaxin1A to the plasma membrane. It is also possible that at low concentrations Munc18c fails to hold syntaxin1A in a closed (SNARE-pairing inactive) conformation, causing the mislocalization of both proteins. Indeed, the open (SNARE-pairing active) conformation is known to promote ectopic SNARE-SNARE binding interactions within intracellular membranes (Medine, Rickman et al. 2007).

Effect of syntaxin conformation on trafficking of Munc18 and syntaxin – The SNARE-pairing inactive binding mode (closed conformation) of syntaxin1A seen in the Munc18a-syntaxin1A crystal structure (Misura, Scheller et al. 2000) is important for the proper targeting of both Munc18a and syntaxin1A to the PM (Rowe, Corradi et al. 1999; Rowe, Calegari et al. 2001; Liu, Ernst et al. 2004). We questioned whether the ability of Munc18c and syntaxin4 to properly target to the plasma membrane also requires a closed conformation of syntaxin4. To rigorously test this hypothesis, we examined the membrane targeting of Munc18 a or c co-expressed with the constitutively open LE mutants of their cognate syntaxins (syntaxin1A, L165A/E166A;

syntaxin4, L173A/E174A). Importantly to our assay, it should be noted that the membrane localization of cYFP-Munc18s in these experiments mainly resulted from Munc18 binding to the exogenously expressed syntaxins, as a principally cytosolic signal was observed when the cYFP-Munc18s were expressed alone ($TF_{Munc18c}$= 0.79±0.01, *n*=20; $TF_{Munc18a}$= 0.82±0.02, *n*=25). Figure 2.13A compares the subcellular distribution of cYFP-Munc18c when co-expressed with CFP-syntaxin4 or CFP-syntaxin4LE in HEK293-S3 cells. In both treatments, Munc18c exhibited distinct plasma membrane localization. Substantial differences in SM-syntaxin interaction were observed in the inability of CFP-syntaxin1ALE to facilitate plasma membrane targeting of co-expressed cYFP-Munc18a, consistent with a previous demonstration by FRET that Munc18a-syntaxin1ALE maintain only a low affinity interaction (Liu, Ernst et al. 2004). Averaged results from numerous cells are shown in Figure. 2.13B. Thus, based on the ability of syntaxin4LE to properly localize Munc18c to the PM, a closed conformation of syntaxin is not strictly required for targeting Munc18/syntaxin PM targeting.

Given that Munc18c can bind and target to multiple conformations of syntaxin4, we next examined the possibility that Munc18c utilizes the N-terminus of syntaxin to facilitate the targeting of CFP-syntaxin4 (Fig. 2.12 B and C). To test this possibility we characterized a mutant of syntaxin4, I241A, which eliminated binding of Munc18c to both closed and open syntaxin4 in our FRET assay (Fig. 2.6). When co-expressed with cYFP-Munc18c, CFP-syntaxin4^{I241A} targeted correctly to the plasma membrane (Fig. 2.13 C and D). Control cells co-expressing cYFP-Munc18c and CFP-syntaxin4$^{\Delta H3/TM}$, which lacks its H3 (SNARE) domain and transmembrane anchor and exhibits cytosolic localization, were also analyzed to provide a quantitative comparison of TFs for cYPF-Munc18c and syntaxin4^{I241A}. Taken together, the results of Fig. 2.12 and 2.13 suggest the unexpected finding that the presence of Munc18c is required (*i.e.*, that its expression strongly facilitates syntaxin4 targeting), but that binding to syntaxin4 is not required for proper plasma membrane targeting.

Examination of SM-syntaxin specificity in exocytotic fusion reactions – A central goal of our experiments was to determine how Sec1/Munc18 proteins, by acting as chaperones for specific syntaxins at sites of exocytosis, confer identity to specific membrane trafficking pathways. In particular, within the exocytotic pathways of most neuroendocrine cells (e.g., neurons, adrenal chromaffin cells, pancreatic β-cells, etc.), genetic evidence suggests that Munc18c/syntaxin4-SNARE complexes mediate constitutive secretion while Munc18a/syntaxin1A-SNARE complexes facilitate fast Ca^{2+}-stimulated secretion (Toonen and Verhage 2003; Jahn and Scheller 2006). It remains unclear how these two exocytotic pathways are discerned in vivo, and to what extent there is crosstalk. Both syntaxin4/ and syntaxin1A/Q-SNARE complexes form functional membrane receptors for the vesicular SNARE VAMP2 and both are present in the same cells. To probe this question we developed an assay to test the fusion competency of various SM-syntaxin pairings in the pheochromocytoma cell line PC-12. In this assay, human growth hormone (hGH) was used as a functional reporter of regulated secretory pathway specifically from transfected cells (Wick, Senter et al. 1993). The BotC light chain, which cleaves syntaxin1A and precludes it from catalyzing membrane fusion (Schiavo, Rossetto et al. 1994), was co-transfected to eliminate potentially confounding effects of endogenous syntaxin1A in these cells. Resistance of the transfected syntaxin1A constructs to BotC was accomplished by substituting Ile in place of Lys at residue 253 within the BotC cleavage site (Lam, Tryoen-Toth et al. 2008). Syntaxin1A^{K253I} and Munc18a have been previously shown to both target correctly to the plasma membrane and rescue hGH secretion in PC-12 cells co-expressing BotC (Lam, Tryoen-Toth et al. 2008).

Initially we examined the contribution of syntaxin1A to constitutive secretion. Shown in Figure 2.14A, BotC cleavage of endogenous syntaxin1A reduced resting hGH secretion by 50%. To test if the BotC secretion defect was due specifically to endogenous syntaxin1A knockdown, we overexpressed BotC-resistant syntaxin1A^{K253I} with Munc18a. A partial restoration of

constitutive secretion was observed in cells expressing Munc18a with syntaxin1A^{K253I} (73±13%, *n*=8) or CFP-syntaxin1A^{K253I} (69±9%, *n*=8). Importantly, previous studies employing this assay have shown that syntaxin1A^{K253I} or Munc18a do not rescue hGH secretion alone, nor does syntaxin1A^{WT} (which is susceptible to BotC cleavage) cotransfected with Munc18a (Lam, Tryoen-Toth et al. 2008). When we examined whether the deficiency in basal exocytosis could be rescued by syntaxin4-Munc18c complexes in the presence of BotC, we found that the extent of secretion in cells overexpressing Munc18c and CFP-syntaxin4 (85±7%, *n*=8) was equivalent those rescued with Munc18a/syntaxin1A^{K253I}. Thus, Munc18a/synaxin1A or Munc18c/syntaxin4 are capable of substituting for each other, at least for constitutive secretion.

The above results prompted us to test whether fast, Ca^{2+}-stimulated exocytosis, may also be catalyzed by Munc18c and syntaxin4 when Munc18a/syntaxin1A is inhibited by Bot C. For these experiments we directly depolarized the cells with 50 mM K^+. Compared with PC-12 cells expressing pCMV-Neo control plasmid alone, K+-stimulated hGH secretion was reduced to 42±3% (*n*=8) in cells expressing BotC and pCMV-Neo control plasmid (Fig. 2.14B). Clearly, at endogenous levels, syntaxin4 and Munc18c are unable to compensate for the BotC defect although syntaxin4 is not cleaved by BotC (Schiavo, Rossetto et al. 1994). As expected, the further addition of overexpressed syntaxin1A^{K253I} and Munc18a restored secretion to control levels. Next, we tested whether raising the levels of CFP-syntaxin4 and Munc18c above those found endogenously could rescue K^+-induced hGH secretion in the presence of BotC. This experiment served an additional purpose, to assess whether N-terminally labeled syntaxins, which retain their membrane targeting function (Figs. 2.12 and 2.13) and have been used extensively in this study (Figs. 2.3, 2.4, 2.6, 2.10, and 2.11), are furthermore fusion-competent. CFP-syntaxin4 and Munc18c rescued 77±4% (*n*=8) of the BotC secretion defect. This treatment exhibited equivalent hGH secretion as cells containing CFP-syntaxin1A^{K253I} and Munc18a (Fig. 2.14B). Therefore, based on the ability of SM-syntaxin pairs to substitute for each other, our results

demonstrate that the preference of Munc18c/syntaxin4 and Munc18a/syntaxin1A for constitutive and Ca2+-stimulated exocytosis, respectively, is strictly dependent on the levels of each protein. Additionally, our results indicate that N-terminally fluoroprotein-labeled syntaxins, while not as effective in catalyzing secretion as unlabeled syntaxin, are fusion competent.

Discussion

Syntaxin molecules utilize Sec1/Munc18 (SM) proteins as high-affinity chaperones beginning with their synthesis and insertion into intracellular membranes, and throughout their transport to the plasma membrane (PM), where together they participate in exocytosis. In this study we have focused on characterizing the factors underlying the *specificity* of SM-syntaxin binding interactions which allow these complexes to traffic and catalyze fusion. Using optical approaches to monitor their movement *in vivo*, we have shown that the efficient and rapid targeting of syntaxin to the plasma membrane, in 3T3L1 adipocytes and HEK293 cells, requires the presence of equivalent or higher levels of Munc18. However, low-affinity mutants of both Munc18c and syntaxin4 have suggested that direct and stable binding of the two proteins is not required for this process. Furthermore, as Munc18c targets constitutively open syntaxin4^{LE} to the plasma membrane, Munc18 interaction with a closed conformation of syntaxin is not a universal requirement for the proper PM targeting of SM-syntaxin pairs. Finally, using hGH secretion assays we provide evidence that elevated levels of syntaxin4/Munc18c can substitute for syntaxin1A/Munc18a to catalyze fast, Ca^{2+}-stimulated membrane fusion.

The validity of these experiments utilizing fluoroprotein-tagged Munc18 and syntaxin is predicated on the idea that the fluoroproteins do not disrupt the normal ability of Munc18 and syntaxin to (1) properly target to the plasma membrane and (2) form functional acceptor complexes for exocytosis at the plasma membrane. One concern is that CFP and cYFP, which form a three-dimensional β-barrel, are relatively inflexible (Palm and Wlodawer 1999). Furthermore, the addition of CFP to the 34 kDa syntaxin nearly doubles the molecular weight of the protein. We showed here that fluoroprotein-labeled Munc18 and syntaxin localize properly to

the plasma membrane. Moreover, Munc18a together with CFP-labeled syntaxin1A was able to rescue secretion in BotC-transfected PC-12 cells to 77±4% of control levels, while unlabeled syntaxin1A completely rescued secretion. We therefore conclude that while N-terminal labels on syntaxin might partially impair function, they do not prevent targeting or fusion. These results furthermore validate our approach of using fluoroprotein-labeled syntaxin4 to study exocytosis in 3T3L1 adipocytes.

It has been reported that cellular feedback mechanisms act to maintain Munc18 and syntaxin proteins in a 1:1 ratio in most cell types examined (Voets, Toonen et al. 2001; Oh, Spurlin et al. 2005). For example, syntaxin4 heterozygous mice exhibit 40% reduction in Munc18c in adipocytes and skeletal muscle (Yang, Coker et al. 2001), and Tlg2p/syntaxin is down-regulated in the absence of Vps45p in yeast (Bryant and James 2001). Furthermore, in response to acute cleavage of syntaxin1A with BotC, Munc18a accumulation is reduced, as are its levels at the plasma membrane (Schutz, Zilly et al. 2005; de Wit, Cornelisse et al. 2006). Syntaxin1A levels are also reduced by 70% in Munc18a-null mice, with the remaining 30% targeting to the plasma membrane correctly (Toonen, de Vries et al. 2005). One interpretation of this finding is that Munc18a is not required for syntaxin targeting. However, our findings highlight a strong correlation between the efficiency of syntaxin membrane localization and the expression levels of Munc18. Using FRET to rigorously quantify the molar ratio of Munc18:syntaxin, we found that at limiting Munc18 levels (Munc18/syntaxin ratio < 0.1-0.5), syntaxin clusters intracellularly. At excess levels (Munc18/syntaxin ratio > ~1), the low-affinity binding partner Munc18c is nonetheless capable of preventing syntaxin1A from ectopically localizing on intracellular membranes. Therefore, although it remains untested, compensation by Munc18c binding to syntaxin1A (*i.e.*, priming) could potentially occur in the synapses of Munc18a-null mice (Voets, Toonen et al. 2001; Toonen, de Vries et al. 2005).

In addition to strongly facilitating exocytosis (Latham, Lopez et al. 2006; Dulubova, Khvotchev et al. 2007; Shen, Tareste et al. 2007), SM proteins in a bimolecular complex with

syntaxin are also capable of preventing the formation of SNARE complexes (Figs. 2.7-9; (Pevsner, Hsu et al. 1994; Araki, Tamori et al. 1997)). Fitting well with this are extensive data on syntaxin1A (Dulubova, Sugita et al. 1999; Misura, Scheller et al. 2000; Yang, Steegmaier et al. 2000) and now syntaxin4 indicating this feature is specifically due to Munc18 stabilizing a closed conformation of syntaxin4. Thus, SM proteins may additionally function as chaperones to protect the syntaxin SNARE domain en route to the site of action. Indeed, our data on Munc18c in 3T3L1 adipocytes is well supported by multiple studies showing that Munc18a prevents deleterious effects of syntaxin overexpression in transfected HEK293, Caco2, and MDCK cells (Rowe, Corradi et al. 1999; Rowe, Calegari et al. 2001; Liu, Ernst et al. 2004). However, this hypothesis seems inconsistent with our data indicating that syntaxin4 PM localizes when expressed with either Munc18c^{R240L} or mutated at residue I241, and both manipulations disrupt the SM-syntaxin binding interaction. That the I241A syntaxin mutant furthermore eliminates high-affinity binding of Munc18c to both closed and open syntaxin suggests that maintaining a closed conformation of syntaxin4 is irrelevant for its membrane targeting. Unambiguously, constitutively-open syntaxin4^{LE} traffics to the PM when co-expressed with Munc18c. A probably explanation for these seemingly contradictory data is that Munc18 levels are somehow required to be equivalent to syntaxin, but at least for membrane targeting their stable binding interaction is dispensable.

It has been suggested that SM proteins serve as syntaxin chaperones to confer specificity between particular membrane trafficking pathways (Toonen and Verhage 2003). This hypothesis is based on the finding that SNARE motifs are not selective for particular SNARE complexes *in vitro* (Yang, Gonzalez et al. 1999), while SM proteins bind specifically and with high affinity to one or two syntaxins (Dulubova, Yamaguchi et al. 2003). Indeed, specific SM-syntaxin pairs are uniquely localized to various cellular compartments (*e.g.*, Munc18a/syntaxin1A to the plasma membrane, and Sly1/syntaxin5 to the Golgi apparatus). Yet, the question remains how specificity is determined *within* a particular trafficking pathway, particularly when multiple SM/syntaxin

pairs are present. The exocytotic pathway, for instance, contains four syntaxins (1-4) and three SM proteins (Munc18 a/b/c). Based on the experiments described here, we propose that the levels of the Munc18a/syntaxin1A and Munc18c/syntaxin4 pairs determine their propensity for Ca^{2+}-dependent vs. constitutive secretion seen in neuroendocrine cells *in vivo*. Indeed, expressed Munc18c and CFP-syntaxin4 were able to rescue secretion when Munc18a-syntaxin1A levels were limited by BotC expression. This rescue was furthermore equivalent to cells which were rescued instead by Munc18a and BotC-resistant CFP-syntaxin1A^{K253I}. Thus, it is clear that Munc18c/syntaxin4 can participate in regulated, Ca^{2+}-dependent secretion. However, the supraphysiologic levels required for their participation in fast exocytosis may reflect their lower affinity for other vesicle-PM scaffolding proteins (*e.g.*, Rab and Rab effectors) compared with Munc18a/syntaxin1A. This interpretation would explain why syntaxin4 and syntaxin1A are unable compensate for each others absence in genetic ablation studies in mice (Verhage, Maia et al. 2000; Kanda, Tamori et al. 2005).

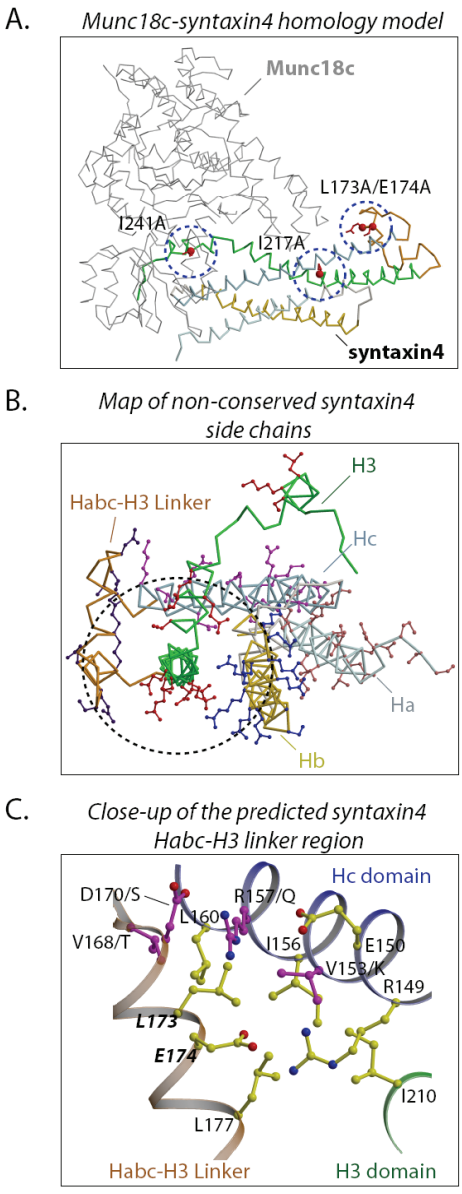

Figure 2.1. **Homology modeling of the Munc18c-syntaxin4 complex based on the Munc18a-syntaxin1A crystal structure**. *A*, Munc18c and syntaxin4 were threaded directly into the Munc18a-syntaxin1A crystal structure based on a ClustalW alignment. Munc18c is colored gray and the syntaxin4 helical domains are colored as follows: Ha in pale blue, Hb in gold, Hc in cyan, H3 in green, and the Habc-H3 linker region in orange. The syntaxin4 point mutants used in this study (red) are mapped onto the Munc18c-syntaxin4 structural model: L173A/E174A, LE; I217A; I241A. *B*, Structural map of non-conserved syntaxin4 residues viewed down the axis of the syntaxin4 H3 domain (green) as it packs against the Habc helices. Side chains of non-conserved residues are shown. A region of highly conserved packing between SNARE (H3) domain and the N-terminal helices is circled (coloring: Ha, rust; Hb, blue; Hc, magenta; H3, red; Habc-H3 linker, indigo). *C*, All contacts proposed to interact with the syntaxin4 linker residues L173 and E174 are colored as conserved (yellow) and non-conserved (magenta); differing syntaxin1A residues are shown after a slash. Residue numbers correspond to the rat syntaxin4 sequence (GenBank, NP_112387).

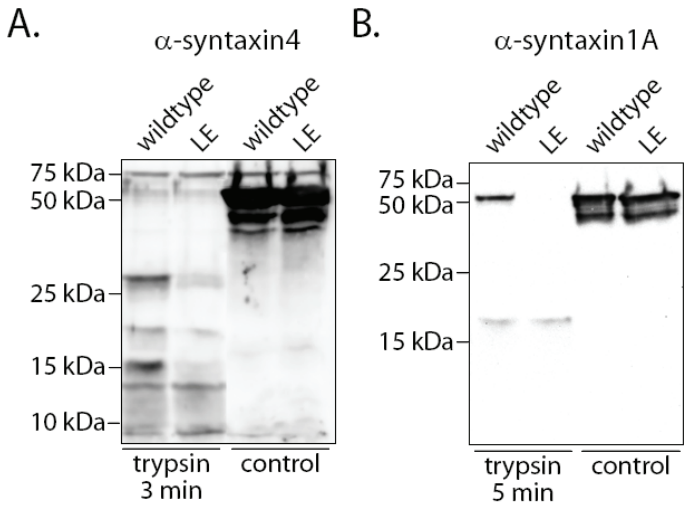

Figure 2.2. **Comparison of trypsin proteolysis between wildtype and mutant syntaxin4^{LE}**. *A*, Immunoblot comparing the effect of trypsin digest (60 nm, 3 min) on GST-syntaxin4$_{1-275}$ wildtype and GST-syntaxin4$_{1-275}^{LE}$ (L173A/E174A). Cleavage products were fractionated on SDS PAGE, and visualized by Western blot using a syntaxin4 polyclonal antibody. Equivalent amounts of each undigested protein (*control*) are also shown. *B*, Immunoblot as in (A), comparing the products of trypsin digest of wildtype or mutant GST-syntaxin1A$_{1-267}^{LE}$ (L165A/E166A), visualized using an anti-syntaxin1A monoclonal antibody. Representative blots were chosen from four independent experiments.

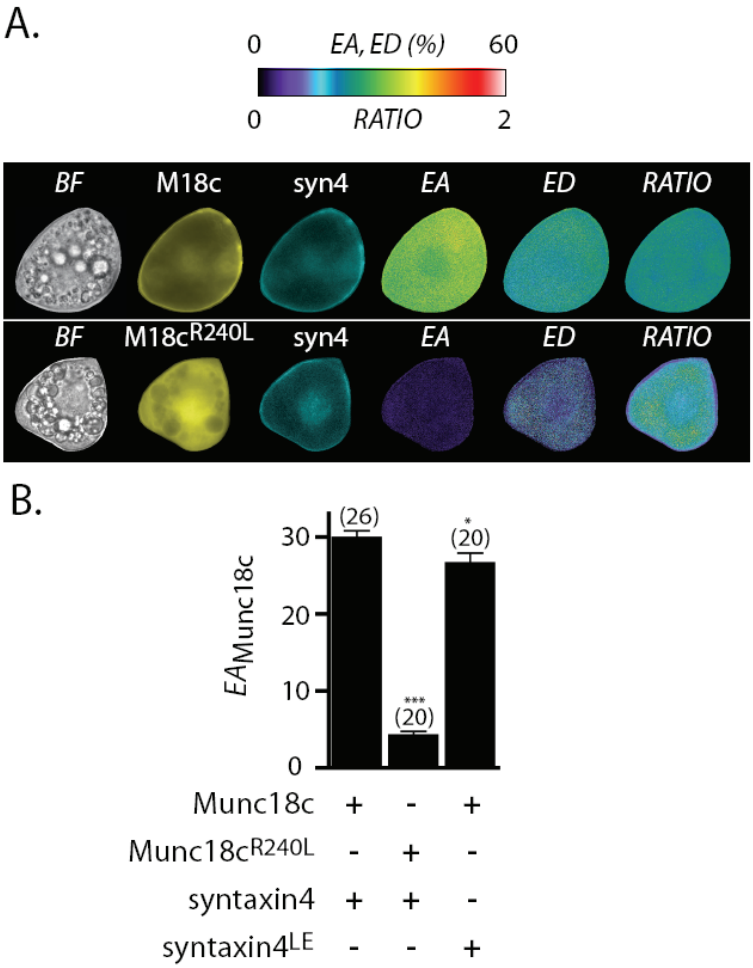

Figure 2.3. **FRET measurements of direct Munc18c and syntaxin4 interaction in 3T3L1 adipocytes**. *A*, FRET measured by sensitized emission in living 3T3L1 adipocytes transfected with cYFP-Munc18c and CFP-syntaxin4 or mutants as indicated. E_A and E_D are the apparent FRET efficiencies for the acceptor (cYFP-Munc18c) and donor (CFP-syntaxin4) in complex, respectively. *RATIO* is the mole fraction cYFP/CFP. The pseudocolored E_A, E_D, and *RATIO* images represent a spatial map of FRET efficiency; the color bar indicates scaling. *B*, Averaged E_A values for each co-transfection condition. Cells with a similar *RATIO* (averaging 0.9-1.1) were chosen for comparison. Numbers above columns indicate number of cells imaged. Significant differences are from the wildtype Munc18c-syntaxin4 treatment: *, $p<0.05$; **, $p<0.01$; ***, $p<0.001$.

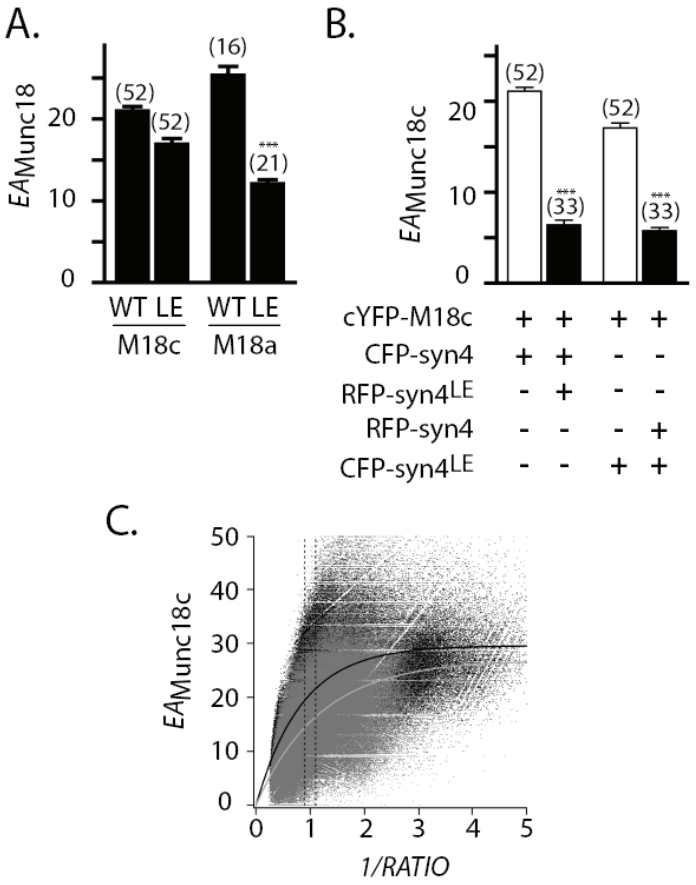

Figure 2.4. **Comparison of syntaxin4 and syntaxin1A LE mutants on SM protein binding**. *A*, Averaged apparent energy transfer (E_A) between the indicated isoforms of cYFP-Munc18 and CFP-syntaxin or CFP-syntaxin^{LE} co-expressed in HEK293-S3 cells. *RATIO*s between 0.9-1.1 were selected. *B*, Competition by RFP-syntaxin4^{LE}/CFP-syntaxin4 or RFP-syntaxin4/CFP-syntaxin4^{LE} pairs for binding to cYFP-Munc18c as measured by the energy transfer between the CFP and cYFP probes in living HEK293-S3 cells. Cells selected for analysis exhibited similar average *RATIO* (2.0±0.10 for both treatments). The number of observations is indicated above each column. *, p<0.05; **, p<0.01, ***; p<0.001. *C*, E_A at each image pixel was plotted against its corresponding inverse *RATIO* value for FRET between cYFP-Munc18c and CFP-syntaxin4 (black, *n*=61) or CFP-syntaxin4^{LE} (gray, *n*=67). Data were fit with a single exponential; the 95% confidence interval is displayed. Vertical dashed lines indicate the RATIO range over which E_A values were averaged for FRET experiments shown in (A).

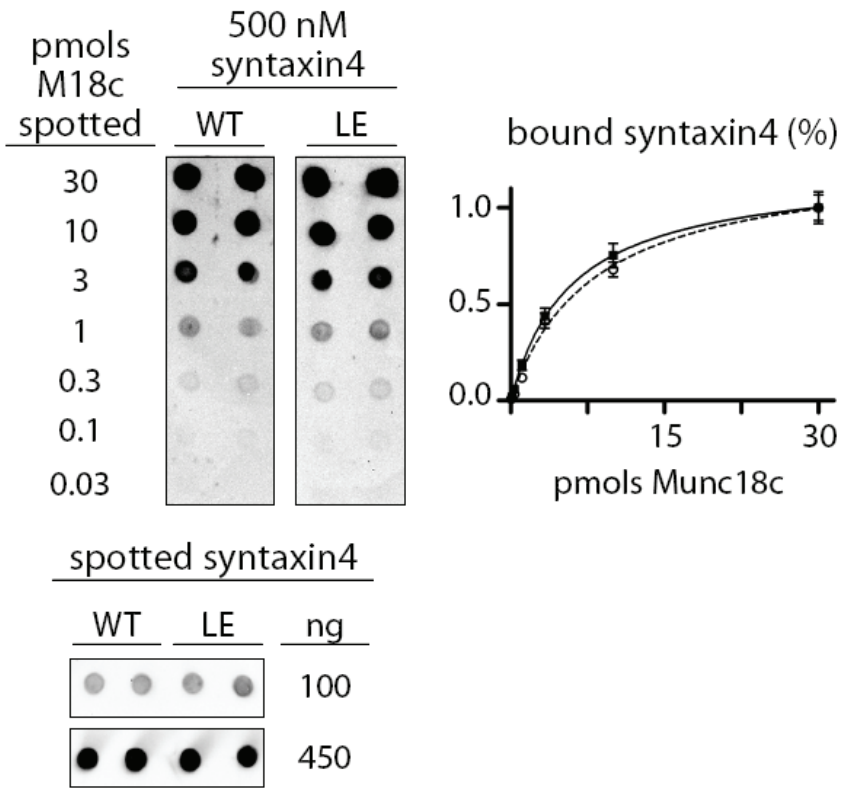

Figure 2.5. **In vitro binding relationship between Munc18c and syntaxin4^{WT} or syntaxin4^{LE}.** Immunoblots of the binding reaction between bacterially expressed and purified 500nM syntaxin4$_{1\text{-}275}$ (black squares, solid line) or syntaxin4$_{1\text{-}275}^{LE}$ (open circles, dashed line) and given quantities of Munc18c spotted on nitrocellulose. The syntaxin4 immunoreactive signal was quantified as a percent maximal binding (*n*=4 spots per condition); averaged results (*right*) are from three independent experiments. Syntaxin4$_{1\text{-}275}$ and syntaxin4$_{1\text{-}275}^{LE}$ used for binding were spotted on nitrocellulose to verify that equivalent amounts were used for binding and demonstrate equivalent immunoreactivity (*below*).

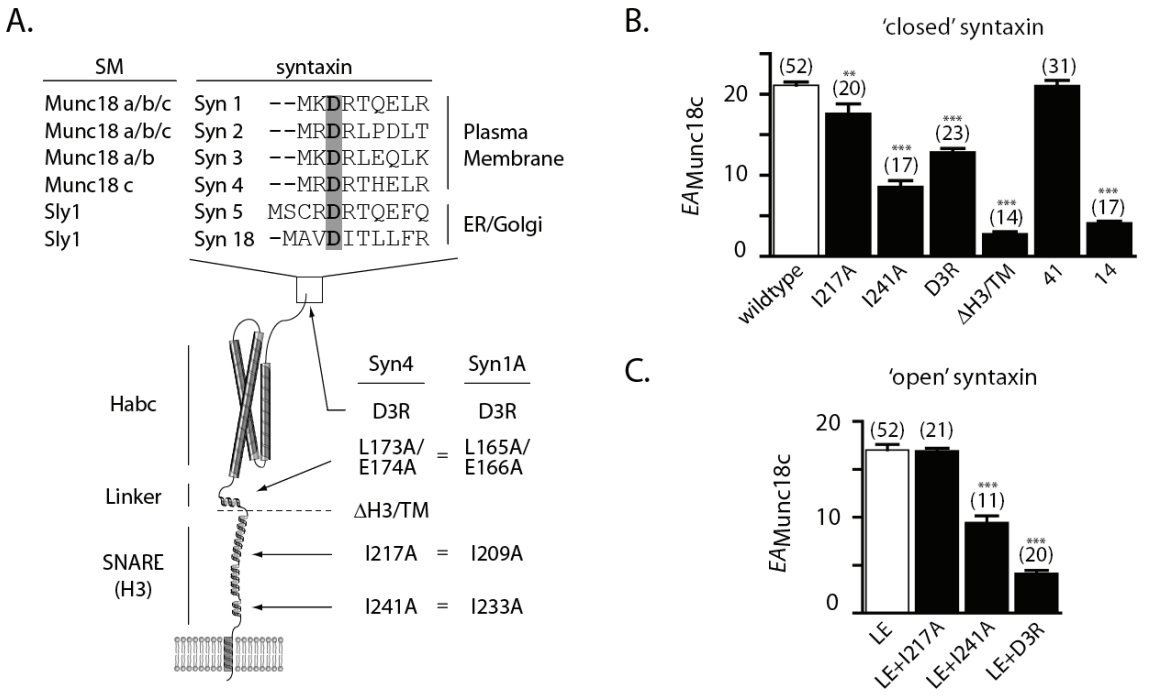

Figure 2.6. **Identification of the syntaxin4 domains required for Munc18c binding**. *A*, Diagram illustrating the relative position of syntaxin4 mutants used to identify interacting sites with Munc18c. Alignments of the syntaxin N-termini are shown for the four vertebrate exocytotic isoforms, as well as syntaxins 5 and 18 (Sed5p and Ufe1p in yeast, respectively). The aspartic acid residue mutated in syntaxin4^{D3R} is highlighted in gray. The SM binding partners for each syntaxin isoform are listed, although not all combinations exhibit equal affinity (Yamaguchi, Dulubova et al. 2002). In syntaxin4 chimeric mutants, termed 14 and 41 (not pictured), the syntaxin4 Habc or H3 domains were replaced with syntaxin1A sequence upstream or downstream of L189 as detailed in *Methods*. Syntaxin4$^{\Delta H3/TM}$ contains a stop codon in place of L189. *B*, Averaged apparent energy transfer (E_A) between cYFP-Munc18c and the indicated mutants of CFP-syntaxin4. Averaged E_A values determined for FRET *RATIO*s of 0.9-1.1 were selected. Significant differences are relative to syntaxin4^{WT} or syntaxin4^{LE} (white bars; controls redisplayed from Fig. 4A). Numbers of observations are indicated above bars. *, $p<0.05$; **, $p<0.01$, ***, $p<0.001$.

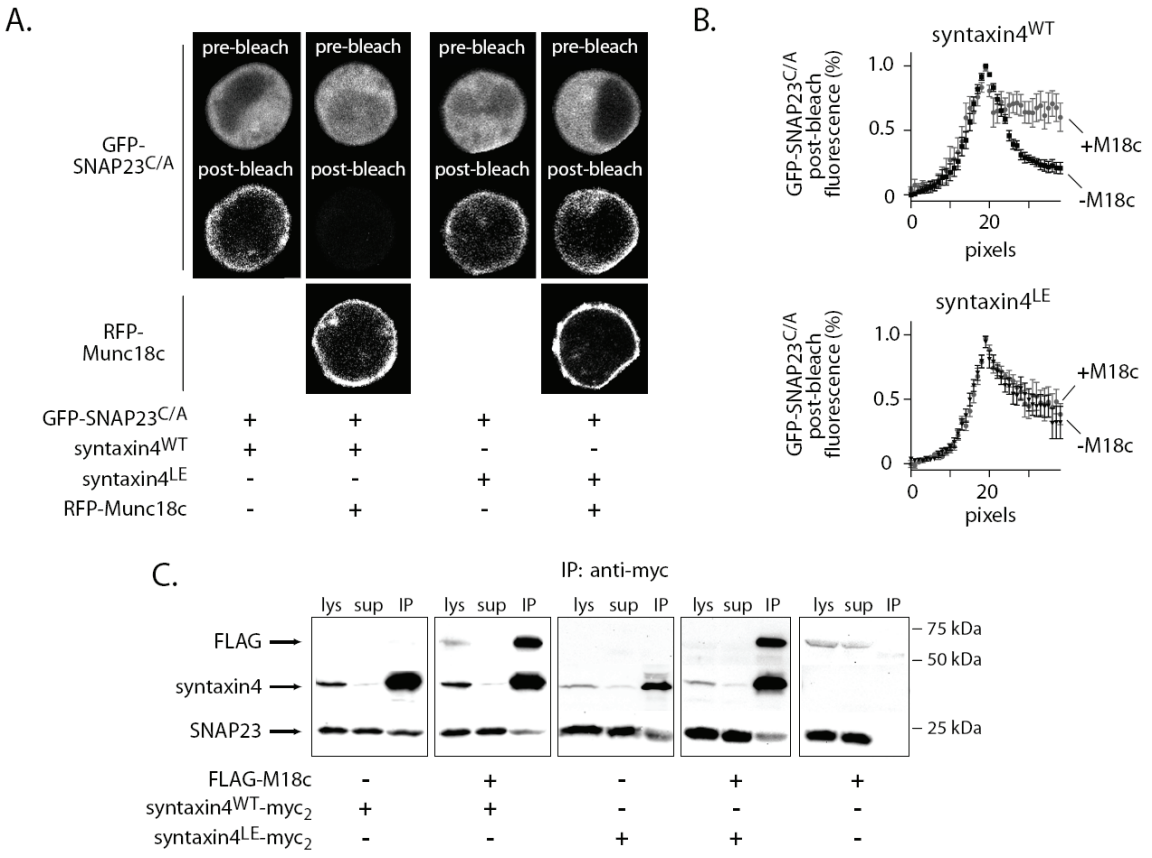

Figure 2.7. **Munc18c effects on Q-SNARE complex nucleation**. *A*, Confocal images of HEK293-S3 cells expressing GFP-SNAP23$^{C/A}$ and syntaxin4 in the absence or presence of RFP-Munc18c are shown after 1 min photobleach (488 nm) of a region in the cytosol. The localization of diffusible GFP-SNAP23$^{C/A}$ after cytosolic photobleach was used as an optical reporter for SNARE pairings with syntaxin4. *B*, Averaged GFP-SNAP23$^{C/A}$ fluorescence intensity remaining after photobleach was quantified by plotting the average GFP pixel intensity across the plasma membrane region for cells co-expressing syntaxin4 (*upper*) or syntaxin4^{LE} (*lower*) in the absence (*black squares*) or presence (*gray circles*) of RFP-Munc18c. Linescans are normalized to peak GFP intensity (n=8-12 cells analyzed per experiment; three independent experiments). *C*, Immunoblots showing co-immunoprecipitation of endogenous SNAP23 from HEK293-S3 cell lysates containing expressed syntaxin4^{WT}-myc$_2$ or syntaxin4^{LE}-myc$_2$ in the presence or absence of expressed FLAG-Munc18c. Lysates were incubated with anti-myc monoclonal antibody (9B11), pulled down with ProteinG-Sepharose, and subject to 12% SDS PAGE fractionation and Western Blot analysis. Blots were cut, and separately exposed to rabbit polyclonal antibodies against syntaxin4, SNAP23, and FLAG. Cell lysates (*Lys*) and supernatants (*Sup*) are shown for reference. No SNAP23 or FLAG-Munc18c pulldown was observed when syntaxin4-myc$_2$ was absent (*right*) (n=4).

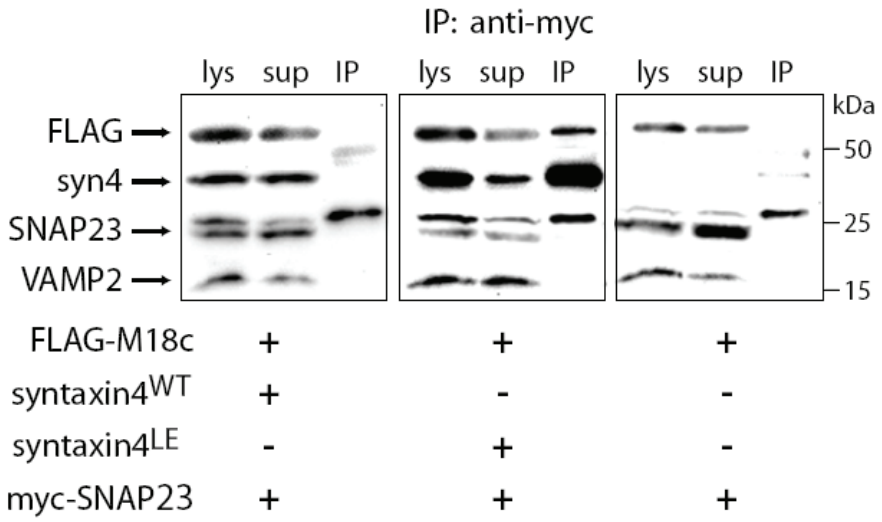

Figure 2.8. **Munc18c interaction with syntaxin4^{LE}-SNAP23 Q-SNARE complexes**. HEK293-S3 cell lysates expressing either syntaxin4^{WT} or syntaxin4^{LE} with FLAG-Munc18c and myc-SNAP23 were subject to immunoprecipitation (as detailed in Fig. 7C) using myc antibodies (*left, middle*). Expression conditions for each co-immunoprecipitation are indicated below immunoblots. Syntaxin4 was omitted in a control experiment (*right*). Blots were probed for SNAP23 and VAMP2 in addition to the overexpressed proteins syntaxin4 and FLAG-Munc18c (*n*=3).

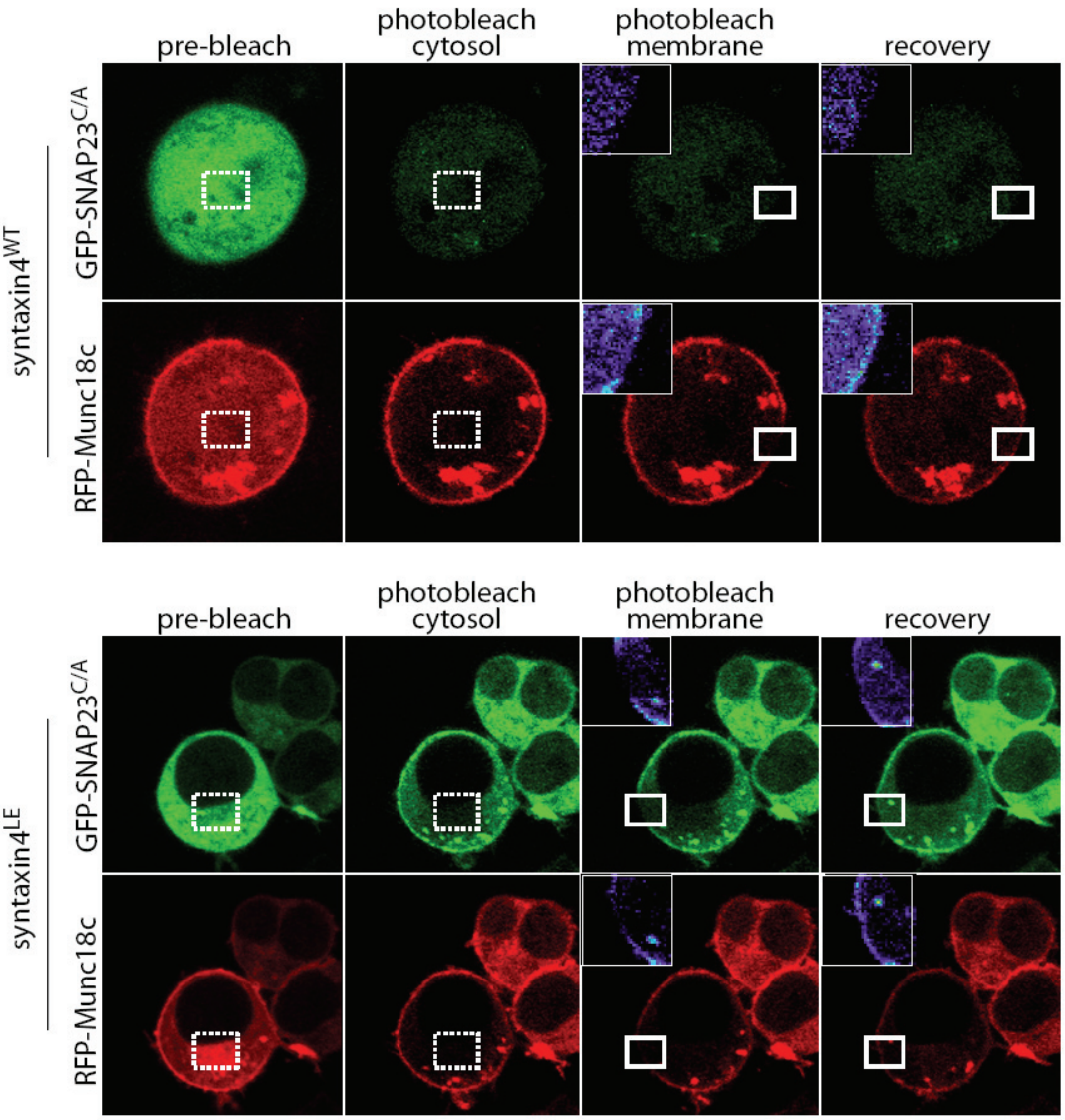

Figure 2.9. **FRAP reveals the presence of RFP-Munc18c/syntaxin4^{LE}/SNAP23$^{C/A}$ tripartite complexes on the plasma membrane of living HEK293 cells**. Representative confocal images of HEK293 cells expressing syntaxin4^{WT} (*upper*) or syntaxin4^{LE} (*lower*) with GFP-SNAP23$^{C/A}$ and RFP-Munc18c. Images show GFP and RFP fluorescence before and after 1 min photobleach (simultaneous 488 nm and 543 nm emission to bleach both GFP and RFP) of a region in the cytosol (dashed box). Photobleach of the cytosol was followed by a 10 sec photobleach (>50%) of a membrane region (box; magnified at inset) and a subsequent recovery period of 1.5 min. For the cytosolic photobleach, >90% bleach was obtained for both GFP and RFP signals. With exception to the pre-bleach images, the images have been scaled equivalently to visualize FRAP after the subsequent membrane photobleach. $n \geq 8$ for each treatment.

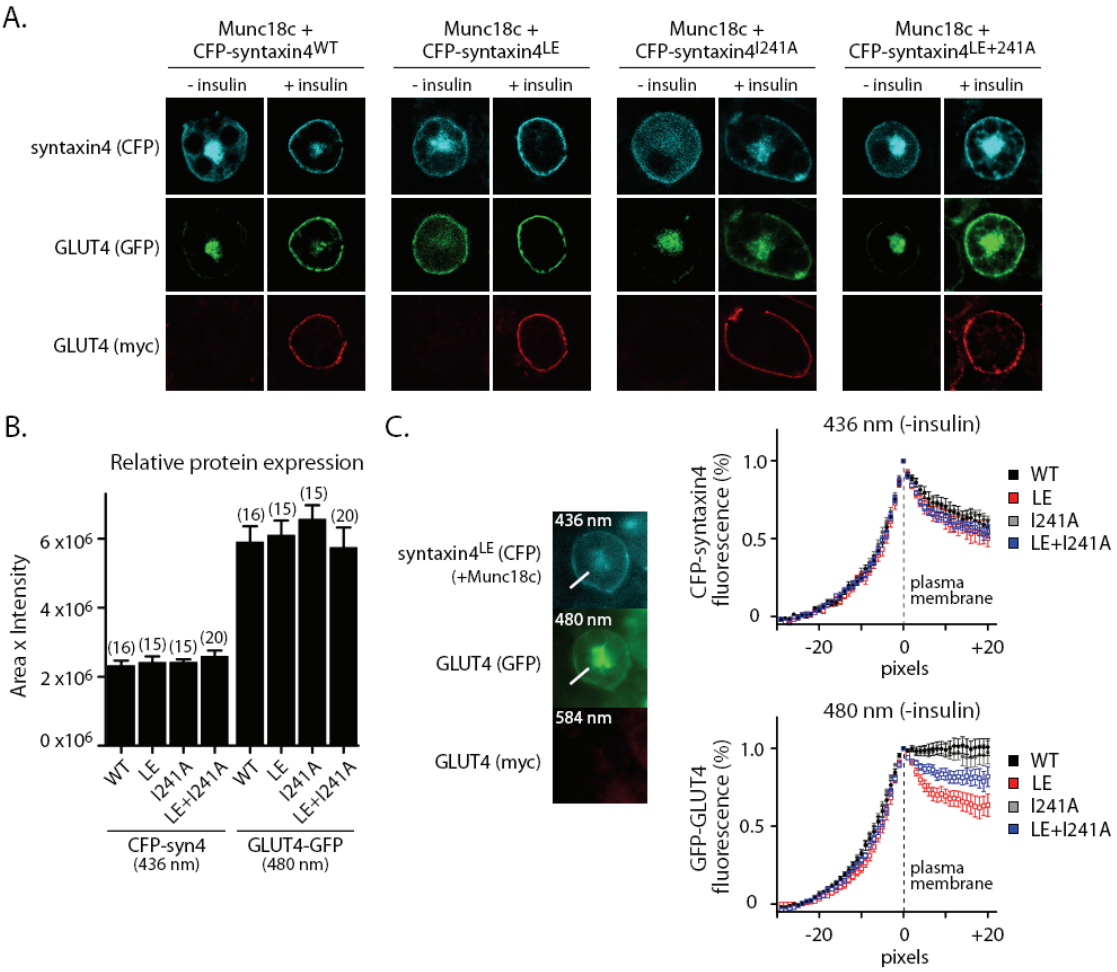

Figure 2.10. **Effects of syntaxin4 conformation and Munc18c complexation on GLUT4 vesicle docking in 3T3L1 adipocytes**. *A*, Confocal images of differentiated 3T3L1 adipocytes stably expressing myc$_7$-GLUT4-GFP, transfected with Munc18c and CFP-syntaxin4^{WT}, CFP-syntaxin4^{LE}, or CFP-syntaxin4^{I241A} as indicated. Cells were fixed before or after treatment with 100 nM insulin (30 min at 37C), and stained without permeabilization against the myc epitope located in the first exofacial loop of GLUT4. *B*, Relative expression levels of CFP-syntaxin4 (or mutants as indicated) and myc$_7$-GLUT4-GFP were determined in adipocytes based on fluorescence intensity. Munc18c was coexpressed for each condition and results were quantified from non-insulin stimulated cells. Numbers above columns indicate number of cells imaged. No significant differences in CFP or GFP expression were found between treatments. *C*, Relative plasma membrane localization of CFP-syntaxin4 (436 nm) and myc$_7$-GLUT4-GFP (480 nm) for cells in (B). Fluorescence intensity along a 10 pixel-width linescan was determined for each cell. The plasma membrane is set at pixel 30. Plots show averaged data (±SEM). A representative cell expressing Munc18c, CFP-syntaxin4^{LE}, and myc$_7$-GLUT4-GFP is shown for clarity with a typical region selected for linescan (*left*).

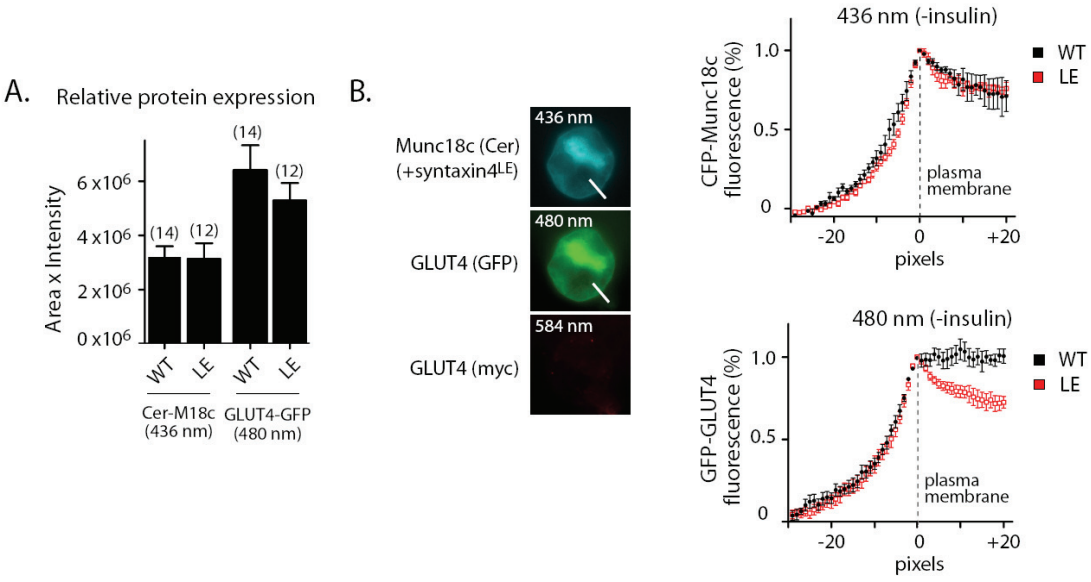

Figure 2.11. **3T3L1 adipocytes coexpressing syntaxin4^{LE}/Cerulean-Munc18c exhibit abnormal vesicle docking in the absence of insulin**. *A*, Relative expression levels of Cerulean-Munc18c and myc$_7$-GLUT4-GFP were quantified based on fluorescence intensity from images of differentiated 3T3L1 adipocytes stably expressing myc$_7$-GLUT4-GFP and transiently transfected with Cerulean-Munc18c and syntaxin4^{WT} (WT) or syntaxin4^{LE} (LE). Cells were fixed after 3 hour serum starvation, and stained without permeabilization against the myc epitope located in the first exofacial loop of GLUT4. Numbers above columns indicate number of cells imaged. No significant differences in CFP or GFP expression were found between treatments. *B*, Relative plasma membrane localization of Cerulean-Munc18c (436 nm) and myc$_7$-GLUT4-GFP (480 nm) for cells in (A). Fluorescence intensity along a 10 pixel-width linescan was determined for each cell. The plasma membrane is set at pixel 30. Plots show averaged data (±SEM). A representative cell expressing Cerulean-Munc18c, syntaxin4^{LE}, and myc$_7$-GLUT4-GFP is shown for clarity with a typical region selected for linescan (*left*).

Figure 2.12**. Visualizing Munc18 and syntaxin subcellular localization in living cells**. *A*, To facilitate subcellular localization of syntaxin and Munc18 in living 3T3L1 adipocytes, we engineered fusion proteins to spectral variants of green-fluorescent protein (GFP) from the hydromedusa *Aequoria victoria*. Syntaxin 1 and 4 isoforms were labeled with monomeric cyan-fluorescent protein (CFP) and Munc18 a and c isoforms with monomeric citrine (cYFP), a pH insensitive mutant of yellow-fluorescent protein. For both syntaxin and Munc18, the N-termini were chosen for the fluoroprotein label based on their steric availability, which is evident in the crystal structure of syntaxin1A in complex with Munc18-1 (Misura, Scheller et al. 2000). *B*, Differentiated 3T3L1 adipocytes were electroporated with 200 μg each of the CFP- or cYFP-tagged proteins as indicated, and visualized using conventional fluorescence microscopy. Cotransfection conditions (not pictured) are indicated in parentheses. *C*, Plasma membrane targeting factors (TF) for cYFP-Munc18c or -Munc18a were calculated based on the ability of specific isoforms of syntaxin to localize Munc18 to the PM in 3T3L1 adipocytes. Mean values are expressed as the ratio of average fluorescence intensity in the membrane region compared with the average fluorescence intensity measured over the cytosol, corrected for area (see *Experimental Procedures* for equation). Numbers above columns indicate numbers of cells imaged. Significant differences are from the Munc18c-syntaxin4 treatment. *D*, HEK293-S3 cells were transfected with 2 μg each of the CFP- or cYFP-tagged proteins as indicated. *E*, TFs for Munc18 were calculated from images of HEK293-S3 cells as in *C*. *F*, HEK293-S3 cells were imaged following transfection with 2 μg each of the CFP- or cYFP-tagged proteins as indicated. *, $p<0.05$; **, $p<0.01$; ***, $p<0.001$.

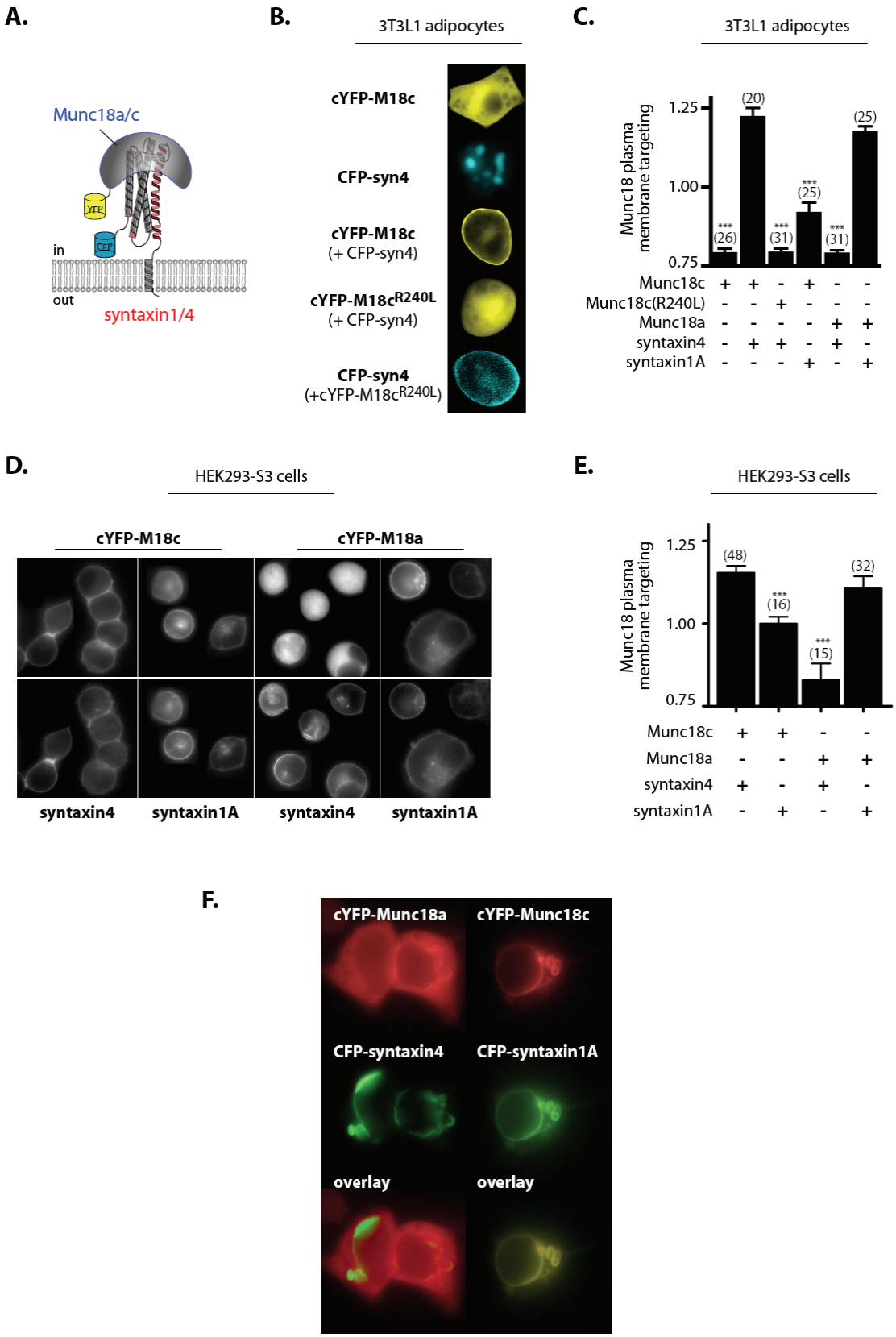
A.
Munc18a/c
YFP
CFP
in
out
syntaxin1/4
B.
3T3L1 adipocytes
cYFP-M18c
CFP-syn4
cYFP-M18c
(+ CFP-syn4)
cYFP-M18cR240L
(+ CFP-syn4)
CFP-syn4
(+cYFP-M18cR240L)
C.
3T3L1 adipocytes
Munc18 plasma membrane targeting
1.25
1.00
0.75
(20)
(25)
***
(26)
***
(31)
***
(25)
***
(31)
Munc18c + + - + - -
Munc18c(R240L) - - + - - -
Munc18a - - - - + +
syntaxin4 - + + - + -
syntaxin1A - - - + - +
D.
HEK293-S3 cells
cYFP-M18c
cYFP-M18a
syntaxin4
syntaxin1A
syntaxin4
syntaxin1A
E.
HEK293-S3 cells
Munc18 plasma membrane targeting
1.25
1.00
0.75
(48)
***
(16)
***
(15)
(32)
Munc18c + + - -
Munc18a - - + +
syntaxin4 + - + -
syntaxin1A - + - +
F.
cYFP-Munc18a
cYFP-Munc18c
CFP-syntaxin4
CFP-syntaxin1A
overlay
overlay

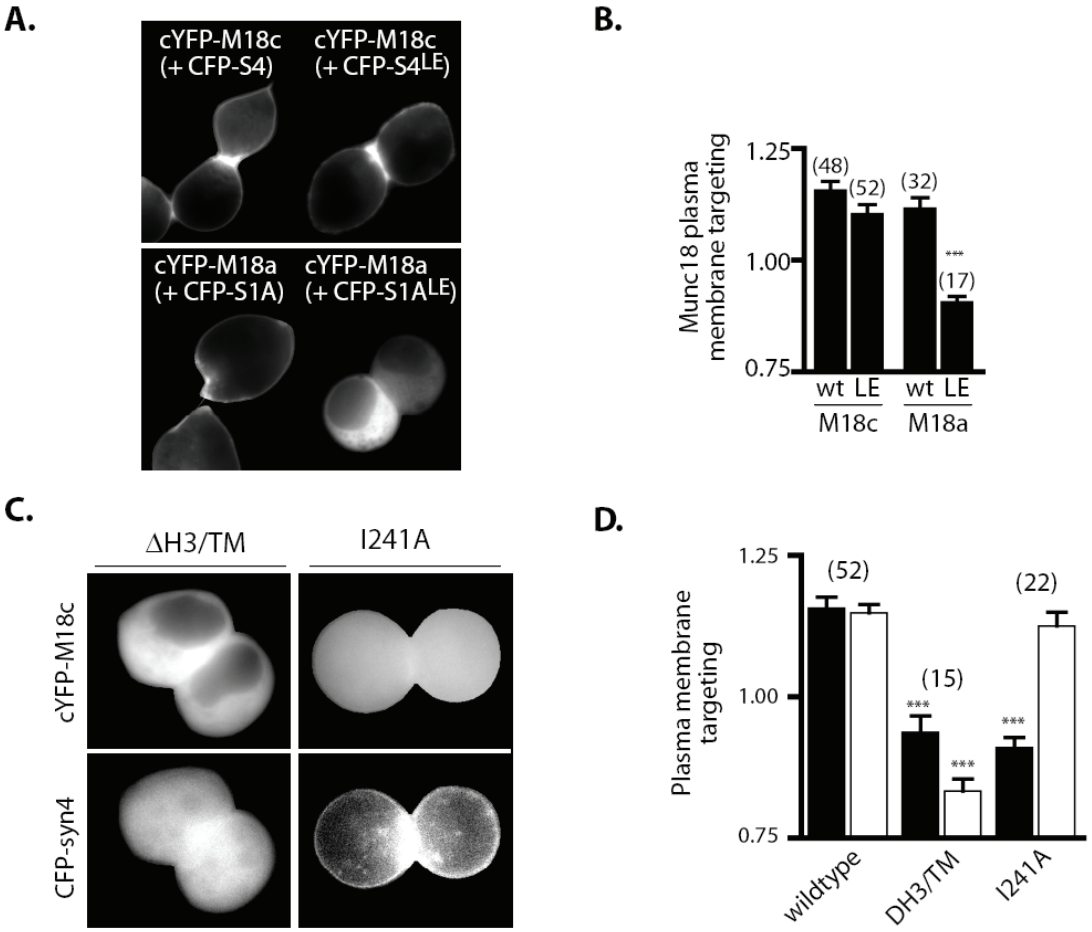

Figure 2.13. **Effect of syntaxin conformation on Munc18 plasma membrane localization.** *A*, HEK293-S3 cells were transfected with either cYFP-Munc18c or cYFP-Munc18a, with co-transfected wildtype or constitutively open (LE) syntaxin as indicated in parenthesis. B, Averaged targeting factors for each transfection condition in *A*. *C*, Epifluorescence images of HEK293-S3 cells expressing cYFP-Munc18c and syntaxin4^{I241A} (eliminates Munc18c binding) or syntaxin4$^{dH3/TM}$ (lacks the SNARE (H3) and transmembrane (TM) domains). D, Quantification of membrane targeting of Munc18c (black bars) and syntaxin4 (white bars). Numbers above columns indicate numbers of cells imaged. *, $p<0.05$; **, $p<0.01$, ***, $p<0.001$.

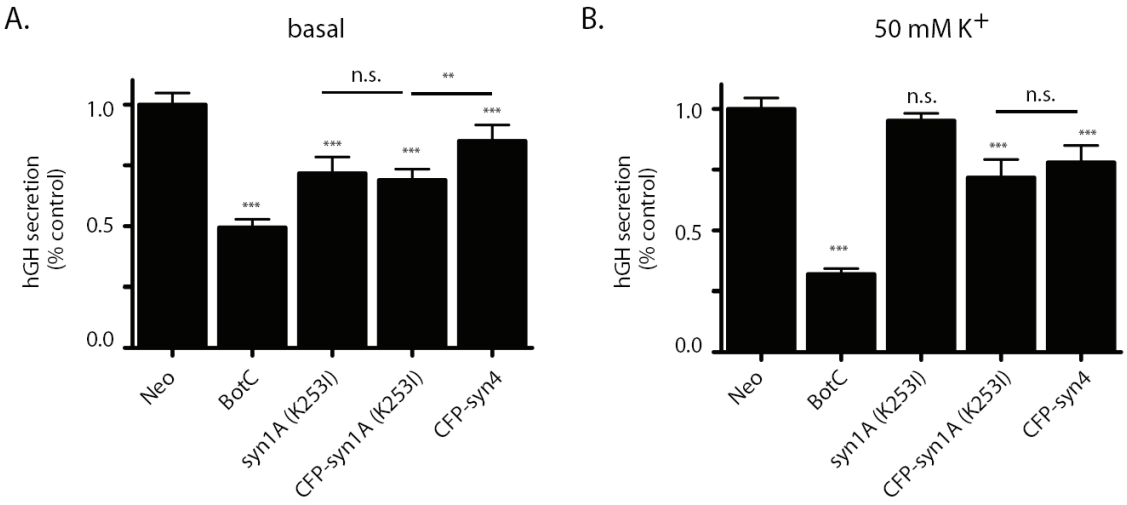

Figure 2.14. **BotC knockdown allows testing of functional effects of exogenous syntaxin constructs in living secretory cells.** Rescue of BotC knockdown of human growth hormone (hGH) secretion under basal or stimulatory (50 mM K^+, 6 min) conditions was measured from transfected PC12 cells. CFP-Syntaxin1A^{K253I} (BotC resistant) and CFP-syntaxin4^{WT} were transfected with equimolar amounts of Munc18a or Munc18c, respectively. Secretion was normalized to total hGH content. Significant differences are from control cells transfected with pCMV-Neo: *, $p<0.05$; **, $p<0.01$; ***, $p<0.001$. Bars, means ± SEM.

	no insulin		
Transfection conditions	***GLUT4***	***myc***	
Munc18c + CFP-syntaxin4^{WT}	18 ± 10%	2.5 ± 1.5%	*n*=75
Munc18c + CFP-syntaxin4^{LE}	79 ± 3%	5 ± 3%	*n*=100
Munc18c + CFP-syntaxin4^{I241A}	12 ± 4%	2.5 ± 1.5%	*n*=75
Munc18c + CFP-syntaxin4$^{LE+I241A}$	40 ± 6%	4.5 ± 0.5%	*n*=60

	insulin		
Transfection conditions	***GLUT4***	***myc***	
Munc18c + CFP-syntaxin4^{WT}	83 ± 4%	46 ± 2%	*n*=114
Munc18c + CFP-syntaxin4^{LE}	92 ± 6%	52 ± 2%	*n*=125
Munc18c + CFP-syntaxin4^{I241A}	92 ± 2%	65 ± 1%	*n*=75
Munc18c + CFP-syntaxin4$^{LE+I241A}$	88 ± 4%	45 ± 2%	*n*=60

Table 2.1. **Effects of syntaxin4 mutants on GLUT4 trafficking and fusion in 3T3L1 adipocytes**. 3T3L1 adipocytes stably expressing myc$_7$-GLUT4-GFP were transfected with the indicated constructs, fixed before or after treatment with 100 nM insulin for 30 min at 37C, and stained with myc antibody. The percentage of CFP-positive cells exhibiting peripheral GLUT4 (as detected by GFP fluorescence) or GLUT4 externalization (as detected by indirect myc immunofluorescence) are displayed ± SEM (data are averaged from 3 independent experiments).

References

Araki, S., Y. Tamori, et al. (1997). "Inhibition of the binding of SNAP-23 to syntaxin 4 by Munc18c." Biochem Biophys Res Commun **234**(1): 257-62.

Arunachalam, L., L. Han, et al. (2008). "Munc18-1 Is Critical for Plasma Membrane Localization of Syntaxin1 but Not of SNAP-25 in PC12 Cells." Mol Biol Cell **19**(2): 722-734.

Bhattacharya, S., B. A. Stewart, et al. (2002). "Members of the synaptobrevin/vesicle-associated membrane protein (VAMP) family in Drosophila are functionally interchangeable in vivo for neurotransmitter release and cell viability." Proc Natl Acad Sci U S A **99**(21): 13867-72.

Bogan, J. S., A. E. McKee, et al. (2001). "Insulin-responsive compartments containing GLUT4 in 3T3-L1 and CHO cells: regulation by amino acid concentrations." Mol Cell Biol **21**(14): 4785-806.

Bose, A., S. Robida, et al. (2004). "Unconventional myosin Myo1c promotes membrane fusion in a regulated exocytic pathway." Mol Cell Biol **24**(12): 5447-58.

Bryant, N. J. and D. E. James (2001). "Vps45p stabilizes the syntaxin homologue Tlg2p and positively regulates SNARE complex formation." Embo J **20**(13): 3380-8.

Bryant, N. J. and D. E. James (2003). "The Sec1p/Munc18 (SM) protein, Vps45p, cycles on and off membranes during vesicle transport." J Cell Biol **161**(4): 691-6.

Calakos, N., M. K. Bennett, et al. (1994). "Protein-protein interactions contributing to the specificity of intracellular vesicular trafficking." Science **263**(5150): 1146-9.

Cao, X., N. Ballew, et al. (1998). "Initial docking of ER-derived vesicles requires Uso1p and Ypt1p but is independent of SNARE proteins." Embo J **17**(8): 2156-65.

Carr, C. M., E. Grote, et al. (1999). "Sec1p binds to SNARE complexes and concentrates at sites of secretion." J Cell Biol **146**(2): 333-44.

Chang, L., S. H. Chiang, et al. (2006). "TC10{alpha} is Required for Insulin-Stimulated Glucose Uptake in Adipocytes." Endocrinology.

de Wit, H., L. N. Cornelisse, et al. (2006). "Docking of secretory vesicles is syntaxin dependent." PLoS ONE **1**: e126.

Dugani, C. B. and A. Klip (2005). "Glucose transporter 4: cycling, compartments and controversies." EMBO Rep **6**(12): 1137-42.

Dulubova, I., M. Khvotchev, et al. (2007). "Munc18-1 binds directly to the neuronal SNARE complex." Proc Natl Acad Sci U S A.

Dulubova, I., S. Sugita, et al. (1999). "A conformational switch in syntaxin during exocytosis: role of munc18." Embo J **18**(16): 4372-82.

Dulubova, I., T. Yamaguchi, et al. (2003). "Convergence and divergence in the mechanism of SNARE binding by Sec1/Munc18-like proteins." Proc Natl Acad Sci U S A **100**(1): 32-7.

Dulubova, I., T. Yamaguchi, et al. (2002). "How Tlg2p/syntaxin 16 'snares' Vps45." Embo J **21**(14): 3620-31.

Gengyo-Ando, K., H. Kitayama, et al. (1996). "A murine neural-specific homolog corrects cholinergic defects in Caenorhabditis elegans unc-18 mutants." J Neurosci **16**(21): 6695-702.

Gladycheva, S. E., C. S. Ho, et al. (2004). "Regulation of syntaxin1A-munc18 complex for SNARE pairing in HEK293 cells." J Physiol **558**(Pt 3): 857-71.

Gonzalez, E. and T. E. McGraw (2006). "Insulin signaling diverges into Akt-dependent and -independent signals to regulate the recruitment/docking and the fusion of GLUT4 vesicles to the plasma membrane." Mol Biol Cell **17**(10): 4484-93.

Graham, M. E., J. W. Barclay, et al. (2004). "Syntaxin/Munc18 interactions in the late events during vesicle fusion and release in exocytosis." J Biol Chem **279**(31): 32751-60.

Hodgkinson, C. P., A. Mander, et al. (2005). "Protein kinase-zeta interacts with munc18c: role in GLUT4 trafficking." Diabetologia **48**(8): 1627-36.

Hoppe, A., K. Christensen, et al. (2002). "Fluorescence resonance energy transfer-based stoichiometry in living cells." Biophys J **83**(6): 3652-64.
Jahn, R. and R. H. Scheller (2006). "SNAREs--engines for membrane fusion." Nat Rev Mol Cell Biol **7**(9): 631-43.
Jhun, B. H., A. L. Rampal, et al. (1992). "Effects of insulin on steady state kinetics of GLUT4 subcellular distribution in rat adipocytes. Evidence of constitutive GLUT4 recycling." J Biol Chem **267**(25): 17710-5.
Kanda, H., Y. Tamori, et al. (2005). "Adipocytes from Munc18c-null mice show increased sensitivity to insulin-stimulated GLUT4 externalization." J Clin Invest **115**(2): 291-301.
Kee, Y., R. C. Lin, et al. (1995). "Distinct domains of syntaxin are required for synaptic vesicle fusion complex formation and dissociation." Neuron **14**(5): 991-8.
Khvotchev, M., I. Dulubova, et al. (2007). "Dual modes of Munc18-1/SNARE interactions are coupled by functionally critical binding to syntaxin-1 N terminus." J Neurosci **27**(45): 12147-55.
Lam, A. D., P. Tryoen-Toth, et al. (2008). "SNARE-catalyzed Fusion Events Are Regulated by Syntaxin1A-Lipid Interactions." Mol Biol Cell **19**(2): 485-97.
Lang, T., M. Margittai, et al. (2002). "SNAREs in native plasma membranes are active and readily form core complexes with endogenous and exogenous SNAREs." J Cell Biol **158**(4): 751-60.
Latham, C. F., J. A. Lopez, et al. (2006). "Molecular dissection of the munc18c/syntaxin4 interaction: implications for regulation of membrane trafficking." Traffic **7**(10): 1408-19.
Liu, J., S. A. Ernst, et al. (2004). "Fluorescence resonance energy transfer reports properties of syntaxin1a interaction with Munc18-1 in vivo." J Biol Chem **279**(53): 55924-36.
Lizunov, V. A., H. Matsumoto, et al. (2005). "Insulin stimulates the halting, tethering, and fusion of mobile GLUT4 vesicles in rat adipose cells." J Cell Biol **169**(3): 481-9.
Margittai, M., J. Widengren, et al. (2003). "Single-molecule fluorescence resonance energy transfer reveals a dynamic equilibrium between closed and open conformations of syntaxin 1." Proc Natl Acad Sci U S A **100**(26): 15516-21.
Medine, C. N., C. Rickman, et al. (2007). "Munc18-1 prevents the formation of ectopic SNARE complexes in living cells." J Cell Sci **120**(Pt 24): 4407-15.
Misura, K. M., R. H. Scheller, et al. (2000). "Three-dimensional structure of the neuronal-Sec1-syntaxin 1a complex." Nature **404**(6776): 355-62.
Oh, E., B. A. Spurlin, et al. (2005). "Munc18c heterozygous knockout mice display increased susceptibility for severe glucose intolerance." Diabetes **54**(3): 638-47.
Palm, G. J. and A. Wlodawer (1999). "Spectral variants of green fluorescent protein." Methods Enzymol **302**: 378-94.
Parlati, F., J. A. McNew, et al. (2000). "Topological restriction of SNARE-dependent membrane fusion." Nature **407**(6801): 194-8.
Parlati, F., T. Weber, et al. (1999). "Rapid and efficient fusion of phospholipid vesicles by the alpha-helical core of a SNARE complex in the absence of an N-terminal regulatory domain." Proc Natl Acad Sci U S A **96**(22): 12565-70.
Peng, R. and D. Gallwitz (2002). "Sly1 protein bound to Golgi syntaxin Sed5p allows assembly and contributes to specificity of SNARE fusion complexes." J Cell Biol **157**(4): 645-55.
Peng, R. and D. Gallwitz (2004). "Multiple SNARE interactions of an SM protein: Sed5p/Sly1p binding is dispensable for transport." Embo J **23**(20): 3939-49.
Pevsner, J., S. C. Hsu, et al. (1994). "Specificity and regulation of a synaptic vesicle docking complex." Neuron **13**(2): 353-61.
Richmond, J. E., R. M. Weimer, et al. (2001). "An open form of syntaxin bypasses the requirement for UNC-13 in vesicle priming." Nature **412**(6844): 338-41.
Rowe, J., F. Calegari, et al. (2001). "Syntaxin 1A is delivered to the apical and basolateral domains of epithelial cells: the role of munc-18 proteins." J Cell Sci **114**(Pt 18): 3323-32.

Rowe, J., N. Corradi, et al. (1999). "Blockade of membrane transport and disassembly of the Golgi complex by expression of syntaxin 1A in neurosecretion-incompetent cells: prevention by rbSEC1." J Cell Sci **112 (Pt 12)**: 1865-77.

Satoh, S., H. Nishimura, et al. (1993). "Use of bismannose photolabel to elucidate insulin-regulated GLUT4 subcellular trafficking kinetics in rat adipose cells. Evidence that exocytosis is a critical site of hormone action." J Biol Chem **268**(24): 17820-9.

Schiavo, G., O. Rossetto, et al. (1994). "Clostridial neurotoxins as tools to investigate the molecular events of neurotransmitter release." Semin Cell Biol **5**(4): 221-9.

Schutz, D., F. Zilly, et al. (2005). "A dual function for Munc-18 in exocytosis of PC12 cells." Eur J Neurosci **21**(9): 2419-32.

Scott, B. L., J. S. Van Komen, et al. (2004). "Sec1p directly stimulates SNARE-mediated membrane fusion in vitro." J Cell Biol **167**(1): 75-85.

Shen, J., D. C. Tareste, et al. (2007). "Selective activation of cognate SNAREpins by Sec1/Munc18 proteins." Cell **128**(1): 183-95.

Tamori, Y., M. Kawanishi, et al. (1998). "Inhibition of insulin-induced GLUT4 translocation by Munc18c through interaction with syntaxin4 in 3T3-L1 adipocytes." J Biol Chem **273**(31): 19740-6.

Tellam, J. T., S. L. Macaulay, et al. (1997). "Characterization of Munc-18c and syntaxin-4 in 3T3-L1 adipocytes. Putative role in insulin-dependent movement of GLUT-4." J Biol Chem **272**(10): 6179-86.

Tellam, J. T., S. McIntosh, et al. (1995). "Molecular identification of two novel Munc-18 isoforms expressed in non-neuronal tissues." J Biol Chem **270**(11): 5857-63.

ter Beest, M. B., S. J. Chapin, et al. (2005). "The role of syntaxins in the specificity of vesicle targeting in polarized epithelial cells." Mol Biol Cell **16**(12): 5784-92.

Thurmond, D. C., B. P. Ceresa, et al. (1998). "Regulation of insulin-stimulated GLUT4 translocation by Munc18c in 3T3L1 adipocytes." J Biol Chem **273**(50): 33876-83.

Thurmond, D. C. and J. E. Pessin (2000). "Discrimination of GLUT4 vesicle trafficking from fusion using a temperature-sensitive Munc18c mutant." Embo J **19**(14): 3565-75.

Toonen, R. F., K. J. de Vries, et al. (2005). "Munc18-1 stabilizes syntaxin 1, but is not essential for syntaxin 1 targeting and SNARE complex formation." J Neurochem **93**(6): 1393-400.

Toonen, R. F. and M. Verhage (2003). "Vesicle trafficking: pleasure and pain from SM genes." Trends Cell Biol **13**(4): 177-86.

Verhage, M., A. S. Maia, et al. (2000). "Synaptic assembly of the brain in the absence of neurotransmitter secretion." Science **287**(5454): 864-9.

Voets, T., R. F. Toonen, et al. (2001). "Munc18-1 promotes large dense-core vesicle docking." Neuron **31**(4): 581-91.

Vogel, K., J. P. Cabaniols, et al. (2000). "Targeting of SNAP-25 to membranes is mediated by its association with the target SNARE syntaxin." J Biol Chem **275**(4): 2959-65.

Vogel, S. S., C. Thaler, et al. (2006). "Fanciful FRET." Sci STKE **2006**(331): re2.

Weber, T., B. V. Zemelman, et al. (1998). "SNAREpins: minimal machinery for membrane fusion." Cell **92**(6): 759-72.

Wick, P. F., R. A. Senter, et al. (1993). "Transient transfection studies of secretion in bovine chromaffin cells and PC12 cells. Generation of kainate-sensitive chromaffin cells." J Biol Chem **268**(15): 10983-9.

Widberg, C. H., N. J. Bryant, et al. (2003). "Tomosyn interacts with the t-SNAREs syntaxin4 and SNAP23 and plays a role in insulin-stimulated GLUT4 translocation." J Biol Chem **278**(37): 35093-101.

Wu, M. N., T. Fergestad, et al. (1999). "Syntaxin 1A interacts with multiple exocytic proteins to regulate neurotransmitter release in vivo." Neuron **23**(3): 593-605.

Yamaguchi, T., I. Dulubova, et al. (2002). "Sly1 binds to Golgi and ER syntaxins via a conserved N-terminal peptide motif." Dev Cell **2**(3): 295-305.

Yang, B., L. Gonzalez, Jr., et al. (1999). "SNARE interactions are not selective. Implications for membrane fusion specificity." J Biol Chem **274**(9): 5649-53.
Yang, B., M. Steegmaier, et al. (2000). "nSec1 binds a closed conformation of syntaxin1A." J Cell Biol **148**(2): 247-52.
Yang, C., K. J. Coker, et al. (2001). "Syntaxin 4 heterozygous knockout mice develop muscle insulin resistance." J Clin Invest **107**(10): 1311-8.
Yang, X., P. Xu, et al. (2006). "Domain requirement for the membrane trafficking and targeting of syntaxin 1A." J Biol Chem **281**(22): 15457-63.
Zilly, F. E., J. B. Sorensen, et al. (2006). "Munc18-Bound Syntaxin Readily Forms SNARE Complexes with Synaptobrevin in Native Plasma Membranes." PLoS Biol **4**(10).

CHAPTER III

RAB27A-DEPENDENT ACTIONS ON VESICLE DOCKING AND PRIMING IN PANCREATIC β-CELLS

Abstract

The small GTPase Rab27a, along with the isoforms of Rab3, is present on insulin secretory granules and has been implicated in regulation of Ca^{2+}-triggered exocytosis. We have used membrane capacitance measurements to define the role of Rab27a in regulating the size and refilling of distinct pools of insulin granules by comparison of evoked secretory responses from Rab27a-null *ashen* and strain-matched wildtype control pancreatic β-cells. We find that *ashen* β-cells display a kinetic defect in refilling of readily-releasable and immediately-releasable vesicle pools (RRP and IRP, respectively) in response to depolarization-evoked Ca^{2+} influx. The deficit in IRP refilling was not observed in the presence of stimulatory glucose concentrations (16.7 mM), though incomplete refilling of the RRP persisted. Comparatively, β-cells from $Rab3a^{-/-}$ mice exhibited complete refilling of the IRP and RRP, demonstrating that Rab27a and Rab3a exert distinct roles in the insulin granule secretory pathway. Further, depletion of the RRP in *ashen* β-cells was two-fold faster than that of control β-cells. These deficits in refilling and exocytotic rate in *ashen* β-cells were absent when cAMP-regulatory pathways were activated. Elevated cAMP increased the RRP pool size, and complete refilling of the RRP occurred in *ashen* β-cells; responses were comparable to wildtype controls. These effects of cAMP were largely eliminated by Rp-cAMP inhibition of PKA, indicating that PKA acts on vesicle priming downstream or via pathways independent of Rab27a. In summary, Rab27a exerts dual roles in

glucose-mediated insulin granule exocytosis, facilitating refilling of releasable granule pools while also limiting the rate of release from these pools.

Introduction

Glucose initially evokes insulin release from pancreatic β-cells by increasing ATP production, which closes K_{ATP} channels and results in the opening of voltage-dependent Ca^{2+} channels, stimulating Ca^{2+}-triggered insulin granule exocytosis. Kinetically slower secretion-amplifying pathways that are dependent on glucose metabolism but independent of the K_{ATP} channel also occur, and their relevance has been extensively reviewed (Eliasson *et al.* 1997; Takahashi *et al.* 1997). Additionally, hormones and neurotransmitters modulate the magnitude of secretion through a number of G-protein coupled receptor pathways. For example, GLP-1 and GIP generate intracellular second messenger signals that include cAMP, which then directly activates protein kinase A (PKA) and Epac2 (exchange protein directly activated by cAMP) leading to a robust enhancement of the secretory response (Jones *et al.* 1986; Ammala *et al.* 1993; Renstrom *et al.* 1997; Wan *et al.* 2004; Yang and Gillis 2004; Shibasaki *et al.* 2007). The net effect of the secondary metabolic and cAMP amplifying pathways is to increase the number of insulin containing granules that are immediately competent for release. These pools of release competent granules include the 'readily-releasable' pool (RRP), a subset of which is the 'immediately-releasable' pool (IRP) that is spatially positioned adjacent to Ca^{2+}-channels, and a small highly Ca^{2+}-sensitive pool (HCSP) that is distinct from the RRP (Wan *et al.* 2004; Yang and Gillis 2004). The number of secretory granules in each pool, the rate of pool refilling, and the rate at which fusion is regulated from these pools largely determines the short-term secretory response of a β-cell.

Rab proteins, which belong to the Ras-related superfamily of small monomeric GTPases, are central mediators of membrane trafficking in all eukaryotic cells. Rab proteins continuously

cycle between GTP and GDP bound states, interacting and activating effector molecules when GTP-bound (Fukuda 2005). With respect to regulated exocytosis, Rab proteins regulate a series of steps including: vesicle/granule transport along cytoskeletal tracts, physical attachment of the vesicles/granules to the plasma membrane (*i.e.*, docking/tethering), priming reactions that allow assembly of the molecular machinery for membrane fusion, and soluble N-ethylmaleimide-sensitive factor attachment protein receptor (SNARE)-catalyzed fusion (Burgoyne and Morgan 2003). Rab27a, along with four isoforms of Rab3 (a/b/c/d), are localized to secretory granules in a number of cell types, and have been directly implicated in the regulation of Ca^{2+}-dependent exocytosis in β-cells (Fukuda 2005). While Rab27a mutants locked in the GTP-bound and GDP-bound states strongly facilitate and potently inhibit insulin secretion, respectively (Yi *et al.* 2002; Fukuda 2003), it is becoming increasingly apparent that it is the rate at which GTP/GDP cycles on Rab proteins that determine the level of their control on a physiologic function (Kondo *et al.* 2006).

Rab27a deficiency results in multiple defects in *ashen* mice (Wilson *et al.* 2000), which are glucose intolerant owing to strongly reduced first- and second-phase glucose-stimulated insulin secretion (Kasai *et al.* 2005). Part of the β-cell secretory defect is reportedly due to a deficit in the replenishment of docked granules, a phenotype evident in other Rab27a-null secretory cells including melanosomes and cytotoxic T-lymphocytes (resulting in the ashen coat-color and immunodeficiency) (Hume *et al.* 2001; Stinchcombe *et al.* 2001; Wu *et al.* 2002). In addition, there are indications that insulin granule priming may be reduced in *ashen* β-cells based on total internal reflection microscopy (TIRFM) imaging showing a reduced release of insulin granules that are docked to the plasma membrane in *ashen* β-cells with respect to that in control β-cells (Kasai *et al.* 2005). As a potential mechanism for these defects, Rab27a effectors are known to directly interact with SNARE proteins and SNARE regulators, for example: Slp4a with Munc18/syntaxin (Torii *et al.* 2002; Tsuboi and Fukuda 2006; Tomas *et al.* 2008), Noc2 with

Munc13-1 (Cheviet *et al.* 2004; Matsumoto *et al.* 2004), and rabphilin with SNAP-25 (Deak *et al.* 2006). Consistently, ablation of certain of these Rab/Rab effector binding partners (*e.g.*, Munc18, syntaxin, Munc13) reduces vesicle docking and priming (Voets *et al.* 2001; de Wit *et al.* 2006; Kang *et al.* 2006; Gulyas-Kovacs *et al.* 2007).

Our goal in the present investigation was to identify and characterize the specific parameters in the insulin secretory pathway that are altered by Rab27a deficiency in *ashen* mice. To accomplish this we have used high temporal resolution membrane capacitance measurements to measure secretion from single pancreatic β-cells, allowing us to define the role of Rab27a in regulating the size, rate of release from and refilling of (*i.e.*, priming into) specific functionally defined insulin granule pools. In addition, we examined the effects of glucose and cAMP enhancing pathways on the actions of Rab27a. Our results are novel in demonstrating (1) that *ashen* β-cells exhibit a time-dependent kinetic defect in vesicle priming into both the IRP and RRP granule pools, and (2) that Rab27a regulates the rate of insulin granule release from the RRP. By comparison, Rab3a-null mice demonstrate normal IRP and RRP refilling and rates of release demonstrating that Rab27a and Rab3a act in different β-cell priming pathways. Finally, we demonstrate that cAMP increases both the RRP and IRP pool sizes in *ashen* β-cells to an extent similar to that observed in control β-cells, suggesting that the cAMP augmentation of secretion is largely independent of Rab27a. The effects of cAMP on refilling of the granule pools were largely PKA dependent.

Methods

Mice and tissue preparation – All experiments were carried out according to rules and regulations of the University Committee on Use and Care of Animals (UCUCA). The *ash/ash* mice (C3H/He background) were kindly provided by N.A. Jenkins in cooperation with Jackson Laboratories (National Cancer Institute, Frederick, Maryland). C3H/He mice were purchased

from Jackson Labs (Bar Harbor, ME). In *ashen* mice (Wilson *et al.* 2000; Kasai *et al.* 2005), a single A-to-T transversion in the splice donor site downstream of exon 4 results in a larger than normal transcript due to the insertion of 235 or 252 base pairs of intron into the Rab27a message. An in-frame stop codon in the intron sequence leads to the production of a non-functional Rab27a protein lacking two critical domains of the GTP-binding pocket. $Rab3a^{-/-}$ mice (C57Bl/6 background) and control C57Bl/6 mice were provided by K. Engisch (Wright State University, Dayton, OH). Mice were sacrificed by cervical dislocation and islets were isolated by retrograde perfusion of the pancreatic duct with 4 ml 0.6-8 mg/ml collagenase (Roche Liberase RI, Roche Diagnostics) in physiologic saline solution (PSS, in mM: 137 NaCl, 5.6 KCl, 1.2 $MgCl_2$, 0.5 NaH_2PO_4, 4.2 HCO_3, 2.6 $CaCl_2$, 2.5 glucose, pH 7.4, 310 mOsm). The pancreas was immediately excised and further digested for 35-40 min at 37°C. Islets were hand-picked after washing the tissue twice in 20 ml PSS containing 5 mg/ml BSA. 130-180 islets were dispersed into single cells and small clusters by 10 min incubation at room temperature in 10 ml Ca^{2+}-free PSS (PSS lacking $CaCl_2$ and containing 2 mM EGTA), followed by 5 min gentle shaking in 1 ml Ca^{2+}-free PSS containing 0.025% trypsin at 37°C (Invitrogen). The dispersed cells were washed twice in 10 ml RPMI 1640 media containing 5 mM glucose and 10% (v/v) FBS supplemented with penicillin (100U/ml) and streptomycin (100 μg/ml), before plating on glass-bottom dishes coated with poly(L)-lysine. Cells were kept in a 37°C incubator at 5% CO_2 and recorded from 2-3 days after preparation.

Imaging of Intracellular Ca^{2+} – Mouse pancreatic β-cells plated on glass-bottom dishes were incubated in PSS containing 2 μM Fura2-AM (Molecular Probes) for 15 min at 37°C. Subsequently the dish volume was reduced to 0.5 ml, and the cells were equilibrated in PSS at a flow rate of 1 ml/min in a heated chamber (30-33°C). After >10 min, cells were incubated in PSS containing 16.7 mM glucose, and fluorescence of individual β-cells was elicited using alternating

excitation wavelengths of 340 and 380 nm (Till Polychrome V), a 410dlcp beamsplitter, and a D510/80 wide band emission filter (Chroma). Emission intensity was collected with a Photometrics Quant-EM camera at 2 Hz.

Electrophysiology – Whole-cell patch clamp measurements were performed at 30-33°C using an EPC-9 amplifier and Patchmaster acquisition software (HEKA electronics, Lambrecht/Pfalz, Germany). Pipettes (3-5 MΩ) were pulled from borosilicate glass (A-M systems, Carlsborg, WA), coated with Slygard 184 (Dow Corning, Midland, MI), and fire-polished. The pipette was held at a DC potential of -70 mV except during membrane depolarization. Capacitance measurements were performed using the software Lock-in extension of the Patchmaster software (dc+sine) using a sinusoid applied with an amplitude of 20 mV and a frequency of 1250 Hz. R_s was typically < 10 MΩ.

All reagents were from Sigma unless stated otherwise. The standard bath solution consisted of 113 mM NaCl, 5.5 mM KCl, 1.2 mM $MgCl_2$, 4.8 $NaHCO_3$, 10 mM $CaCl_2$, 20 mM TEA-Cl, 5 glucose, and 10 mM HEPES titrated to pH 7.3 with NaOH (310 mOsm). The standard pipette solution contained 125 mM Cs-glutamate, 10 mM CsCl, 10 mM NaCl, 0.25 mM EGTA, 0.16 mM $CaCl_2$, 3 mM Mg-ATP, 0.01 mM Na-GTP, and 5 mM HEPES titrated to pH 7.2 using CsOH (300 mOsm). The initial $[Ca^{2+}]_i$ was estimated to be 272 nM (WebMAXC software). TEA^+ and Cs^+ eliminated the contribution of K^+ efflux, allowing calculation of Q_{Ca} by integration of leak-subtracted (P/4) I_{Ca} during a 15 ms pulse given 1 min after membrane rupture and 2 min prior to the stimulus train. As described previously (Kinard and Satin 1995; Miley *et al.* 1999), a large slow onset Cl^- influx was observed during the stimulus protocol (Fig. 3.1A), possibly activated by our intracellular clamp of ATP at 3 mM as well as the cell-swelling associated with the whole-cell patch configuration, prohibiting quantification of I_{Ca} during measurement of the

RRP. In some experiments, the pipette solution was supplemented with 100 μM cAMP, 100 μM 8-pCPT-2'-*O*-Me-cAMP (Axxora), or 500 μM Rp-cAMP (Axxora).

Statistics – Statistical analysis was performed using InStat (Graphpad). Two-tailed paired t tests, assuming Gaussian distribution (parametric), were used to determine differences between mean IRP and RRP size measured from pairs of depolarization trains (see Fig. 3.1A) on each cell. Two-tailed unpaired t tests, assuming equal standard deviations, were used to compare mean IRP and RRP size between treatments (*e.g.*, wildtype vs. *ashen*).

Results

Ashen mice display a time-dependent kinetic defect in vesicle pool refilling – Our initial goal was to determine the kinetic parameters within the exocytotic pathway that are specifically altered by Rab27a deficiency using cultured mouse β-cells isolated from control C3H/He and *ashen* mice, which lack functional Rab27a protein (Wilson *et al.* 2000). High-resolution membrane capacitance measurements were used to monitor exocytosis. We devised a voltage-clamp depolarization protocol to separately stimulate vesicle release from the immediately-releasable and readily-releasable pools (IRP and RRP, respectively), which consist of docked and primed granules. The stimulation protocol consisted of a series of five 50-ms depolarizations (ΔCm_5) to deplete the IRP, followed by eight 500-ms depolarizations (ΔCm_8) to elicit secretion from the RRP, each from a holding potential of -70 mV to +20 mV (Fig. 3.1A), with a 100 ms inter-pulse interval. In wildtype β-cells we observed a small capacitance increase (8±1 fF, n=33) after ΔCm_5 corresponding to release from the IRP (Fig. 3.1B, 3.1D). From Figure 3.1B it can be seen that there is little additional capacitance change after the first two pulses, indicating depletion of the IRP without significant stimulation of release from the RRP. As an alternative estimation of the IRP size, a subset of the wildtype β-cell ΔCm_5 responses fit the criteria for a '2-

pulse' protocol (using the first two successive 50 ms pulses which are separated by 100 ms) for estimating the IRP as previously described (Gillis *et al.* 1996). In a comparable fashion to measuring IRP at the end of ΔCm_5, this analysis estimated the IRP size (B_{max}) as 7±1 fF (*n*=19) in wildtype β-cells (Fig. 3.1D). The magnitude of the IRP in *ashen* β-cells was comparable to C3H/He cells as shown in Figure 3.1B and D. Stimulated release from the RRP in wildtype cells (114±24 fF, *n*=33) was not significantly different than *ashen* cells (128±22 fF, *n*=33) using the ΔCm_8 stimulation train. The membrane conductance (Gm) in both control and *ashen* β-cells also exhibited similar patterns to the step depolarization protocol (Fig. 3.1C). Assuming 1.7 fF/granule measured previously in mouse β-cells (Ammala *et al.* 1993), the fast kinetic phase corresponding to the IRP was estimated at ~5 granules while ΔCm_8 released ~75 granules, which by other reports of mouse β-cells employing flash photolysis corresponds to the majority and perhaps the entire RRP under the equivalent conditions of 5 mM glucose (Renstrom *et al.* 1997; Wan *et al.* 2004; Yang and Gillis 2004). Interestingly, kinetic analysis of Figure 3.1B indicates that secretion from *ashen* β-cells progresses significantly faster (2X) than from control C3H/He β-cells, based on single exponential fits of the ΔCm_8 secretory response (*ashen*, $1/\tau$=0.63±0.09 s^{-1}; C3H/He, $1/\tau$=0.32±0.06 s^{-1}). The increased rate of secretion in *ashen* β-cells indicates that Rab27a participates in a rate-limiting step in the final stages of glucose-regulated exocytosis.

Our above results are novel in indicating that the defect in glucose-stimulated insulin secretion previously observed in *ashen* islets (Kasai *et al.* 2005) is not due to a limited initial size of the RRP. However, perfused islets from ashen mice exhibit a strong deficit in insulin secretion with respect to control islets in response to sustained elevated glucose exposure. Therefore, we next examined if Rab27a affects the rate at which the IRP and RRP refill, as may be necessary for sustained secretory responses. To examine refilling of the RRP and IRP pools that is reflective of the rate of insulin granule priming, the IRP and RRP were initially depleted and then the entire ΔCm_5 and ΔCm_8 stimulation train was applied a second time following a 2 min recovery period to

measure extent to which refilling of the IRP and RRP occurred. A 2 min recovery period was chosen as it provided sufficient time for both the IRP and RRP pools to completely refill in wildtype cells (Fig. 3.1 B and D). Comparatively, the ΔCm_5 response in *ashen* cells exhibited a ~70% deficit in pool refilling while a ~40% deficit was observed in the refilling of the RRP (Fig. 3.1B and D).

Since intracellular calcium $[Ca^{2+}]_i$ is both a stimulus for secretion as well as an important determinant of secretory granule priming (Gillis and Misler 1992; Eliasson *et al.* 1996; Barg *et al.* 2001), differences in calcium dynamics between wildtype and *ashen* β-cells could potentially confound interpretation of the results. To determine if such differences occurred we quantified the total Ca^{2+} influx (integrated current, Q_{Ca}) during a 15 ms depolarizing pulse (-70 mV to +20 mV) 2 min prior to the first stimulus train under each condition. This depolarization was insufficient to evoke secretion, consistent with other reports (Barg *et al.* 2001). No difference in Q_{Ca} was found between wildtype and *ashen* β-cells (Fig. 3.1E). We also examined voltage activation relationships for the Ca current, using 100 ms depolarizing pulses from the holding potential (-70 mV) to voltages between -70 mV and +50 mV. Peak current was elicited comparably in both wildtype and *ashen* β-cells at voltages between +20 and +30mV (Fig. 3.2A). Important to our investigations was demonstration that isolated *ashen* β-cells retain sensitivity to glucose stimulation equivalent to that observed in β-cells from C3H/He controls. For this determination we measured the increase in $[Ca^{2+}]_i$ in *ashen* and control β-cells loaded with Fura-2 in response to 16.7 mM glucose stimulation. After a delay which varied from 2-4 min, the Fura-2 340/380 intensity ratio increased 3- to 5-fold and without significant difference in both C3H/He and *ashen* β-cells in response to glucose (n=6). Representative glucose-stimulated changes in Fura-2 fluorescence are displayed in Figure 3.2B. Taken together, our results indicate that the deficit in vesicle pool refilling of both the IRP and RRP in *ashen* β-cells results from the absence of Rab27a and not altered Ca^{2+} dynamics or glucose responsiveness. In addition, as a reduced

release of pre-docked vesicles was previously observed in *ashen* β-cells by TIRF microscopy (Kasai *et al.* 2005), our results suggest that Rab27a normally facilitates vesicle priming.

Rab27a and Rab3a act in distinct secretion amplifying pathways – In addition to Rab27a, isoforms of the small GTPase Rab3 (a/b/c/d) are present on pancreatic β-granules (Tsuboi and Fukuda 2006). Perfused Rab3a-null islets reportedly exhibit a decreased (by 50%) secretory response to elevated glucose (16.7 mM), when administered over 1 h (Yaekura *et al.* 2003). To compare the effects of Rab3 deficiency with that of Rab27a deficiency we measured exocytosis from pancreatic β-cells isolated from Rab3a-null mice elicited in response to the voltage depolarization protocol outlined in Figure 3.1A. The IRP measured from Rab3a-null β-cells (13±3 fF) was comparable to wildtype C57Bl/6 cells (15±2 fF), and was completely refilled after a 2 min recovery period (Fig. 3.3 A and B. Ca^{2+} influx between these two treatments was not significantly different (Fig. 3.3C). In response to 500 ms step depolarizations, the RRP secretory responses exhibited similar kinetics in both $Rab3a^{-/-}$ and C57Bl/6 control β-cells ($Rab3a^{-/-}$, $1/\tau=0.30\pm0.06\ s^{-1}$; C57Bl/6, $1/\tau=0.35\pm0.06\ s^{-1}$). However, the initial size of the RRP in Rab3a-null β-cells was substantially (27±8%) smaller than C57Bl/6 cells, a deficit which was not observed in *ashen* β-cells (Fig. 3.1A, 1B). Also in contrast to *ashen* β-cells, the Rab3a-null cells demonstrated full recovery of the RRP over the 2 min period as indicated by responses to the second stimulus train (Fig. 3.3A, 3.3B). These results indicate that while Rab3a is more important for initial RRP size, Rab27a is a rate-limiting step in IRP and RRP refilling. This difference indicates that Rab27a and Rab3a have certain functionally distinct roles in the final signaling pathways governing insulin secretion.

Glucose-dependent vesicle priming in ashen β-cells – As established by multiple studies of single vesicle release, glucose possesses the ability to potently increase insulin secretion from pancreatic β-cells through increased priming of insulin granules into the functionally identified granule pools (Wan *et al.* 2004; Yang and Gillis 2004). We therefore next determined the effects

of a >10 min pre-incubation in 16.7 mM glucose on the IRP and RRP pool size in β-cells from *ashen* and background control mice. Figure 3.4A presents the averaged capacitance responses following glucose treatment using the stimulation protocol of Figure 3.1A. This treatment resulted in a 28±6% increase in Q_{Ca} as measured by a 15 ms depolarization measured prior to the ΔCm_5 and ΔCm_8 stimulus train. Two principal differences in secretion were observed between *ashen* cells incubated in 5 mM (Fig. 3.1A, 1D) and 16.7 mM glucose (Figs. 3.4A, 3.4B). First, the rate of secretion was dramatically increased by 16.7 mM glucose, as measured by an increase in the rate constant from $1/\tau=0.63\pm0.09$ s^{-1} to $1/\tau=1.36\pm0.07$ s^{-1} measured across the ΔCm_8. Secondly, although the magnitude of the IRP was unaffected by increasing glucose to 16.7 mM, the IRP measured after a second stimulus train completely recovered in *ashen* cells incubated in 16.7 mM glucose (Figs. 3.4A, 3.4B), whereas those in 5 mM glucose exhibited a ~70% deficit using the same stimulation protocol (Fig. 3.1A, D). However, this 'rescue' was limited to the IRP, as refilling of the RRP after 2 min remained incomplete (by 42±7% and 30±7%, respectively), and was comparable in both 5 mM and 16.7 mM glucose. Thus, our results indicate that at high concentration glucose maintains a Rab27a-independent mechanism for increasing the rate of β-granules movement from the RRP into the IRP, while the glucose-induced priming into the RRP continues to be limited by the absence of Rab27a.

cAMP-dependent vesicle priming and vesicle pool refilling in ashen β-cells – As a second messenger, cAMP stimulates exocytosis for a given Ca^{2+} influx from release-ready β-cell vesicle pools (Jones *et al.* 1986; Ammala *et al.* 1993; Renstrom *et al.* 1997; Wan *et al.* 2004; Yang and Gillis 2004). To determine the role of Rab27a in the cAMP pathway we next compared secretory responses (IRP and RRP size and rate of refilling) from *ashen* and wildtype β-cells using the stimulation protocol depicted in Figure 3.1A. As shown in Figures 3.5A and 3.5B inclusion of 100 μM cAMP in the recording pipette solution resulted in an increase in the size of the initial IRP and RRP response that was statistically equivalent for wildtype (C3H/He) and

Rab27a-null β-cells. The secretory response from C3H/He and *ashen* β-cells recorded in the absence of exogenously added cAMP are redisplayed from Figure 3.1A for comparison. Notably, the presence of added cAMP the ΔCm_5 elicited stepwise increases in membrane capacitance that continued throughout the series of step depolarizations, suggesting that the ΔCm_5 response may have included contribution from the RRP. As an alternative strategy, the size of the IRP was evaluated using analysis of the first two 50 ms pulses of ΔCm_5. Figure 3.5B shows that cAMP induced a ~300% increase in the IRP size to 18±3 fF in wildtype and 23±4 fF in *ashen* β-cells. By comparison, the RRP increased ~40% to 185±16 fF in wildtype and 190±17 fF in *ashen* β-cells. In part, the increase in secretory response may be attributable to an observed effect of cAMP to slow Ca^{2+}-current inactivation in both wildtype and *ashen* β-cells (Fig. 3.5C). Of importance, *ashen* and wildtype β-cell responses evoked in response to the second stimulus train were found to be equivalent to the first secretory response when cAMP was present (Fig. 3.5A, 5B), demonstrating that the IRP and RRP are capable of complete refilling in the absence of Rab27a when cAMP signaling pathways are activated. Inclusion of cAMP in the recording pipette was also observed to result in a decrease in the rate of capacitance increase in *ashen* β-cells during the ΔCm_8 of the first stimulus train. The rate constant ($1/\tau$) of secretion without cAMP was 0.64±0.09 s^{-1} while in its presence it was 0.40±0.07 s^{-1}. The reduction in the rate of capacitance increase in *ashen* β-cells with cAMP resulted in a rate approximately equivalent to C3/He cells in the presence (0.43±0.05 s^{-1}) of 100 μM cAMP. Thus, activation of cAMP signaling pathways is able to circumvent the rate-limiting effects of Rab27a on secretion.

The relative contribution of cAMP effector pathways differ in wildtype and ashen β-cells – As the addition of cAMP eliminated the secretory deficit observed in *ashen* β-cells (Fig. 3.5), it suggested that one or more cAMP effectors facilitates priming by acting in exocytotic signaling pathways parallel to or downstream of Rab27a. Protein kinase A (PKA) is one such effector that directly binds cAMP and strongly modulates Ca^{2+}-triggered exocytosis in pancreatic β-cells

(Gillis and Misler 1992; Ammala *et al.* 1993; Ammala *et al.* 1994; Wan *et al.* 2004; Yang and Gillis 2004). We, therefore, next determined the effects of PKA on cAMP-potentiated (100 μM) insulin secretion and vesicle pool refilling in *ashen* β-cells by modifying the pipette solution to include 500 μM Rp-cAMP, which inactivates PKA (Renstrom *et al.* 1997; Wan *et al.* 2004; Yang and Gillis 2004). As shown in Figure 3.6A and 3.6B, the capacitance responses to the initial set of ΔCm_5 and ΔCm_8 stimulus depolarizations (*i.e.*, the IRP and RRP) in the presence of cAMP and Rp-cAMP remained equivalent to that in cells treated with cAMP alone (*c.f.*, Figs. 3.5A and 3.5B). These results suggest that the initial enhancement of secretion by cAMP is largely facilitated by PKA-independent pathways. By comparison, the capacitance increases to application of the second pulse train after a 2 min recovery period demonstrated that while refilling of the IRP remained PKA-independent, refilling of the RRP in both wildtype and *ashen* β-cells was strongly PKA-dependent (Fig. 3.5B). Notably, this second pulse train elicited a 122±12 fF response in C3H/He cells treated with cAMP and Rp-cAMP (Fig. 3.6), a response that was nearly identical to wildtype cells in the absence of cAMP (Fig. 3.1; 114±14 fF). This comparison indicates that within a 2 min time period, PKA-dependent pathways comprise almost all (>90%) of cAMP actions to refill the RRP in C3H/He cells. Surprisingly, in *ashen* β-cells treated with cAMP/Rp-cAMP the second pulse train elicited a greater response (Fig. 3.6; 104±12 fF) than *ashen* cells in the absence of cAMP (Fig. 3.1; 75±14 fF), potentially indicating that cAMP-independent pathways are upregulated in the absence of Rab27a. Collectively, these experiments argue for considerable PKA-independent actions downstream of Rab27a.

Contribution of Epac2 to cAMP facilitation of secretion in ashen β-cells – The experiments described above indicate glucose-dependent deficits in pool refilling occur in *ashen* β-cells (Figs. 3.1 and 3.3). In addition, we demonstrated above that cAMP-dependent pathways remain potent secretory activators in *ashen* β-cells, particularly those independent of PKA. These pathways are capable of increasing the RRP size, but are insufficient (*i.e.*, require PKA action) to

increase the rate of pool refilling following its depletion (Fig. 3.6). In pancreatic β-cells, PKA-independent effects of cAMP have been reported, in part, to involve activation of Epac2 (exchange protein directly activated by cAMP). This Epac2 pathway can be selectively activated by pharmacologic ESCAs (Epac selective cAMP analogues; here, 8-pCPT-2'-*O*-Me-cAMP) (Kang *et al.* 2003; Holz *et al.* 2008). Therefore, to determine the contribution of Epac2 to PKA-independent actions of cAMP in *ashen* β-cells we measured capacitance increases to ΔCm_5 and ΔCm_8 when 100 μM ESCA was included in the pipette solution. As shown in Fig. 3.7, the IRP (17±3 fF) and RRP size (185±22 fF) measured in response to application of the initial series of depolarizing steps were similar to wildtype or *ashen* cells treated with cAMP (Fig. 3.5) or cAMP and Rp-cAMP (Fig. 3.6). This results shows that Epac2 is directly responsible for the PKA-independent boost in the IRP and RRP observed by evaluation of the first induction of pool depletion. By comparison, evaluation of refilling of the pools by application of a second stimulus series demonstrated that the IRP recovered completely while the RRP recovered to only ~80% of its initial size. Thus, the majority of PKA-independent actions in *ashen* β-cells utilize Epac2, while PKA action is responsible for most of cAMP actions on pool refilling.

Discussion

The targeting and docking of secretory granules to the plasma membrane involves the activity of Rab-GTPases. Yet, the specific functional sites that Rab proteins act in the exocytotic pathway to mediate their actions, as well as the molecular complexes that assemble and disassemble to perform their functions, remain ill defined. In this study we have used a functional analysis of secretion to identify specific steps in the final stages of insulin secretion where Rab27a acts. The experiments compared secretory responses from *ashen* β-cells (which lack Rab27a protein) and $Rab3a^{-/-}$ β-cells with appropriate background control β-cells. Multiple sites of Rab27a action were identified including regulation of the rate of refilling of specific

readily-releasable granule pools. In addition, we identify a role for Rab27a that limits the rate of granule fusion from these pools with the plasma membrane. Moreover, we find that these functions are unique to Rab27a, as Rab3a, which is also present on insulin secretory granules, did not exert regulation at these steps. Both the deficit in pool refilling in the *ashen* β-cells, as well as the increased rate of pool depletion were not observed in the presence of cAMP, owing largely to PKA-dependent pathways. Collectively, our results suggest that glucose-dependent enhancement of insulin secretion involves priming pathways that utilize Rab27a while, by comparison, receptor-mediated cAMP-dependent pathways that amplify secretory responses work primarily downstream of, or in parallel to, Rab27a.

What are the sites of Rab27a action in the pancreatic β-cell secretory pathway?

We have used stimulus-induced changes in membrane capacitance as a time resolved measurement of insulin release from the readily-releasable pool (RRP) of insulin granules (~60 granules), and its kinetically-distinct subset of ~10 Ca^{2+} channel-associated immediately-releasable granules (IRP) (Barg *et al.* 2001; Wan *et al.* 2004; Yang and Gillis 2004). The functional significance of this *in situ* measurement is that *in vivo*, IRP and RRP release are believed to account for first-phase insulin secretion (via K_{ATP} channel-dependent pathways), while the sustained second-phase release requires their refilling from a reserve pool (involving K_{ATP} channel-independent pathways) (Eliasson *et al.* 1996; Barg *et al.* 2001; Barg *et al.* 2002; Olofsson *et al.* 2002; Straub and Sharp 2002). Notably, the rate of secretion using membrane depolarization to induce Ca^{2+} influx is artificially high (~75 granules s^{-1}) (Kanno *et al.* 2004), at least ~300-fold faster than glucose-stimulated first-phase release (~0.25 granules s^{-1}) (Bratanova-Tochkova *et al.* 2002; Straub and Sharp 2002), thereby allowing us to completely deplete both the IRP and RRP, and examine refilling processes in a shortened time-frame. Using this approach,

we were able to define multiple rate-limiting sites of Rab27a action in the vesicle secretory pathway.

A remarkable finding of our study was that following depletion, the refilling of the RRP and IRP was incomplete even after a 2 min recovery in Rab27a-null *ashen* β-cells, compared with complete recovery seen in background control (C3H/He) cells. This result is highly significant, as a previous study suggests that the RRP recovers with a time constant of 31 s, and only 60 s is required for complete recovery (Gromada *et al.* 1999). The currently available literature on Rab27a, which has been largely derived from *ashen* mice, suggests three possible sites of Rab27a action in the secretory pathway which could potentially explain this phenomenon: granule recruitment, docking, and priming. The role of Rab27a in recruitment is evidenced by the failure of melanosomes to target to the PM, accumulating around the nucleus in *ashen* melanocytes because a Rab27a-MyRIP-myosin Va tripartite complex is required for their transfer from microtubules to actin filaments (Fukuda *et al.* 2002; Strom *et al.* 2002; Waselle *et al.* 2003). Rab27a is also known to participate in granule docking. In cytotoxic T-cells (CTLs) derived from *ashen* mice, EM analysis has revealed that lytic granules polarize correctly to the immunological synapse (*i.e.*, recruitment processes are functional), but the CTLs are unable to secrete granzyme A or hexoaminidase because the lytic granules stop short of docking (Stinchcombe *et al.* 2001). However, recruitment/docking seem unlikely to completely account for the Rab27a-dependent secretory deficit we find in *ashen* β-cells, since EM analysis has shown that the granule density at/near the PM (within 500 nm) is nearly identical in unstimulated Rab27a-null and C3H/He β-cells (Kasai *et al.* 2005), and is not affected by RNAi directed against Rab27a (Waselle *et al.* 2003). We additionally demonstrated that functionally, the initial secretory responses between *ashen* and control β-cells were similar, yielding a ~10 fF IRP (~6 granules) and a ~115 fF RRP (~68 granules), which is comparable to control responses reported in prior studies.

In addition to potential roles at recruitment or docking steps, we propose that Rab27a participates in glucose-dependent *priming* pathways in pancreatic β-cells. The hypothesis that Rab27a participates in priming was suggested by a dramatically reduced release of pre-docked granules seen in the TIRFM field following glucose stimulation in *ashen* β-cells (Kasai *et al.* 2005). That priming of granules occurs in β-cells was originally suggested by quantitative comparisons between EM ultrastructural analysis and membrane capacitance measurements. That is, out of the ~10-13,000 granules in the β-cell, ~600 (~5% in total) are docked at the plasma membrane and yet only ~60 granules (~0.5% in total) comprise the RRP (Dean 1973; Renstrom *et al.* 1997; Bratanova-Tochkova *et al.* 2002; Olofsson *et al.* 2002). The conversion of reserve/docked granules into readily- and immediately-releasable granules, requiring priming, is believed to be a biochemical process with the rate and extent of priming dependent on time, temperature, $[Ca^{2+}]_i$, $[ATP]_i$, and importantly, glucose concentration (Grodsky 1972; Grodsky 1972; Gromada *et al.* 1999; Barg *et al.* 2002; Yang and Gillis 2004). Although a number of readily-releasable granules have been found by TIRFM to be released without an extended docking step (a.k.a. restless newcomer) during first phase-secretion under glucose stimulation (Shibasaki *et al.* 2007), this population is far less affected by the absence of Rab27a than the docked pool (Kasai *et al.* 2005). We have found additionally that movement from the RRP into the IRP is strongly dependent on Rab27a at 5 mM glucose, but independent of Rab27a when extracellular glucose is raised to 16.7 mM. Coincident with this glucose-dependent bypass of Rab27a action, the rate of RRP emptying in *ashen* cells also increases by ~2-fold upon raising extracellular glucose (*ashen*/5 mM glucose, $1/\tau=0.63\pm0.09$ s^{-1}; *ashen*/16.7 mM glucose, $1/\tau=1.36\pm0.07$ s^{-1}).

The role of Rab27a effectors in glucose and Rab27a-dependent priming

Both the glucose-dependent deficit in granule pool refilling and the increased rate of RRP depletion we find in *ashen* β-cells are consistent with the known properties of Rab27a effector interactions in priming. For example, reduction of the Rab 3/27a effector Noc2 by RNAi decreases insulin secretion from INS-1 β-cells. *In vitro*, Noc2 has been reported to bind the essential priming factor Munc13 (Cheviet *et al.* 2004). Another principal Rab27a effector is Slp4a/granuphilin (Fukuda 2005). Rab27a-dependent pool refilling could also be explained, in part, by the finding that β-cells deficient in either Rab27a (Kasai *et al.* 2005) or Slp4a (Gomi *et al.* 2005) have reductions in the number of insulin granules docked to the plasma membrane, although the defect is substantially larger in Slp4a-null β-cells as measured by EM. Consistently, overexpression of Slp4a in neuroendocrine PC12 cells significantly increases the number of vesicles docked prior to stimulation (Tsuboi and Fukuda 2006). Although the docking of β-granules to the plasma membrane is strongly facilitated by Rab27a and Slp4a, these vesicles may be forced into an inactive and unprimed state since secretion is strongly inhibited by Slp4a overexpression (Coppola *et al.* 2002; Torii *et al.* 2002), and because Slp4a interacts strongly with only the closed and SNARE-pairing inactive Munc18/syntaxin complex (Coppola *et al.* 2002; Torii *et al.* 2002; Gomi *et al.* 2005; Tsuboi and Fukuda 2006). This biochemical state could explain the Rab27a-dependent clamp on granule release absent in *ashen* β-cells. Indeed, the clamp may be released upon stimulation, since Rab27a is activated and interacts with effectors only in the GTP bound state, and GTP hydrolysis is known to accompany stimulation (Kondo *et al.* 2006).

The interplay of Rab27a and Rab3a in priming pathways

Islets isolated from either Rab27a-null (Kasai *et al.* 2005) or Rab3a-null (Yaekura *et al.* 2003) animals are reported to exhibit glucose intolerance as well as a ~50% defect in glucose-stimulated insulin secretion, although these approaches preclude identification of specific granule

pools affected or quantitative analysis on refilling rates of specific granule pools. Our results identify the site of the Rab27a-dependent secretion deficit as a glucose-dependent defect in IRP and RRP refilling, yet as we see no initial deficit in the RRP size, it is surprising that Rab27a-null animals are glucose intolerant (Kasai *et al.* 2005). Notably, the functionally defined Rab27a deficits in secretion were not observed in Rab3a-null β-cells, suggesting that the two molecules do not function redundantly in pancreatic β-cells. This is an important determination when one considers that some redundancy exists in Rab27/Rab3 effector interactions. For example, rabphilin and Noc2, which were first characterized as Rab3a effectors (Kotake *et al.* 1997; Haynes *et al.* 2001), also function in concert with Rab27a (Cheviet *et al.* 2004; Fukuda *et al.* 2004). Slp4a, however, is believed to form an endogenous complex only with Rab27a based on its high affinity interaction (Mahoney *et al.* 2006), despite its interaction with Rab3a *in vitro* (Coppola *et al.* 2002). Moreover, the Munc13-1 binding protein RIM (Betz *et al.* 2001) only binds to Rab3a (Fukuda 2005). The situation in other cell types may be different. For example, in PC12 cells, RNAi knockdown of Rab27a and Rab3a has an additive effect to reduce secretion (Tsuboi and Fukuda 2006). It seems more likely, though, that Rab3a is redundant with the other three isoforms present on β-granules (*i.e.*, Rab a/b/c/d) (Iezzi *et al.* 1999). Deletion of all four Rab3 isoforms in mice (which is lethal owing to respiratory defects) resulted in only a ~30% decrease in evoked secretion from hippocampal neurons (Schluter *et al.* 2004; Schluter *et al.* 2006), suggesting Rab3a is redundant with Rab3 b, c, and d, at least for synaptic transmission.

Rab27a and amplifying pathways of secretion

cAMP is a powerful potentiator of insulin secretion (Holst and Gromada 2004), via its contribution to both the initial size and the rate of refilling of multiple secretory granule pools (Gromada *et al.* 1998; Yang *et al.* 2002; Wan *et al.* 2004; Yang and Gillis 2004; Kwan and Gaisano 2005). The effects of cAMP to augment secretion are furthermore additive with those

seen under conditions of elevated glucose (Wan *et al.* 2004; Yang and Gillis 2004), suggesting that at least some glucose and cAMP signaling intermediates act in independent pathways. We have found that the actions of cAMP have two principal effects independent of the glucose/Rab27a-dependent pathways on pool size and refilling. First, cAMP can quickly enhance (in <3 min) the initial IRP and RRP magnitude in *ashen* β-cells to an equivalent extent as in control β-cells. Second, cAMP can obviate the Rab27a-dependent deficit in pool refilling seen in the *ashen* cells. The intracellular mediators of these cAMP effects are separable into PKA-independent and PKA-dependent pathways, respectively.

Our results indicate that cAMP-mediated refilling of the RRP is strongly dependent on PKA, since Rp-cAMP completely blocks the ability of cAMP to refill the RRP in both wildtype and *ashen* β-cells. Consequently, we find no Rab27a-dependence of PKA action. Interestingly, we found that Rp-cAMP has no effect in limiting the initial enhancement of the IRP and RRP by cAMP. This is surprising, since previous reports using the same inhibitor describe a partial (Rosengren *et al.* 2002) or complete block (Wan *et al.* 2004; Yang and Gillis 2004) of an initial cAMP-induced enhancement of depolarization-induced exocytosis. Perhaps the inhibition by Rp-cAMP lags behind cAMP activation, in spite of the high Rp-cAMP concentration we used in the patch pipette. On the other hand, it may be that the activity of PKA is only evident after stimulation, during the refilling of the IRP and RRP (*i.e.*, the observed initial boost in RRP size prior to its depletion is likely to be mediated by PKA-independent pathways). Renstrom and colleagues (Renstrom *et al.* 1997) previously reported that neither Rp-cAMP nor PKI (PKA inhibitory peptide) affected cAMP potentiation of granule release evoked by a single 500 ms depolarizing pulse, but when additional pulses are applied at 1 Hz over tens of seconds, where RRP refilling processes would predominate, the effects of cAMP to enhance secretion are severely reduced by PKA inhibition. Consistent with this latter hypothesis, we found that direct activation of Epac2 in *ashen* cells with the ESCA 8-pCPT-2'-O-Me-cAMP increased the initial

RRP size (closely mimicking the treatment of *ashen* cells with cAMP/Rp-cAMP), but failed to support complete refilling of the RRP.

By fitting the time course of RRP depletion, which occurred during closely spaced repetitive depolarizing steps, to a single exponential, and comparing the results between *ashen* and control β-cells, we have discovered that Rab27a exerts a previously unknown rate-limiting action on vesicle release. The results establish a ~2-fold faster pool depletion in *ashen* β-cells than in wildtype β-cells incubated in 5 mM glucose (*ashen*, $1/\tau=0.63\pm0.09$ s^{-1}; C3H/He, $1/\tau=0.32\pm0.06$ s^{-1}), that is further enhanced in 16.7 mM glucose ($1/\tau=1.36\pm0.07$ s^{-1}). A role for Rab27a action immediately proximal to secretion is evidenced by a corresponding hydrolysis of Rab-GTP upon stimulation (Kondo *et al.* 2006). This regulatory effect of Rab27a on rate of pool depletion is not recapitulated by deletion of Rab3a ($Rab3a^{-/-}$, $1/\tau=0.30\pm0.06$ s^{-1}; C57Bl/6, $1/\tau=0.35\pm0.06$ s^{-1}). Rab27a control over vesicle pool depletion is, however, bypassed by the actions of cAMP (*ashen*/cAMP, $1/\tau=0.40\pm0.07$ s^{-1}; C3H/He/cAMP, $1/\tau=0.43\pm0.05$ s^{-1}). These results support a convergence of cAMP and glucose-dependent priming pathways proximal to secretion.

Several distinct molecular mediators can be postulated for the effect of cAMP effect on priming of insulin granules. One possibility is activation of the small GTPase Rap1 by Epac2, which serves as a GEF (Shibasaki *et al.* 2007). Epac2 also directly binds the Rab3a effector molecules Munc13-1 and Rim2, which serve as vesicle priming factors (Fujimoto *et al.* 2002; Shibasaki *et al.* 2004; Kwan *et al.* 2007). This mechanism is influenced by PKA-dependent processes, owing to direct phosphorylation of Rim2 (Lonart *et al.* 2003) as well as the SNARE protein SNAP25 (Hepp *et al.* 2002), although these events have not been directly correlated with enhanced secretion. Further studies probing Rab3 and other small GTPase (*e.g.*, Rap1, RalA (Lopez *et al.* 2008), *etc.*) pathways may address these possibilities.

Summary

Interactions between Rab27a-GTPase and its effectors on secretory granule membrane are believed to act in concert with SNAREs on the plasma membrane to facilitate docking and secretion. In this study we have investigated the mechanisms by which insulin secretion is regulated by Rab27a in mouse pancreatic β-cells, focusing specifically on the glucose- and cAMP-dependent priming pathways. Our results indicate that Rab27a is a central effector upon which glucose-dependent β-cell signaling pathways converge to regulate refilling of and rate of release from specific releasable pools of secretory granules. Moreover, Rab27a and Rab3a appear not to be redundant in their actions. Finally, cAMP amplification of insulin secretion acts primarily downstream of or independent of Rab27a, suggesting Rab27a is a critical regulator of glucose-induced secretion and an important mediator of both first and second phase of glucose stimulated insulin secretion.

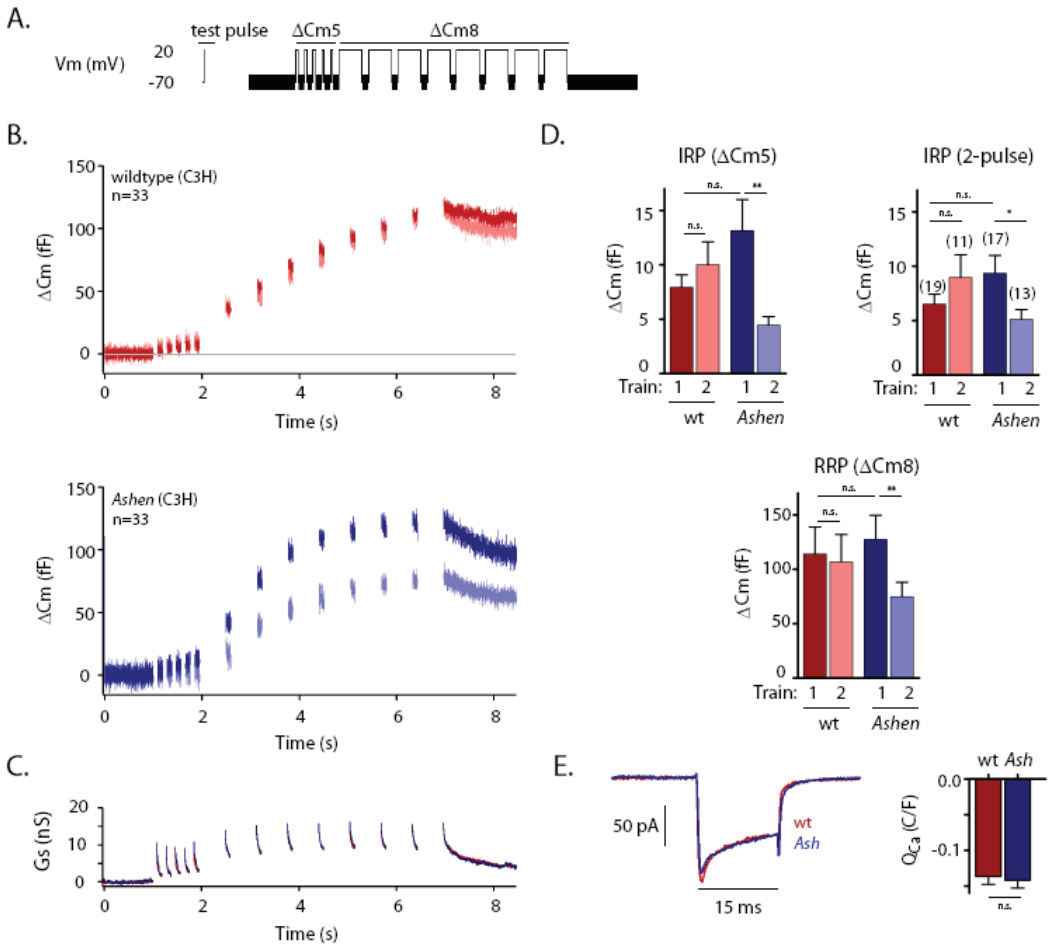

Figure 3.1. ***Ashen* mice exhibit kinetic defects in refilling of the IRP and RRP.** *A*, Mouse pancreatic β-cells under whole cell voltage clamp were depolarized from a holding potential of -70 mV to +20 mV to elicit exocytosis of β-granules. The stimulus train consisted of five 50-ms depolarizations (ΔCm_5) to exhaust the IRP, which was immediately followed by eight 500-ms depolarizations (ΔCm_8) to stimulate release from the RRP. The inter-pulse interval was 100 ms. The entire stimulus train was repeated twice for each experiment, allowing 2 min between trains for vesicle pool recovery. A 15 ms test depolarization was given 2 min prior to the first stimulus train to measure the properties of I_{Ca}. *B*, Averaged capacitance increases measured from wildtype (C3H/He) (*dark red, light red*) and *ashen* β-cells (*dark blue, light blue*) in response to the pulse train in A. *C*, Averaged membrane conductance measured from wildtype (C3H/He) (red) and *ashen* (blue) β-cells during the first stimulus train in (B). *D*, Averaged capacitance increases measured after ΔCm_5 (IRP) or ΔCm_8 (RRP) from cells in (B). The IRP was also estimated using the equation $S/(1-R^2)$, where S is the sum of the first two capacitance responses and R is the ratio of the first two responses (2-pulse) (Gillis *et al.* 1996). Cells were selected for analysis only when the capacitance increase following the first depolarizing pulse was greater than 60% of the capacitance increase following the second depolarizing pulse of ΔCm_5. *E*, Averaged leak-subtracted I_{Ca} measured during a 15 ms depolarization given 30 s prior to the stimulatory pulses in B. The bar graph displays integrated current (Q_{Ca}) normalized to cell size. *, $p<0.05$; **, $p<0.01$; ***, $p<0.001$. Bars, means ± SEM. Number of observations (β-cell recordings) is indicated above each averaged trace.

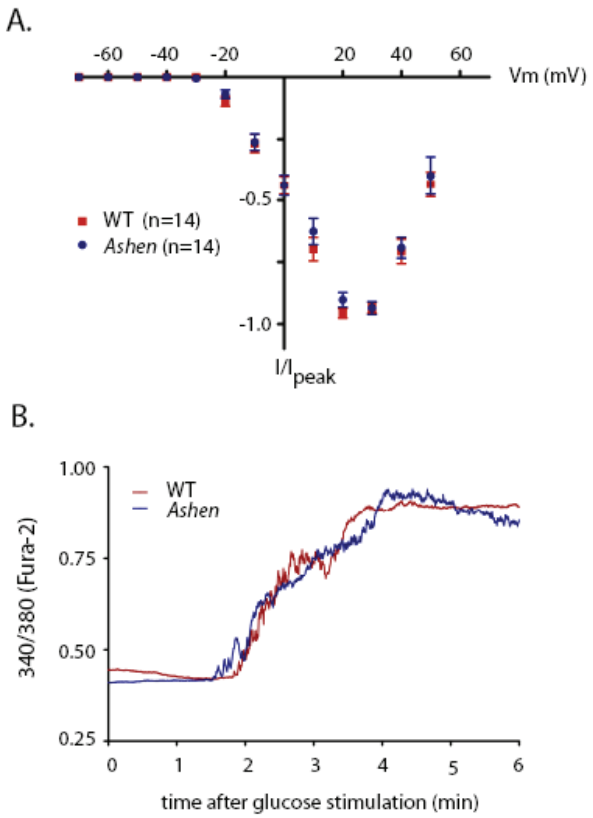

Figure 3.2. **Comparison of *ashen* and wildtype β-cell voltage-gated calcium influx and of intracellular Ca^{2+} responses to glucose stimulation.** *A*, current-voltage relationship of I_{Ca} in control C3H/He or *ashen* β-cells measured in response to 100 ms step depolarizations applied at 1 Hz from a holding potential of -70 mV. *B*, Changes in intracellular Ca^{2+} measured from single wildtype C3H/He (*red*) and *ashen* (blue) β-cells loaded with Fura-2 in response to 16.7 mM glucose. Representative traces are shown, *n*=6.

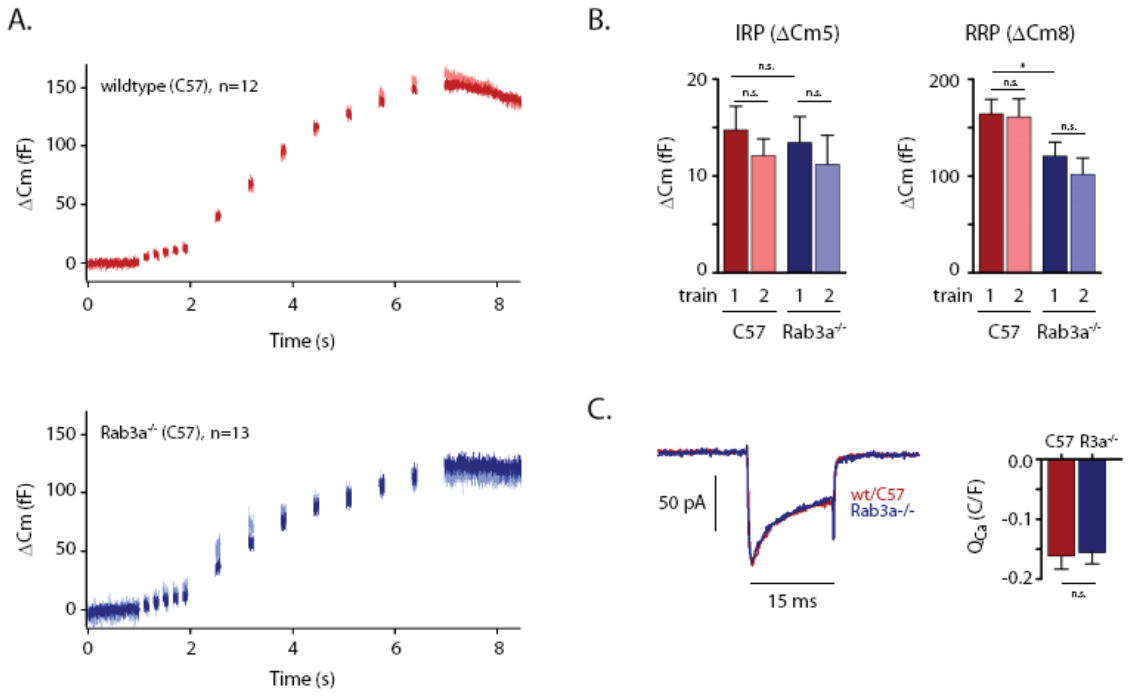

Figure 3.3. **Measurement of IRP and RRP pool sizes and refilling in Rab3a-null β-cells**. *A*, Averaged capacitance changes measured from background control (C57) (*dark red, light red*) and Rab3a$^{-/-}$ β-cells (*dark blue, light blue*) in response to the pulse protocol described in Fig. 3.1A. *B*, Averaged capacitance increases measured after ΔCm_5 (IRP) or ΔCm_8 (RRP) from cells in A. *C*, Averaged leak-subtracted I_{Ca} measured during a 15 ms depolarization given 30 s prior to the stimulatory pulses in A. The bar graph displays integrated current (Q_{Ca}) normalized to cell size. *, p<0.05; **, p<0.01; ***, p<0.001. Bars, means ± SEM.

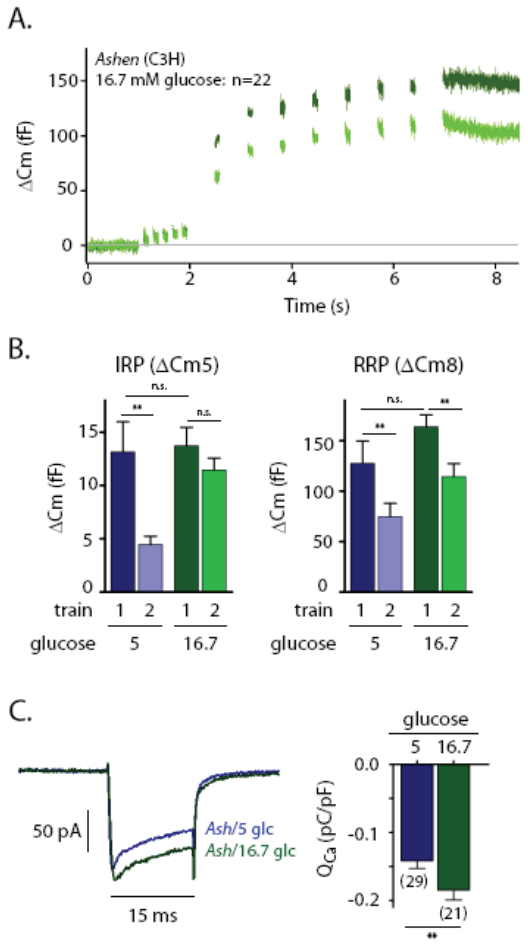

Figure 3.4. **Glucose-dependent increases in priming of the RRP are deficient in *ashen* β-cells**. *A*, Averaged capacitance changes measured from *ashen* β-cells (*dark green, light green*) incubated in 16.7 mM glucose for >10 min. The stimulus protocol is detailed in Fig. 3.1A. *B*, Averaged capacitance increases measured after ΔCm_5 (IRP) or ΔCm_8 (RRP) from cells in A. *C*, Averaged leak-subtracted I_{Ca} measured during a 15 ms depolarization given 30 s prior to the stimulatory pulses in A. The bar graph displays integrated current (Q_{Ca}) normalized to cell size. *, $p<0.05$; **, $p<0.01$; ***, $p<0.001$. Bars, means ± SEM.

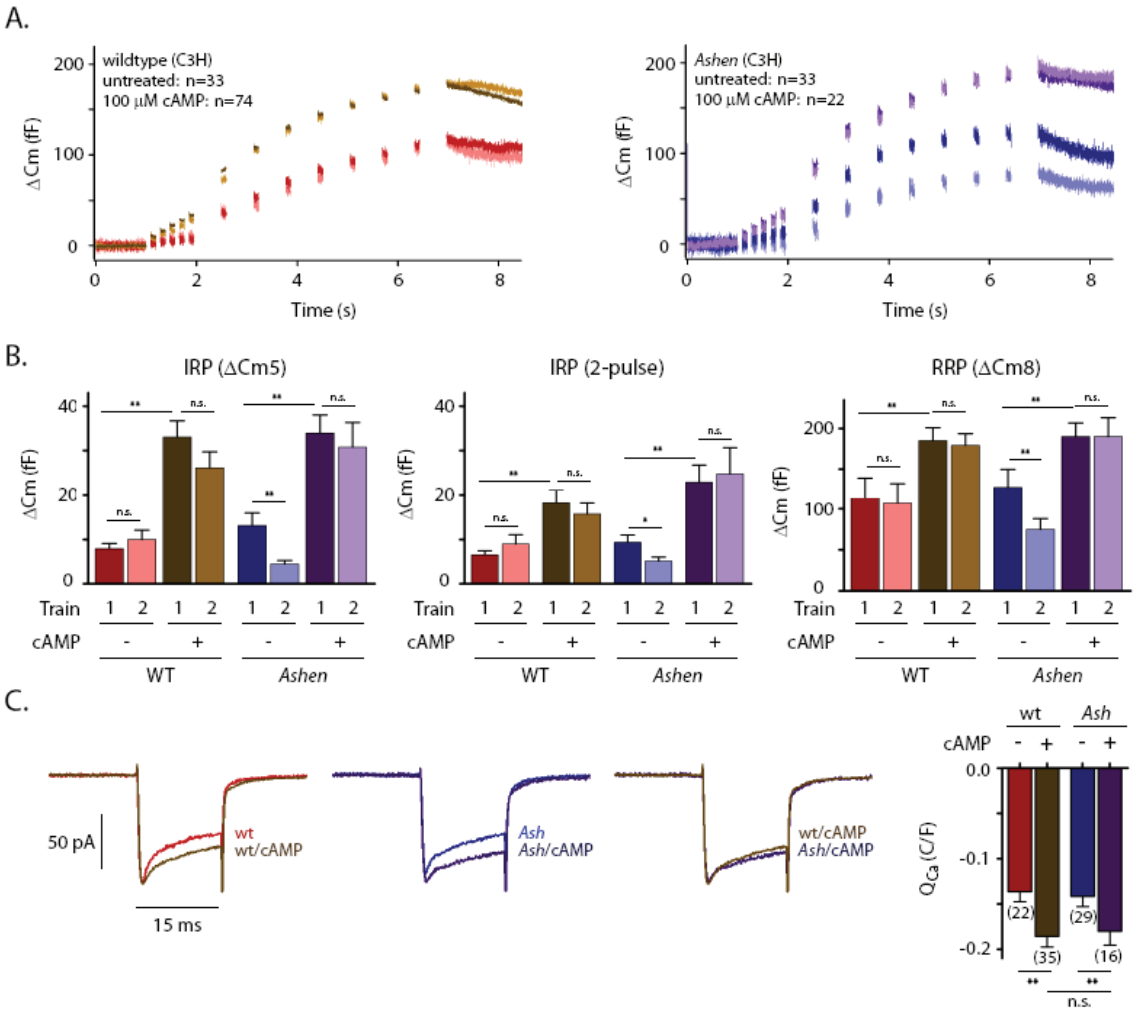

Figure 3.5. **Effects of cAMP on evoked changes in membrane capacitance in *ashen* β-cells**. *A*, Averaged capacitance increases measured in response to 100 µM cAMP from wildtype (C3H/He) (*dark brown, light brown*) and *ashen* β-cells (*dark purple, light purple*) in response to the pulse train in Fig. 3.1A. Capacitance changes from control untreated cells are redisplayed from Fig. 3.1B for comparison. *B*, Averaged capacitance increases measured following ΔCm_5 or ΔCm_8 from cells in A. The IRP was analyzed by the 2-pulse procedure described in Fig. 3.1D. *C*, Averaged leak-subtracted I_{Ca} measured during a 15 ms depolarization given 30 s prior to the stimulatory pulses in A. The bar graph displays integrated current (Q_{Ca}) normalized to cell size. *, $p<0.05$; **, $p<0.01$; ***, $p<0.001$. Bars, means ± SEM.

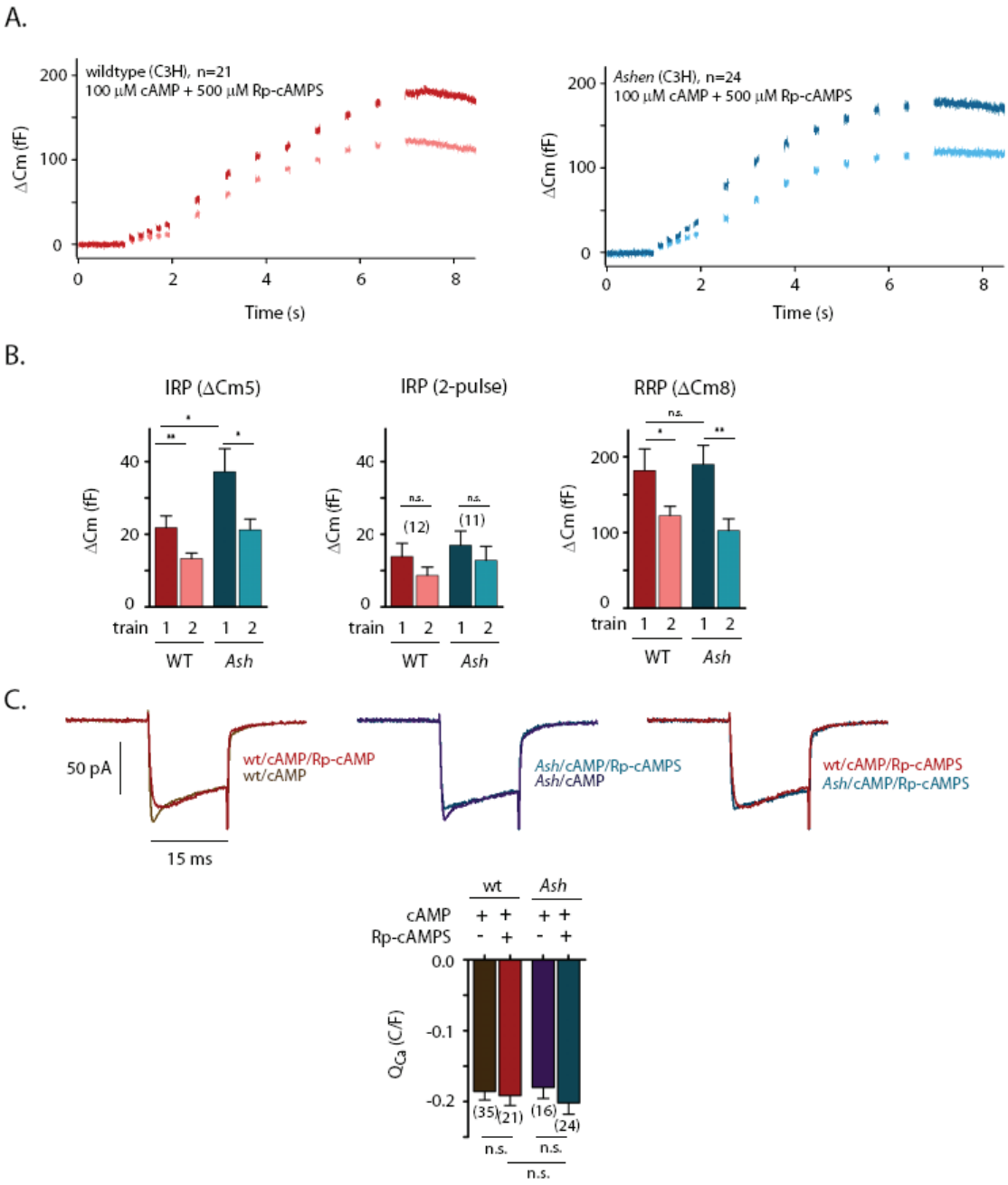

Figure 3.6. **A PKA-dependent step downstream of Rab27a facilitates RRP pool refilling**. *A*, Averaged capacitance increases recorded from wildtype (C3H/He) (*dark red, light red*) and *ashen* β-cells (*dark blue, light blue*) with 100 µM cAMP and 500 µM Rp-CAMP (PKA inhibitor) in the pipette soluion. Cells were stimulated by two pulse trains 2 min apart as described in Fig. 3.1A. *B*, Averaged capacitance increases measured following ΔCm_5 or ΔCm_8 from cells in A. The IRP was analyzed by the 2-pulse procedure as described in Fig. 3.1D. *C*, Averaged leak-subtracted I_{Ca} measured during a 15 ms depolarization given 30 s prior to the stimulatory pulses in A. The bar graph displays integrated current (Q_{Ca}) normalized to cell size. I_{Ca} and Q_{Ca} from cells treated with cAMP are redisplayed from Fig. 3.4C. *, $p<0.05$; **, $p<0.01$; ***, $p<0.001$. Bars, means ± SEM.

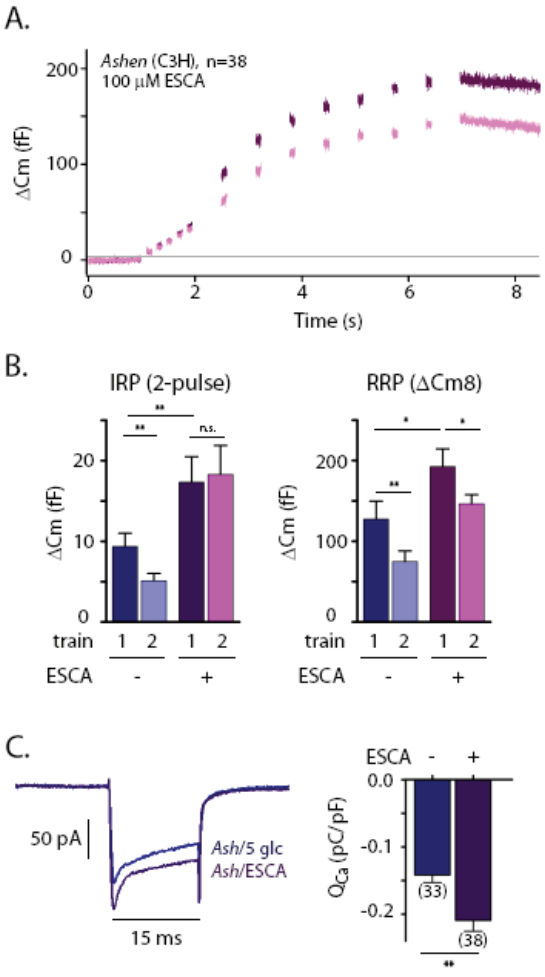

Figure 3.7. **Effects of Epac2 activation on IRP and RRP size and refilling in *ashen* β-cells.** *A*, Averaged capacitance changes measured from *ashen* β-cells (*dark purple, light purple*) in the presence of 100 µM 8-pCPT-2'-*O*-Me-cAMP (ESCA) in response to the pulse protocol described in Fig. 3.1A. *B*, Averaged capacitance increases measured after ΔCm_5 (IRP) or ΔCm_8 (RRP) from cells in A. *C*, Averaged leak-subtracted I_{Ca} measured during a 15 ms depolarization given 30 s prior to the stimulatory pulses in A. The bar graph displays integrated current (Q_{Ca}) normalized to cell size. *, $p<0.05$; **, $p<0.01$; ***, $p<0.001$. Bars, means ± SEM.

References

Ammala, C., *et al.* (1993). "Calcium-independent potentiation of insulin release by cyclic AMP in single beta-cells." Nature **363**(6427): 356-8.

Ammala, C., *et al.* (1994). "Activation of protein kinases and inhibition of protein phosphatases play a central role in the regulation of exocytosis in mouse pancreatic beta cells." Proc Natl Acad Sci U S A **91**(10): 4343-7.

Ammala, C., *et al.* (1993). "Exocytosis elicited by action potentials and voltage-clamp calcium currents in individual mouse pancreatic B-cells." J Physiol **472**: 665-88.

Barg, S., *et al.* (2002). "A subset of 50 secretory granules in close contact with L-type Ca2+ channels accounts for first-phase insulin secretion in mouse beta-cells." Diabetes **51 Suppl 1**: S74-82.

Barg, S., *et al.* (2001). "Fast exocytosis with few Ca(2+) channels in insulin-secreting mouse pancreatic B cells." Biophys J **81**(6): 3308-23.

Betz, A., *et al.* (2001). "Functional interaction of the active zone proteins Munc13-1 and RIM1 in synaptic vesicle priming." Neuron **30**(1): 183-96.

Bratanova-Tochkova, T. K., *et al.* (2002). "Triggering and augmentation mechanisms, granule pools, and biphasic insulin secretion." Diabetes **51 Suppl 1**: S83-90.

Burgoyne, R. D. and A. Morgan (2003). "Secretory granule exocytosis." Physiol Rev **83**(2): 581-632.

Cheviet, S., *et al.* (2004). "The Rab-binding protein Noc2 is associated with insulin-containing secretory granules and is essential for pancreatic beta-cell exocytosis." Mol Endocrinol **18**(1): 117-26.

Coppola, T., *et al.* (2002). "Pancreatic beta-cell protein granuphilin binds Rab3 and Munc-18 and controls exocytosis." Mol Biol Cell **13**(6): 1906-15.

de Wit, H., *et al.* (2006). "Docking of secretory vesicles is syntaxin dependent." PLoS ONE **1**: e126.

Deak, F., *et al.* (2006). "Rabphilin regulates SNARE-dependent re-priming of synaptic vesicles for fusion." EMBO J **25**(12): 2856-66.

Dean, P. M. (1973). "Ultrastructural morphometry of the pancreatic -cell." Diabetologia **9**(2): 115-9.

Eliasson, L., *et al.* (1996). "PKC-dependent stimulation of exocytosis by sulfonylureas in pancreatic beta cells." Science **271**(5250): 813-5.

Eliasson, L., *et al.* (1997). "Rapid ATP-dependent priming of secretory granules precedes Ca(2+)-induced exocytosis in mouse pancreatic B-cells." J Physiol **503 (Pt 2)**: 399-412.

Fujimoto, K., *et al.* (2002). "Piccolo, a Ca2+ sensor in pancreatic beta-cells. Involvement of cAMP-GEFII.Rim2.Piccolo complex in cAMP-dependent exocytosis." J Biol Chem **277**(52): 50497-502.

Fukuda, M. (2003). "Slp4-a/granuphilin-a inhibits dense-core vesicle exocytosis through interaction with the GDP-bound form of Rab27A in PC12 cells." J Biol Chem **278**(17): 15390-6.

Fukuda, M. (2005). "Versatile role of Rab27 in membrane trafficking: focus on the Rab27 effector families." J Biochem (Tokyo) **137**(1): 9-16.

Fukuda, M., *et al.* (2004). "Rabphilin and Noc2 are recruited to dense-core vesicles through specific interaction with Rab27A in PC12 cells." J Biol Chem **279**(13): 13065-75.

Fukuda, M., *et al.* (2002). "Slac2-a/melanophilin, the missing link between Rab27 and myosin Va: implications of a tripartite protein complex for melanosome transport." J Biol Chem **277**(14): 12432-6.

Gillis, K. D. and S. Misler (1992). "Single cell assay of exocytosis from pancreatic islet B cells." Pflugers Arch **420**(1): 121-3.

Gillis, K. D., *et al.* (1996). "Protein kinase C enhances exocytosis from chromaffin cells by increasing the size of the readily releasable pool of secretory granules." Neuron **16**(6): 1209-20.
Gomi, H., *et al.* (2005). "Granuphilin molecularly docks insulin granules to the fusion machinery." J Cell Biol **171**(1): 99-109.
Grodsky, G. M. (1972). "A threshold distribution hypothesis for packet storage of insulin and its mathematical modeling." J Clin Invest **51**(8): 2047-59.
Grodsky, G. M. (1972). "A threshold distribution hypothesis for packet storage of insulin. II. Effect of calcium." Diabetes **21**(2 Suppl): 584-93.
Gromada, J., *et al.* (1998). "Glucagon-like peptide 1 (7-36) amide stimulates exocytosis in human pancreatic beta-cells by both proximal and distal regulatory steps in stimulus-secretion coupling." Diabetes **47**(1): 57-65.
Gromada, J., *et al.* (1999). "CaM kinase II-dependent mobilization of secretory granules underlies acetylcholine-induced stimulation of exocytosis in mouse pancreatic B-cells." J Physiol **518 (Pt 3)**: 745-59.
Gulyas-Kovacs, A., *et al.* (2007). "Munc18-1: sequential interactions with the fusion machinery stimulate vesicle docking and priming." J Neurosci **27**(32): 8676-86.
Haynes, L. P., *et al.* (2001). "A direct inhibitory role for the Rab3-specific effector, Noc2, in Ca2+-regulated exocytosis in neuroendocrine cells." J Biol Chem **276**(13): 9726-32.
Hepp, R., *et al.* (2002). "Differential phosphorylation of SNAP-25 in vivo by protein kinase C and protein kinase A." FEBS Lett **532**(1-2): 52-6.
Holst, J. J. and J. Gromada (2004). "Role of incretin hormones in the regulation of insulin secretion in diabetic and nondiabetic humans." Am J Physiol Endocrinol Metab **287**(2): E199-206.
Holz, G. G., *et al.* (2008). "Epac-selective cAMP analogs: new tools with which to evaluate the signal transduction properties of cAMP-regulated guanine nucleotide exchange factors." Cell Signal **20**(1): 10-20.
Hume, A. N., *et al.* (2001). "Rab27a regulates the peripheral distribution of melanosomes in melanocytes." J Cell Biol **152**(4): 795-808.
Iezzi, M., *et al.* (1999). "Subcellular distribution and function of Rab3A, B, C, and D isoforms in insulin-secreting cells." Mol Endocrinol **13**(2): 202-12.
Jones, P. M., *et al.* (1986). "Regulation of insulin secretion by cAMP in rat islets of Langerhans permeabilised by high-voltage discharge." FEBS Lett **205**(2): 205-9.
Kang, G., *et al.* (2003). "Epac-selective cAMP analog 8-pCPT-2'-O-Me-cAMP as a stimulus for Ca2+-induced Ca2+ release and exocytosis in pancreatic beta-cells." J Biol Chem **278**(10): 8279-85.
Kang, L., *et al.* (2006). "Munc13-1 is required for the sustained release of insulin from pancreatic beta cells." Cell Metab **3**(6): 463-8.
Kanno, T., *et al.* (2004). "Large dense-core vesicle exocytosis in pancreatic beta-cells monitored by capacitance measurements." Methods **33**(4): 302-11.
Kasai, K., *et al.* (2005). "Rab27a mediates the tight docking of insulin granules onto the plasma membrane during glucose stimulation." J Clin Invest **115**(2): 388-96.
Kinard, T. A. and L. S. Satin (1995). "An ATP-sensitive Cl- channel current that is activated by cell swelling, cAMP, and glyburide in insulin-secreting cells." Diabetes **44**(12): 1461-6.
Kondo, H., *et al.* (2006). "Constitutive GDP/GTP exchange and secretion-dependent GTP hydrolysis activity for Rab27 in platelets." J Biol Chem **281**(39): 28657-65.
Kotake, K., *et al.* (1997). "Noc2, a putative zinc finger protein involved in exocytosis in endocrine cells." J Biol Chem **272**(47): 29407-10.
Kwan, E. P. and H. Y. Gaisano (2005). "Glucagon-like peptide 1 regulates sequential and compound exocytosis in pancreatic islet beta-cells." Diabetes **54**(9): 2734-43.

Kwan, E. P., *et al.* (2007). "Interaction between Munc13-1 and RIM is critical for glucagon-like peptide-1 mediated rescue of exocytotic defects in Munc13-1 deficient pancreatic beta-cells." Diabetes **56**(10): 2579-88.
Lonart, G., *et al.* (2003). "Phosphorylation of RIM1alpha by PKA triggers presynaptic long-term potentiation at cerebellar parallel fiber synapses." Cell **115**(1): 49-60.
Lopez, J. A., *et al.* (2008). "The RalA GTPase is a central regulator of insulin exocytosis from pancreatic islet beta-cells." J Biol Chem.
Mahoney, T. R., *et al.* (2006). "Regulation of synaptic transmission by RAB-3 and RAB-27 in Caenorhabditis elegans." Mol Biol Cell **17**(6): 2617-25.
Matsumoto, M., *et al.* (2004). "Noc2 is essential in normal regulation of exocytosis in endocrine and exocrine cells." Proc Natl Acad Sci U S A **101**(22): 8313-8.
Miley, H. E., *et al.* (1999). "Regulation of a volume-sensitive anion channel in rat pancreatic beta-cells by intracellular adenine nucleotides." J Physiol **515 (Pt 2)**: 413-7.
Olofsson, C. S., *et al.* (2002). "Fast insulin secretion reflects exocytosis of docked granules in mouse pancreatic B-cells." Pflugers Arch **444**(1-2): 43-51.
Renstrom, E., *et al.* (1997). "Protein kinase A-dependent and -independent stimulation of exocytosis by cAMP in mouse pancreatic B-cells." J Physiol **502 (Pt 1)**: 105-18.
Rosengren, A., *et al.* (2002). "Glucose dependence of insulinotropic actions of pituitary adenylate cyclase-activating polypeptide in insulin-secreting INS-1 cells." Pflugers Arch **444**(4): 556-67.
Schluter, O. M., *et al.* (2006). "Rab3 superprimes synaptic vesicles for release: implications for short-term synaptic plasticity." J Neurosci **26**(4): 1239-46.
Schluter, O. M., *et al.* (2004). "A complete genetic analysis of neuronal Rab3 function." J Neurosci **24**(29): 6629-37.
Shibasaki, T., *et al.* (2004). "Interaction of ATP sensor, cAMP sensor, Ca2+ sensor, and voltage-dependent Ca2+ channel in insulin granule exocytosis." J Biol Chem **279**(9): 7956-61.
Shibasaki, T., *et al.* (2007). "Essential role of Epac2/Rap1 signaling in regulation of insulin granule dynamics by cAMP." Proc Natl Acad Sci U S A **104**(49): 19333-8.
Stinchcombe, J. C., *et al.* (2001). "Rab27a is required for regulated secretion in cytotoxic T lymphocytes." J Cell Biol **152**(4): 825-34.
Straub, S. G. and G. W. Sharp (2002). "Glucose-stimulated signaling pathways in biphasic insulin secretion." Diabetes Metab Res Rev **18**(6): 451-63.
Strom, M., *et al.* (2002). "A family of Rab27-binding proteins. Melanophilin links Rab27a and myosin Va function in melanosome transport." J Biol Chem **277**(28): 25423-30.
Takahashi, N., *et al.* (1997). "Multiple exocytotic pathways in pancreatic beta cells." J Cell Biol **138**(1): 55-64.
Tomas, A., *et al.* (2008). "Munc 18-1 and granuphilin collaborate during insulin granule exocytosis." Traffic **9**(5): 813-32.
Torii, S., *et al.* (2002). "Granuphilin modulates the exocytosis of secretory granules through interaction with syntaxin 1a." Mol Cell Biol **22**(15): 5518-26.
Tsuboi, T. and M. Fukuda (2006). "Rab3A and Rab27A cooperatively regulate the docking step of dense-core vesicle exocytosis in PC12 cells." J Cell Sci **119**(Pt 11): 2196-203.
Tsuboi, T. and M. Fukuda (2006). "The Slp4-a linker domain controls exocytosis through interaction with Munc18-1.syntaxin-1a complex." Mol Biol Cell **17**(5): 2101-12.
Voets, T., *et al.* (2001). "Munc18-1 promotes large dense-core vesicle docking." Neuron **31**(4): 581-91.
Wan, Q. F., *et al.* (2004). "Protein kinase activation increases insulin secretion by sensitizing the secretory machinery to Ca2+." J Gen Physiol **124**(6): 653-62.
Waselle, L., *et al.* (2003). "Involvement of the Rab27 binding protein Slac2c/MyRIP in insulin exocytosis." Mol Biol Cell **14**(10): 4103-13.

Wilson, S. M.*, et al.* (2000). "A mutation in Rab27a causes the vesicle transport defects observed in ashen mice." Proc Natl Acad Sci U S A **97**(14): 7933-8.
Wu, X.*, et al.* (2002). "Rab27a is an essential component of melanosome receptor for myosin Va." Mol Biol Cell **13**(5): 1735-49.
Yaekura, K.*, et al.* (2003). "Insulin secretory deficiency and glucose intolerance in Rab3A null mice." J Biol Chem **278**(11): 9715-21.
Yang, Y. and K. D. Gillis (2004). "A highly Ca2+-sensitive pool of granules is regulated by glucose and protein kinases in insulin-secreting INS-1 cells." J Gen Physiol **124**(6): 641-51.
Yang, Y.*, et al.* (2002). "A highly Ca2+-sensitive pool of vesicles is regulated by protein kinase C in adrenal chromaffin cells." Proc Natl Acad Sci U S A **99**(26): 17060-5.
Yi, Z.*, et al.* (2002). "The Rab27a/granuphilin complex regulates the exocytosis of insulin-containing dense-core granules." Mol Cell Biol **22**(6): 1858-67.

CHAPTER IV

Discussion

The purpose of the investigations forming this dissertation was to provide information on the sites of Munc18c and Rab27a action in vesicle docking and priming in two tissues which exhibit exocytotic defects in the diabetic state, adipocytes and pancreatic β-cells. In this section I will summarize the experimental results that address the Specific Aims identified in the Introduction, highlighting their significance within the broader literature. In doing so, I will describe the features identified for each molecule that contribute to temporal regulation of exocytotic events, as both molecules were studied in the context of regulated exocytotic events. Finally, I will describe the major limitations of each chapter's results, and propose future studies to forward progress in the field.

Significance of the Specific Aims addressed in Chapters II and III

In our initial characterization of the molecular requirements for the Munc18c-syntaxin4 interaction, we found using mutational analysis that multiple binding states for Munc18c exist depending on the conformation of syntaxin4. This result rectified apparent inconsistencies in the model for Munc18c action proposed in past literature. Long established models of Munc18 action proposed that Munc18-syntaxin binding interactions were eliminated upon formation of SNARE complexes, thereby indicating that Munc18s interacted only with closed conformations of syntaxin (Dulubova *et al.* 1999; Misura *et al.* 2000). More recently, Munc18c, was shown to

bind SNARE complexes *in vitro* (Widberg *et al.* 2003), and biochemical analysis suggested that the N-terminus of syntaxin4 could support Munc18c binding (Latham *et al.* 2006). Our data tested this interaction scenario in an *in situ* situation, and the results strongly agree with the latter model.

Supporting the interpretation of multiple Munc18c binding states was the preparation of a constitutively open mutant of syntaxin4 (L173A/E174A; LE). This mutant was found by an intermolecular FRET assay *in situ* to interact with Munc18c to a similar extent as with wildtype syntaxin4. The nature of Munc18c-syntaxin4^{LE} interaction required the N-terminus of syntaxin4, as demonstrated by point mutants of syntaxin4^{LE} (D3R and I233A) that eliminated interaction with Munc18c. During completion of our Munc18c research, a Munc18a-Q-SNARE complex was suggested to serve as a vesicle docking platform in chromaffin cell plasma membranes (Zilly *et al.* 2006). We, therefore, searched for such an analogous complex for Munc18c. Our results demonstrated the existence of a Munc18c-syntaxin4^{LE}-SNAP23 complex using immunoprecipitation in HEK293 cells. Supporting this result was a novel optical assay in which a cytosolic mutant of GFP-SNAP23 was protected from cytosolic photobleach through binding to a Munc18c-syntaxin4^{LE} complex, but not the Munc18c-syntaxin4^{WT} complex, at the PM. These studies highlight the role of Munc18c, as outlined in Specific Aim 1, as a syntaxin chaperone that initially regulates syntaxin-SNARE interactions.

The investigations associated with Specific Aim 2 extended our analysis of the binding modes between Munc18c and syntaxin4 to determine whether Munc18c control over syntaxin4 conformation affects the competency of GLUT4 vesicle docking. We showed that 3T3L1 adipocytes expressing Munc18c together with syntaxin4^{LE}, but not syntaxin4^{WT}, syntaxin4^{D3R} (a mutant that eliminates Munc18c binding to the syntaxin4 N-terminus), or syntaxin4^{I233A} (a mutant that eliminates Munc18c binding to both closed and open forms of syntaxin4), is sufficient for GLUT4 vesicle docking to the PM. To our knowledge, this is the first evidence demonstrating a positive role for Munc18c in GSV trafficking. This is particularly significant as our studies,

together with recent studies of the neuronal homologue Munc18a (Dulubova *et al.* 2007; Khvotchev *et al.* 2007; Shen *et al.* 2007), now have agreement with older studies of Sec1p in yeast (Carr *et al.* 1999; Scott *et al.* 2004) showing that SM proteins can facilitate secretion. Collectively, these results support a consensus model of SM interactions with exocytotic syntaxins in which multiple binding and functional states are necessary to maintain temporal regulation of exocytosis.

These studies furthermore support the following sequence of events in the docking, priming, and fusion of GSVs with the PM. Following vesicle transport to the plasma membrane, Munc18c binding to closed syntaxin4 puts a clamp on vesicle docking and priming, by preventing syntaxin4 entry into SNARE complexes. As signaled by insulin, priming factors subsequently assist the opening of syntaxin4, transitioning Munc18c to an N-terminal binding interaction with the open conformation of syntaxin4. Exposure of the syntaxin4 SNARE domain supports the formation of Q-SNARE complexes with SNAP23, and the resulting binary complex serves as an acceptor for VAMP2 on the vesicle, towards completion of priming which is ultimately necessary to provide the force necessary for GSV fusion.

What then, is the direct stimulus for priming reactions and SNARE complex assembly? Numerous experiments now indicate that Rab/Rab effector/Munc18/syntaxin interactions comprise the end-stage events in exocytosis, which include the processes of vesicle docking, priming, and fusion. First, it was discovered in yeast that the loss of Rab GTPase (Ypt1) in ER-to-Golgi trafficking can be bypassed by the SM protein Sly1, suggesting that Rab and SM proteins function in the same pathways (Peng and Gallwitz 2002). Second, biochemical interactions between Rab effector proteins and the SM-syntaxin complex have been reported *in vitro* (Torii *et al.* 2002; Fukuda 2003). Most recently, a direct protein-protein interaction between Rab3a and Munc18a has been reported in neuroendocrine PC12 cells (Graham *et al.* 2008). Finally, in mammals, genetic ablation of Rab GTPases, a subset of their effectors (*e.g.*, Slp4a, rabphilin), and SM proteins exhibit very similar defects, principally reported as defects in vesicle

docking and priming (Voets *et al.* 2001; Weimer *et al.* 2003; Gomi *et al.* 2005; Kasai *et al.* 2005; Korteweg *et al.* 2005; Deak *et al.* 2006).

Of significant interest to this work, a marked deficit in both first and second phase insulin secretion was evident during glucose stimulation in islets isolated from Rab27a-null *ashen* mice, resulting in glucose intolerant animals (Kasai *et al.* 2005). In response to a single meal, ~5% of the ~13,000 β-granules are released during two biochemically separate periods. First phase secretion (*i.e.*, K_{ATP}-channel dependent) depends on exocytosis of readily- and immediately-releasable granules that are fully primed (~50 to 60 granules) (Barg *et al.* 2001; Olofsson *et al.* 2002), while the second phase (*i.e.*, K_{ATP}-channel independent) relies on transition of non-primed granules to a fully-primed state as well and recruitment of granules to the PM region for exocytosis (Eliasson *et al.* 1997; Kanno *et al.* 2004). From the initial studies of *ashen* β-cells, it was unclear whether absence of Rab27a resulted in a limited readily-releasable pool size or the replenishment of that pool as the islets were continuously exposed to stimulatory concentrations of glucose, or both. Thus, the initial goal of Specific Aim 3 was to characterize the kinetic parameters of vesicle exocytosis that differed in Rab27a-null β-cells from background matched control β-cells. To accomplish this we used patch-clamp measurements of membrane capacitance changes in response to a stimulation protocol that could simultaneously assay the size as well as refilling competence of the functionally distinct β-granule pools (*i.e.*, the IRP and RRP). Membrane capacitance measurements are independent of morphological characterizations of the secretory pathways (*e.g.*, docking as assayed by TIRFM or EM), allowing us to isolate the sites of Rab27a action in the exocytotic pathway based discretely on Rab27a function. Measurements of membrane capacitance changes do, however, represent a net measurement of both exocytotic and endocytotic activity. As endocytosis is kinetically slower that exocytosis, the results using our brief stimulation protocol are predominated by exocytotic activity.

We have identified the principal defect in *ashen* β-cells as the inability to replenish both the IRP and RRP. Notably, the initial size of both pools was comparable to that measured in control β-cells in our experiments, and by others (Eliasson *et al.* 1997; Barg *et al.* 2001). This result indicates the Rab27a-dependent deficit is time-dependent, and reflective of Rab27a working in conjunction with other unknown mechanisms to refill the pools (*i.e.*, Rab27a is not strictly required). The deficit in *ashen* cells with respect to the RRP cannot be offset by elevated glucose-stimulation, as it persists even as glucose was elevated from mildly (5 mM) to strongly (16.7 mM) stimulatory concentrations. By comparison, our results demonstrated that high glucose concentrations can obviate Rab27a for priming into the IRP. In considering the mechanism for this response, there are several possible signaling intermediates/pathways that have been proposed to account for the dose-dependent glucose augmentation of secretion, including long chain acyl-CoA (Prentki 1996; Prentki and Corkey 1996), nucleotides (Henquin 2000), and protein kinases (PKA, PKC, and AMPK) (Nesher *et al.* 2002). We investigated the cAMP/PKA-dependent priming pathway and its interactions/requirements with Rab27a regulated pathways.

The secondary goal of Specific Aim 3 was to provide missing information on the specific signaling pathways responsible for Rab27a activation. In addition to glucose-dependent pathways, cAMP-dependent pathways strongly augment secretion (Ammala *et al.* 1993; Gromada *et al.* 1998; Yang *et al.* 2002; Wan *et al.* 2004; Yang and Gillis 2004; Kwan and Gaisano 2005). Most of effects of cAMP can be attributed to the direct binding of either protein kinase A (PKA) or Epac2 (exchange protein directly activated by cAMP) (Ozaki *et al.* 2000). Both PKA and Epac2 have proximal effects on β-cells via regulation of ion channel activity, thereby increasing Ca^{2+} influx (Ammala *et al.* 1993; Kang *et al.* 2001; Shibasaki *et al.* 2004). Consistently, we measured a significant retardation in the I_{Ca} inactivation kinetics, increasing the net Ca^{2+} influx by ~20% in response to direct activation of both pathways. However, up to 80% of the effects of

cAMP on exocytosis are believed to be downstream of Ca^{2+}, through direct interaction with the secretory machinery (Ammala *et al.* 1993). Yet, no prior studies had examined whether these distal cAMP actions are upstream, downstream, or parallel to Rab27a.

As Rab27a is known to participate in such diverse steps in membrane trafficking as transport (Hume *et al.* 2001; Wu *et al.* 2002), docking/tethering (Stinchcombe *et al.* 2001; Gomi *et al.* 2005; Kasai *et al.* 2005), and priming (Kasai *et al.* 2005), it seems plausible that Rab27a is inherent to cAMP-dependent, as well as glucose-dependent, processes. Yet, we found two principal effects of cAMP that are not affected by the absence of Rab27a in *ashen* β-cells. First, both the IRP and RRP amplitude and refilling rate could be augmented through direct activation of Epac2, in the absence of Rab27a. Second, the ability of the IRP and RRP to refill in both *ashen* and wildtype β-cells is strongly dependent on PKA-dependent processes. Therefore, as it has been reported that the actions of glucose and cAMP to augment secretion are additive (Wan *et al.* 2004; Yang and Gillis 2004), we now know that cAMP actions on the final stages of the exocytotic pathway happen independent of or downstream of Rab27a. As discussed in a subsequent section, Rab3 GTPases may be possible mediators of cAMP-dependent effects.

Limitations and Future Directions of Chapter II Results

The overall goal of our experiments in adipocytes was to produce a detailed functional map of the protein-protein interactions that are required to dock GLUT4 vesicles to the PM, and assist in their priming. We have made significant progress towards this goal. Our main finding was that the priming factor Munc18c, through binding to the open conformation of syntaxin4, promotes GLUT4 vesicle docking in 3T3L1 adipocytes. Still unclear are the critical proteins linking the vesicle and PM. Until recently, the identities of the Rab proteins involved in GLUT4 trafficking were unknown. Particularly, Rab10 appears important to the process, since overexpression of a Rab10 mutant defective in GTP hydrolysis increases basal surface GLUT4

and Rab10 knockdown inhibits the rate of exocytosis (Sano *et al.* 2007). Rab 2A, 8A, and 14 have also been shown to interact with PI3K-dependent Rab-GAP AS160 (Miinea *et al.* 2005), but no functional effects of the Rab molecules has been identified. Therefore, in contrast to the situation in β-cells described in this work, in which the Rab27a and Rab3 effectors in insulin secretion have been identified (*e.g.*, Slp4a, Noc2, and rabphilin), very little information exists on the Rab effectors in adipocytes. Future studies, using the techniques described below, may address this discrepancy.

Perhaps the central limitation of our GSV study is that our correlations between the distinct conformational states of syntaxin4 and functional effects on the GLUT4 translocation pathways were performed on fixed cells with limited optical resolution of the PM afforded by confocal microscopy. The use of dynamic FRET measurements in combination with TIRF (total internal reflection fluorescence) microscopy, which was not previously accessible, is currently being developed as an ideal tool to address this issue. TIRF microscopy utilizes an evanescent wave to visualize between 100-250 nm of the cell proximal to the PM, allowing examination of both GSV docking and fusion events at the PM. Recently, the application of TIRF microscopy in adipocytes has revealed a previously undiscovered insulin-regulated step in GSV docking/priming (Bai *et al.* 2007; Huang *et al.* 2007). Based on our findings, we propose that this step is likely to involve PI3K- and Akt2-dependent activation of Munc18c, although this hypothesis has not been tested. In addition to TIRFM, we are currently using FRET to directly report the CFP-Rab27a and CFP-Rab3a interactions with cYFP-Slp4a, as well as cYFP-Slp4a interaction with CFP-syntaxin4 in β-cells. This same system can be utilized in adipocytes as a companion to TIRFM. A potential hindrance to this idea is our discovery that the use of N-terminally labeled syntaxin (1 or 4), which clearly permits GSV docking in adipocytes, is mildly inhibitory in hGH secretion assays. This will require the design of an alternative to our Munc18c-syntaxin4 FRET-based assay appropriate to adipocytes. With the joining of TIRF and

FRET technologies, the objective of these studies will be to produce a real-time spatial map of the vesicle-PM protein-protein interactions underlying insulin-stimulated GSV docking and fusion.

Limitations and Future Directions of Chapter III Results

We used membrane capacitance measurements to monitor insulin secretion from single pancreatic β-cells to functionally test for sites of Rab27a action on specific functional vesicle pools. With currently available technology, this electrophysiologic approach yields a substantially better time resolution than optical or immunological measurements of insulin secretion and simultaneously provides an integrated readout of β-cell secretion augmentation pathways. One caveat of our β-cell electrophysiology study is the assertion that single pancreatic β-cells behave the same as intact islets. Several studies support this hypothesis. First, insulin secretion measured *in situ* from both single β-cells and pancreatic islets is biphasic, as observed in peripheral blood *in vivo* (Satin 2000; Dahlgren *et al.* 2005; Dahlgren *et al.* 2005; Nunemaker *et al.* 2005; Nunemaker *et al.* 2006). Second, a similar pattern of electrical oscillations elicited in response to glucose is observed in intact islets and single β-cells (Gopel *et al.* 1999). Third, these action potentials give rise to oscillations in intracellular Ca^{2+} (Satin 2000; Dahlgren *et al.* 2005; Dahlgren *et al.* 2005; Nunemaker *et al.* 2005; Nunemaker *et al.* 2006). Still unclear is whether the synchronization of insulin secretion between islets seen *in vivo* and *in situ* extends to the single cell level. Of course, our measurements of membrane capacitance require voltage clamp of the β-cell membrane potential. While this procedure departs from glucose-stimulated insulin secretion, control over Ca^{2+} influx was necessary to facilitate strong stimulation of the β-cells to completely deplete the IRP and RRP, allowing us to monitor for rate-limiting steps in their refilling.

We have reported a significant glucose-dependent secretory defect in Rab27a-mediated RRP refilling in *ashen* β-cells that does not exist in Rab3a-deficient cells. An important question

remaining is whether Rab27a and Rab3a are functionally redundant. Our results indicate that Rab27a is almost certainly not redundant, probably because the closely related Rab27b isoform is not present in pancreatic β-cells. In fact, the defects in vesicle trafficking in *ashen* mice have been shown to only exist in cells where one Rab27 isoform is present. These cell types include Rab27a-dependent defects in melanosomes, cytotoxic T-lymphocytes, and pancreatic β-cells, which underlie the albinism, immunodeficiency, and glucose intolerance in *ashen* mice (Stinchcombe *et al.* 2001; Tolmachova *et al.* 2004).

Whether Rab3a is redundant with the other Rab3 isoforms is still a matter of debate. All four isoforms are present on the same insulin secretory granules (Regazzi *et al.* 1996; Iezzi *et al.* 1999). Rab3a-null islets are reported to exhibit a ~50% defect in glucose-stimulated insulin secretion, suggesting that Rab3a is not redundant with other Rab proteins (Yaekura *et al.* 2003). Yet, we measured only a small deficit in the RRP size in Rab3a$^{-/-}$ β-cells, which seems to be too small account for the defect seen in intact islets. Comparatively, deletion of all four Rab3 isoforms (which is lethal owing to respiratory defects) in studies of hippocampal neurons resulted in only a ~30% decrease in evoked secretion (Schluter *et al.* 2004; Schluter *et al.* 2006), suggesting Rab3a is redundant with Rab3 b, c, and d, at least for synaptic transmission. However, the situation in hippocampal neurons may not be analogous to the condition in β-cells, as no defects in vesicle docking or priming were discovered (Geppert *et al.* 1994).

The potential for redundancy between Rab27 and Rab3, and amongst the Rab3 isoforms, makes it difficult to determine whether Rab27a and Rab3a have overlapping roles within the glucose- and cAMP-dependent priming pathways. Our results indicate that cAMP bypasses Rab27a-dependent actions in pool refilling, suggesting that Rab27a acts independently of the cAMP-dependent priming pathway. However, an alternative interpretation is that Rab3 isoforms are compensating for the Rab27a deficiency, and that Rab27a normally exerts an overlapping function with Rab3 in the cAMP-dependent pathway. If the latter is true, future experiments

might focus on eliminating the contribution of multiple Rab isoforms to secretion simultaneously, allowing the isolation of particular priming pathways. For example, adenoviral expression of the unique Rab-specific GDI might prevent the Rab3 and Rab27a cycling necessary for function (Takai *et al.* 2001; van Weering *et al.* 2007). Alternatively, knockdown of the GEF specific for Rab3 and Rab27a (known as Rab3GEP; Figueiredo *et al.* 2008) could further reduce the normally slow Rab cycle (Becker *et al.* 1991; Kondo *et al.* 2006) by inactivating both Rab3 and Rab27a. In fact, deletion of the GEF for Rab3 and Rab27 in *C. elegans*, AEX-3 (Iwasaki and Toyonaga 2000), has a much more severe phenotype than elimination of either Rab protein alone (Mahoney *et al.* 2006). Unfortunately, no GEF is known to act exclusively upon Rab27a, although a more highly-specific GEF for Rab3 (GRAB) has been shown to activate Rab3a (Luo *et al.* 2001). However, two putative Rab27a GAPs have been identified (EPI64 and FLJ13130/Rab27a-GAPβ) (Itoh and Fukuda 2006; Itoh *et al.* 2006), which upon overexpression, may be effective to specifically reduce the activity of Rab27a by functionally eliminating its effector interactions. This same strategy could be employed to assess the contribution of other small GTPases thought to act in the cAMP pathway. A third potential target is the small GTPase Rap1, which has been implicated in the cAMP-induced increases in vesicle priming downstream of its GEF Epac2 (Ozaki *et al.* 2000; Shibasaki *et al.* 2007). These future studies may shed new light on the function of Rab27a and Rab3a as they act to fine-tune glucose-stimulated insulin release.

Future Studies: using technology to understand the heterogeneous causes of glucose intolerance and the diabetic state

Type 2 diabetes mellitus accounts for between 80-90% of all diabetes in most countries (Gerich 1998; King *et al.* 1998). However, this disorder presents in a highly heterogeneous fashion, as 5-10% of patients have maturity-onset diabetes of youth (MODY) (Fajans 1989), and another 5-10% acquire diabetes secondary to rare genetic disorders (Moller and Flier 1991; Taylor 1992). Unfortunately, the etiology of the remaining ~80% of cases remains further

divided by the relative strength of genetic (polygenic) and environmental (acquired) factors (Hamman 1992; Kahn 1994; Bouchard 1995; Turner *et al.* 1995) as well as the quantitative contribution of insulin resistance and impaired insulin secretion (Gerich 1998). It is therefore imperative to test how these phenotypes display at the tissue and cellular level.

It is important to point out that the approaches used in this dissertation, particularly the use of FRET to study protein-protein interactions, and electrophysiologic studies of insulin secretion, provide nearly unparalleled spatial and temporal resolution of vesicle/granule movements *in situ*. Clearly the critical next step in the evolution of controlling the diabetic state is the application of these technologies to compare between normal physiologic processes and models of the diabetic state that accurately reflect the heterogeneity of type 2 diabetes presentations and treatments. These models should encompass: (1) mouse genetic models of the identified diabetes susceptibility genes which differ between populations (*e.g.*, NIDDM1 (Hanis *et al.* 1996) in Mexican Americans is different from NIDDM2 (Mahtani *et al.* 1996) found in Finnish families), (2) studies of cell secretory function in both insulin-secreting and insulin-sensitive tissues in response to changes in newly discovered adipose-derived hormones (*e.g.*, leptin, adiponectin, resistin, *etc.*) as well as circulating factors known to affect insulin secretion or activity (*e.g.*, circulating free fatty acids), and (3) studies of pharmacologic activators of insulin secretion, to identify their specific sites of action and potential side effects (*e.g.*, Liraglutide, Exenatide/Byetta and other GLP-1 analogs that act to increase pancreatic β-cell insulin secretion and decrease pancreatic α-cell glucagons secretion).

For each of these three genetic or pharmacologic manipulations, information desired is the specific steps at which membrane trafficking is disrupted or accelerated. Therefore, it would be useful to adapt the techniques we describe to monitor the functional output of granule/vesicle movement to the surface: *i.e.*, the IRP, RRP, and HCSP size and refilling can be monitored electrophysiologically in β-cells; optical measurements of labeled GLUT4 can be used to follow

the Golgi- or endosomally-derived GSV pools in adipocytes and skeletal muscle, as well as their fusion with the PM. Apart from the cell's net functional secretory capacity, morphological analysis of vesicle number, size and location (by EM, for example) can be combined with TIRFM analysis of the kinetics of granule movements near the PM to additionally screen for aberrations in vesicle translocation, docking and fusion. Upstream of fusion, the direct triggers for exocytosis can be monitored. For example, specifically in pancreatic β-cells, current clamp experiments can be used to determine whether specific pharmacologic manipulations alter electrical activity (including the action potential), and simultaneous loading of cells with Fura-2 can serve as a monitor of intracellular Ca^{2+} handling. Comparatively, as stimulus-secretion coupling in adipocytes is mediated specifically through insulin-receptor pathways (*i.e.*, independent of action potentials and Ca^{2+}), our knowledge of real-time changes in protein-protein interactions at critical nodes of the pathway can potentially be advanced by the creation of novel FRET pairs to monitor specific signaling pathways: *e.g.*, PI3K/Akt2, an early-stage node at which the insulin-IR pathway diverges; Akt2/AS160, to monitor Akt2 movement to the PM as it activates AS160 GAP activity; or Rab10/Munc18c, a putative interaction which may prove useful to assess vesicle docking/priming events. In summary, the use of genetic approaches to pursue specific molecules controlling glucose homeostasis as pharmacological targets can be combined with the technology employed in this dissertation to provide the added benefit of understanding the likely functional outcome of such manipulations.

Conclusion

When taken together, the results of the investigations forming this dissertation support a role for Munc18c and Rab27a in controlling both the timing and magnitude of vesicle docking and priming at the plasma membrane, thereby acting as crucial regulators in the regulated exocytotic pathways in glucose regulatory tissues. It is our hope that information gleaned from this work can assist in mitigating the diabetes epidemic worldwide.

References

Ammala, C., *et al.* (1993). "Calcium-independent potentiation of insulin release by cyclic AMP in single beta-cells." Nature **363**(6427): 356-8.

Bai, L., *et al.* (2007). "Dissecting multiple steps of GLUT4 trafficking and identifying the sites of insulin action." Cell Metab **5**(1): 47-57.

Barg, S., *et al.* (2001). "Fast exocytosis with few Ca(2+) channels in insulin-secreting mouse pancreatic B cells." Biophys J **81**(6): 3308-23.

Becker, J., *et al.* (1991). "Mutational analysis of the putative effector domain of the GTP-binding Ypt1 protein in yeast suggests specific regulation by a novel GAP activity." Embo J **10**(4): 785-92.

Bouchard, C. (1995). "Genetics of obesity: an update on molecular markers." Int J Obes Relat Metab Disord **19 Suppl 3**: S10-3.

Carr, C. M., *et al.* (1999). "Sec1p binds to SNARE complexes and concentrates at sites of secretion." J Cell Biol **146**(2): 333-44.

Dahlgren, G. M., *et al.* (2005). "Substrate effects on oscillations in metabolism, calcium and secretion in single mouse islets of Langerhans." Biochim Biophys Acta **1724**(1-2): 23-36.

Dahlgren, G. M., *et al.* (2005). "Effect of intracellular delivery of energy metabolites on intracellular Ca2+ in mouse islets of Langerhans." Life Sci **77**(23): 2986-97.

Deak, F., *et al.* (2006). "Rabphilin regulates SNARE-dependent re-priming of synaptic vesicles for fusion." EMBO J **25**(12): 2856-66.

Dulubova, I., *et al.* (2007). "Munc18-1 binds directly to the neuronal SNARE complex." Proc Natl Acad Sci U S A.

Dulubova, I., *et al.* (1999). "A conformational switch in syntaxin during exocytosis: role of munc18." Embo J **18**(16): 4372-82.

Eliasson, L., *et al.* (1997). "Rapid ATP-dependent priming of secretory granules precedes Ca(2+)-induced exocytosis in mouse pancreatic B-cells." J Physiol **503 (Pt 2)**: 399-412.

Fajans, S. S. (1989). "Maturity-onset diabetes of the young (MODY)." Diabetes Metab Rev **5**(7): 579-606.

Fukuda, M. (2003). "Slp4-a/granuphilin-a inhibits dense-core vesicle exocytosis through interaction with the GDP-bound form of Rab27A in PC12 cells." J Biol Chem **278**(17): 15390-6.

Geppert, M., *et al.* (1994). "The role of Rab3A in neurotransmitter release." Nature **369**(6480): 493-7.

Gerich, J. E. (1998). "The genetic basis of type 2 diabetes mellitus: impaired insulin secretion versus impaired insulin sensitivity." Endocr Rev **19**(4): 491-503.

Gomi, H., *et al.* (2005). "Granuphilin molecularly docks insulin granules to the fusion machinery." J Cell Biol **171**(1): 99-109.

Gopel, S., *et al.* (1999). "Voltage-gated and resting membrane currents recorded from B-cells in intact mouse pancreatic islets." J Physiol **521 Pt 3**: 717-28.

Graham, M. E., *et al.* (2008). "A gain-of-function mutant of Munc18-1 stimulates secretory granule recruitment and exocytosis and reveals a direct interaction of Munc18-1 with Rab3." Biochem J **409**(2): 407-16.

Gromada, J., *et al.* (1998). "Glucagon-like peptide 1 (7-36) amide stimulates exocytosis in human pancreatic beta-cells by both proximal and distal regulatory steps in stimulus-secretion coupling." Diabetes **47**(1): 57-65.

Hamman, R. F. (1992). "Genetic and environmental determinants of non-insulin-dependent diabetes mellitus (NIDDM)." Diabetes Metab Rev **8**(4): 287-338.

Hanis, C. L., *et al.* (1996). "A genome-wide search for human non-insulin-dependent (type 2) diabetes genes reveals a major susceptibility locus on chromosome 2." Nat Genet **13**(2): 161-6.
Henquin, J. C. (2000). "Triggering and amplifying pathways of regulation of insulin secretion by glucose." Diabetes **49**(11): 1751-60.
Huang, S., *et al.* (2007). "Insulin stimulates membrane fusion and GLUT4 accumulation in clathrin coats on adipocyte plasma membranes." Mol Cell Biol **27**(9): 3456-69.
Hume, A. N., *et al.* (2001). "Rab27a regulates the peripheral distribution of melanosomes in melanocytes." J Cell Biol **152**(4): 795-808.
Iezzi, M., *et al.* (1999). "Subcellular distribution and function of Rab3A, B, C, and D isoforms in insulin-secreting cells." Mol Endocrinol **13**(2): 202-12.
Itoh, T. and M. Fukuda (2006). "Identification of EPI64 as a GTPase-activating protein specific for Rab27A." J Biol Chem **281**(42): 31823-31.
Itoh, T., *et al.* (2006). "Screening for target Rabs of TBC (Tre-2/Bub2/Cdc16) domain-containing proteins based on their Rab-binding activity." Genes Cells **11**(9): 1023-37.
Iwasaki, K. and R. Toyonaga (2000). "The Rab3 GDP/GTP exchange factor homolog AEX-3 has a dual function in synaptic transmission." EMBO J **19**(17): 4806-16.
Kahn, C. R. (1994). "Banting Lecture. Insulin action, diabetogenes, and the cause of type II diabetes." Diabetes **43**(8): 1066-84.
Kang, G., *et al.* (2001). "cAMP-regulated guanine nucleotide exchange factor II (Epac2) mediates Ca2+-induced Ca2+ release in INS-1 pancreatic beta-cells." J Physiol **536**(Pt 2): 375-85.
Kanno, T., *et al.* (2004). "Large dense-core vesicle exocytosis in pancreatic beta-cells monitored by capacitance measurements." Methods **33**(4): 302-11.
Kasai, K., *et al.* (2005). "Rab27a mediates the tight docking of insulin granules onto the plasma membrane during glucose stimulation." J Clin Invest **115**(2): 388-96.
Khvotchev, M., *et al.* (2007). "Dual modes of Munc18-1/SNARE interactions are coupled by functionally critical binding to syntaxin-1 N terminus." J Neurosci **27**(45): 12147-55.
King, H., *et al.* (1998). "Global burden of diabetes, 1995-2025: prevalence, numerical estimates, and projections." Diabetes Care **21**(9): 1414-31.
Kondo, H., *et al.* (2006). "Constitutive GDP/GTP exchange and secretion-dependent GTP hydrolysis activity for Rab27 in platelets." J Biol Chem **281**(39): 28657-65.
Korteweg, N., *et al.* (2005). "The role of Munc18-1 in docking and exocytosis of peptide hormone vesicles in the anterior pituitary." Biol Cell **97**(6): 445-55.
Kwan, E. P. and H. Y. Gaisano (2005). "Glucagon-like peptide 1 regulates sequential and compound exocytosis in pancreatic islet beta-cells." Diabetes **54**(9): 2734-43.
Latham, C. F., *et al.* (2006). "Molecular dissection of the munc18c/syntaxin4 interaction: implications for regulation of membrane trafficking." Traffic **7**(10): 1408-19.
Luo, H. R., *et al.* (2001). "GRAB: a physiologic guanine nucleotide exchange factor for Rab3A, which interacts with inositol hexakisphosphate kinase." Neuron **31**(3): 439-51.
Mahoney, T. R., *et al.* (2006). "Regulation of synaptic transmission by RAB-3 and RAB-27 in Caenorhabditis elegans." Mol Biol Cell **17**(6): 2617-25.
Mahtani, M. M., *et al.* (1996). "Mapping of a gene for type 2 diabetes associated with an insulin secretion defect by a genome scan in Finnish families." Nat Genet **14**(1): 90-4.
Miinea, C. P., *et al.* (2005). "AS160, the Akt substrate regulating GLUT4 translocation, has a functional Rab GTPase-activating protein domain." Biochem J **391**(Pt 1): 87-93.
Misura, K. M., *et al.* (2000). "Three-dimensional structure of the neuronal-Sec1-syntaxin 1a complex." Nature **404**(6776): 355-62.
Moller, D. E. and J. S. Flier (1991). "Insulin resistance--mechanisms, syndromes, and implications." N Engl J Med **325**(13): 938-48.
Nesher, R., *et al.* (2002). "Beta-cell protein kinases and the dynamics of the insulin response to glucose." Diabetes **51 Suppl 1**: S68-73.

Nunemaker, C. S., *et al.* (2006). "Insulin secretion in the conscious mouse is biphasic and pulsatile." Am J Physiol Endocrinol Metab **290**(3): E523-9.
Nunemaker, C. S., *et al.* (2005). "Individual mice can be distinguished by the period of their islet calcium oscillations: is there an intrinsic islet period that is imprinted in vivo?" Diabetes **54**(12): 3517-22.
Olofsson, C. S., *et al.* (2002). "Fast insulin secretion reflects exocytosis of docked granules in mouse pancreatic B-cells." Pflugers Arch **444**(1-2): 43-51.
Ozaki, N., *et al.* (2000). "cAMP-GEFII is a direct target of cAMP in regulated exocytosis." Nat Cell Biol **2**(11): 805-11.
Peng, R. and D. Gallwitz (2002). "Sly1 protein bound to Golgi syntaxin Sed5p allows assembly and contributes to specificity of SNARE fusion complexes." J Cell Biol **157**(4): 645-55.
Prentki, M. (1996). "New insights into pancreatic beta-cell metabolic signaling in insulin secretion." Eur J Endocrinol **134**(3): 272-86.
Prentki, M. and B. E. Corkey (1996). "Are the beta-cell signaling molecules malonyl-CoA and cystolic long-chain acyl-CoA implicated in multiple tissue defects of obesity and NIDDM?" Diabetes **45**(3): 273-83.
Regazzi, R., *et al.* (1996). "Expression, localization and functional role of small GTPases of the Rab3 family in insulin-secreting cells." J Cell Sci **109 (Pt 9)**: 2265-73.
Sano, H., *et al.* (2007). "Rab10, a target of the AS160 Rab GAP, is required for insulin-stimulated translocation of GLUT4 to the adipocyte plasma membrane." Cell Metab **5**(4): 293-303.
Satin, L. S. (2000). "Localized calcium influx in pancreatic beta-cells: its significance for Ca2+-dependent insulin secretion from the islets of Langerhans." Endocrine **13**(3): 251-62.
Schluter, O. M., *et al.* (2006). "Rab3 superprimes synaptic vesicles for release: implications for short-term synaptic plasticity." J Neurosci **26**(4): 1239-46.
Schluter, O. M., *et al.* (2004). "A complete genetic analysis of neuronal Rab3 function." J Neurosci **24**(29): 6629-37.
Scott, B. L., *et al.* (2004). "Sec1p directly stimulates SNARE-mediated membrane fusion in vitro." J Cell Biol **167**(1): 75-85.
Shen, J., *et al.* (2007). "Selective activation of cognate SNAREpins by Sec1/Munc18 proteins." Cell **128**(1): 183-95.
Shibasaki, T., *et al.* (2004). "Interaction of ATP sensor, cAMP sensor, Ca2+ sensor, and voltage-dependent Ca2+ channel in insulin granule exocytosis." J Biol Chem **279**(9): 7956-61.
Shibasaki, T., *et al.* (2007). "Essential role of Epac2/Rap1 signaling in regulation of insulin granule dynamics by cAMP." Proc Natl Acad Sci U S A **104**(49): 19333-8.
Stinchcombe, J. C., *et al.* (2001). "Rab27a is required for regulated secretion in cytotoxic T lymphocytes." J Cell Biol **152**(4): 825-34.
Takai, Y., *et al.* (2001). "Small GTP-binding proteins." Physiol Rev **81**(1): 153-208.
Taylor, S. I. (1992). "Lilly Lecture: molecular mechanisms of insulin resistance. Lessons from patients with mutations in the insulin-receptor gene." Diabetes **41**(11): 1473-90.
Tolmachova, T., *et al.* (2004). "A general role for Rab27a in secretory cells." Mol Biol Cell **15**(1): 332-44.
Torii, S., *et al.* (2002). "Granuphilin modulates the exocytosis of secretory granules through interaction with syntaxin 1a." Mol Cell Biol **22**(15): 5518-26.
Turner, R. C., *et al.* (1995). "Type II diabetes: clinical aspects of molecular biological studies." Diabetes **44**(1): 1-10.
van Weering, J. R., *et al.* (2007). "The role of Rab3a in secretory vesicle docking requires association/dissociation of guanidine phosphates and Munc18-1." PLoS ONE **2**: e616.
Voets, T., *et al.* (2001). "Munc18-1 promotes large dense-core vesicle docking." Neuron **31**(4): 581-91.
Wan, Q. F., *et al.* (2004). "Protein kinase activation increases insulin secretion by sensitizing the secretory machinery to Ca2+." J Gen Physiol **124**(6): 653-62.

Weimer, R. M.*, et al.* (2003). "Defects in synaptic vesicle docking in unc-18 mutants." Nat Neurosci **6**(10): 1023-30.

Widberg, C. H.*, et al.* (2003). "Tomosyn interacts with the t-SNAREs syntaxin4 and SNAP23 and plays a role in insulin-stimulated GLUT4 translocation." J Biol Chem **278**(37): 35093-101.

Wu, X.*, et al.* (2002). "Rab27a is an essential component of melanosome receptor for myosin Va." Mol Biol Cell **13**(5): 1735-49.

Yaekura, K.*, et al.* (2003). "Insulin secretory deficiency and glucose intolerance in Rab3A null mice." J Biol Chem **278**(11): 9715-21.

Yang, Y. and K. D. Gillis (2004). "A highly Ca2+-sensitive pool of granules is regulated by glucose and protein kinases in insulin-secreting INS-1 cells." J Gen Physiol **124**(6): 641-51.

Yang, Y.*, et al.* (2002). "A highly Ca2+-sensitive pool of vesicles is regulated by protein kinase C in adrenal chromaffin cells." Proc Natl Acad Sci U S A **99**(26): 17060-5.

Zilly, F. E.*, et al.* (2006). "Munc18-Bound Syntaxin Readily Forms SNARE Complexes with Synaptobrevin in Native Plasma Membranes." PLoS Biol **4**(10).